Dynamic Simulation of Semi-Active Suspension Systems for Durability Analysis

By

Rahizar Ramli

BSc.(Mech.), MEng.Sc.

Submitted in accordance with the requirements for the degree of

Doctor of Philosophy

University of Leeds

School of Mechanical Engineering

February 2007

Dedication

In loving memory of

Haji Ramli B. Man

(14^{th} April 1941 – 4^{th} June 2006)

Acknowledgements

I would like to express my sincere gratitude to the following people who have contributed and assisted me throughout the entire research directly and indirectly.

Sincere thanks are due to my academic supervisor Dr. M.C. Levesley for his unmatched guidance, invaluable advice, and knowledge during the course of this research. Thanks to Professor D.A. Crolla for his contribution on publications, Dr. O.M. Querin, and Dr. P.C. Brooks for their expert advice and constructive suggestions on finite element analysis and fatigue analysis.

An acknowledgement is also made to my sponsor, the University of Malaya for funding this research. Thanks are also due to Robert Cawte and Tony Goff of *nCode International Ltd.* for their invaluable suggestions on FE-Fatigue, and Tony Eckersley of *MSC.Software Ltd.* The supports from *Leyland Technical Centre Ltd. (LTC)* and *MIRA* have been significantly helpful and are highly appreciated.

A mention must also be given to the past and present colleagues in the G54B laboratory that includes Dr. Neil Stembridge, Dr. Mark Selby, Matt Pownall, Muhammad Zahir Hassan, Afandi Dzakaria, Bo Zhu, Ziad Chaaban, and Franz Manns for their knowledgeable assistance, contributions and suggestions throughout my studies.

I am also indebted to the technical staffs, Mr. Mick Martin and Mr. Dave Readman for utility and laboratory supports, Dr. G.J. Blyth, Mrs. M.I. Gibson, and Mr. E. Allwood for prompt and efficient IT assistance.

Finally, thanks are due to my wife, Rozilawati and my three wonderful children, Rahiman, Rezamir, and Rafiqah Alia for their love, patience and encouragement throughout many long days and nights of work. Not forgetting to my mother, and relatives for their endless supports, prayers and encouragement during these difficult times.

Abstracts

The benefits of vehicles with semi-active suspension systems have been widely accepted, mainly for improvement in ride and handling, over the passive system. However, the durability of the suspension components resulting from this implementation received very little attention. Therefore, this research aims to examine the effect of employing a selection of semi-active control strategies on the components' durability. To achieve this early in the design cycle, accurate representations of the load histories must be generated as these histories are the prerequisite in predicting fatigue life. This requires an alternative modelling and simulation approach capable of combining the complexity of vehicle suspensions with semi-active controller models, and at the same time capable of maintaining accurate dynamic responses.

In realizing this objective, a multi-body cosimulation approach has been proposed to predict these loads. Initially, efforts are centred on verifying the proposed method against conventional modelling and simulation techniques. This is followed by the evaluating the responses of vehicle suspension models of different complexities fitted with a selection of semi-active control strategies when subjected to transient and random road inputs. In an attempt to demonstrate the flexibility of MBS cosimulation, a magnetorheological damper model derived from experimental data is introduced, in which its dynamic characteristics and dynamic response are examined.

It is concluded that the proposed method is capable of producing reasonably accurate load histories but at the expense of increasing solution time. Evaluation of the durability of a lower suspension arm of a multi-purpose passenger vehicle suggested that the two-state semi-active strategies with skyhook damping control produced shorter fatigue life than from the conventional passive suspension systems.

Table of Contents

Lists of Figures

Lists of Tables

Lists of Abbreviations

2D	Two-dimensional
3D	Three-dimensional
ABC	Active bounce control
ARC	Active roll control
ASTM	American Society for Testing and Materials
B	Semi-active optimised controller gain
a_m	Maximum jerk
CAD	Computer aided design
CAE	Computer-aided-engineering
CG	Centre of gravity
CPU	Central processing unit
CVD	Continuously variable damper
C_{hard}	High damping coefficient
C_s	Viscous damping coefficient
C_{soft}	Low damping coefficient
d_{F_LHS}	Damper force on the front left hand side
d_{F_RHS}	Damper force on the front right hand side
d_{R_LHS}	Damper force on the rear left hand side
d_{R_RHS}	Damper force on the rear right hand side
d_{wb}	Wheelbase distance
DOF	Degree of freedom
ECU	Electronic control unit
EGH	Extended ground-hook control
EPS	Electric power steering
ER	Electrorheological damper
F_d	Damper force
F_t	Vertical tyre force
f	Natural frequency in Hz
FEM	Finite element method
FFT	Fast Fourier transformation

FVM	Full vehicle model
G	Optimised controller gain
K_s	Passive suspension stiffness
K_t	Tyre stiffness
K_{eq}	Ride rate
LDE	Lifetime dissipated energy
LTC	Leyland Technical Centre
MBS	Multi-body system
MR	Magnetorheological damper
m_b	Vehicle body mass or sprung mass
m_w	Wheel mass or unsprung mass
m_h	Hub mass
P	Instantaneous mechanical power converted to heat in MR/ER device
PID	Proportional-Integral-Derivative controller
PSD	Power spectral density
QVM	Quarter vehicle model
RMS	Root mean square
RMS_{ACC}	RMS acceleration
SA	Semi-active
TSS	Two-state switchable
TSS1 PnR	Two-state switchable with pitch and roll control
TSS2	Two-state switchable with damper force switching parameters
TSS3	Two-state switchable semi-active with current switching parameters
t_d	Time delay between the front and the rear wheel.
V	Volume of MR/ER fluid
v	Constant forward velocity
x	Displacement road profile
x_s	Sine wave amplitude.
z	Displacement of vehicle components
$\dot{z}$	Velocity of vehicle components
$\ddot{z}$	Acceleration of vehicle components
$\dot{z}_2$	Sprung mass velocity
$\dot{z}_1$	Unsprung mass velocity
α	Vibration sensor distance between the front and the rear of FVM
β	Vibration sensor distance between the right and the left hand side

δ	Logarithmic decrement
σ_x	Normal stress in x-direction
σ_y	Normal stress in y-direction
σ_z	Normal stress in z-direction
τ_{xy}	Shear stress in xy-plane
τ_{yz}	Normal stress in yz-plane
τ_{zx}	Normal stress in zx-plane
θ_x	Angular acceleration about x-axis (pitch acceleration)
θ_y	Angular acceleration about y-axis (roll acceleration)
ζ	Damping ratio
ω	Natural frequency in radian/s

CHAPTER ONE

Introduction

1.1 Overview

In the global automotive market, automotive manufacturers are forced to remain competitive. This imposes challenges to produce new and innovative models, improve on safety and reliability of components, shorten the development time while at the same time keeping production costs down. The typical automotive development cycle includes stages of conceptual design, prototype and production. Each of these stages requires an enormous amount of test and analysis comprising of physical and virtual techniques, thus significantly affecting time and cost. Many automotive manufacturers are adopting ways to overcome this problem by slowly reducing the number of traditional physical tests with equivalent virtual methods.

Durability plays a significant role in the automotive industry, particularly in promoting reliability and safety issues. Conventional methods for evaluating vehicle components' durability rely on physical testing. The technique produces accurate and reliable results but at the expense of extensive work and cost. In addition, problems can only be detected at the very end of the development cycle. With increasing innovation in software and hardware capabilities, virtual durability assessment is becoming a realistic alternative to physical durability testing. It helps to reduce the number of design changes, consequently curtailing production time and cost. Eventually virtual methods permit structural optimisation where radical and creative design solutions can be ascertained.

Typical virtual durability techniques in the automotive industry involve multidisciplinary simulation that integrates vehicle dynamics, finite element analysis, fatigue analysis and structural optimisation. In order to include this approach early in

the development process, accurate service load histories of critical components must firstly be obtained from vehicle dynamic simulation. Here, the components can be tested and analysed under a variety of road profiles, tyre and suspension models, and driving conditions. These load data are then applied to the desired components to determine stress distribution via finite element methods. Once the component stresses have been identified, the regions of high stress intensities will be selected for fatigue life estimation. Structural optimisation process allows removal of sections with lower stresses such that the final product becomes lighter without sacrificing its structural integrity.

The use of multi-body system (MBS) simulation to predict component load histories has generated considerable attention and has recently become feasible for the automotive world. Complex non-linear passive damper models can now be integrated into the suspension system. One inherent limitation of traditional passive suspension is that it has restricted capability in satisfying the conflicting design requirements of ride and handling. Controllable suspension systems such as active control suspensions, offer a better alternative in overcoming these differing needs but at the cost of an increase in payload, power consumption, the need for fairly complex control laws and hence are much more expensive. Conversely, semi-active systems, particularly those using magnetorheological (MR) dampers appear to provide a balance between the two suspension systems needs. It works on the principle of reducing the input vibration energy by means of dissipating the energy with minimal power consumption. This implies that the system does not require bulky and expensive energy supplies which in turn reduce extra payload and cost. Additionally, the control laws are much simpler to be developed, thereby presenting a more cost effective solution.

Nonetheless, incorporating semi-active suspension in the MBS program may not be practical due to limited functional capability for developing the controller model. Generally, controller development is done in mathematical software that allows real time simulation and provides efficient interfacing with the hardware. In the same manner, building complex vehicle suspension models in a mathematical environment may pose great difficulty as the degrees of freedom get larger, especially with the introduction of non-linear elements within the model. The use of a single computer program to obtain the service loads may require simplifications that would result in

inaccuracies. Therefore, an alternative simulation approach is needed to efficiently integrate these programs. The approach should allow vehicle suspension geometries and semi-active controller models of different complexities to be built within their own respective and specialized programs. Once each module has been individually analysed and verified, these subsystems can be integrated and simultaneously simulated.

At present extensive applications of semi-active control systems mainly focus on improving ride and handling performances. The outcome of employing these controller models on the suspension component fatigue life has received very little attention. Based on these circumstances, this research aims to examine the effect of suspension component loads and hence fatigue life when semi-active control is implemented. The task can be accomplished by introducing an approach that is capable of combining these modules.

1.2 Research Aims and Objectives

The main aim of this research is to evaluate the durability of suspension components when semi-active control systems are utilised. This consists of predicting minimum fatigue life and identifying sections which are susceptible to damage to the suspension components. To achieve this demands accurate prediction of service load histories of the selected component. Since the problem requires accurate representation of the suspension systems and necessitates evaluation of many control strategies, an alternative modelling and simulation method is required to integrate the two. By doing this, the two subsystems can be modelled and simulated in their respective programs. Hence, it provides flexibility in simulation in which critical vehicle sub systems such as the vehicle suspension models, damper models, tyre models and road profiles can be developed in modular form allowing dynamic simulation to be performed more efficiently.

1.3 Proposed Method and Scope of Work

Earlier work by Haiba [1] has provided the groundwork for current research. He established load histories of a dynamically loaded component for a passive suspension system using a purely multi-body approach. Since the present work comprises of the

application of semi-active suspension system, an approach that incorporate the two is proposed. The term "MBS cosimulation" is introduced to represent this integrated method.

The work begins by validating the dynamic response of a simple lumped vehicle model with conventional modelling techniques. In a similar manner, a simple semi-active controller model is developed in the mathematical environment. Gradually, vehicle suspensions with greater degrees of freedom are introduced in line with the increasing complexity of the semi-active controller models. The scope of the proposed method covers aspects of ride in which only vertical dynamics is taken into consideration for the road profiles and the tyre models. A virtual durability proving ground is used to ascertain loads on a particular suspension component that will be used in the durability analysis.

Once the load prediction is completed, the research enters its final phase. Finite element analysis generates stress distribution from the applied load histories on the suspension component. Each of the nodal stress and strain undergoes cycle counting to yield a stress/strain range with corresponding load cycles. This information is then used to calculate fatigue life of the component. Finally, assessment of minimum life and damage distributions is made between the passive and the semi-active models.

1.4 Organisation of Thesis

Chapter 2 provides a broad review of current literature related to virtual durability, comprising of MBS simulation in vehicle dynamics, semi-active control systems and fatigue analysis. This includes descriptions of conventional terms used within each area. The chapter concludes by identifying gaps in current research and underlining the importance of employing an alternative simulation method to achieve accurate load histories. Several control strategies are discussed and recommended for adoption in this research.

Chapter 3 evaluates the proposed method (MBS cosimulation) against the purely MBS method and the conventional mathematical approach. This involves validation of a lumped quarter vehicle model (QVM) with passive suspension system subjected to

different vertical tyre models and road events. Findings from this chapter are used as the basis for the following two chapters

Chapter 4 involves implementing the MBS cosimulation method for a multi-purpose vehicle (MPV) with a conventional passive suspension system. The work includes a QVM with a realistic suspension model which is extended to determine an equivalent lumped QVM that will be used in attaining dynamic response of a full vehicle model (FVM). Responses from the vehicle models are evaluated by traversing transient and random road profiles at several forward constant velocities.

Chapter 5 investigates the influence of semi-active suspension on the load histories of the MPV. Several semi-active control laws are adopted, developed and analysed. The vehicle dynamic responses of a lumped mass and realistic quarter vehicle model are considered with reference to the passive systems. For the full vehicle model, two types of semi-active control strategies are implemented. The first type applies a switchable controller derived from the quarter vehicle model to all suspension corners to represent an independent semi-active suspension system. Similar assumptions are employed for the passive suspension system. The second type of semi-active controller considers the effect of vehicle body pitch and roll motions, where it calculates the response to estimate the appropriate damper force setting at all four actuators that gives a minimum acceleration response. The chapter also includes evaluation of control laws derived from an actual magnetorheological (MR) damper.

Chapter 6 describes the fatigue life estimation using finite element analysis. Quasi-static durability analysis computes the damage accumulation and identifies the region that would contribute to minimum life and potential damage locations. Fatigue analysis is then executed to the lower suspension arm and the effects of implementing several semi-active control methods on the component are assessed.

Finally, Chapter 7 presents the conclusions of the current research, a statement of achievements and knowledge contributions, along with suggestions for further work.

Appendix I contain full documents of the three publications the author has produced during the course of his research. The first two were presented in an international

symposium and conference, highlighting the author's proposed simulation method. The third is a refereed journal paper accepted for publication focussing on semi-active applications and their effects on the vehicle dynamic response.

Appendix II explains mathematically the steps involving the determination of equivalent lumped parameters for the two degrees of freedom quarter vehicle model, from the realistic suspension model.

In Appendix III, descriptions of sprung and unsprung mass resonances of a lumped mass quarter vehicle model are presented. The information is useful for verifying responses of vehicle models of different complexities, and is used in investigating the effect of resonance in the semi-active damper models.

Descriptions of routines for obtaining power spectral density and the RMS values, using MATLAB, employed throughout the analysis chapters are available in Appendix IV.

Appendix V shows the method of calculating total dynamic stress histories from ANSYS load cases and MSC.visualNastran load histories.

CHAPTER TWO

Review on the Durability of Semi-Active Suspension Systems

2.1 Introduction

Durability can be defined as the ability of a structure to resist failure principally originating from fatigue. It determines the duration for which the structure or component can withstand a given service condition. Though other factors such as wear and corrosion are likely to affect durability, failure caused by fatigue is the most dominant [2]. Fatigue happens under repetitive loading smaller than the ultimate static strength of the structure where cracks initiate prior to failure. Three major inputs are required in estimating fatigue life, namely load histories, geometric details, and material properties. Among these three, obtaining accurate load data is crucial since it has direct influence from the varying external inputs such as road excitations and suspension types. Component geometry and material properties remain unchanged unless structural optimisation is conducted towards the later stage of the design process.

Load histories can be obtained either experimentally using strain gauges and load cells, or analytically using computer simulations. The former method is widely practiced and produces reliable results but at the expense of extensive work and cost. It requires component prototypes, thus limiting the ability to assess fatigue early in the design phase. With the rapid improvement in computing resources, attaining load data by means of computer simulations offers a better solution. Costly prototypes are no longer needed as component geometry and other details are created in a virtual environment. Similarly, various forms of suspension designs, controller models, road profiles, and

driving conditions can be developed and analysed without the need of physical testing. This allows fatigue life assessment to be implemented early in the design cycle, encouraging analysts to come up with creative and radical design changes.

Figure 2.1 illustrates four possible approaches in durability assessment in the automotive industry. The first two methods consist of proving ground tests and physical laboratory tests. These are physical methods of durability analysis where actual components are tested either through actual durability roads or as simulated road inputs. Kyoung *et al.* [3] of Hyundai Motor Company evaluate virtual durability method that replicates physical in-laboratory body-in-white (automotive body without trims) test. Similar studies by Ferry *et al.* [4] describe in detail the durability process particularly in relation to establishing load histories from multi-body simulation. Another strand of virtual durability analysis employs virtual road profiles that imitate the actual proving ground as studied by Edara *et al.* [5]. The technique is suitable to analyse potentially damaging loads due to transient road events such as bumps and potholes over which drivers may find it difficult to control an actual vehicle.

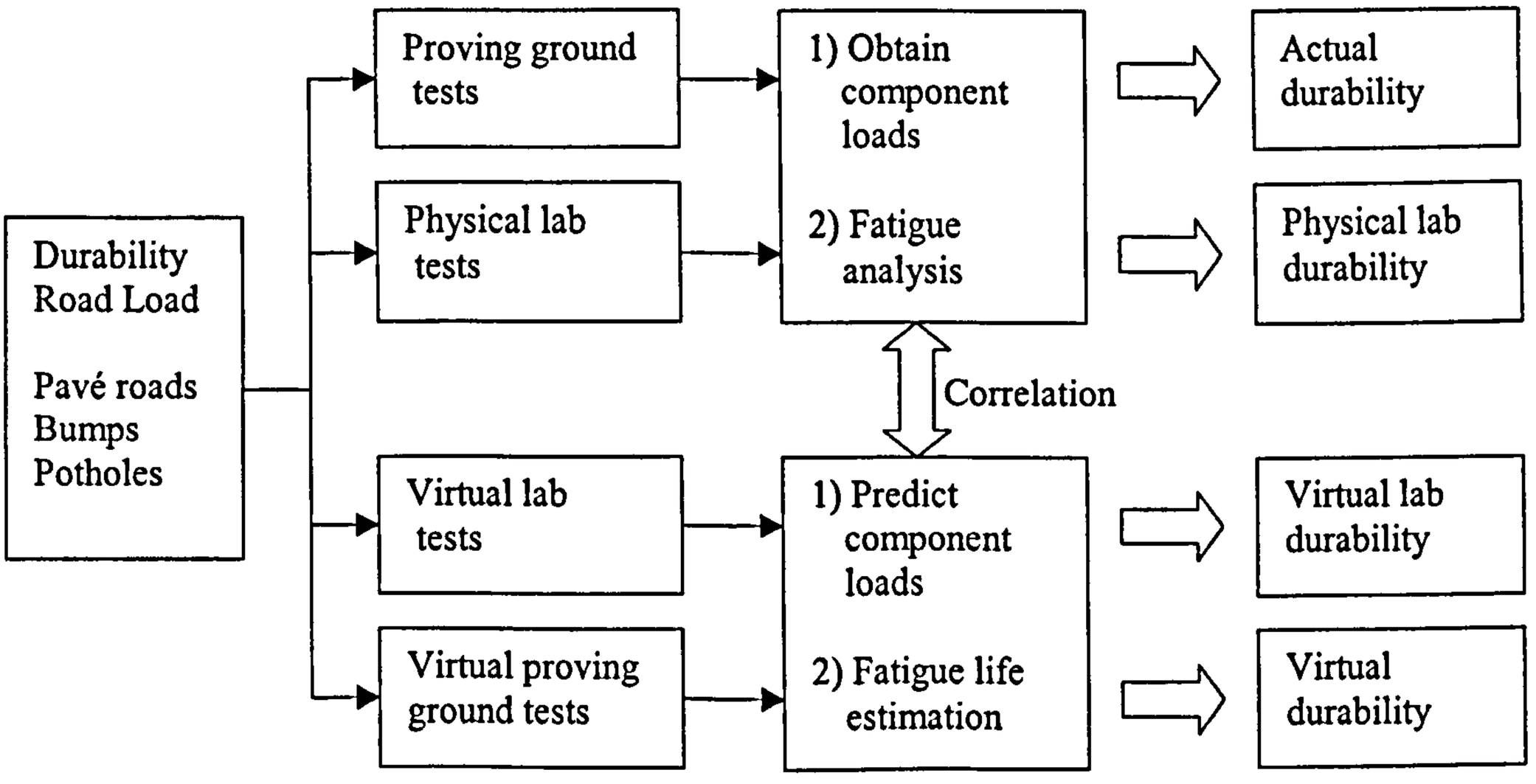

Figure 2.1: Durability Assessment of Vehicle Components

In general, virtual durability analysis requires component load histories extracted from either MBS simulation or from wheel force transducers as shown in Figure 2.2. These load data are the precursor to ascertain the stress and strain distributions within the component by employing finite element analysis. The fatigue life is predicted after performing cycle counting of regions with high stress or strain intensities.

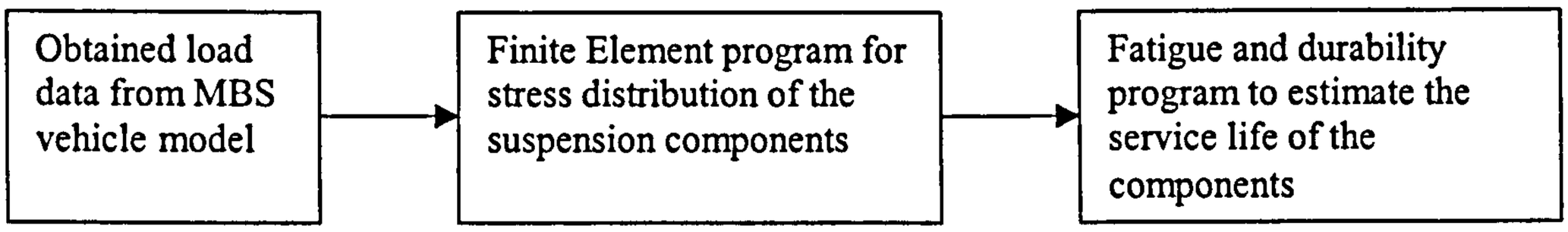

Figure 2.2: Typical Virtual Durability Process Involving MBS Simulation

This chapter provides a comprehensive review of these three stages. A summary is presented at the end of this chapter indicating the gaps in current research this thesis will address.

2.2 Obtaining Load from a Multi-body Vehicle Model

Nowadays, the use of multi-body system (MBS) simulation in predicting durability loads has become feasible and widely used [2-4, 6-9]. The key element for this is the ability of the simulation method to accurately predict dynamic response which will be the prerequisite in virtual durability analysis. Mousseau *et al.* [10] argue that employing MBS simulation alone for vehicle ride analysis and for durability issues, will not be accurate due to presence of high frequency modes of the tyre and the vehicle body. In order to improve the accuracy of the simulation, they propose integration of a multi-body vehicle model, with a non-linear finite element (FE) model for the tyre. However, large FE-models will generate large degrees of freedom, and thus require longer and extensive computational resources as pointed out by Frieberg and Eriksson [11]. Further evidence has been demonstrated by Edara *et al.* [5] in investigating virtual durability for a heavy vehicle traversing on various virtual road surfaces purely with an FE method. In order to achieve accurate results, the simulation on a single central processing unit (CPU) with dual processor took nearly 25 days. Additionally, large memory and storage space are required for the data. They claimed that a significant reduction in simulation time can be accomplished when parallel processing is implemented.

Simulation accuracy does not solely depend on the number of degrees of freedom. Other factors for instance vehicle models contribute to the accuracy of the response. Haiba *et al.* [8] demonstrate that a full vehicle model developed purely in a multi-body environment is capable of producing good load histories correlation with the

experimental setup, compared to those from the quarter vehicle model. Though the difference in the degrees of freedom is clear, they argue that the influence of body motions for the full vehicle model has significantly affected the overall dynamic response. This argument is supported by Levesley *et al.* [6] when evaluating a variety of vehicle models developed in MBS that were subjected to potentially damaging transient road inputs.

However, the use of MBS as a stand-alone program to generate load histories may not be commercially attractive. With the rapid advancement in computer technology, solutions from integrated system are sought. Pompetzki [2] reviews the accuracy and analysis time of traditional durability methods comprising of load-based and location-based methods, with those that integrate MBS and FE. Significant levels of accuracy can be achieved with the latter technique but at the expense of increase simulation time.

Based on these instances, the concept of virtual durability can be extended to examine durability of semi-active systems. The selection of semi-active controller models should be based on achieving better ride comfort rather than improving handling response. This is because, according to Decker and Savaidis [12], damage to suspension components are more susceptible to driving at a forward constant velocity compared to failures from driving manoeuvres such as acceleration, braking and cornering. MBS appears to be the obvious choice to generate accurate load histories but have to be integrated with the semi-active control modelling. FE methods in predicting fatigue life shows a promising trend in which the results can be further employed in structural optimisation

2.2.1 Describing a Multi-body System

According to Shabana [13], MBS can be described as an assembly of subsystems made up of bodies, components and substructure. It originates from multi-body dynamics consisting of arrays of interlinked rigid and flexible bodies. A rigid three-dimensional body has six degrees of freedom. The first three are translational components having the principal axes perpendicular to each other, and the remaining three rotational components rotate around each of the principal axes. A body is said to be rigid when

there exists no relative motion between two arbitrary points on the object. In contrast, relative motion exists between two arbitrary points on a flexible body. From a finite element perspective, a rigid body exhibits a non-zero displacement with zero strain energy [14].

A joint connects the bodies and it is described by constraint equations. The function of joints in MBS is to reduce the number of degree of freedom between the connected bodies. For example, a spherical joint removes all translational degrees of freedom leaving only the rotational components. Other forms of joints are spring, bush, damper and actuator that connect bodies using force, which are dependent on motions (displacement or velocity). Motions of a rigid body that consider a centroidal body coordinate system can be calculated from Newton-Euler equations. Translational components utilise Newton formulation while rotational components use Euler equations, expressed as acceleration and forces acting on the body.

In MBS simulation, component loading exists in the forms of design loads and service loads, as reported by Blundell and Harty [15]. Design loads are calculated on the assumption of the maximum possible loads a component can withstand. They refer to them as 'abuse loads' where the vehicle is expected to exhibit some operational defects but not physical damage. For example, a vehicle striking a curb or a pothole causes steering misalignment. The design events are somewhat fictitious and can be computed with minimal information about the vehicle using a static or quasi-static method. This can be exercised during the conceptual suspension design allowing the analysts to have meaningful insight of their design. In contrast, service loads are a form of load that would not impose damage to components. Their loading events such as road profiles are well defined therefore enabling accurate fatigue life assessment. Unlike design loads, predicting service loads would lead to increasing computational time thus limiting fatigue prediction to only critical components.

In virtual durability analysis, the predicted load histories via MBS simulation can be explained in a flowchart as shown in Figure 2.3. Firstly, vehicle suspension geometry is created in a computer aided design (CAD) package. An interface within the program translates the geometrical information into a universal file format that can be read into the MBS code. Here, appropriate definitions of mechanical and material properties

along with excitation inputs and initial conditions are required and fed to the converted MBS vehicle model prior to executing the simulation. Once the load histories are obtained, the analysts can validate the model by comparing data from it with either experimental results, published data or from other verified simulation codes.

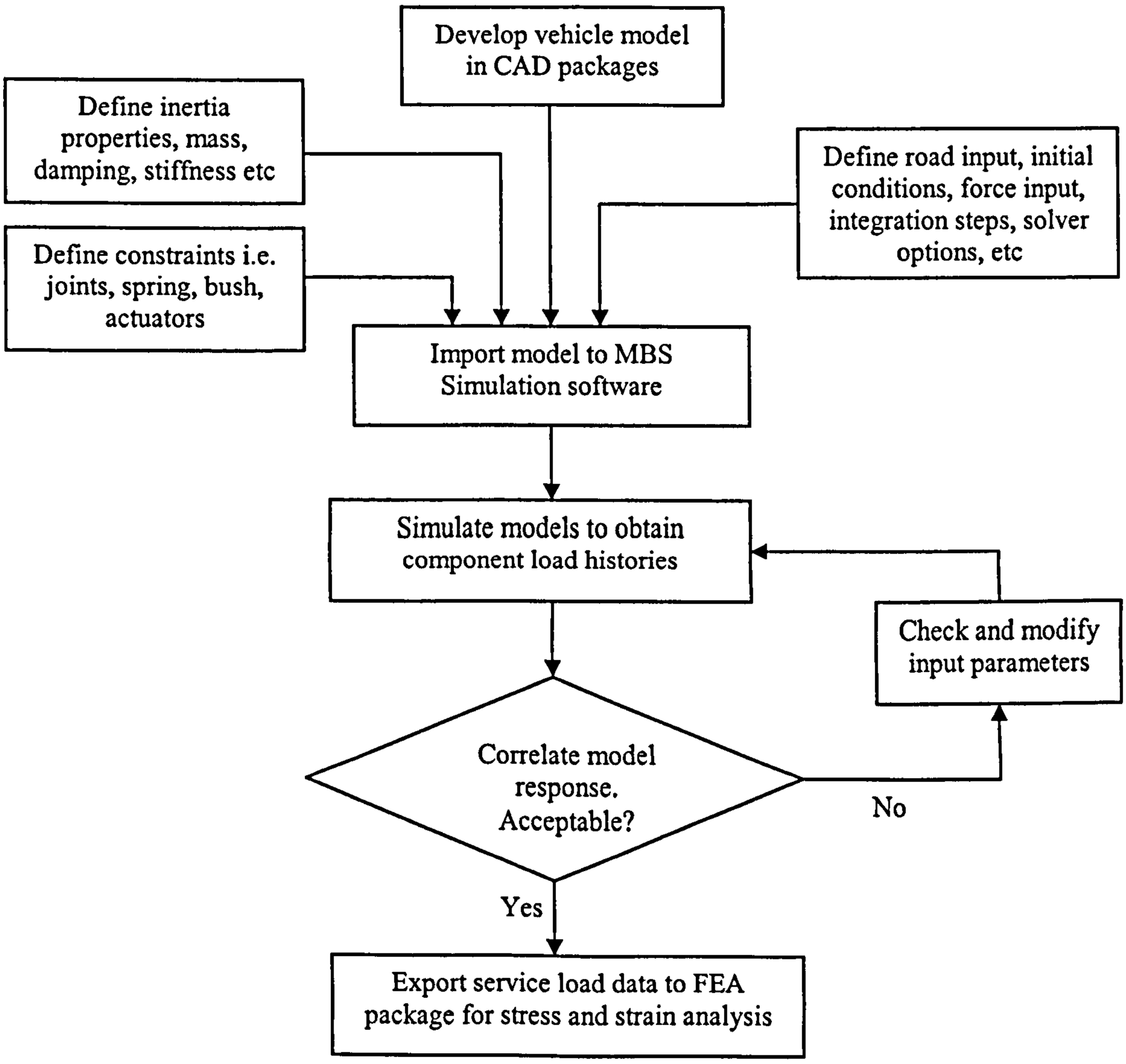

Figure 2.3: Obtaining Load Histories from MBS Simulation

2.2.2 Multi-body System for Vehicle Dynamic Simulation

In the application of computer methods in vehicle dynamic simulation, Crolla *et al.* [16] categorise two main streams when applying computer methods in vehicle dynamics to derive the equations of motions. The first strand requires the user to define the equations of motions, whereas for the second strand, the computer generates the equations of motions. The former method, according to Kortum and Sharp [17], is highly erroneous and take a considerable amount of time to numerically solve the

equation of motions. The latter, known as MBS modelling, allows the computer to generate the equations. The users are only required to provide the vehicle model parameters, which include mass properties (vehicle body, wheel, suspensions arms etc.), mechanical properties (spring stiffness, damping constant/curve, and joint's degrees of freedom), and geometrical properties (component's centre of gravity, mass moment of inertia) either in spatial form, three-dimensional (3D) form or in plane, two-dimensional (2D) form. Crolla *et al.* [18] further categorise the MBS method, into four approaches. They are simulation software based on specific vehicle design, MBS software with a numerical form such as MSC.ADAMS, MBS software with algebraic form in which equations are produced in symbolic form, and the toolkit approach, for example MATLAB. They introduce Vehicle Dynamics Analysis Software (VDAS) operating based on toolkit approach. The concept relies on the accumulation of procedures to generate specific vehicle models, creating equations and solving for specific problems such as ride and handling, natural frequencies and mode shapes. Another strand of the MBS technique that is attaining wide attention is the cosimulation approach.

2.2.3 MBS Cosimulation Approach

Cosimulation refers to a simulation method where two or more software packages are integrated and concurrently simulated in each respective environment. The purpose is to allow specific modelling tasks to harness the full potential of each dedicated program. The first known implementation of this technique dates back to the early 90's. In studying the severity of service load histories on a suspension component of a heavy vehicle, Prior [7] implicitly integrates subsystems for tyre models and driving inputs. These subsystems are then incorporated into the full vehicle model. He reports the method offers flexibility in developing, examining and validating each of the subsystem, independently.

An experimental study by Venhovens *et al.* [19], implements cosimulation on a passenger car. They investigate handling dynamics when semi-active attitude control is applied on Volvo 480ES. The cosimulation involves integration of a full vehicle model developed using a Bond graph based Algorithm for Modelling Multibody Systems (BAMMS), with a proportional-integral-derivative (PID) controller for the body

attitude control. They achieve considerable reduction in body roll but at higher frequencies the lateral and longitudinal accelerations generate noise caused by road undulations, creating instability in the feedforward PID controller.

Another example of practical cosimulation work was conducted by Nell and Styen [20]. They introduce a global two-state semi-active control that take into account pitch and roll motions of vehicle body and implement it to an off-road vehicle. The full vehicle model is developed using DADS multi-body package while the controller model utilizes similar hardware setup as [19]. They achieve perceivable improvement in ride comfort over the passive system as the road surfaces become rougher. Nevertheless, the controller strategy does not provide significant ride improvement when analysed at higher constant velocities.

Liao and Du [21] evaluate the influence of electric power steering (EPS) control on the handling response. They employ a cosimulation approach that integrates a full vehicle model, created using MSC.ADAMS, and an EPS control module developed in MATLAB/Simulink. Simulation results showed reasonable agreement in handling response with the experimental data particularly the magnitude and the response signatures. Additionally, the EPS control showed a better reduction in peak amplitudes and shorter settling time at selected suspension components compared to the response without EPS.

In a related development, Danesin *et al.* [22] present another example of cosimulation using MSC.ADAMS and MATLAB/Simulink. A full vehicle model of a FIAT saloon 3.0L is developed using MSC.ADAMS/Car and integrated with a fuzzy logic control for a continuously variable damper system. The work highlights some issues concerning virtual simulation and the capability of a fuzzy logic controller in predicting basic handling problems.

Kortum *et al.* [23] employ a cosimulation approach to verify the effect of a continuously variable damper with ground-hook control on tyre forces, obtained from an experimental setup. They develop two full vehicle models using SIMPACK which consist of a ten-wheeled platform truck and an eighteen-wheeled semi-trailer truck. Both trucks are equipped with continuously variable semi-active dampers on the driven

axles complete with sensors. MATLAB/Simulink is utilised for the development of extended ground-hook (EGH) control with the primary aim to minimise road damage by means of reducing tyre loads. Reasonable accuracy in dynamic tyre force has been achieved between cosimulation and experimental data, suggesting that the use of semi-active damping can improve road friendliness resulted from lower dynamic tyre forces compared to passive damping. This enables further studies in enhancing not only the vehicle models and the related control systems but also those involving existing regulations imposed on heavy vehicles.

Despite the examples reported above, until recently, cosimulation has not received widespread attention in the automotive industry. One major intricacy faced by analysts relates to inconsistent communication between software packages, as pointed out by Blundell and Harty [15]. Software developers often overlooked this aspect during software upgrades as the process differs from one software package to another.

Nevertheless, the past few years has seen an increasing interest in enhancing the technique particularly for those involving multidisciplinary applications. Maiorana *et al.* [24] employ cosimulation for a full vehicle model with active suspension control focussing on ride characteristics of a truck modelled in MSC.ADAMS whilst the active and semi-active control systems are created in MATLAB/Simulink. They discover that both fully active and semi-active systems provide improvement ride comfort with a reduction in roll motion but at the cost of greater suspension travel. In a related development, Lepold *et al.* [9], examine the effect of active suspension roll control (ARC) and active bounce control (ABC) on component durability. A cosimulation method is employed to integrate the dynamic vehicle suspension model in MBS using MSC.ADAMS, with the active roll control modelled using MATLAB/Simulink. Their finding showed mixed results in terms of stress levels when compared to the passive suspension system.

Ieluzzi *et al.* [25] adopt a cosimulation approach to evaluate the effect of semi-active suspension control on a heavy truck's ride and handling performances. The controller model combines vertical, lateral, and longitudinal dynamics control in an attempt to simultaneously improve ride comfort, reduce body roll and minimizing pitch, respectively. This unique controller model is developed in MATLAB/Simulink while

the truck is modelled using MSC.ADAMS/Car. Acceleration responses from the truck with a passive suspension system indicate reasonable agreement between the model and those from the experiment. Then, the semi-active controller model is implemented on the virtual vehicle model using a cosimulation approach. Once a desired result has been achieved, the controller model is then converted into C-code compiled using MATLAB Real-Time-Workshop before downloading the code into the truck electronic control unit (ECU). They report up to 25 percent reduction in body acceleration can be achieved with the implementation of the skyhook control in comparison with the response from passive suspension. Similar improvement has been observed during handling and braking manoeuvres resulted from the lateral and longitudinal controls.

Perhaps, the most comprehensive review of integrated MBS simulation is discussed by Vaculin *et al.* [26]. They classify and evaluate the effectiveness of simulation time for several cosimulation interfaces using SIMPACK for the MBS tool and MATLAB/Simulink for the controller design. Further development in the area of variable time data exchange, developing programs for real-time applications and model optimisation for hardware-in-the-loop are in progress. The findings promote additional investigation [27] for evaluating the effect of semi-active control laws on the ride characteristics of a commercial truck.

Based on these advances, applying MBS cosimulation for the prediction of durability of semi-active suspension systems appears to be the best available technique. The present author will face challenges in integrating a variety of vehicle suspension models with a selection of semi-active control strategies. The expected outcome from this integration will be in the form of accuracy in the dynamic response which will then be utilised to ascertain fatigue life of suspension components. The following section will focus on suspension technology along with a comprehensive review of semi-active control systems.

2.3 Suspension Systems

In vehicle dynamics, the function of the suspension systems is to provide good isolation between the tyre-road interface and the vehicle body, as well as good road holding characteristics. Additionally, it should also provide good steering control

during manoeuvring and maintain an acceptable response to cornering, braking and accelerating [28]. Traditional passive suspension systems have limited capability in satisfying the two conflicting design requirements of ride and handling.

Good ride comfort can be achieved by means of minimising body acceleration, utilising low spring and damper rates resulting in softer suspension. Having a softer suspension imposes greater suspension travel, which eventually leads to wheel hop and unstable body attitude caused by varying load. The vehicle will experience an increase in lateral load that directly affect lateral force of the tyres causing poor handling capability. On the contrary, good handling exists when the wheels are capable of following road irregularities. The use of high spring rates and damper rates generates stiffer suspension, preventing wheel hop motion which in turn minimizing the load variation in the tyres. Consequently, the vehicle body has less inclination to roll, maintaining stable body attitude from less suspension travel. Nonetheless, the body acceleration will increase resulting in poor ride comfort.

Vehicle components are subjected to a variety of excitations ranging from tyre and road interaction, vehicle aerodynamics, and from the engine and transmissions. Suspension components in particular, are exposed to two forms of excitation largely from the tyre and road interaction. They are transient and random excitations. The former is likely to be due to the vehicle travelling through bumps and potholes, while the latter occurs when the vehicle traversing at constant speed on a normal or a rough road undulations. Both excitations generate forces over a wide frequency range. These excitations cause resonance of the vehicle structures as well as the suspension components, when the excitation frequencies coincide with any of the components natural frequencies. In general, resonance can be decomposed into two forms; rigid body modes and the flexible modes as described in section 2.2.1.

A typical passive suspension system consists of a conventional spring that functions as an energy storage device and a hydraulic damper that acts as an energy dissipater, arranged in parallel with the spring. The damper rate and spring rate are generally fixed and time invariant limiting its ability to provide optimum performance under a variety of road input and driving manoeuvres. Sharp and Crolla [29] describe these limitations and inherent problems facing the suspension designers. Optimising ride

will certainly sacrifice handling capability. Nevertheless, this suspension system is still widely used in the production of ground vehicles largely due to design and manufacturing simplicity, in addition to easy maintenance, and inexpensive parts replacement.

2.3.1 Controllable Suspension Systems

In controllable suspension systems, the role of conventional springs and dampers are substituted with sensors and actuators primarily aimed at overcoming the limitation of the passive system. There are a number of controllable suspension schemes, for example self-levelling systems, adaptive systems, semi-active systems and fully active systems.

Self-levelling systems as introduced by Citroen aim at sustaining the vehicle ride height such that the available suspension working space remains unaffected by the changes in static loads [30]. It works with the use of external power to raise or lower the suspension according to the static loading conditions. With the cheaper and rapid improvement in electronics and microprocessor technology, more responsive suspension systems have been developed.

Adaptive suspension systems [30, 31] work by producing adjustment to the control signal as a result of various vehicle operating conditions. More than a decade ago, Toyota introduced electronically adjustable dampers capable of switching state to a softer setting to improve comfort, under normal driving conditions. Once a more demanding driving condition is sensed, for instance accelerating, braking or manoeuvring, the controller switches its damping state to a hard setting to enhance handling performance.

By far, the best form of controllable suspension is achieved with the use of a fully active suspension system. In theory, an ideal fully active control system is capable of producing any desired force to cancel out ground excitation. The control laws and the response of the actuators dictate the efficacy of producing such forces. One of the most widely used control method is the application of linear quadratic optimum control theory [30, 32-35]. The suspension system is optimised based on a quadratic

performance index that applies weighting functions to body acceleration, suspension working space, dynamic tyre load, overall stiffness, and control force. Application of this control theory can be observed in the preview control of road input as investigated by [32, 33, 36-38]. The simplest form of preview control assumes a time delay of the road input at the rear wheel from the front axle. A more advanced form is the "look-ahead" preview where information about the road profiles can be identified at a finite distance in front of the wheel. Theoretically, preview methods show promising results but actual implementation of such systems may not be feasible. For example, measuring road undulations with sensors attach to the vehicle body can be difficult and impractical.

Even though fully active suspension systems offer great potential in overcoming the compromise between ride and handling issues, benefits still cannot compensate for the manufacturing costs. Sharma [34] points out that the system must accomplish much higher improvement in order to substantiate its implementation. In contrast, semi-active suspension systems provide a potentially effective form of alternative solution compared to passive and fully active systems.

2.3.2 Semi-active Control Systems

In general semi-active suspension works on the principle of reducing the input vibration energy by means of manipulating the damper orifice/valve or controlling magnetic or electromagnetic fields across the damper with the use of a minimum external energy. Unlike full active control, semi-active systems require no auxiliary power supply to dissipate the energy, utilise minimal power consumption, reduce production and maintenance costs, reduce vehicle weight addition, and allow development of simpler control algorithms. It is considered a hybrid between a passive suspension and a fully active suspension system, representing a compromise between performance and simplicity in operation [38]. The first concept of a semi-active control system was proposed by Karnopp *et al.* [39], who introduce the skyhook concept, using generalized velocity feedback for improving ride comfort performance.

Performance of semi-active systems in providing improvement in ride and handling issues over passive systems has been studied extensively for more than three decades.

For ride, the performance criteria relate to body acceleration, suspension working space, and dynamic tyre loads that centre on vertical dynamics. Aspects of lateral and longitudinal dynamics are included in handling performance involving roll stability, body attitude, and road holding. Most of the control algorithms developed intends to improve these performance parameters by adopting a variety of control strategies, depending on vehicle types and their applications.

In conventional passive suspension systems, the performance is a function of relative velocity measured between the sprung and the unsprung masses. However, for semi-active systems, the applied force is as a function of absolute velocity of the sprung mass. This improves sprung mass isolation at the expense of increase suspension working space with minimal effect on dynamic tyre load. Theoretically, this imposes no significant influence on suspension component durability but the outcome has not been widely investigated.

Semi-active control strategies can commonly be categorised as switchable (on-off) and continuously variable. The switchable damper relies on rapid switching between different damper forces by using either hard or soft settings [30, 40-45]. The control law demands a discrete switching between the damper settings based on the relative and the absolute motions of the sprung and unsprung masses. In contrast, continuously variable dampers continuously generate a force demand through manipulation of the damper fluid viscosities. Both semi-active strategies are discussed in the following sections.

2.3.3 Switchable Damper Strategy

A two-state switchable (TSS) damper is the basic form of a switchable semi-active system. The switching mechanism is based on the absolute velocity of the sprung and unsprung masses, and the relative velocity across the damper (damper velocity). When the absolute velocity of the sprung mass and the relative velocity have the same sign (refer to Figure 2.4), the damper will resist the motion by generating large damper forces acting in the direction opposite to the sprung mass motion. In contrast, if the sign between the two velocities is opposite, then no force is exerted on the sprung mass to resist the motion, allowing the controller to switch to a lower setting. This type of

control is known as skyhook control. A detailed description of this control theory is presented in section 2.3.5.

More advanced switchable damper strategies can be seen with the introduction of multiple state switchable dampers [45-47]. A three-state switchable controller for a passenger vehicle may consist of a soft, a normal, and hard setting. It provides better performance than the two-state switchable damper in terms of body accelerations as reported by El-Tawwab and Crolla [45], Sharma *et al.* [46], and Vannucci [47]. However, Nell and Styen [20] argue that a two-state switchable strategy is sufficient since generally the damper switching is distributed between the hard and the soft settings. It is based on an experimental assessment in which, for about 80 percent of the driving time, the damper is switched to the soft state, followed by 12 percent in hard setting, and for the remaining time, the damper is switched to the normal setting.

One fundamental problem with the switchable damper is that it suffers from transient forces known as jerk when the system switches from one damping state to another. Miller and Nobles [40] discovered that the discontinuity in force switching is more prominent when the damper switches from the higher damping rates to the lower states. The finding is supported by Yoo and Jin [48] when they experimentally investigate the dynamic characteristics of a semi-active damper. They discover that the force discontinuity causes resonance to the upper section of the damper resulting in poor reduction in body acceleration. Ahmadian *et al.* [49, 50] explain that the discontinuity occurs as the relative velocity crosses zero in a conventional skyhook control. They point out that the discontinuity not only happens when the damper switches from higher setting to the lower state, but also from the lower setting to the higher setting as illustrated in Figure 2.4. This phenomenon causes a sudden increase in sprung mass acceleration and consequently minimises the benefits of switchable control. Jerk occurs either in a two-state system or in systems with multiple damping states. It can be defined as the time rate of change of acceleration [51]. Consider a sine wave, the maximum jerk, a_m will occur when:

$$a_m = \omega^2 . x_s \qquad \textbf{Eq 2. 1}$$

where, $\omega = 2\pi f$ is equivalent to natural frequency in radians/s, f is natural frequency in Hz and x_s is the sine wave amplitude.

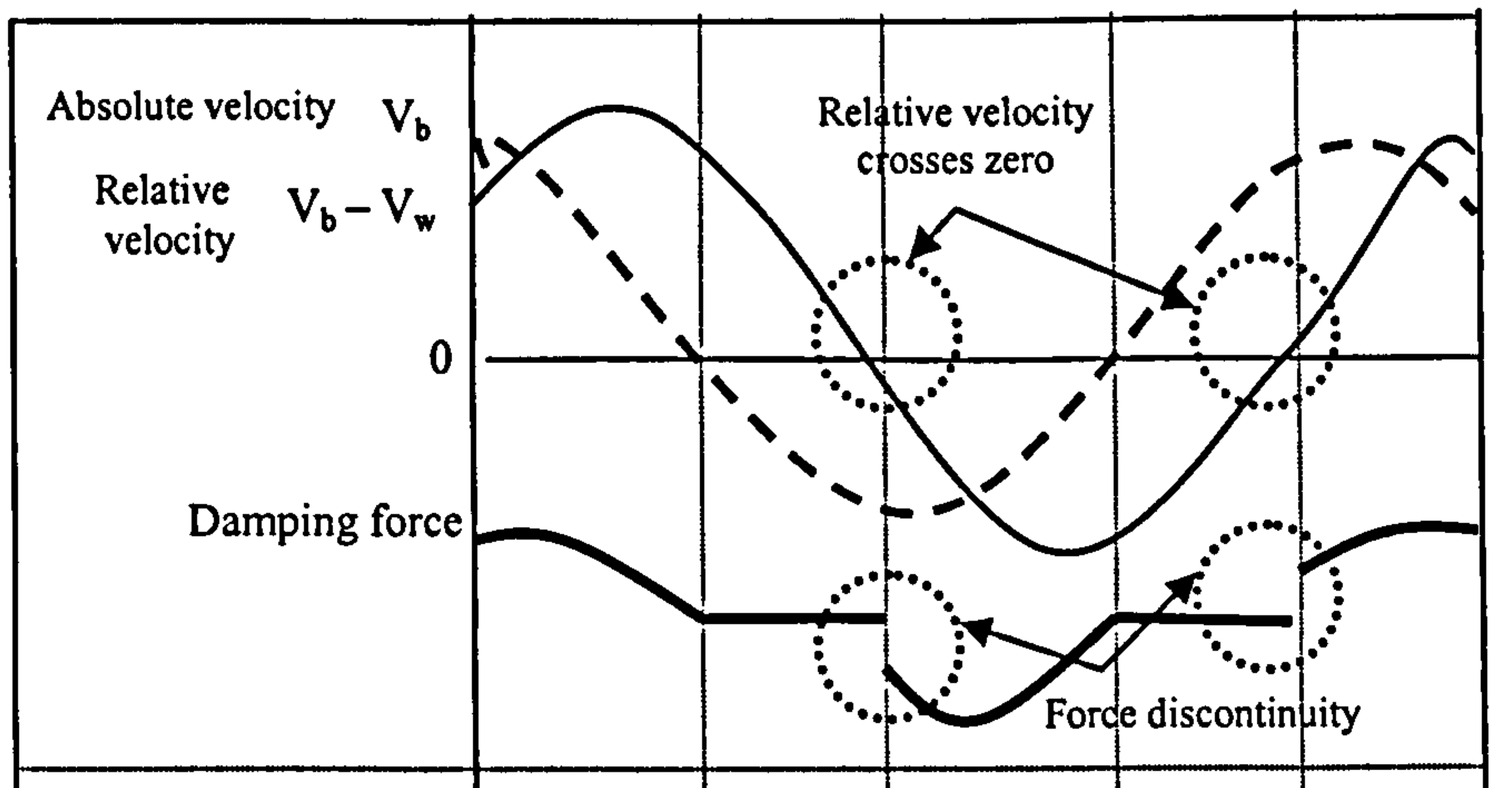

V_b	+	+	-	+	+
$V_b - V_w$	+	-	-	-	+
$V_b (V_b - V_w)$	+	-	+	-	+
Damping force	F_{sa}	F_{min}	F_{sa}	F_{min}	F_{sa}

Figure 2.4: Effect of Relative Velocity on Force Discontinuity [49]

Attempts to minimize jerk have been studied by many. This includes the use of multi-level switching [52], preview control incorporating jerk [53], and modified skyhook control [44, 49]. Among these solutions, [49, 50] provides a simpler approach. Governing equations for an ideal skyhook control of a two-degree of freedom QVM in Figure 2.5(a) can be described as:

$$\begin{aligned} For \quad v_b.(v_b - v_w) &> 0; \quad F_{sa} = c_{sky}.v_b \\ v_b.(v_b - v_w) &\leq 0; \quad F_{sa} = 0 \end{aligned} \qquad \textbf{Eq 2.2}$$

where, v_b and v_w are the velocity of sprung mass and unsprung mass, respectively, (v_b - v_w) is the relative velocity or the damper velocity, F_{sa} is the damper force for an ideal skyhook, and c_{sky} is the skyhook gain. To eliminate the effect of force discontinuity, Ahmadian *et al.* [49] suggest that the skyhook damping should be a function of relative velocity. Their experimental results showed perceivable reduction in the acceleration jump at the seat when the modified skyhook is introduced compared to the passive system.

2.3.4 Continuously Variable Damper Strategy

Typical continuously variable dampers (CVD) consist of a controllable damper arranged in parallel with a conventional spring. The damper/actuator is expected to reproduce a force demand signal continuously. In cases when the actuator fails to reproduce the required force, it is simply switched off, and the suspension temporarily becomes a passive system. Generally, there are two forms of semi-active CVDs i.e. variable orifice dampers [32, 54, 55] and variable fluid dampers [56-58]. Unlike fully active systems, CVD requires minimal external energy to manipulate the fluid damping characteristics. Aurell [59], Wilkinson [60], Katsuda *et al.* [56] and Besinger *et al.* [57] suggest that a continuous variable damper strategy has a better capability in minimising body acceleration and dynamic tyre force, compared to the switchable (on-off) strategy. In a theoretical investigation on the effect of tyre forces of heavy vehicles on road wear, Aurell [59] concludes that vehicles with CVD can reduce dynamic tyre load by 17 percent and up to 25 percent reduction can be achieved in sprung mass acceleration. Another finding based on simulation of laden heavy vehicles by Wilkinson suggests improvement in vertical tyre loads and body acceleration with a reduction of 13 percent and 23 percent, respectively compared with passive air suspension.

Recently, implementation of magnetorheological (MR) [61-63] and electrorheological (ER) [64-66] dampers has received considerable attention for improvement in ride comfort. The variable force from the damper is controlled by either the magnetic particles in the damper fluid or the electrically charge fluid. The fluid can change its characteristics from low viscosity (low damping) to highly viscous (high damping) proportional to the magnetic or electrical charge from the controller.

A major advantage of utilising the MR and ER dampers is due to its capability to produce variable forces within the minimum and maximum limit. In other words, the fluids are able to change their characteristics from a Newtonian fluid to semi-solids within milliseconds [67]. Additionally, the yield strength and the stability of the damper fluids allow them to be used in a broad range of dynamic applications. Nevertheless, the non-linearity between the damper force and the velocity across damper impose a challenging task to researchers. The damper fluids also suffer from

irreversible progressive thickening over a long-term use as noted by Carlson [68]. When examining the characteristics of MR fluid, he points out that the deterioration of the fluids depend on the shear rate, the operating temperature, and amount of radiation the fluids are exposed to. The life of MR fluid can be predicted and is defined as:

$$LDE = \frac{1}{V}\int_0^{life} P.dt \qquad \textbf{Eq 2. 3}$$

where, LDE is the fluid lifetime dissipated energy, V is the volume of the fluid, and P is the instantaneous mechanical power converted to heat in the device.

Even though the characteristics of the damper fluids suffer from long term usage, conventional dampers and other vehicle components such as suspension bushes also degenerate under similar circumstances. Over the years, significant benefits offered by this type of damper may outweigh the cost of part replacement.

2.3.5 Semi-active Control Theories

There are many control laws developed and employed for both the switchable and continuously variable dampers over the past forty years. Some of these control theories are analysed by means of simulations, by experiments, or by validation between simulations and experiments. In simulation, many of these control laws are developed based on quarter vehicle models, half vehicle models, and on full vehicle models with the aim of improving ride comfort, better handling and road holding capabilities, reducing roll, minimising road damage, etc. Among the control theories that have received extensive attention are skyhook control [39, 41, 44, 49, 52, 69-71], linear quadratic regulator (LQR) control [32-34, 38, 43, 72] and preview control [53, 73-77]. Other forms of more recent control models such as controller models based on genetic algorithms [42] for damper optimisation , fuzzy logic control [63], and hybrid control [50, 78, 79], generally have similar control objectives but are achieved from different perspectives.

Skyhook damping control, originally proposed by Karnopp *et al.* [39], aims at improving ride comfort by means of reducing body acceleration. Unlike a passive damper that produces a force to minimise relative velocity (damper velocity), skyhook control generates a force to reduce absolute velocity of the sprung mass. The logic

behind this concept is that the skyhook control emulates the passive suspension hooked between the sprung mass and a reference "sky" by a fictitious inertial damping as illustrated in Figure 2.5(b). This suggests that the unsprung mass will have no damping and the response would reach infinity at wheel hop frequency. However, in practice the response is still affected by damping since the semi-active damper is mounted between the sprung and unsprung mass.

Valasek *et al.* [71] highlight two main reasons why the skyhook concept remains important in suspension control. It is used as a reference for comparison with other concepts, and it served as the basis of semi-active practical implementation. Throughout more than three decades, skyhook control has been applied to switchable and continuously variable dampers, typically in passenger vehicle and still remains an important concept in theoretical and experimental studies. The disadvantages of this type of control are that it is susceptible to instantaneous acceleration when applied to switchable dampers as previously discussed. Furthermore, its capability in reducing the dynamic tyre loads is not quite as effective, as reported by Wilkinson and Crolla [80], and Besinger [57], in which it is shown to inflict adverse effects on heavy vehicles. Therefore, variations of skyhook control are introduced in order to overcome these problems, namely ground-hook control and hybrid control theories.

Ground-hook control [25, 39, 71, 81-83] aims at minimising tyre load, and is intended for heavy and commercial vehicle applications. A basic ground hook damping control requires an additional damping element between the wheel and the ground, parallel to the tyre, as shown in Figure 2.5(c). Instead of controlling the sprung mass, m_b, ground-hook control attempts to reduce the unsprung mass response. The concept can be explained by treating the relative velocity as positive when the two masses are moving apart and the absolute velocity of the unsprung mass is positive in the upward direction. If the unsprung mass moves downward (negative), the groundhook damping exerts a maximum force, pushing the unsprung mass upward. In contrast, if the unsprung mass velocity is positive or moving upward, groundhook damping applies minimum force to resist the response. Mathematically, this control policy can be expressed as described in [78] as shown in Eq 2.4.

$$
\begin{aligned}
For \quad -v_w.(v_b - v_w) &> 0; \quad F_{sa} = c_{gnd}.v_w \\
-v_w.(v_b - v_w) &\leq 0; \quad F_{sa} = 0
\end{aligned}
\qquad \textbf{Eq 2.4}
$$

where, v_b and v_w are the velocity of sprung mass and unsprung mass, respectively, (v_b - v_w) is the relative velocity or the damper velocity, F_{sa} is the ground-hook damper force, and c_{gnd} is the ground-hook gain in which the full damping range of the damper can be employed.

Cole [83] and Kortum *et al.* [23] design a controller that is capable of exerting a force to reduce the absolute velocity of the unsprung mass, effectively reducing the dynamic tyre load to minimise damage to road surfaces. In a related development, Valasek *et al.* [71] develop an extended ground hook concept with a similar objective of minimising dynamic tyre load, and improving ride comfort for heavy trucks, subjected to a wide range of road irregularities.

In recent studies, Ahmadian *et al.* [50, 78, 81] introduce an alternative control theory that combine skyhook and ground-hook controls attempting to simultaneously reduce the sprung mass acceleration and the dynamic tyre loads in heavy vehicles. This hybrid control, as illustrated in Figure 2.5(d), linearly combines Eq 2.2 and Eq 2.4 and is described by [78] as:

$$F_{sa} = G\left[\alpha F_{sh} + (1-\alpha) F_{gh}\right]$$

for

$$
\begin{aligned}
v_b.(v_b - v_w) &> 0; \quad F_{sh} = v_b \\
v_b.(v_b - v_w) &\leq 0; \quad F_{sh} = 0
\end{aligned}
\qquad \textbf{Eq 2.5}
$$

and

$$
\begin{aligned}
-v_w.(v_b - v_w) &> 0; \quad F_{gh} = v_w \\
-v_w.(v_b - v_w) &\leq 0; \quad F_{gh} = 0
\end{aligned}
$$

The variables F_{sh} and F_{gh} are the skyhook and ground-hook components of the damping force, α is the relative ratio between the skyhook and the ground-hook control, and G is the constant gain. In Eq 2.5, as the relative ratio, α is zero, the hybrid damping acts as a ground-hook control. In contrast, as α approaches one, the hybrid

damping becomes a skyhook control. In an experimental study, Ahmadian and Pare [78] suggest that better stability and ride comfort can be achieved with this control theory when it is combined with adaptive control.

Other control theories such as optimal control work with the objective of attaining a force from the semi-active damper that can produce optimum suspension performance. This control theory often applies to linear systems using a linear quadratic regulator (LQR) in analysis conducted by Katsuda *et al.* [56], Sharma *et al.* [46], Oueslati and Sankar [43], and ElBeheiry and Karnopp [84]. Typically, a performance index in a form of an integral over time of some constraints, are geared to minimising body acceleration, suspension deflection and tyre deflection (proportional to tyre load). When Sharma *et al.* [46] examine two-state and three state switchable dampers with LQR control, they realize that the performance of the semi-active dampers show improved ride comfort on a smooth random road input. However, when subjected to extreme road conditions, the performance of the semi-active systems becomes marginal compared to the passive system. In a computer simulation and experimental investigation on a QVM, Katsuda *et al.* [56] suggest that a continuously variable damper with LQR control is capable of achieving better ride comfort in comparison with the passive and the switchable systems. A theoretical comparative study of three suspension systems by Gordon [72] produces similar finding, but with the introduction of a non-linear optimal controller to take into account the non-linear effect of the dissipative behaviour of the actuator, and tyre deflection. With the addition of these non-quadratic terms in the optimal cost function, the semi-active system showed better ride performance particularly for high amplitude disturbance. A detailed survey by Hrovat [32] on optimal control theory includes, among others, its implementation on a simplified 1 DOF QVM to a 7 DOF full vehicle model for fully active systems and for semi-active systems employing switchable and continuously variable dampers. He concludes that most of the results are based on idealized conditions which might not be accurate in practical applications. For instance, the force actuators are assumed to have infinite bandwidth whereby in reality the actuators operate within a limited frequency range. Moreover, the controller models are developed in reference to simplified lumped vehicle models that do not consider the details required in practical suspension systems.

Another attractive concept in semi-active suspension control is preview control. It is derived from the successful implementation in the fully active system. The main advantage of preview control is that any delay in damper force actuation can be easily corrected. The amount of preview depends on vehicle speed, wheelbase, and control bandwidth [77]. The concept uses the information available from the front suspension dynamic data in order to improve the performance of the rear suspension. A similar control technique is applied with the primary aim of improving ride comfort. Nagai and Hasegawa [74], in studying preview control for improved rear ride quality, propose a quasi-skyhook control concept, which they claim has theoretically increased the pitch damping. At present, this type of control technique is based on theoretical simulations and more inclined towards achieving better ride quality, with minimum improvement in the variation in tyre load, and unsprung mass acceleration.

Among other techniques used, the hardware-in-the-loop simulation (HILS) offers a better concept in evaluating the performance of the control designs, [57, 58, 85]. The technique allows flexibility in changing vehicle parameters. It combines a software simulation and hardware implementation via an interface, thus helping to bridge the gap between software simulation and the high cost of complete hardware system development. Besinger *et al.* [57] and Hwang *et al.* [58] implement this method when investigating the performance of a continuously variable semi-active damper for a quarter vehicle model. It works in a closed loop system with a real time computer simulation controlling the hardware setup consisting of a hydraulic test bench, semi-active damper, and a controller unit with a displacement sensor. Further advancement using this concept has been investigated Choi *et al.* [85]. The effort focuses on studying the performance of an MR damper applied to a full vehicle model.

In summary, most of the semi-active strategies and the adopted control theories aim primarily at either improving ride quality, handling or both. Little attention is given to analyzing the effect these have on the durability of suspension components, which is discussed in the following section.

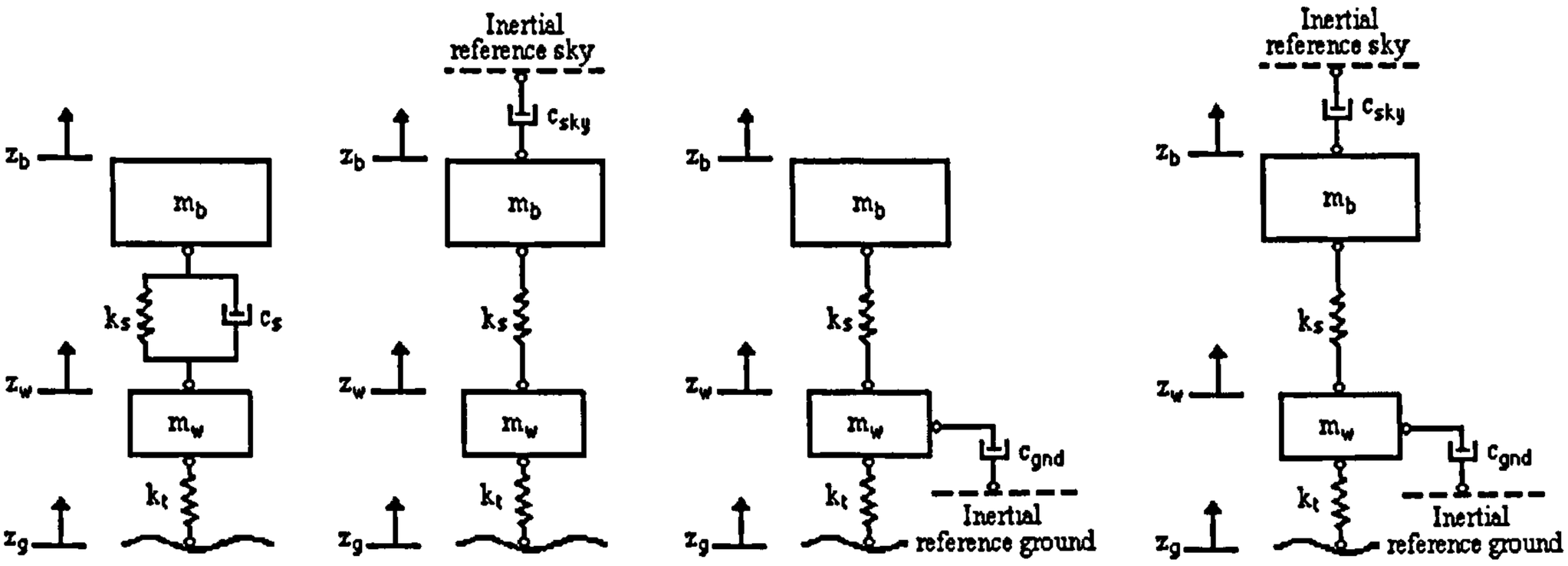

Figure 2.5: QVM Representation of Skyhook Damping Control and its Variations

2.4 Durability of Semi-active Suspension Systems

According to Halfpenny [86], previous studies suggest about 80-90 percent of structural damages are contributed by fatigue. In the automotive industry, fatigue largely affects the durability of vehicle components [2]. Therefore, in this section the term durability refers to the analysis of fatigue performance. With the aim of implementing this early in the design cycle to reduce production time and minimise development costs, virtual models are employed in which critical engineering aspects are considered prior to mass production. Factors such as vehicle ride and handling capabilities, safety, noise, vibration and harshness (NVH), and durability can be analysed and fine-tuned within simulation environments without the need for an actual prototype.

A study involving fatigue life estimation of semi-active suspension systems comprises of multiple disciplines in engineering. This includes simulation of the vehicle model under different road conditions, a variety of tyre models, and a selection of driving inputs at various speeds. The introduction of semi-active control systems requires that the vehicle model must be able to incorporate the controller models to produce accurate simulation results i.e. the load histories which are the prerequisite for fatigue life prediction. Finally, structural modification using structural optimisation can be conducted with data obtained from the fatigue life distribution of the components so that analysts can produce a more radical design modification with improved reliability.

Prediction of fatigue life can either be analysed in the time domain or frequency domain. In the time domain, the service load is in the form of a time history, employed to calculate stress histories using either a quasi-static method or a transient stress method. In the frequency domain, the time histories of the service loads are converted into power spectral density (PSD), in which a harmonic stress or a random stress method is applied to obtain PSD stress representations.

2.4.1 Fatigue Analysis

Fatigue occurs when repetitive loading on a structure or component causes fracture at a load level less than its maximum static strength [86], initiated by imperfections on the surfaces. Fatigue analysis begins by determining the loading of the structure. This information is used to calculate stress or strain either in the time domain or in the frequency domain as explained in the preceding sections.

In the time domain, the repetitive stress or strain histories are categorised into different ranges occurring at specific cycles, and are calculated using the Rainflow Cycle Counting method [87]. The method converts the uneven stress or strain histories into a defined set of constant stress or strain magnitude. According to Downing [88] and Halfpenny [89], a cycle, defined as peak-to-peak (positive or negative), is counted when the successive stress range is greater or equal to the first range. The results are presented in a 3D matrix format in the form of cycles for a given stress range and mean stress. To determine the accumulated damage resulted from these cycles, every cycle of the stress range is summed up using the Palmgren-Miner linear damage rule [90] as follows:

$$\text{Accumulated Damage, } D = \sum_i \frac{N_i}{N_{f_i}} \qquad \textbf{Eq 2. 6}$$

where,

N_i = the number of cycles of a particular stress range and mean

N_f = the number of cycle to cause failure at a specific stress range and mean for a given material stress-life (S-N) curve

i = covers the stress ranges within the matrix

Thus, the fatigue life can be expressed as:

$$\text{Fatigue Life} = \frac{\text{Length of time history}}{\text{Accumulated Damage}} \qquad \textbf{Eq 2. 7}$$

Fatigue life of a structure or component is influenced mainly by dynamic loads, stress and strain resulting from the loads, and the reaction from the material [2]. Therefore, fatigue analysis requires three key inputs, namely component loads, geometrical properties and cyclic material properties. In virtual durability analysis, component loads are attained through MBS simulation. With the absence of an actual prototype, the simulation technique must generate accurate representations of the service load histories. Pompetzki [2] outlines three strategies where durability analysis can be done using these predicted loads. It consists of a load based relative method, a location based method, and a finite element based method.

The load based durability method assumes the geometrical and the cyclical material properties are unchanged. The method is suitable for the study of design problems in the product design stage, since fatigue life can be evaluated quickly. Nevertheless, the accuracy of the result is poor compared to the other strategies. In the location-based analysis, both the component loading and material data are required for fatigue calculation. The method is confined to analysing a critical location of the component, typically in regions with high stress or strain. The results are more accurate than the load-based method, and can be rapidly obtained. One main drawback of this technique is that the fatigue assessment is performed on specific regions on the component, neglecting other critical areas.

The finite element (FE) based method is by far the most capable of producing a more accurate fatigue life prediction than the other two methods, but at the expense of increasing computing time and resources. Here, all three key inputs are needed for the analysis. The benefits of employing this technique is that the entire component is considered in the fatigue calculation. Since this research employs a virtual vehicle model, the fatigue life assessment of the semi-active suspension will be based on the FE method.

This section describes several fatigue analysis techniques employed in the automotive industry. They are the quasi-static durability method, the transient dynamic durability method, and the resonance (harmonic) durability approach. Outcome from the review will highlight the best method to evaluate durability based on fatigue life.

2.4.2 Quasi-static Durability Analysis

Conventional methods in durability assessment of suspension components rely on quasi-static stress analysis in the time domain. The approach is considered simple yet relatively accurate and regularly used as a benchmark to determine component stresses and predicting fatigue in the automotive industry [3, 91-94]. For example, Lee *et al.* [92] compare the durability assessment, of the rear axle of a small size passenger car, between the harmonic stress method and the quasi-static stress approach in which the latter method is used as a reference. The damage results of the two produce good correlation without structural resonance. When the vehicle is subjected to random road input, structural resonances of the axle are present within the bandwidth. It is apparent that the quasi-static stress method generates larger fatigue life than the dynamic (harmonic) stress method since the former method does not consider local and global vibrations.

In contrast, Haiba *et al.* [94] discover the opposite when they examine three life assessment strategies that would produce the most efficient and accurate life distribution for structural optimisation based on fatigue life. They conclude that quasi-static stress with a time domain approach gives better accuracy in terms of predicting minimum life and nodal life distributions, in comparison with the results from the transient dynamic stress approach which is employed as the reference strategy. The minimum life assessment calculated using harmonic stress approach generate unreliable results since it is sensitive to changes in the frequency range, the frequency resolution of the forcing functions and the buffer size for the PSD representation. Selection of these parameters remain subjective from one analyst to another and therefore can be potentially erroneous in predicting minimum fatigue life. However, these parameters do not affect the nodal life distributions even though the locations differ from those obtained using the reference strategy.

Although findings regarding quasi-static stress with the time domain approach from [92] and [94] contradict each other, the fundamental assumption of the effect of local and global vibration on the accuracy of the approach are still valid. In the study from Lee *et al.* [92], the influence of structural resonances exist with the introduction of the random road, which directly improve the accuracy of the fatigue life prediction from the harmonic stress method. In the case of Haiba *et al.* [94], the suspension component employed in their study is not affected by structural resonances since the lowest natural frequency of the flexible mode occurs well above the excitation frequencies.

Assessment of fatigue life using the quasi-static method calculates stress histories based on the product of static load cases and the dynamic load histories. The stress influence coefficients can be obtained by replacing each of the load histories acting on the component with a unit load acting in the same direction as the load history and solve using static analysis. The process is repeated for the other load histories. These static load cases are then multiplied with the corresponding load histories to produce dynamic stress histories. Finally, the superposition principle is applied to ascertain the total dynamic stress of the component. Mathematically, it can be described as

$$\sigma(t) = \sum_{i=1}^{n} \sigma_i F_i(t) \qquad \text{Eq 2.8}$$

where, $\sigma(t)$ is the total stress histories, σ is the static stress load case based on a unit load in the same direction as the load history, F is the dynamic load history obtained either from experiment or through MBS simulation, and i is the number of load cases. In finite element analysis, the dynamic stress histories at each node can be described assuming plane stress conditions for a 2D model consisting of $\sigma_x(t)$, $\sigma_y(t)$, $\tau_{xy}(t)$. For a 3D model, the component stresses comprise of $\sigma_x(t)$, $\sigma_y(t)$, $\sigma_z(t)$, $\tau_{xy}(t)$, $\tau_{yz}(t)$, and $\tau_{zx}(t)$. Details of the mathematical expression for the 3D solid model is presented in Chapter 6. Since the dynamic stress histories generally have variable amplitudes, rainflow cycle counting [87] is employed to determine the number of cycles in each block of stress range. Finally, fatigue life can be estimated by summing the damage for each stress range using Miner's rule as expressed in Eq 2.6.

As mention earlier, the use of this method is restricted to stiff components where the natural frequencies are significantly above the operating frequencies. The method does not identify the regions where global and local vibrations exist [3, 92, 94, 95].

Furthermore, it depends on the linear superposition principal to obtain the total stress. Hence, it is only suitable for linear elastic stress analysis applications, where stresses and strains in the plastic region are not considered [94].

2.4.3 Transient Dynamic Durability Analysis

This technique applies to structures or components in which the natural frequencies are significantly affecting the fatigue life. Generally, this method takes into account local and global vibration in calculating the dynamic stresses. This can be done in two ways either by the direct transient method or by the modal transient method [91, 94, 96].

According to Huang *et al.* [91], obtaining dynamic stress using the direct transient method involves solving the entire equation of motions that accounts for linear and non-linear solutions. This contributes to the need for large computational resources and generally is implemented on specific regions of the structure. In contrast, the modal transient method utilises only the linear solutions when solving for the equation of motions. The method discards high frequency modes of the structure leaving only the problematic low frequency modes as possible resonance occurs from low frequency excitation of the road input, minimising the number of calculations for the dynamic stress. Huang *et al.* [91] describe three different techniques in modal transient analysis. They can be classified as the mode displacement method, the mode stress method, and the component mode synthesis method. Of the three, obtaining the dynamic stress from the mode stress method appears the most efficient in the sense that it does not require large computational resources as do the other two methods.

Haiba [1] suggests another method which is commercially available within finite element packages. The modal superposition transient technique computes the dynamic stress by summing the modal participation histories of every mode with the modal influence coefficient using the linear superposition method. Modal participation histories are obtained from modal transient analysis whilst modal influence coefficients, which are the stress fields of a particular mode, are extracted from modal analysis. He points out two major factors influencing the dynamic stress, namely the number of modes used in the calculation, and the solution time step size used. The minimum life prediction and the nodal life distribution are reduced and converged to a

certain value and pattern as the number of modes considered increases. Similar convergence is observed for the life and the distribution when the solution step size is reduced. On both accounts, although modal transient strategy produces the best accuracy in predicting fatigue life and the nodal life distribution, it requires extensive computational resources. Therefore it is only used as a reference strategy in his study.

2.4.4 Resonance Durability Analysis

Predicting dynamic stress (harmonic stress) using this method assumes the structure or the component behaves linearly. The dynamic stress can be determined by combining the load histories data in frequency domain, expressed in PSD, with the frequency response function obtained from modal analysis. The load histories originally measured in time domain is converted to frequency domain using Fourier transformation. Instead of applying Miner's rule to calculate the fatigue damage, a probability density function (PDF) is utilised to estimate the damage based on the PSD dynamic stress histories.

The first contribution of predicting fatigue damage using a PDF is proposed by Bendat [97] in 1964 when he proposes a narrow band solution for the dynamic stress histories. According to Halfpenny [89], calculating damage using this solution becomes inaccurate and not applicable as a wider band stress histories is selected. He provides a comprehensive review of fatigue analysis using frequency domain methods. Among them includes empirical formulations by Wirsching, Kam and Dover, Hancock, and Dirlik. Of all these formulations, Dirlik's [98] approach provides the best accuracy and robustness during application.

Nevertheless, uncertainties in assigning frequency parameters such as frequency range, frequency resolution as well as the buffer size, as previously discussed in section 2.4.2, have resulted in poor fatigue life prediction. Therefore, the usage of this method in this research is limited to theoretical discussions.

2.5 Conclusions

This chapter provides a comprehensive review of virtual durability of semi-active suspension components comprising of three key areas, namely vehicle dynamic simulation, development of semi-active control systems, and durability analysis based on fatigue life. To successfully predict fatigue life of a semi active suspension component, an integrated simulation method is required. It should combine MBS simulation for accurate service load prediction, with a mathematical simulation program in which a selection of semi-active control algorithms are developed. Then, finite element analysis is employed to predict fatigue life of suspension components subjected to different semi-active control systems. The fatigue life distribution can be used as a precursor for structural optimisation based on fatigue allowing creation of a more durable, lightweight and cost efficient components.

From the literature reviews, it can be concluded that many researchers are more concerned with the effect of their controller models on the ride and handling performances. Hence, the study of the effect of semi-active control systems on the durability of suspension components receives very little attention. Recently, research in this area has started to gain interest mainly due to the rapid advancement in computational capability and resources, although very few results have been published. For example, the investigation by Lepold *et al.* [9] on the influence of suspension components durability resulted from an active suspension system. The fatigue analysis is evaluated at both the component level and full vehicle level under the influence of realistic active roll control (ARC) and active bounce control (ABC). Their study does not include semi-active control. In another development, Haiba [1] reviews several durability analysis approaches and tried to establish the most efficient combination of the two that will be used in structural optimisation algorithm based on fatigue life. He concluded that for dynamically loaded component, the most efficient and accurate combination is with the use of a quasi-static method. It accurately and efficiently predicts the minimum life and the nodal life distributions when compared to the reference method (transient dynamic analysis). However, the study investigates a multi purpose vehicle with a passive suspension system only, instead of with semi-active control systems.

To the best of the author's knowledge, at the time of publication, the author is among the first to study the influence on durability of suspension components with semi-active control systems. In ride and handling, semi-active control systems produce much better performance compared to passive systems. Even though these improvements are less than for the fully active systems, the implementation of such systems are more economical, less weight additions, and produces easier development of control models. Central to this scheme, the main aim of this research is to evaluate several existing semi-active control strategies and their effects on suspension component durability. This is necessary because different control theories would generate different damper forces exerted on the vehicle body as well as other suspension components. These repeated and abrupt changes in damper forces may result in improved ride comfort, minimised road loads, better road holding or manoeuvrability, but simultaneously may inflict high local stresses on suspension components resulting in possibly shorter service lives.

The selection of suitable control strategies is based on the type of vehicle, the driving conditions, the road types, and proper representation of the tyres. Earlier work by Haiba [1] is utilised as the basis of this research. The reasons behind this justification include:

a. His MBS simulation on passive suspension system allows the present author to validate his vehicle suspension models from the proposed modelling strategy.

b. The use of realistic suspension models in his work can be employed to evaluate durability of selected suspension components when semi-active controls are applied. Here, fatigue life of the selected component with a passive suspension system is used as a reference.

c. The comprehensive study on the virtual durability approaches laid out by him has provided a better insight into selecting the appropriate technique in fatigue analysis for the present research. As a result, the quasi-static durability approach shall be used in predicting the minimum life and the nodal life distributions of a selected suspension component.

Building upon these, the selection of semi-active control strategies and the corresponding control theories shall be based on those appropriate for a passenger vehicle. Performance in passenger vehicles is more focussed on aspects of improving ride comfort. Consequently, the most appropriate control theory that is capable of improving ride quality is the skyhook control. As mentioned in a previous section, the skyhook concept remains important in suspension control as it is used as a benchmark for comparison with other concepts, and it served as the basis for semi-active practical implementation [71]. Additionally, this skyhook control will be applied to switchable dampers. These are capable of generating jerk that would exert considerable stress on suspension parts, presumably affecting their service life. A two-state switchable strategy is used as suggested by Nell and Styen [20] since generally the switching occurs between the hard and the soft settings rather than on the intermediate settings in multiple-state switchable systems.

As many semi-active control theories are based on quarter vehicle model, the effect of vehicle body motions are not taken into consideration when implementing these control strategies in a full vehicle model. Findings from Levesley *et al.* [6] and Ramli *et al.* [99] suggest that body motions particularly the pitch and roll motions tend to affect the dynamic response of the unsprung masses. Thus, a suitable semi-active control concept that considers these effects should be adopted using the MBS cosimulation approach. In this study, a two-state semi-active strategy with pitch and roll control as proposed by Nell and Styen [20] is adopted with some modifications. The original control strategy, based on a 3DOF FVM has been modified to suit a 7DOF FVM.

2.6 Outline of the Research

The summary presented in the preceding section has identified gaps in current research. This includes studies relating to component durability under the influence of semi-active control systems. Pursuing this direction, this thesis will undertake a theoretical study to look at the effect of classical semi-active control theories on the fatigue life of suspension components. To achieve this objective, an alternative modelling and simulation approach is proposed. The approach combines a multi-body program for the vehicle models with a mathematical code for the semi-active control

models. The scope of the proposed research can be broadly categorised into four stages.

In the initial stage, the proposed approach known as MBS cosimulation is evaluated against the purely MBS method and the conventional mathematical approach. Here, a selection of vertical tyre models with transient road input are developed as subsystems and are integrated with simple lumped 2DOF quarter vehicle models. The creation of these models as subsystems is another feature of MBS cosimulation which demonstrates the flexibility of the approach. These subsystems are designed such that they allow easy substitution of the parameters within the subsystems without the need to rebuild the entire system from scratch.

Once reasonable criteria have been accomplished, the study continues to investigate the dynamic response of a multi-purpose vehicle (MPV) using the proposed approach. At this stage, several variations of the MPV (from 2DOF QVM to realistic model) with passive suspension systems are developed and analysed subjected to transient and a random road inputs. The findings from this stage will be used as a benchmark for the assessment of semi-active control strategies in the next phase of the research.

The third stage of the research examines the effect of implementing the selected semi-active control strategies on the dynamic responses of the MPV and its critical components. The damper models are obtained from published work and the MR damper model derived from experimental data. These damper models adopt the skyhook control theory and the dynamic responses from several MPV models travelling over transient road and random road inputs are studied. Additionally, the advantages and limitations of MBS cosimulation are addressed particularly with the implementation of the experimentally-derived MR damper models.

In the final stage, the influence of semi-active systems on durability is predicted. The durability based on fatigue life assessment of a particular suspension component is calculated using a quasi-static stress and a time domain life analysis. A finite element model of the suspension component is created to determine the load cases from the quasi-static method. These load cases are multiplied with the corresponding load histories, obtained from earlier stages of research, to produce dynamic stress histories.

The fatigue life of the component is ascertained using the Rainflow Cycle Counting on these variable amplitude stress histories, followed by Miner's rule to estimate the accumulated damage. Since the research focuses on virtual durability, the suspension component fatigue life assessment will be based on relative distribution rather than on exact values.

CHAPTER THREE

Vehicle Modelling Strategies

3.1 Introduction

One of the important elements in virtual durability analysis is to accurately predict the loading histories of the components or structures. This can be achieved with the MBS cosimulation approach. This chapter provides detailed theoretical discussions and assessment of the proposed modelling and simulation strategy. The performance of MBS cosimulation is evaluated against other conventional approaches. It considers the actual computing time and the accuracy of the dynamic response. The accuracy of dynamic response is paramount since it directly affects the load histories, which in turn affect the predicted fatigue life. Other factors affecting the accuracy of the dynamic response are also studied, these include the effect of simulation step size, influence of implementing different tyre models, and the difference between open and closed-loop simulation methods. For simplicity, this chapter is confined only to a lumped two degrees of freedom quarter vehicle model (QVM) with passive suspension system subjected to transient step inputs. Validation of all simulations is achieved by comparison to the quarter vehicle model response with data from Crolla *et al.* [30] and Levesley [100].

3.2 Why MBS Cosimulation?

In automotive durability studies, MBS programs have been recognized by many [2, 7, 8, 26] as an excellent means of predicting dynamic response of vehicles. The accuracy of the dynamic response from MBS simulation depends on how closely it represents the actual system. Among the factors affecting the accuracy include geometrical

properties, material properties and boundary conditions (interaction with adjacent components). As discussed in detail in section 2.2, the MBS method is generally preferred when complex models are involved particularly with presence of non-linear components. For instance, Haiba [8] provides a comprehensive durability study of a multi purpose vehicle with passive suspension. Here, all suspension details such as the hub, suspension arms, tie rods, torsion bars, bushings, bump stop, passive dampers, tyre models and even the road profiles are developed in an MBS program.

However, with the introduction of semi-active control suspension, the use of MBS is currently restricted, as it requires elaborate mathematical functions necessary for the development of control algorithms. This imposes limitations on existing MBS software. Eventually, it leads to unnecessary simplification of controller models in order to satisfy MBS modelling requirements, potentially affecting the accuracy of the dynamic response. On the other hand, control engineers prefer a mathematical program when developing complex controller models. It provides a wide range of control functionality including real time simulation and supports efficient interfacing with hardware. In the development of many semi-active controllers, the descriptions of the vehicle model are often limited to a simple lumped quarter vehicle model [33, 44, 78]. While this enables extensive studies on control strategies to achieve improved vehicle's dynamic response, the model is perhaps oversimplified and hence unrepresentative.

Hence, the use of a single computer code, either an MBS or a mathematical program to predict the service loads, may require simplifications that would generate inaccuracies. With the intention of overcome these shortcomings, an alternative simulation approach is developed to efficiently integrate these two modelling techniques. Both the suspension and semi-active controller models can be built in stages of different complexities, starting with simple models where the results can be firstly validated. The approach includes development of critical suspension components such as the vehicle models, suspension dampers, the tyre models as well as the road irregularities, in a modular form or subsystem allowing easy substitution of these subsystems. This would facilitate simulation by providing faster parameter replacement without the need of developing them from scratch.

The term MBS cosimulation has been adopted in the thesis to separate it from integrated simulation involving flexible multi-body systems. In flexible multi-body systems, both the rigid body motions and elastic body motions are highly coupled and can be modelled by a superimposition method consisting of complex formulation of constraint equations and mass matrix. Incorporating a flexible multi-body system is crucial for durability studies as suggested by Mousseau *et al.* [10], if the intended components have elastic modes in the operating frequency regions. The scope of this research does not account for flexible multi bodies since the selected component previously evaluated [1] has elastic modes much higher than the operating frequency.

3.3 Proposed MBS Cosimulation Method

The adopted approach combines MBS code (MSC.visualNastran) used for modelling complex multi-body vehicle suspensions configurations, with a mathematical program (MATLAB/Simulink) used for the development of the semi-active controllers, tyre and road models. MSC.visualNastran [101] is a computer aided engineering tool for multi-body system analysis. Formerly known as Working Model 2D, it is capable of simulating motions, vibration, stress and thermal analysis. This includes static, kinematics and dynamic analysis involving positions, velocities and accelerations, constraint force, length and torque, joints forces and moments. All interconnected components are assumed to be rigid. It offers additional features with the introduction of integration with MATLAB/Simulink. MATLAB/Simulink is a modelling and simulation tool that translate mathematical functions or models into a graphical block diagrams from a customisable set of block libraries [102]. This modelling and simulation tool is widely applied in control engineering, therefore provides a suitable platform for studying semi-active control systems in this research.

MSC.visualNastran is selected as a tool for vehicle modelling since the realistic vehicle models were previously developed in this environment. This is crucial in properly evaluating the accuracy of the proposed method with the purely MBS method. Additionally, the use of more advanced MBS software such as MSC.ADAMS is not considered, in order to minimise uncertainties during component remodelling due to the absence of geometric details from previous work.

The MBS cosimulation approach integrates the two simulation codes, in which both programs perform their own numerical integration in fixed time steps. It forms a weak coupling between the two programs, as reported by Vaculin *et al.* [26]. MSC.visualNastran continuously integrates inputs from MATLAB/Simulink between the time intervals, and generates outputs at a new time step. Likewise, MATLAB/Simulink performs its numerical integration with the inputs produced from the previous time point in MSC.visualNastran. Further description of the MBS cosimulation concept is illustrated in Figure 3.1. Each program executes numerical integration, where at each time step both codes update one another with new state values before advancing to the next step. MATLAB/Simulink computes the road displacement, x and the tyre force, F_t, at t_o. In calculating the tyre force, the initial displacement input, z, from the MBS hub/unsprung mass is utilized. Similarly, the damper force is calculated with the initial values obtained from MBS, depending on demands of the damper models. The MBS initial state values in the forms of displacements, velocities and accelerations, act as feedback inputs to MATLAB/Simulink subsystems.

The vehicle model in MSC.visualNastran accepts force inputs from MATLAB/Simulink tyre and suspension damper subsystems, which are represented as linear force actuators. In solving the motions, MSC.visualNastran utilizes continuous numerical integration that allows the use of a fixed step or a variable step method. In fixed mode, the integration step is set to the default setting of the animation step, preventing smaller integration step being used. This may violate the overlap tolerance resulting in simulation inaccuracy if a large interval is selected. Conversely, variable integration will automatically adjusts to smaller time steps (not greater than the one specified in animation step) to obtain convergence, in which the overlap tolerance is satisfied. The process is conducted in the background and only the results at the animation step size are displayed.

In the tyre subsystem, various mathematical tyre models can be created, although only two are shown in Figure 3.1 for illustrations purposes. Similarly, non-linear, passive dampers and semi-active damper models are generated in the suspension damper subsystem. This approach allows easy model substitution when evaluating the performance of various suspension systems. Motion histories generated from the MBS

cosimulation are used as key inputs to finite element analysis to calculate the stress distributions and to estimate the fatigue life of suspension components.

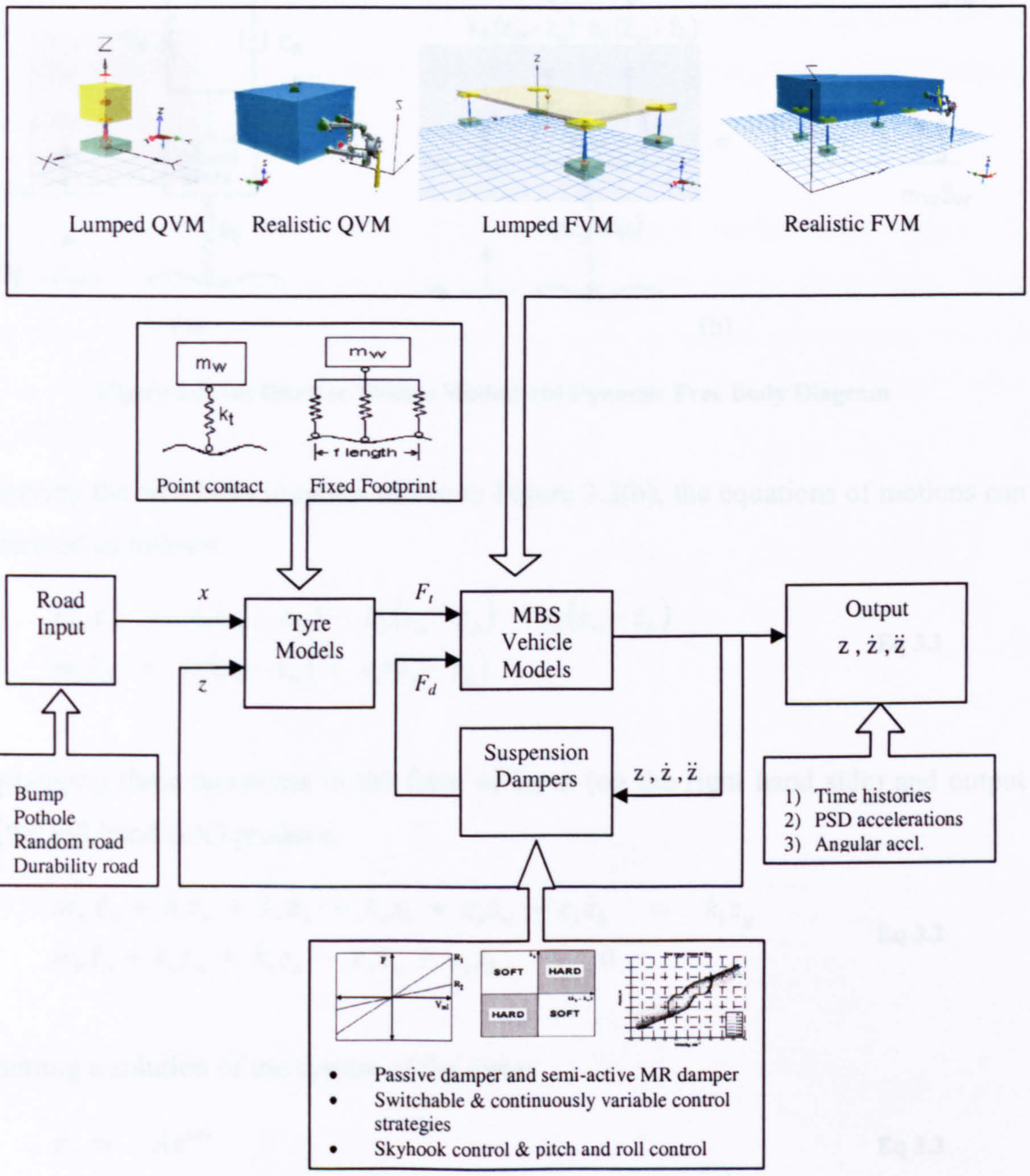

Figure 3.1: MBS Cosimulation Scheme

3.4 Lumped Quarter Vehicle Model

Evaluation of the proposed method begins with a simple two degrees of freedom quarter vehicle model (QVM) as illustrated in Figure 3.2(a).

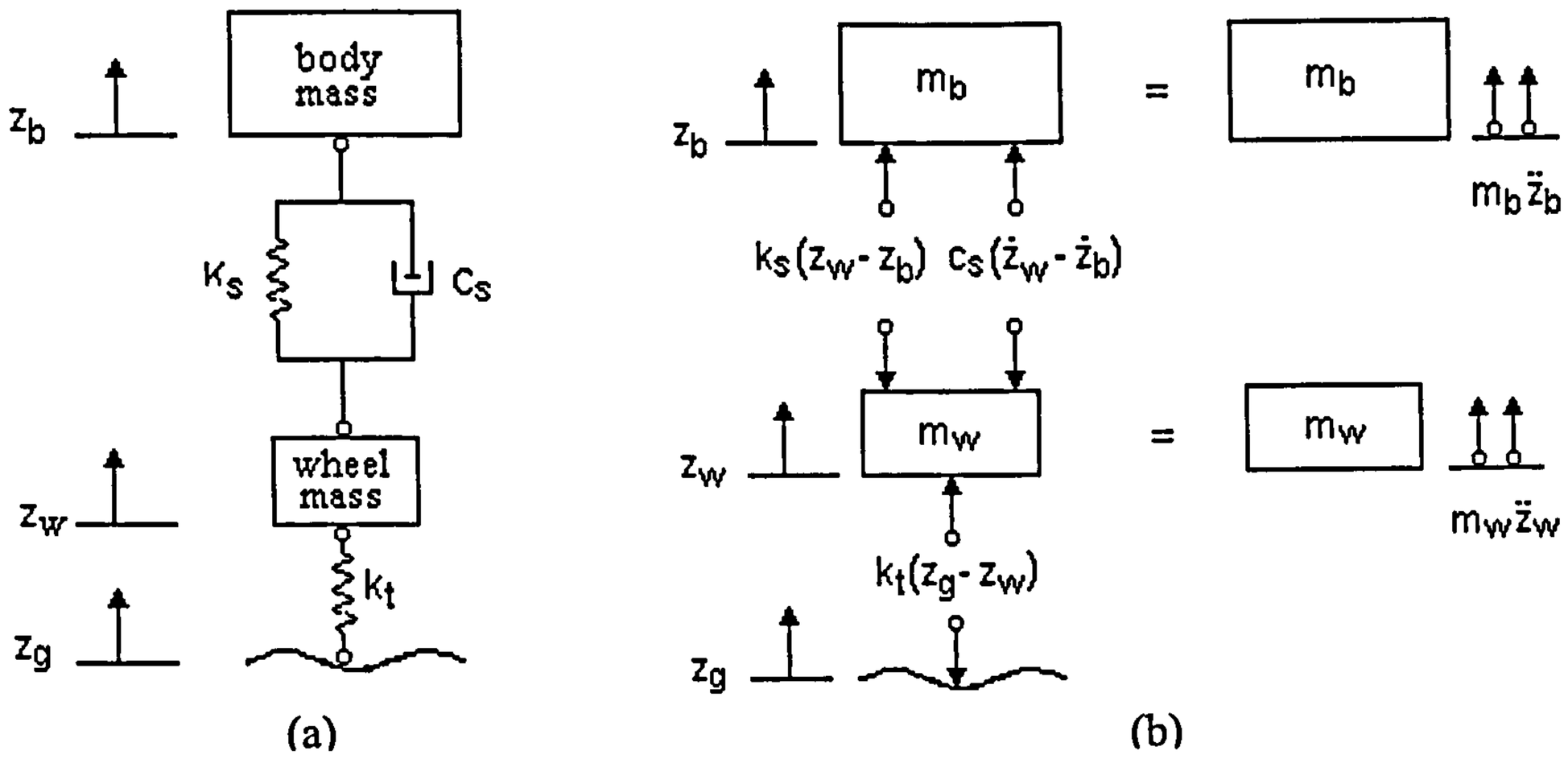

Figure 3.2: (a) Quarter Vehicle Model; (b) Dynamic Free Body Diagram

Observing the free body diagram shown in Figure 3.2(b), the equations of motions can be derived as follows:

$$\begin{aligned} m_w\ddot{z}_w &= k_t(z_g - z_w) - k_s(z_w - z_b) - c_s(\dot{z}_w - \dot{z}_b) \\ m_b\ddot{z}_b &= k_s(z_w - z_b) + c_s(\dot{z}_w - \dot{z}_b) \end{aligned} \qquad \textbf{Eq 3.1}$$

Rearranging these equations in the form of input (on the right hand side) and output (on the left hand side) produce:

$$\begin{aligned} m_w\ddot{z}_w + k_t z_w + k_s z_w - k_s z_b + c_s\dot{z}_w - c_s\dot{z}_b &= k_t z_g \\ m_b\ddot{z}_b - k_s z_w + k_s z_b - c_s\dot{z}_w + c_s\dot{z}_b &= 0 \end{aligned} \qquad \textbf{Eq 3.2}$$

Assuming a solution of the system of the form:

$$z = Ae^{i\omega t} \qquad \textbf{Eq 3.3}$$

By differentiating Eq 3.3 once and twice, with respect to t, the velocity, $\dot{z}$, and the acceleration, $\ddot{z}$, are obtained as:

$$\begin{aligned} \dot{z} &= i\omega . Ae^{i\omega t} \\ \ddot{z} &= -\omega^2 . Ae^{i\omega t} \end{aligned} \qquad \textbf{Eq 3.4}$$

Earlier work by Hudson [103] using the MBS software from MSC.visualNastran shows near exact response to the analytical solution under sinusoidal excitation. Based

on the derivation of Eq 3.2, a QVM is developed employing three modelling techniques comprise of a purely mathematical method with MATLAB/Simulink, a purely MBS method with MSC.visualNastran, and an MBS cosimulation approach that integrates the two simulation codes. The aim of the study is to evaluate the accuracy of the dynamic response and the time needed to complete the simulation when the vehicle undergoes a transient step input.

A MATLAB/Simulink block diagram method employed, as shown in Figure 3.3, allows critical vehicle suspension components to be modelled as subsystems. These subsystems will be used in the MBS cosimulation to represent the damper, tyre and road as shown in Figure 3.5. Similarly, a QVM representation for the purely MBS simulation is as shown in Figure 3.4.

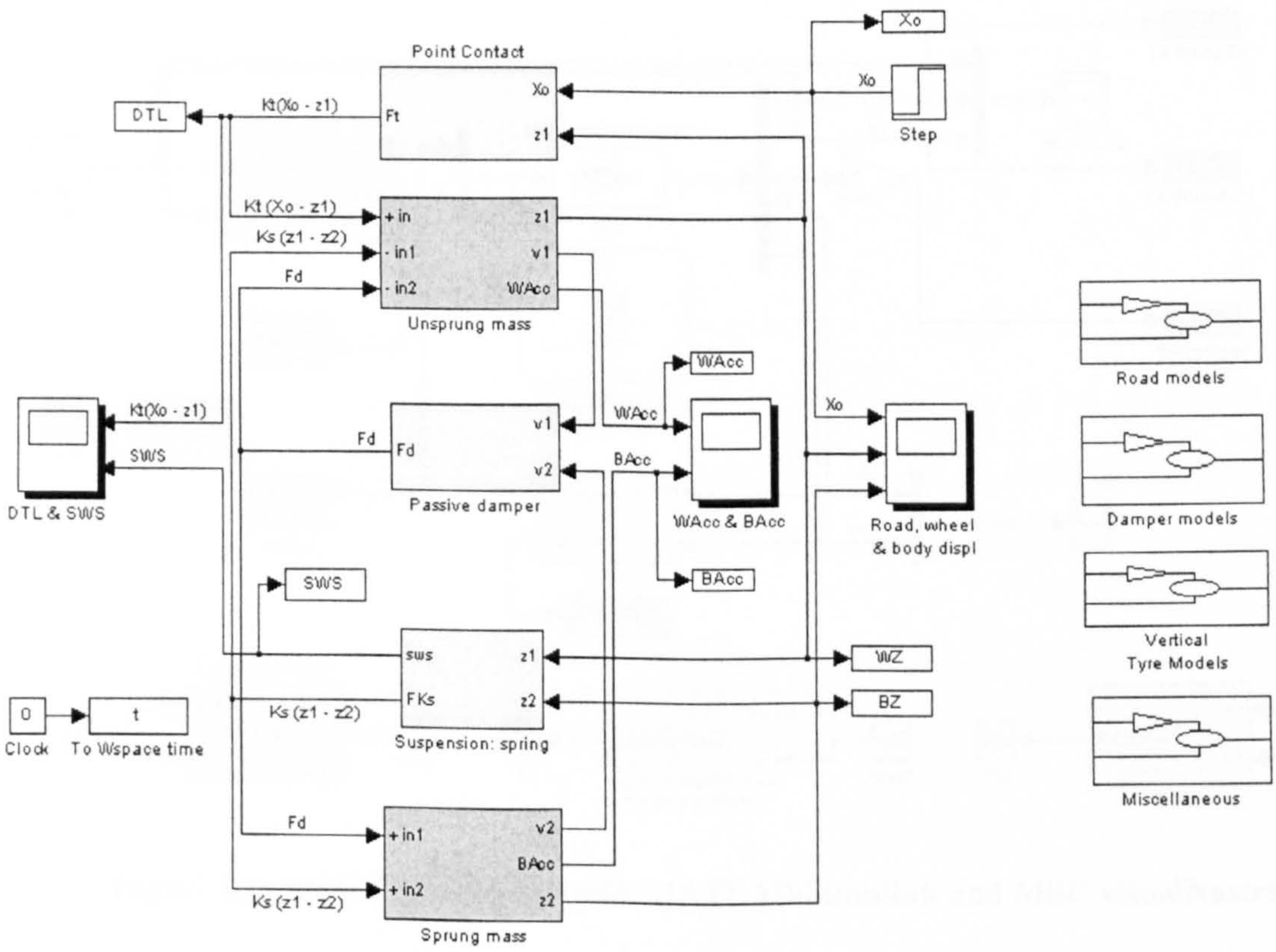

Figure 3.3: MATLAB/Simulink Block Diagram of a QVM

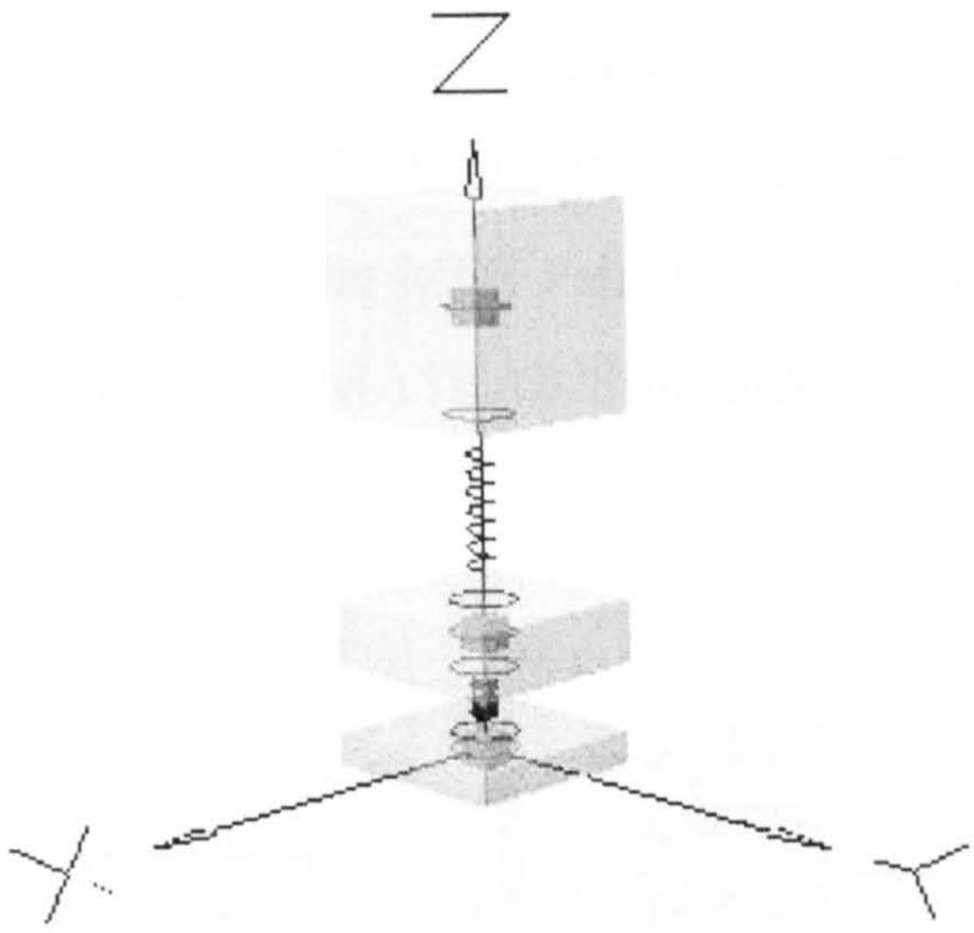

Figure 3.4: MBS Simulation of QVM using MSC.visualNastran

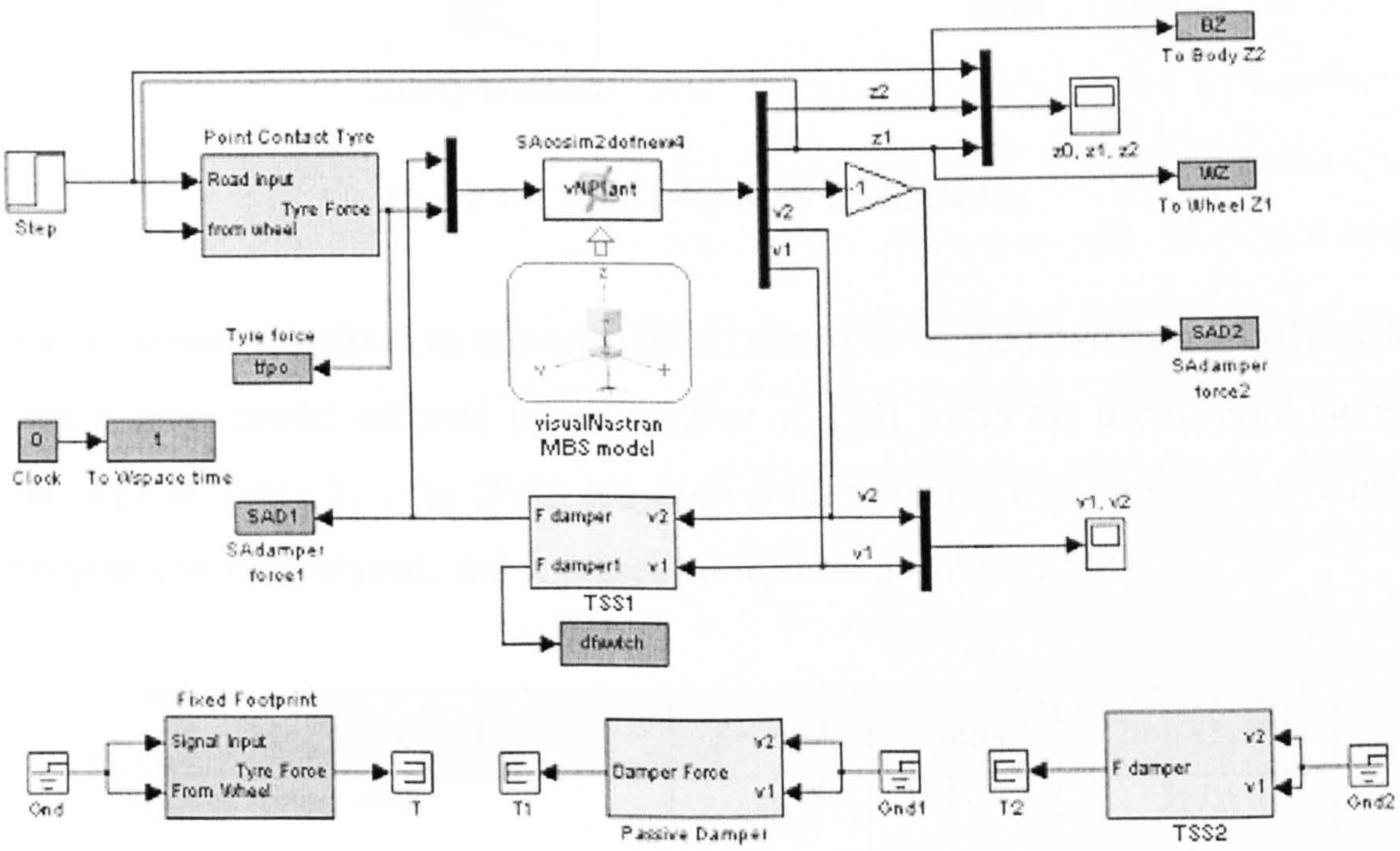

Figure 3.5: MBS Cosimulation with MATLAB/Simulink and MSC.visualNastran

MBS cosimulation with MSC.visualNastran can be implemented in two ways, either in open loop or closed loop. In the open loop format (Figure 3.6), the actuator simply acts as road profile generator applying road amplitude displacements from MATLAB/Simulink as a function of time. Here, all other vehicle parameters are set in MSC.visualNastran. Even though open loop cosimulation produces better accuracy at a faster computational time than the closed loop cosimulation, the technique lacks flexibility. One main disadvantage is that it does not allow subsystems or modules of

critical components to be developed and therefore limits the capability of the approach when investigating problem related to semi-active applications. In contrast, the closed loop MBS cosimulation (Figure 3.5) utilized in the preceding analysis, allows feedback of dynamic signals from the MBS vehicle models. These signals are used as input to the critical subsystems in MATLAB/Simulink and are fed back to the MBS model as force elements.

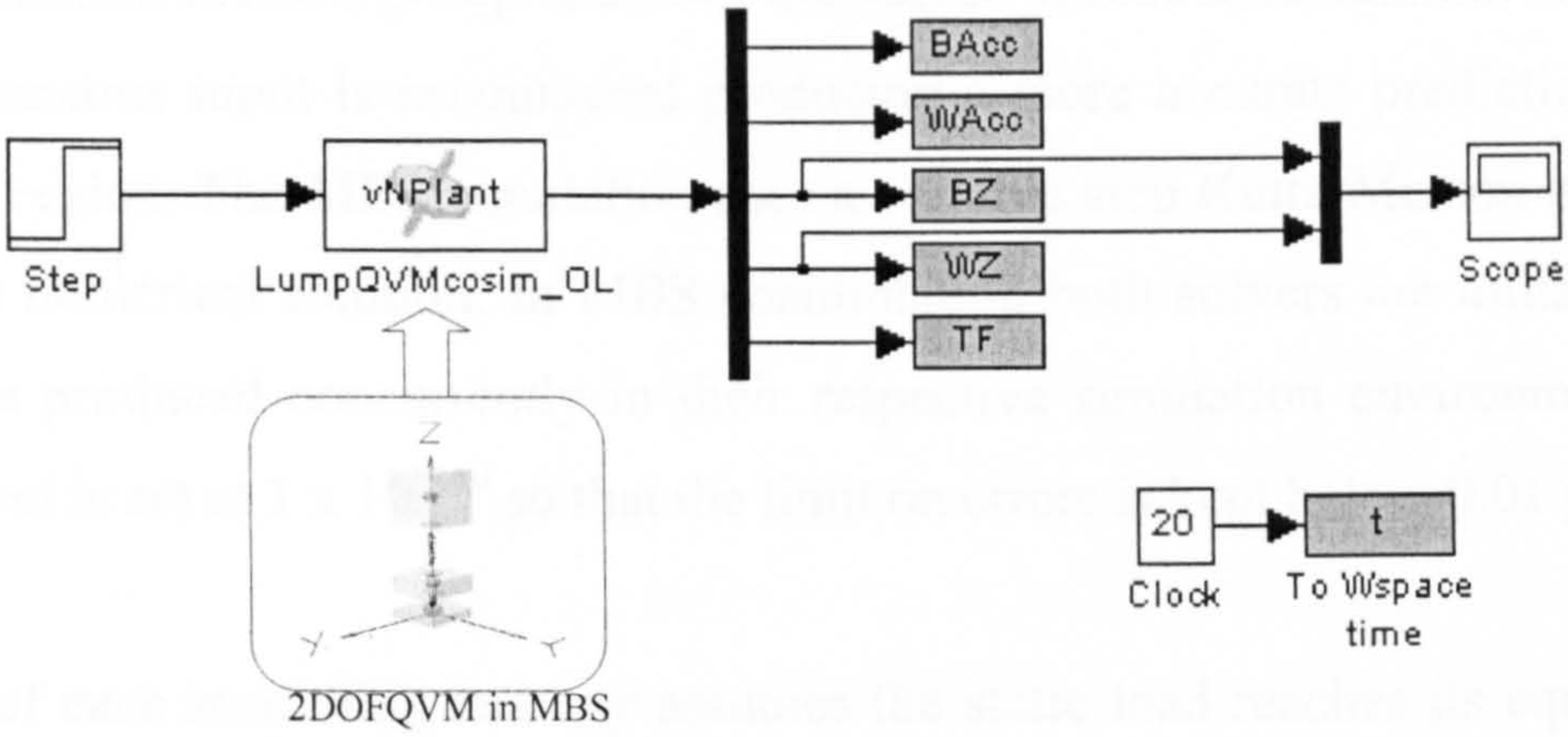

Figure 3.6: Open Loop MBS Cosimulation

The vehicle model utilized in this chapter consists of a lumped two degrees of freedom quarter vehicle model adopted from Crolla *et al.* [30]. With the use of Ford Granada model data in Table 3.1, the QVM response from the three modelling and simulation techniques can be analysed, and is presented in subsequent sections.

Vehicle Parameters	Symbol	Units	2dof QVM
Effective sprung mass	m_b	kg	317.5
Unsprung mass	m_w	kg	45.4
Suspension stiffness	k_s	N/m	22000
Suspension damping	c_s	N.s/m	1500
Tyre stiffness	k_t	N/m	192000

Table 3.1: Quarter Vehicle Model Parameters [30]

3.5 Results and Analysis

In this chapter, assessment of the MBS cosimulation approach is based on the dynamic response of a lumped two degrees of freedom quarter vehicle model with passive

suspension (Table 3.1), subjected to a transient step input. Normalized acceleration and displacement time histories for the sprung and unsprung mass are compared with the response from purely MBS simulation (MSC.visualNastran4D) and the mathematical approach (MATLAB/Simulink).

The mathematical approach using MATLAB/Simulink is used as a reference simulation. It employs a variable step solver using ODE113 based on Adams-Bashforth-Moulton method [104]. It allows the solver to reduce simulation step when large instantaneous input is encountered producing a more accurate prediction in the surrounding region. The MBS simulation uses a variable step Kutta-Merson integrator [101] for its numerical solution. In MBS cosimulation both solvers are utilized since solutions are produced concurrently in their respective simulation environment. The tolerance level is set at 1×10^{-10} so that the limit on errors is kept below 0.01 percent.

Simulation of each modelling strategy assumes the static load reaches its equilibrium state prior to the step excitation. In MBS simulation and MBS cosimulation, the QVM is allowed to settle to its equilibrium by running the simulation with zero input over a long simulation period. The procedure has to be repeated if any adjustments are made to the multi-body dynamic parameters. This includes the sprung and unsprung mass, suspension stiffness and damping and tyre stiffness. All simulations run for 4 seconds with a step input of 20 mm, occurring at 0.5 seconds. They run on a desktop computer with AMD Athlon™ XP 2200+ processor at 1.81 GHz with 512 MB of random access memory (RAM).

3.5.1 Model Solution Methods

The purpose of this evaluation is to determine the effectiveness of the MBS cosimulation method for use in predicting load histories for durability analysis. The proposed method is evaluated against competing modelling strategies, namely the mathematical approach and the MBS approach. Firstly, the efficiency is determined by comparing the actual computing time required to complete the 4 seconds simulation period. Then, the accuracy of the dynamic response is ascertained by correlating them with that of the MATLAB/Simulink variable step approach, which is used as a reference. The evaluation also considers a second MATLAB/Simulink approach

utilizing a fixed step ODE5 Dormant-Prince solver. This is essential to anticipate any significant degradation on the dynamic response as the time step is varied manually.

Several observations can be made following the results presented in Table 3.2 based on 4 seconds of simulation time. The data block on the right hand side of the table is the amount of space required for storing one output, for example sprung mass acceleration response. MATLAB/Simulink simulation with variable step solver achieves among the fastest computing time and generates the smallest data size. This is because the solver constantly adjust the integration step size to maximise simulation speed while maintaining reasonable accuracy. It is capable of overriding a predetermined output step size resulting in faster simulation time and acquire less output data size. With a fixed step solver, MATLAB/Simulink produces relatively fast solution but the accuracy in the response is affected by the selected step size. However, in this exercise, the minimum and the maximum step size limit has minimally affected the accuracy of the response with computing times remain below 1 seconds.

Simulation results from the multi-body method show significant increase in the solution time and the data size in comparison with the reference technique. Of the two MBS techniques, MBS cosimulation requires the longest simulation time requiring more than twice the computing time from the MBS simulation. This is anticipated since the technique has to provide numerical solutions in both the mathematical and the MBS environment. Reducing the simulation step size would result in a drastic increase in solution time. This may be seen as a drawback particularly if the technique is to be integrated within an automated structural optimisation scheme. For example, a 35 seconds simulation period of a simple 2DOF QVM on a virtual durability track, would take more than 40 minutes of actual solution time. It is expected that with increasing complexity in suspension geometry, the approach will require more equations of motion to be solved due to the increase in mass matrix and constraint equations, thus requiring considerable computing time.

Simulation Step Size (s)	Actual Computing Time			Data Block (Bytes)
	Simulink Fixed Step (s)	MBS (s)	MBS Cosimulation (s)	
0.001	0.66	216.50	400.67	32008
0.002	0.54	103.00	222.75	16008
0.003	0.45	78.17	155.19	10672
0.004	0.33	60.20	121.40	8008
0.005	0.26	49.13	100.30	6408
MATLAB/Simulink with Variable Step Size as Reference Model Actual Computing Time: 0.34 s with 2584 bytes of data block size.				

Table 3.2: Comparison of Modelling Methods (Solution Time)

Next, the analysis examines the accuracy of the participating simulation techniques, based on 1 ms step size, against the reference simulation. Of the three approaches, MBS simulation shows the worst correlation. In Figure 3.7, the unsprung mass acceleration of MBS simulation drastically overestimates the peak amplitude when compared to the reference model. This is due to the step input created in MBS program that treats instantaneous signal as a discontinuity resulting in large amplitude responses of the unsprung mass. This high transient amplitude may result in erroneous prediction of the load histories on suspension components. Eventually, this would lead to incorrect stress distribution and poor fatigue life assessment. Similar patterns can be seen in Figure 3.8 and Figure 3.9 but to a lesser extent.

Conversely, the MBS cosimulation data appears to match results from the reference simulation better. Observing the plots for the unsprung mass (Figure 3.7 and Figure 3.8), reveals very minimal differences in both the acceleration and displacement signatures. This implies that the method is capable of generating accurate load histories and is suitable to be used as a tool in virtual durability analysis.

Among the three simulation techniques, MATLAB/Simulink with fixed step solver produces the most accurate response. The acceleration and displacement profiles in Figure 3.7 to Figure 3.10, for both the sprung and unsprung mass, are almost identical with the reference simulation of the variable step solver. Despite being the best method, its usage is limited to simple vehicle models, therefore is considered to be inappropriate for evaluating durability at component levels.

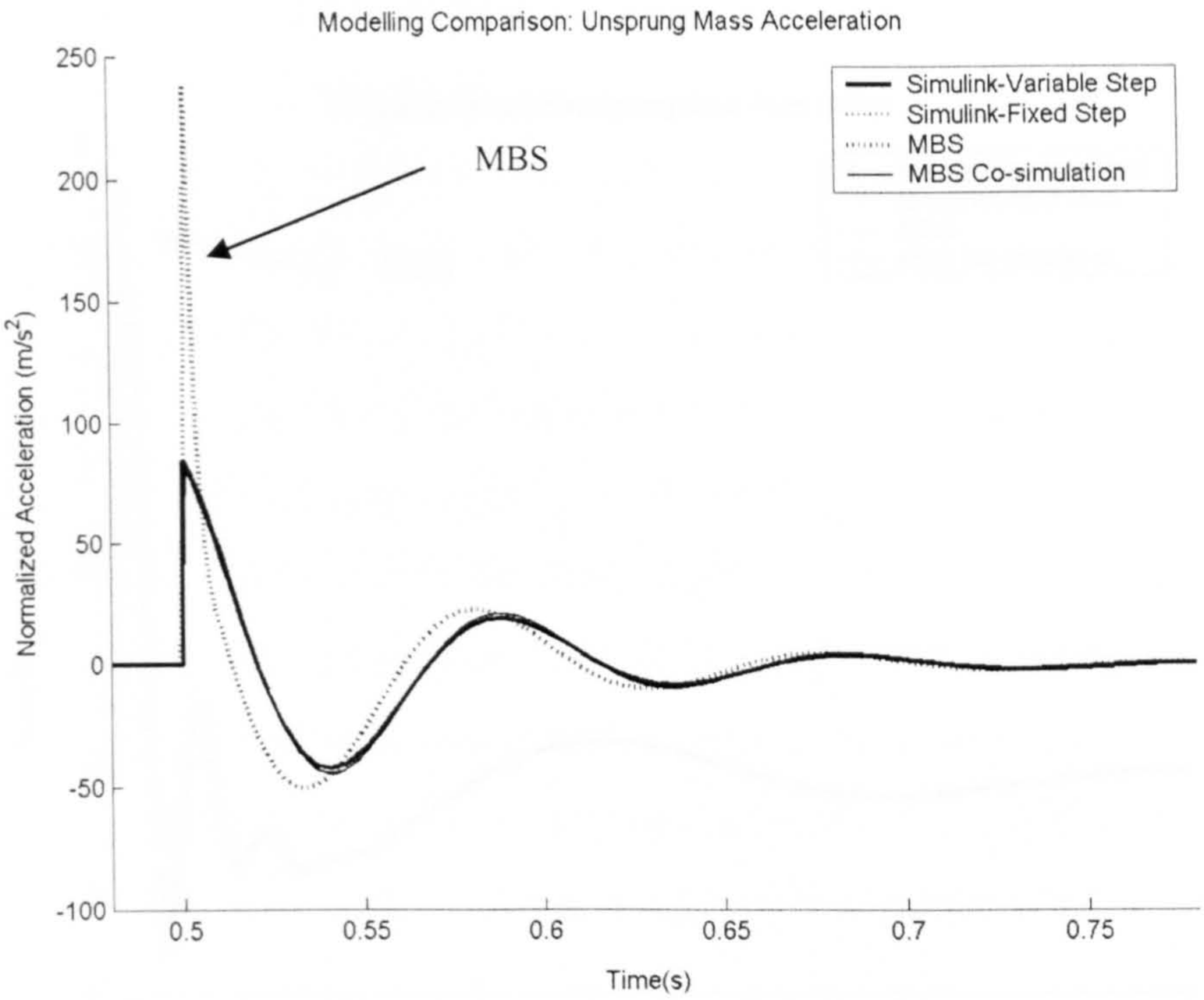

Figure 3.7: Effect of Modelling Strategies on Unsprung Mass Acceleration

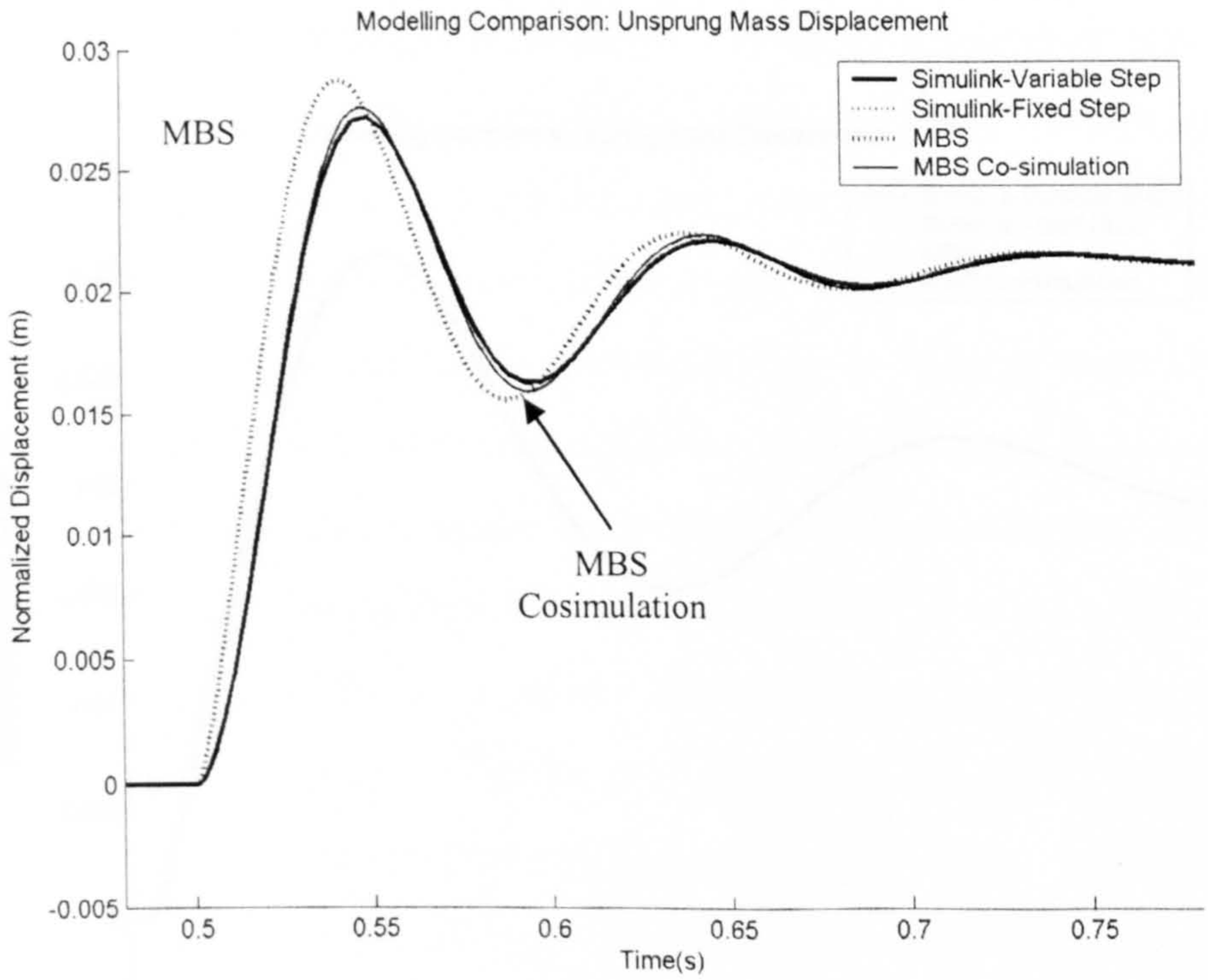

Figure 3.8: Effect of Modelling Strategies on Unsprung Mass Displacement

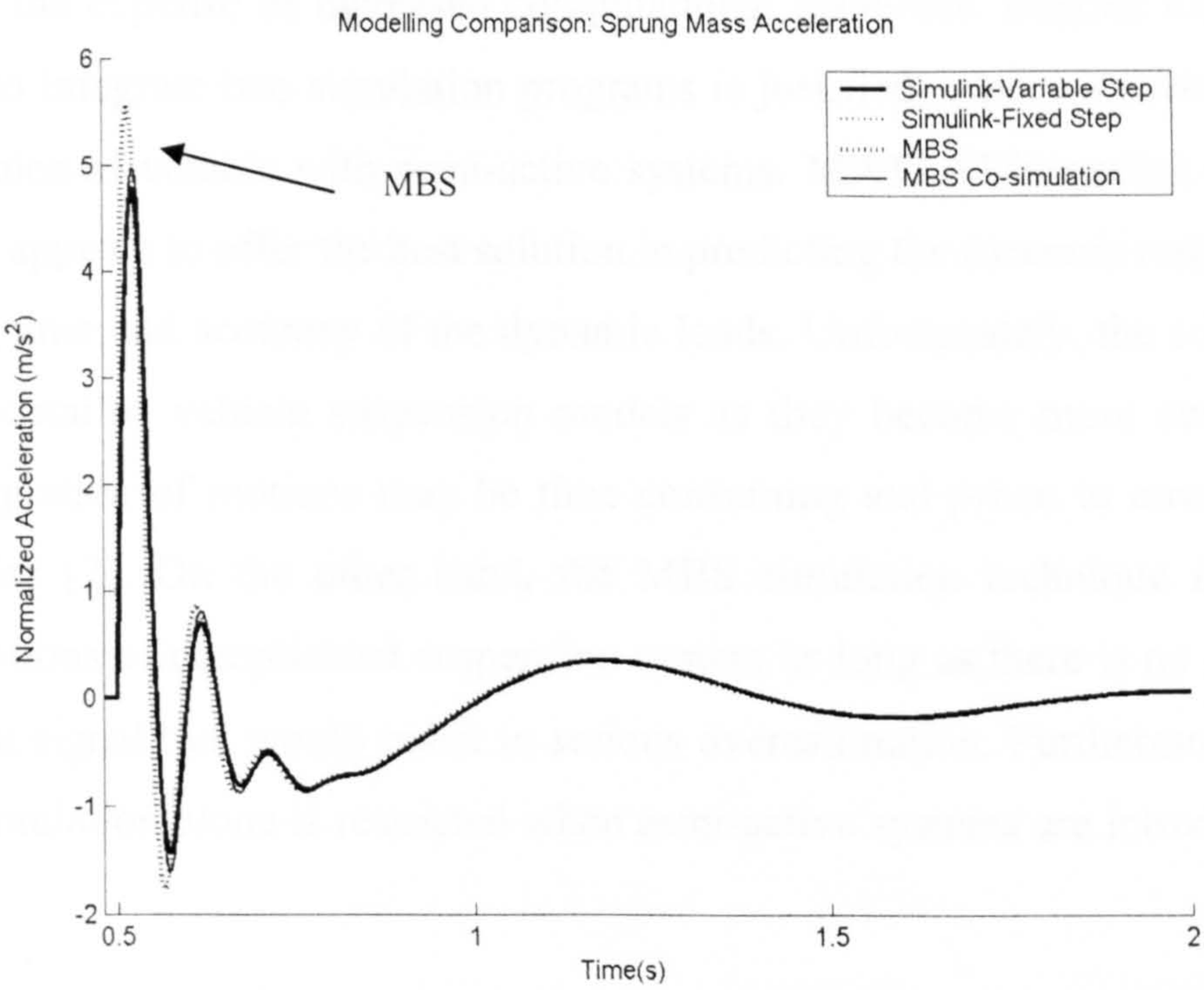

Figure 3.9: Effect of Modelling Strategies on Sprung Mass Acceleration

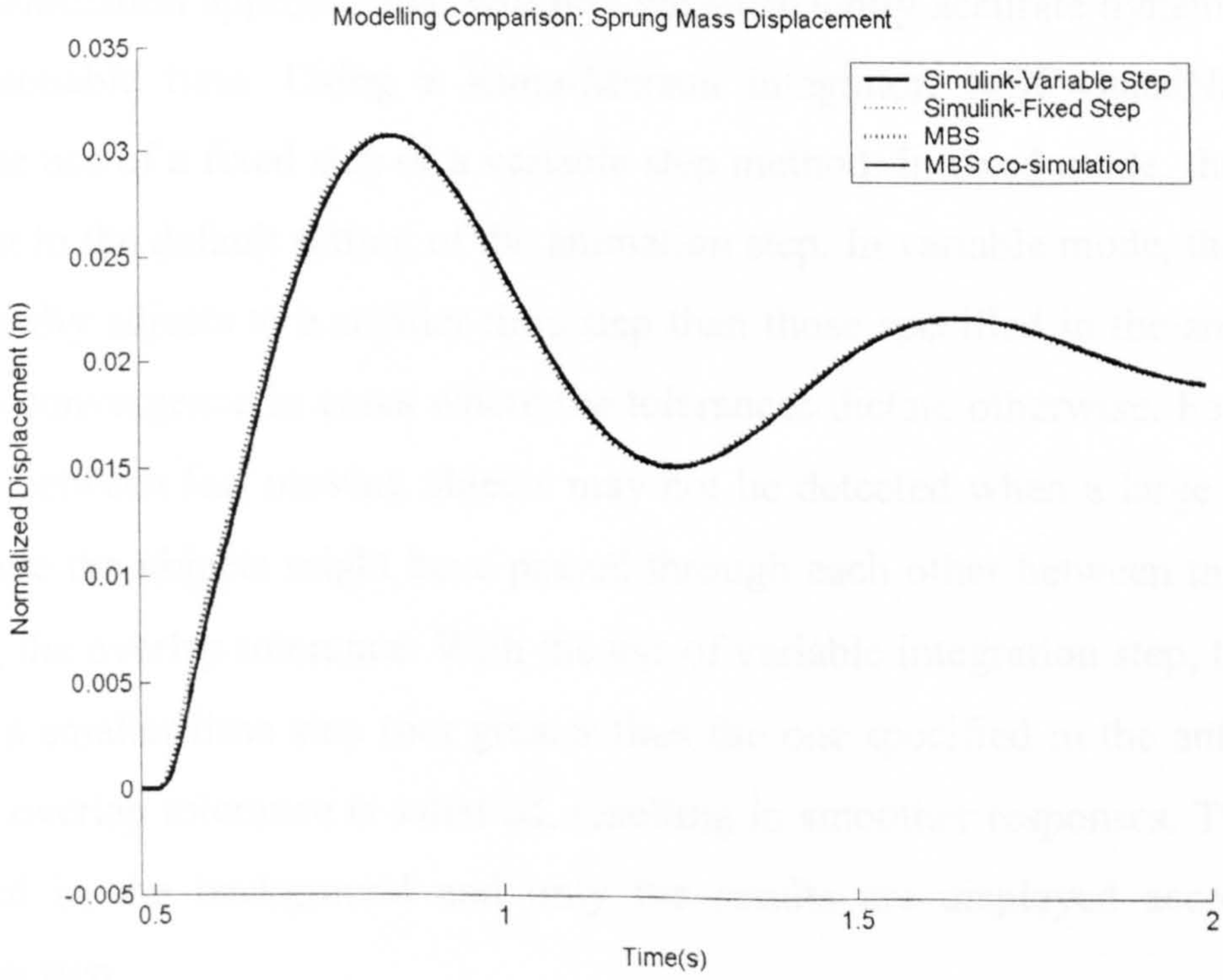

Figure 3.10: Effect of Modelling Strategies on Sprung Mass Displacement

In summary, the analysis of model solution methods suggests that MBS cosimulation can be employed to determine reasonably accurate load histories for use in durability analysis at the expense of increased computational resources. Despite this limitation, its ability to integrate two simulation programs is justified, especially when analysing the dynamics of vehicle with semi-active systems. MATLAB/Simulink with a fixed step solver appears to offer the best solution in predicting the dynamic response both in computing time and accuracy of the dynamic loads. Unfortunately, the software is ill-suited for detailed vehicle suspension models as they become more complex, since deriving equation of motions may be time consuming and prone to error, as pointed out by Prior [7]. On the other hand, the MBS simulation technique is capable of solving motions of complicated suspension system as long as there is no discontinuity in the input signal that would result in serious overestimation. Furthermore, the usage of MBS simulation alone is restricted when semi-active systems are introduced later in the thesis.

3.5.2 Time Step Variation

Analysis in this section attempts to identify a suitable integration time step for the MBS cosimulation approach that will provide sufficiently accurate dynamic responses in a reasonable time. Using a Kutta-Merson integrator, MSC.visualNastran [101] allows the use of a fixed step or a variable step method. In fixed mode, the integration step is set to the default setting of the animation step. In variable mode, the integration automatically adjusts to a smaller time step than those specified in the animation step to obtain convergence in cases where the tolerances dictate otherwise. For example, a collision between fast moving objects may not be detected when a large fixed step is used where the objects might have passed through each other between the time steps, violating the overlap tolerance. With the use of variable integration step, the integrator will use a smaller time step (not greater than the one specified in the animation step) until the overlap tolerance is satisfied, resulting in smoother responses. The process is conducted in the background and only the results are displayed according to the animation step.

The step size in this analysis refers to animation step, since the variable integrator works on a smaller time step than those specified in the animation step. Therefore the

accuracy of vehicle response depends on the time value set in animation step. The simulation begins with the default animation step size of 10 milliseconds (ms) and is reduced to 1 ms. However, the analysis only considers simulation time steps between 1 ms and 5 ms since the dynamic results beyond this range appear to either require too much computational effort or produce results which are less accurate than required for durability studies. The dynamic response resulted from variation in the step size is correlated with those from the reference simulation of MATLAB/Simulink with variable step solver.

Observing the sprung and unsprung mass acceleration and displacement plots shown in Figure 3.11 to Figure 3.13 clearly indicate, as the time step increase the response becomes less accurate as compared to the reference solution. Sprung mass displacement in Figure 3.14 shows minimum amplitude variation, thus may not be a good indicator for this analysis. The effect of the step size variation is more distinguished at the peaks (maximum and minimum). The differences in peak amplitudes with respect to the reference simulation are summarized in Table 3.3, and are calculated as in Eq 3.5.

$$\begin{pmatrix} Percentage \\ Peak\ Amplitude \end{pmatrix} = \frac{Peak\ Ampl_{\ MBS\,Cosim@\Delta t} - Peak\ Ampl_{\ Simulink}}{Peak\ Ampl_{\ Simulink}} \times 100 \qquad \textbf{Eq 3.5}$$

Integration Step Size (s)	Difference in Peak Amplitude w.r.t. MATLAB/Simulink (%)	Actual Computing Duration (s)
0.001	1 - 3	400.67
0.002	3 - 5	222.75
0.003	7 - 9	155.19
0.004	10 - 15	121.4
0.005	13 - 20	100.3

Table 3.3: Effect of Step Size Variations

Employing maximum time step limit of 1 ms may seem to provide the best accuracy but at the expense of considerable computing resources. On the other hand, a 5 ms time step would result in poor results which might have adverse effects on the load histories prediction. In order to maintain the balance between the accuracy and the length of

computing duration, a 2 ms integration step is selected. The actual simulation duration is one half of the 1 ms simulation while keeping the response error within 5 percent. This time step was utilised for dynamic analysis of passenger vehicles with passive suspension system employed in this chapter and in Chapter 4.

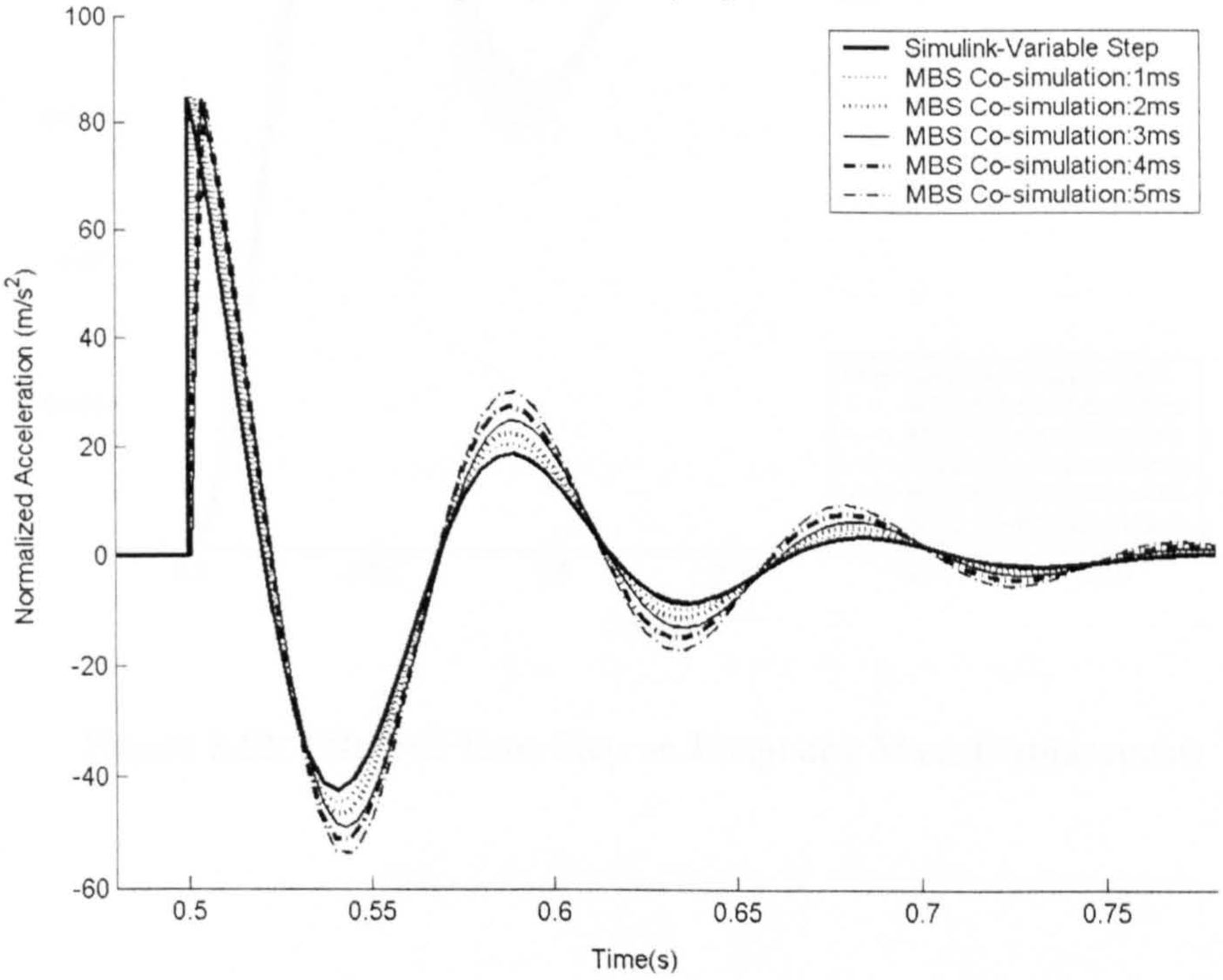

Figure 3.11: Effect of Time Step on Unsprung Mass Acceleration

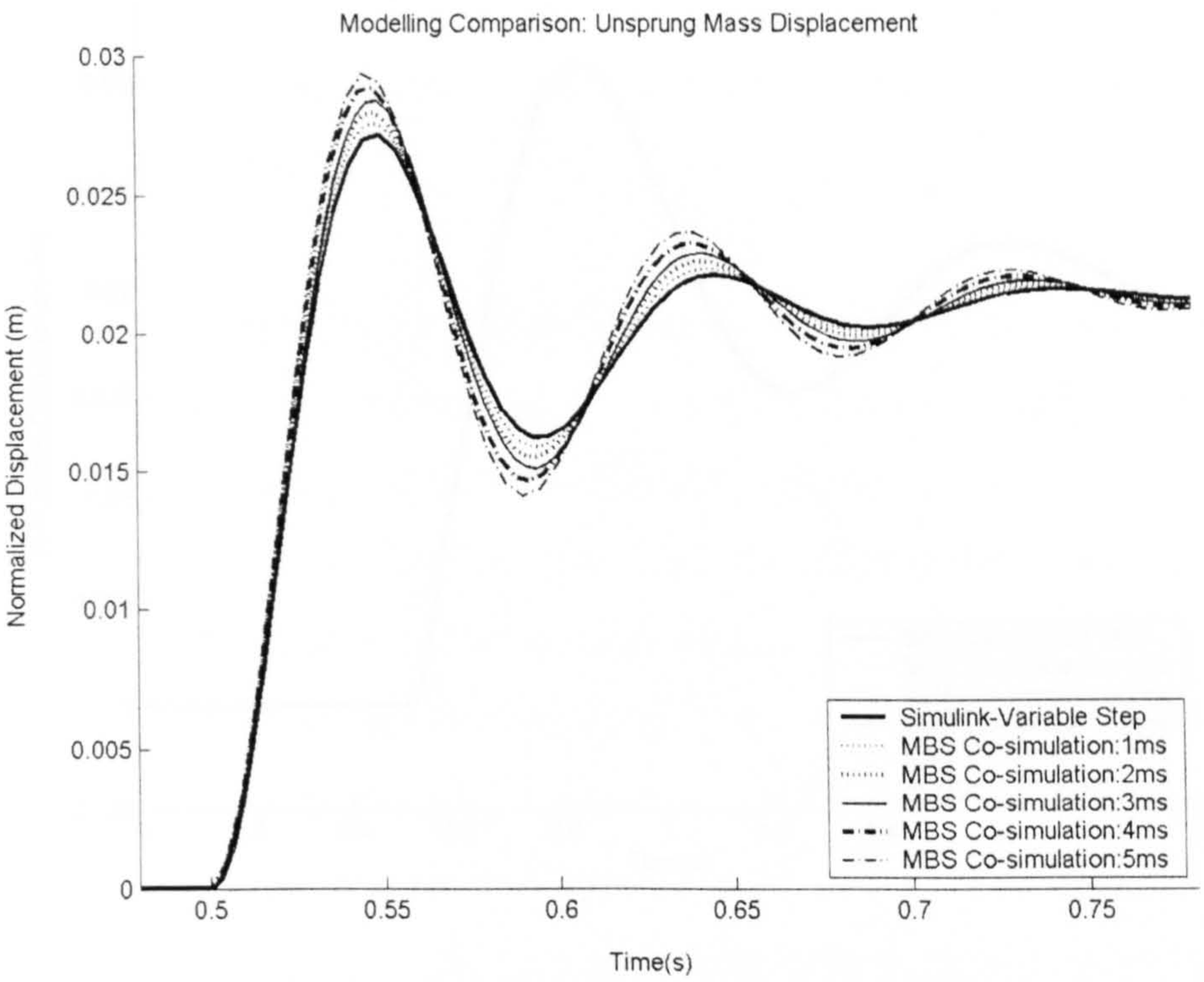

Figure 3.12: Effect of Time Step on Unsprung Mass Displacement

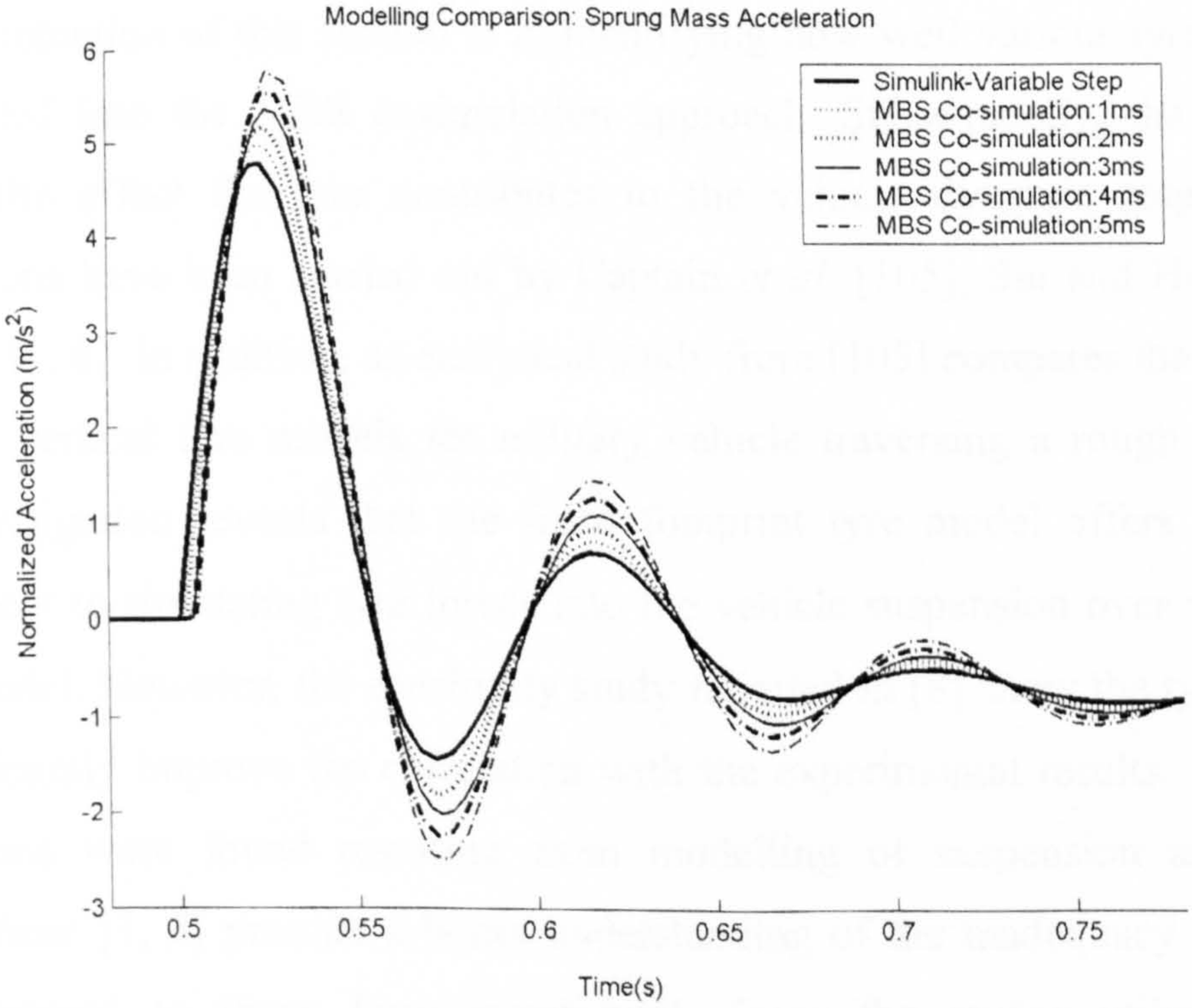

Figure 3.13: Effect of Time Step on Sprung Mass Acceleration

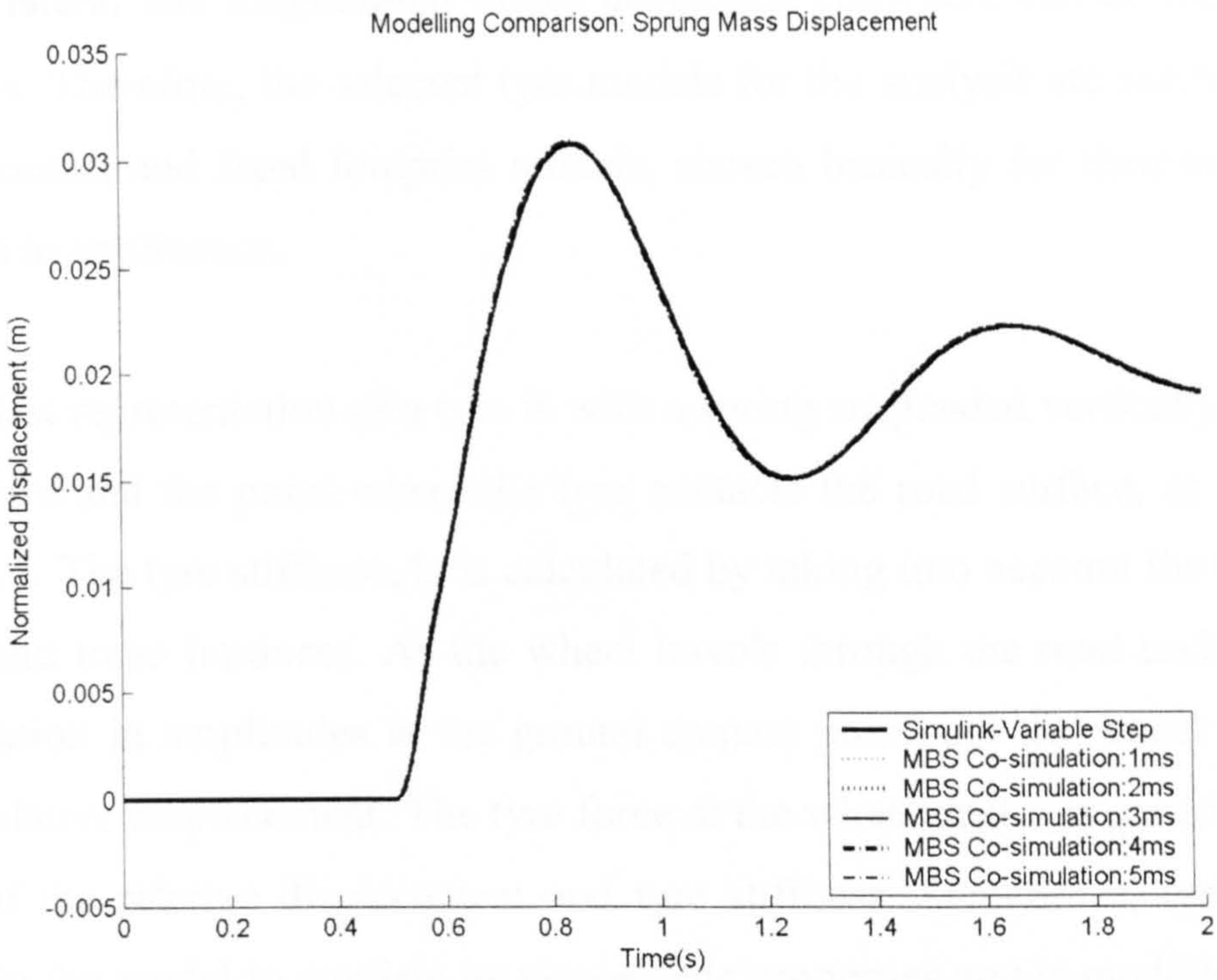

Figure 3.14: Effect of Time Step on Sprung Mass Displacement

3.5.3 Influence of Tyre Models on the Vehicle Dynamic Response

The main intention of this section is in identifying how well various tyre models can be integrated into the MBS cosimulation approach. Subsequently, the section will ascertain the effect the tyre contributes to the vehicle dynamic response. Detail investigations have been carried out by Captain *et al.* [105], Sui and Hirschey [106] and Haiba [1, 8]. In addition, an analytical study from [105] compares the performance of several vertical tyre models for military vehicle traversing a rough road profile. Their investigation reveals that the fixed footprint tyre model offers a substantial improvement in simulating tyre forces into the vehicle suspension over a single point contact model. However, the sensitivity study reported in [8] show the tyre models do not significantly improve the correlation with the experimental results. In fact, many contributions were found resulting from modelling of suspension arm bushings. Findings from [1, 8] provide a better understanding of the inadequacy of simulation work compared to those from experiment. Since the author utilizes the same suspension system as in [1], the effect of tyre models on the load histories is not crucial and the aim primarily focuses on integrating simple tyre models within the

MBS cosimulation scheme. It is anticipated in future more complicated tyre models involving lateral and longitudinal forces developed elsewhere can be incorporated in the scheme. Therefore, the selected tyre models for the analysis are restricted initially to point contact and fixed footprint models, chosen basically for their simplicity and robustness in application.

The simplest representation of a tyre is with a spring suspended vertically between the wheel centre and the point where the tyre contacts the road surface, as illustrated in Figure 3.15. The tyre stiffness, k_t is calculated by taking into account the tyre inflation pressure and tread hardness. As the wheel travels through the road undulation, there exist variation in amplitudes at the ground contact point and the wheel centre in the form of relative displacement. The tyre force at the wheel centre is generated from the product of the relative displacement and tyre stiffness. Sometimes, tyre damping is included in the model to emulate its viscoelastic properties and is modelled as dashpot parallel to the spring element. The corresponding force generated from tyre damping is the product of the damping constant and the relative velocities across the damper. The contribution of tyre damping force is minimal and has little effect on the dynamic histories when traversing normal road surfaces [8]. To the contrary, under large transient event such as striking a kerb or a pothole, the tyre's damping force must be considered. Hanley [107] points out that under these circumstances, a finite modelling approach provides a better accuracy of the forces as compared to the simple spring element models. The differential equation of motion of a QVM with point contact tyre model can be found in the first term of the right hand side of Eq 3.1 i.e. $k_t\left(z_g - z_w\right)$.

In the fixed footprint model, the formulation considers the contact between the tyre and road surface as a contact length rather than as a point, as in the point contact model (Figure 3.16). The tyre force is distributed over the contact patch as it rolls on the road irregularities. The force distribution is determined by the number of spring/damper elements employed within the tyre contact length. In a fixed footprint model that first term is denoted as:

$$\left(\frac{k_t}{n}\right)\int_{i=1}^{n}\left(z_g - z_w\right) \qquad \textbf{Eq 3.6}$$

where the subscript n, denotes the number of the spring elements used.

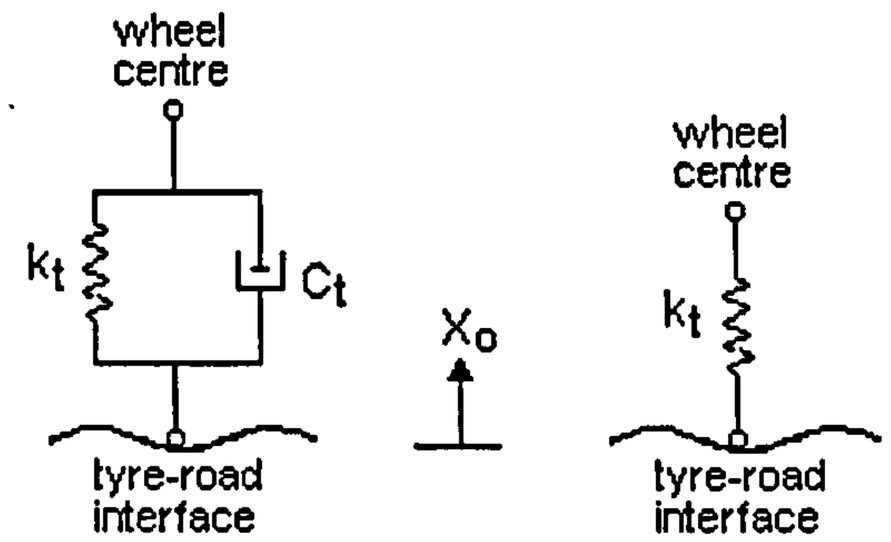

(a) with tyre damping (b) tyre stiffness only

Figure 3.15: Point Contact Tyre Model

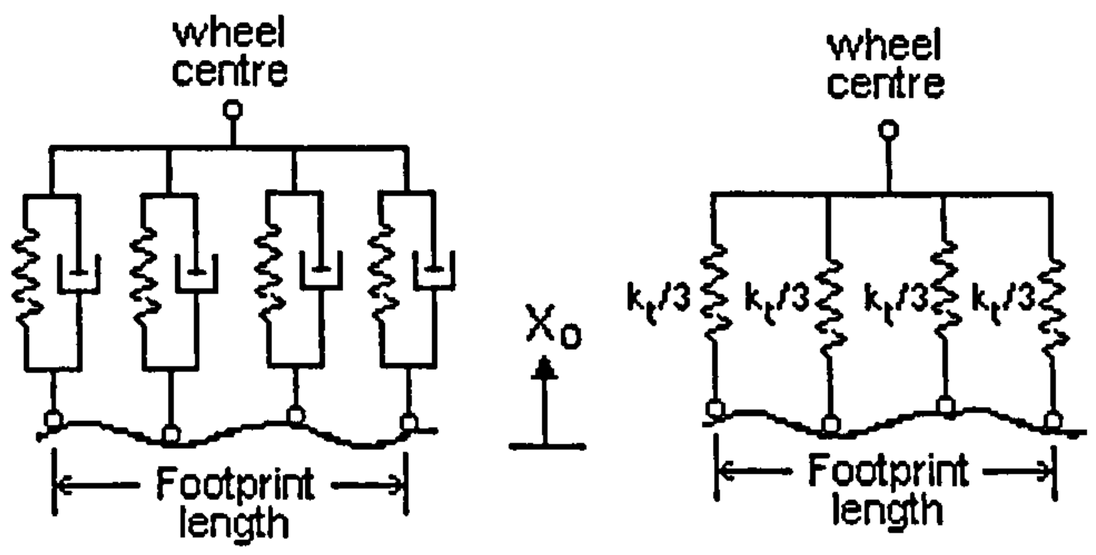

(a) with tyre damping (b) tyre stiffness only

Figure 3.16: Fixed Footprint Tyre Model

In MBS cosimulation, both tyre models demand unsprung mass displacement feedback from the MBS vehicle model generating force output back to the MBS in a form of a linear force actuator. The representation of both vertical tyre models in a MATLAB/Simulink block diagram is created as subsystems as illustrated in Figure 3.17 and Figure 3.18. In this analysis, the fixed footprint model employs four spring elements.

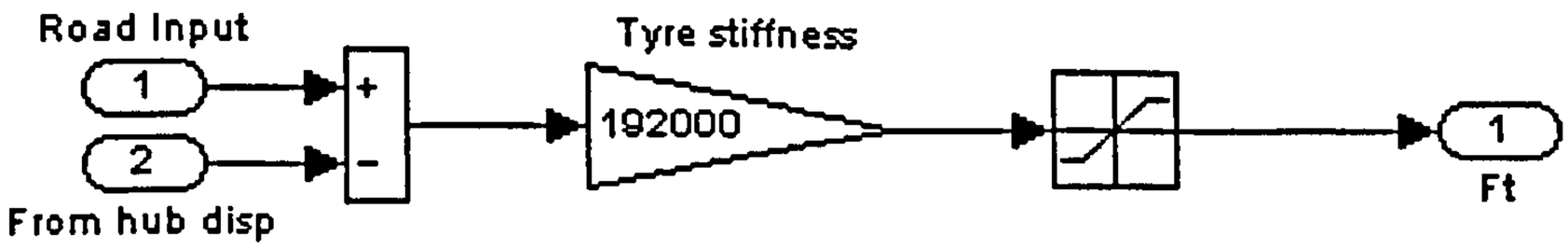

Figure 3.17: Point Contact Tyre Model

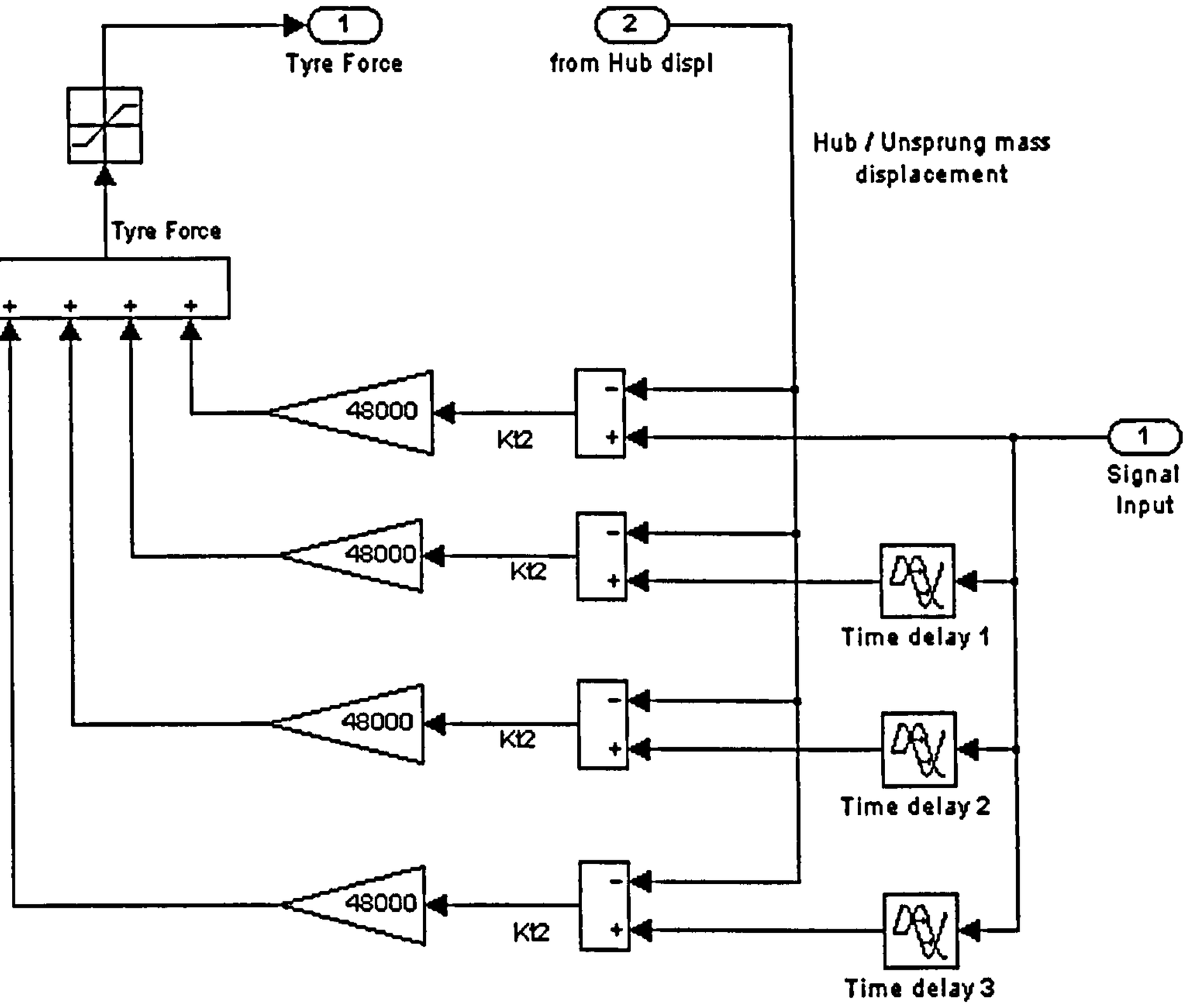

Kt = 192000 N/m is divided by 4 footprint elements = 48000 N/m.
Each time delay is calculated based on the vehicle constant forward velocity, contact patch length and distance between each spring element

Figure 3.18: Fixed Footprint Tyre Model [108]

Both the tyre models require a negative tyre force saturation to facilitate the ability of the tyre to leave the ground if a negative step is encountered. Thus, a force that is less than zero must not exist. This non-linearity feature is the crucial element in the tyre modelling.

Results shown in Figure 3.19 indicate that the peak tyre force from the point contact model exceeds the force from the fixed footprint model by about 7 percent, with the latter lagging by a few milliseconds. Unsprung mass displacement in Figure 3.20, shows similar characteristics to the delay in the tyre force but with smaller differences in peak amplitude. Negligible variation is recorded of the sprung mass response between the two tyre models as illustrated in Figure 3.21. This suggests the tyre models have a small effect on the load histories of the unsprung mass and very little influence on the sprung mass. Similar conclusions were established by Ramli *et al.* [108].

Of the two tyre models, the fixed footprint provides a better physical representation of the tyre force as it rolls over the step, with a gradual increase in force caused by the flexibility and geometry of the tyre. The discrete pattern of the fixed footprint as shown in Figure 3.19 is generated by the number of spring element used in the model; in this case 4 elements are utilized. The discrete increments can still be minimised by either introducing more spring elements to the footprint model or using a rigid roller tyre model as describe by Captain *et al.* [105] and Sui and Hirschey [106].

The analysis highlights the ability to incorporate a tyre model as a subsystem in the MBS cosimulation technique. It offers flexibility for the analysts to evaluate a variety of tyre models quickly and efficiently by allowing easy substitution of tyre models. The influence of implementing different tyre models to obtain load histories was found to be minimal. Similar outcome was discovered by Haiba *et al.* [8] in which the vertical tyre models were created within the MBS program. In light of these findings, a point contact tyre model will be utilized for further analysis in the next few chapters due to its simplicity, faster solution time, with a reasonable accuracy in dynamic response.

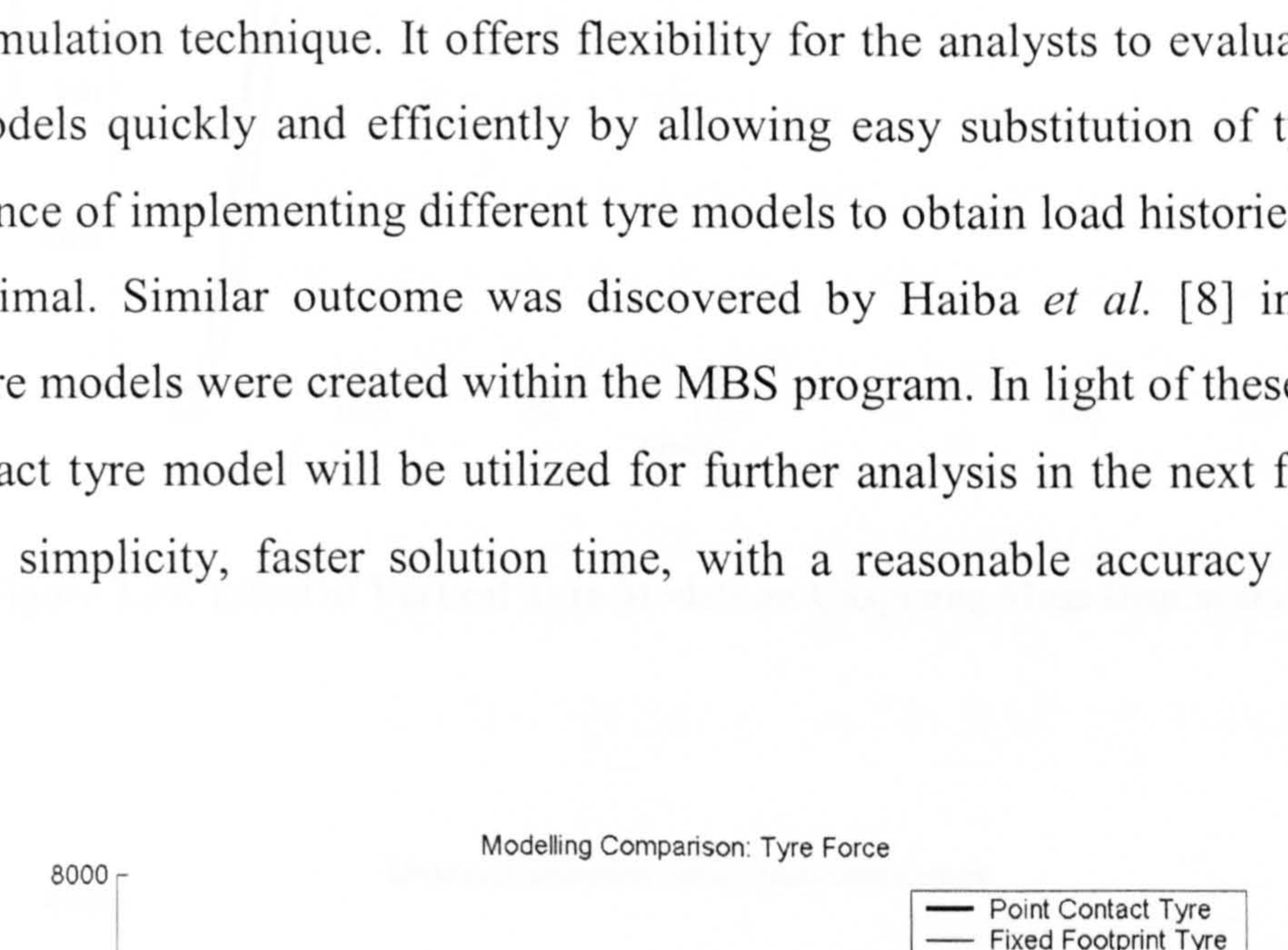

Figure 3.19: Effect of Vertical Tyre Models on Tyre Force

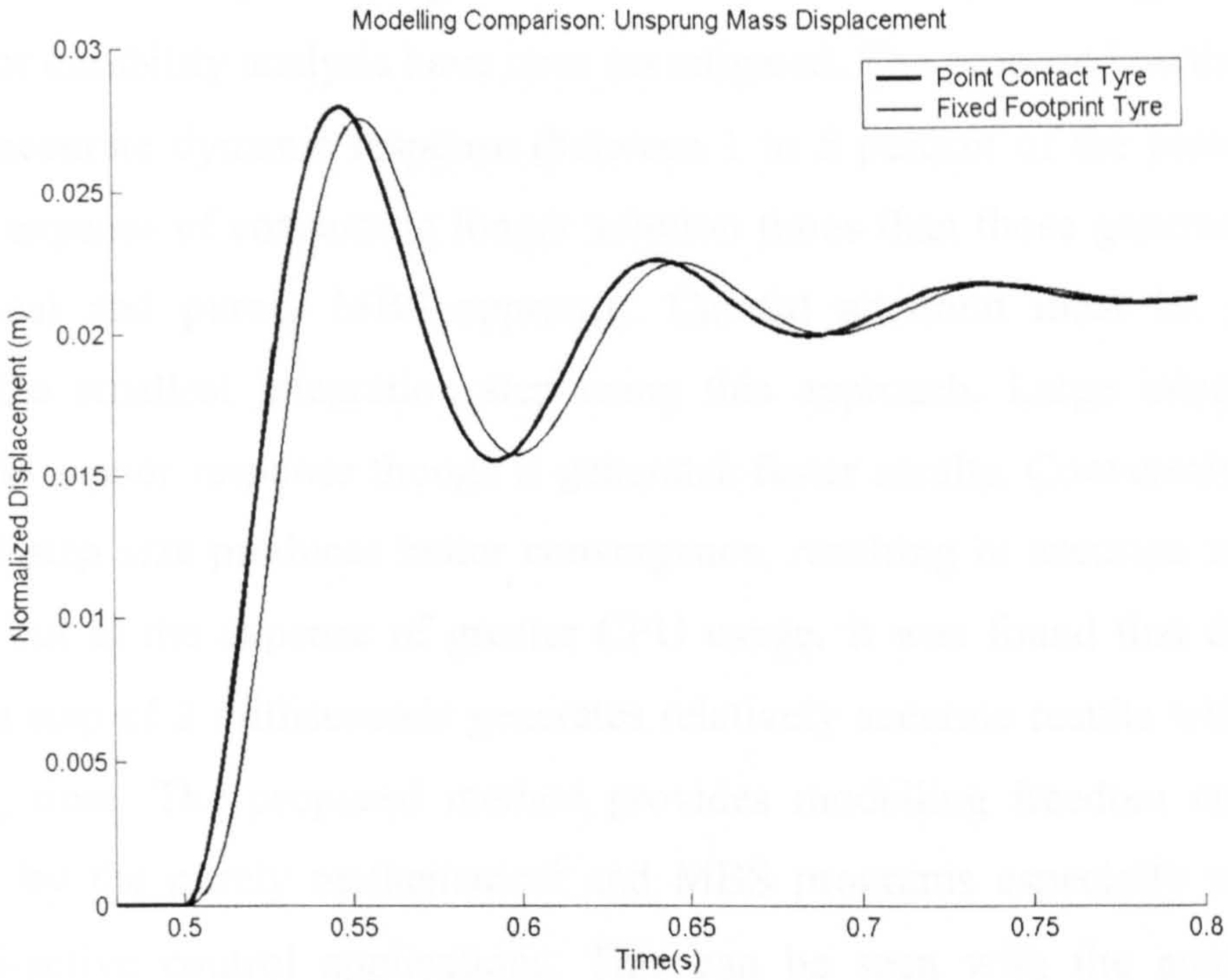

Figure 3.20: Effect of Vertical Tyre Models on Unsprung Mass Displacement

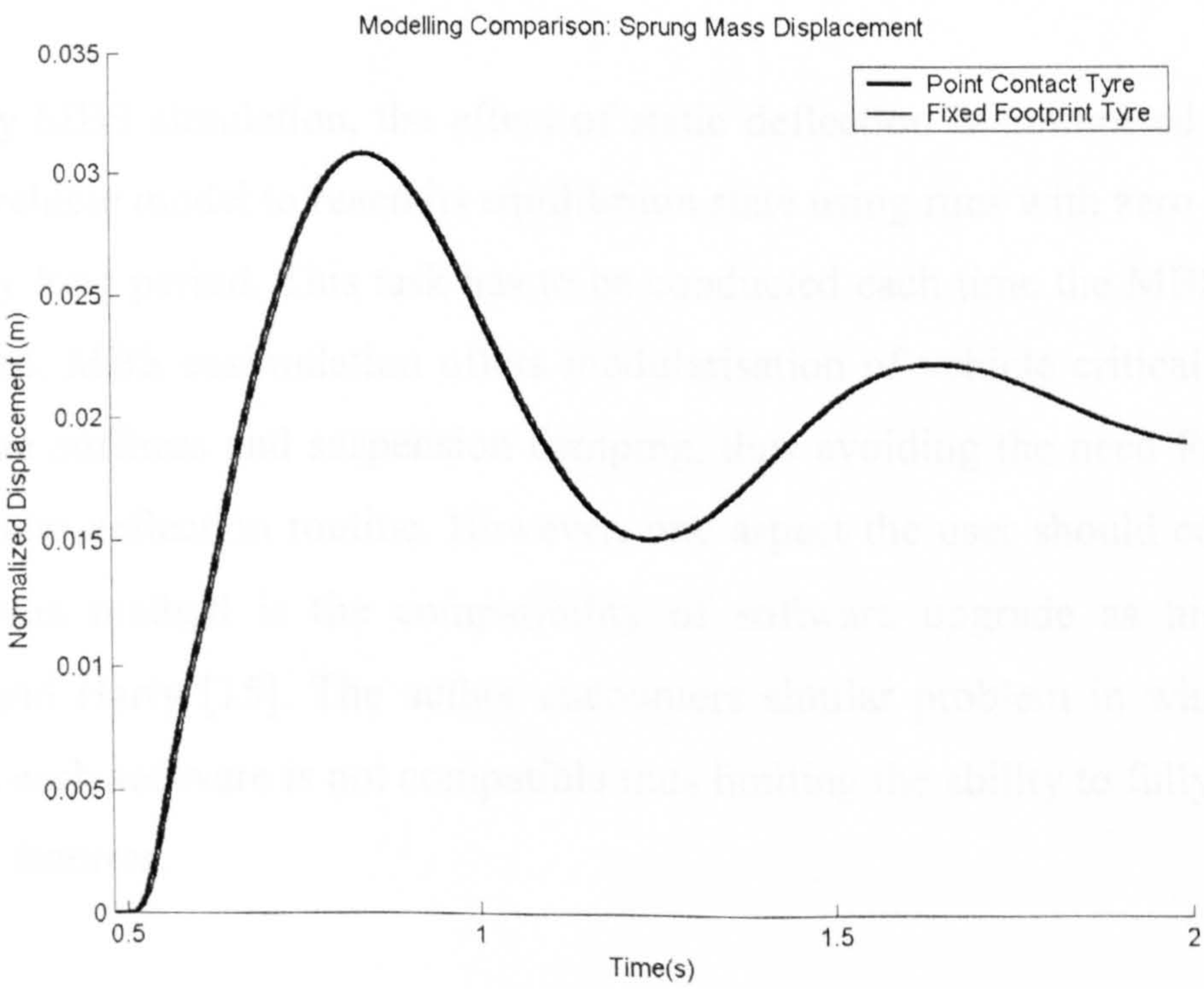

Figure 3.21: Effect of Vertical Tyre Models on Sprung Mass Displacement

3.6 Conclusions

The outcomes of implementing MBS cosimulation for predicting accurate load histories for durability analysis have been investigated. The proposed method produces generally accurate dynamic response (between 1 to 5 percent of the peak amplitude) but at the expense of consuming longer solution times than those generated from the mathematical and purely MBS approach. Careful attention must be given when selecting the smallest integration step using this approach. Large integration steps would yield a poor response though it generates faster results. Conversely, utilizing a very small step size produces better convergence, resulting in accurate and smoother responses but at the expense of greater CPU usage. It was found that the use of an integration step of 2 milliseconds generates relatively accurate results with acceptable computing time. The proposed method provides modelling freedom and flexibility unrivalled by the purely mathematical and MBS programs especially when dealing with semi-active control applications. This can be seen with the analysis of tyre vertical models where different models can be easily substituted and analysed. The effect of tyre models on the load histories was found to be minimal; a similar outcome to that reported by Haiba *et al.* [8] when the tyre models were constructed in a purely MBS environment.

In a purely MBS simulation, the effect of static deflection is minimised by allowing the MBS vehicle model to reach its equilibrium state using runs with zero input over a sufficiently long period. This task has to be conducted each time the MBS parameters are changed. MBS cosimulation offers modularisation of vehicle critical components such as tyre stiffness and suspension damping, thus avoiding the need for the user to run this static deflection routine. However, one aspect the user should consider when adopting this method is the compatibility of software upgrade as highlighted by Blundell and Harty [15]. The author encounters similar problem in which the latest version of each software is not compatible thus limiting the ability to fully exploit their additional features.

It has been demonstrated that the proposed method can be utilised as an effective method in predicting load histories for durability calculation for passive suspension systems. This has been achieved with the use of MSC.visualNastran for generating

MBS vehicle models and MATLAB/Simulink for the development of suspension passive damper, tyre and road models. Nevertheless, the solutions obtained through this method assume all vehicle components act as rigid bodies. The assumption remains valid if the natural frequencies and the corresponding flexible modes of the components are higher than the excitation frequencies. This would impose inaccurate response typically for components with high mass and low stiffness if the flexible modes are within the range of the excitation frequencies i.e. the road input. In this case, other cosimulation packages such as MSC.ADAMS, DADS and SIMPACK which offer integration with flexible bodies may provide better response prediction than the current MBS software being used.

CHAPTER FOUR

MBS Cosimulation of a Multi Purpose Vehicle

4.1 Introduction

Previous work by Haiba [1] provides valuable insights when adopting MBS simulation for durability analysis based on fatigue life. Comparison with experimental results reveals reasonable accuracy in the simulated load histories, except in the longitudinal direction where better modelling of the lower arm bushing may improve the simulation results. Additionally, it was shown that better correlation can be obtained with a full vehicle model but this requires extensive computing time. This limits the functionality of the MBS method within the structural optimisation routine. Regardless of the issue of long solution time, the scope of this work is focussed on determining reasonably accurate load histories for the same suspension configuration as used by [1], when semi-active systems are introduced. Since there was no actual semi-active system used on the existing suspension, the study is limited to theoretical validation from published data. To achieve this requires simplification of the realistic model to a lumped mass 2DOF quarter vehicle model, where many semi-active control strategies can be easily implemented and verified.

The work presented in this chapter explores the use of a realistic suspension model with the MBS cosimulation approach to accurately determine load histories to a specific suspension component. It focuses on evaluating simulation responses of selected vehicle models with increasing suspension complexity and degrees of freedom. Vehicle models under consideration include a lumped two degree-of freedom QVM, a realistic QVM with non-linear elements, and a lumped seven degree-of freedom full vehicle model (FVM). They represent an unladen multi-purpose passenger vehicle with passive suspension system. The dynamic response of these

vehicles will be used as benchmark in Chapter 5 where performance of several semi-active strategies is assessed. Ultimately, MBS cosimulation is employed in generating load histories of a specific suspension component that will be used as a precondition for fatigue life estimation.

4.2 Realistic Quarter Vehicle Model

The intention of simulating a realistic suspension model is to ascertain accurate representation of component load histories for fatigue life estimation. As illustrated in Figure 4.1, the realistic QVM is firstly modelled using a computer aided design (CAD) package. Then, the model is exported to the MBS software, where appropriate mass, inertia properties and joint constraints are assigned. This double wishbone suspension configuration is modelled using MSC.visualNastran and consists of thirteen degrees of freedom calculated using Gruebler equation [15, 109] and is given as:

$$\text{Total DOF} = 6 \times (\text{Number of parts} - 1) - (\text{Number of constraints}) \qquad \textbf{Eq 4. 1}$$

Table 4.1 shows the details of the calculation of degrees of freedom for the QVM. It should be noted that the model has an extra degree of freedom compared to that used by [1] because there is no longitudinal motion constraint to represent the road profile.

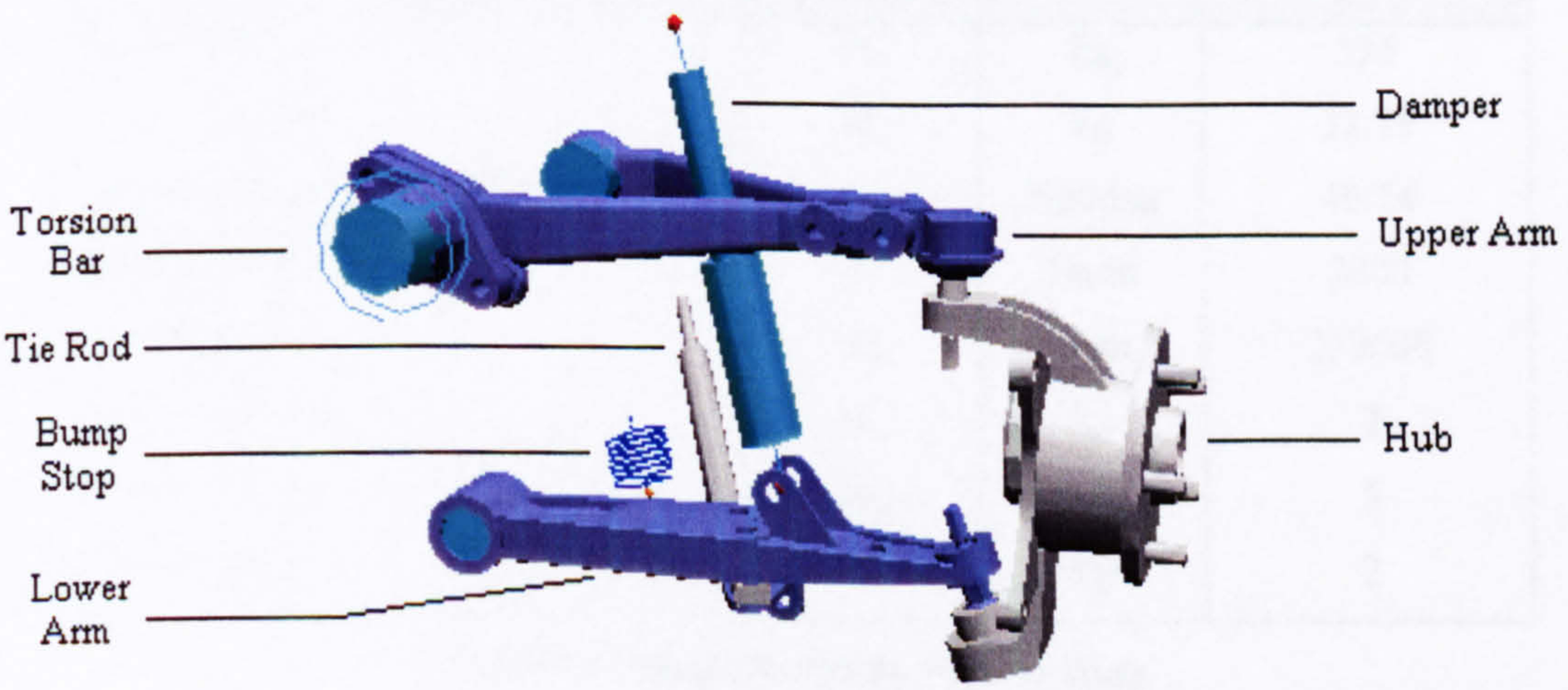

Figure 4.1: Realistic QVM of an MPV

Vehicle Components	Constraints	Number	DOF	ΣDOF
Body, hub, road-tyre interface, bump stop	Translation	4	-5	-20
Body-damper interface, Lower Arm-damper interface, Body-Upper Arm, Body-Lower Arm	Revolute	4	-5	-20
Hub-Upper Arm, Hub-Lower Arm	Spherical	2	-3	-6
	Motion (translational)	1	-1	-1
Total Parts	-	10	6	60 - 47
Total DOF	-	-	-	**13**

Table 4.1: Degrees of Freedom (DOF) Calculation for Realistic QVM

Vehicle data for the unladen realistic QVM model is given in Table 4.2. The realistic model is then used to attain the equivalent vehicle parameters for a lumped mass 2DOF model. This lumped model will be used primarily for modelling various semi-active applications in Chapter 5 and analysis of a lumped full vehicle model.

Vehicle Parameters	Symbol	Units	QVM
Body mass	M_b	kg	535
Front hub mass	M_h	kg	38.75
Suspension torsional stiffness	K_{tor}	Nm/deg	46.74
Suspension damping	C	Ns/m	3800
Tyre stiffness	K_t	N/m	239000
Upper arm mass	M_{ua}	kg	2
Lower arm mass	M_{la}	kg	5
Tie rod mass	M_{tr}	kg	2

Table 4.2: Realistic QVM Vehicle Data

Performing MBS cosimulation using the realistic vehicle model requires a slight modification to the previous MBS model. The passive damper is replaced with a linear force actuator where the input is generated from a MATLAB/Simulink damper subsystem. The subsystem demands relative velocity inputs from the vehicle body and

the unsprung mass. The two locations are denoted as the body-damper interface and the lower arm-damper interface, respectively. Each interface produces component vectors of absolute velocities in x, y, and z directions.

4.3 Derivation of a Two-Degree of Freedom Quarter Vehicle Model

This section describes the derivation of a lumped mass 2DOF QVM from the realistic model. The purpose of this analysis is to calculate vehicle parameters of the lumped model, such that its equivalent suspension parameters will be utilised when developing a local semi-active controller in Chapter 5. There are two methods to derive these parameters, namely using logarithmic decrement [110] and through kinematic analysis [15]. The former method is chosen over the latter since the actual dimensions of the entire realistic suspension model (required for kinematic analysis), are not available. This is vital in order to avoid unnecessary approximation of the dimensions from the MBS model that may affect the values of the parameters.

These parameters shown in Table 4.3, were obtained using logarithmic decrement calculation, δ, of the vehicle body displacement from the realistic QVM. The method determines the equivalent suspension damping, c_s, and stiffness, k_s and assumes vehicle body mass, m_b, and the tyre stiffness, k_t, remain unchanged whilst the unsprung mass, m_w is equivalent to the combination of hub mass and the linkages masses. The mathematical derivation using this method is available in Appendix II.

Once these equivalent parameters for the lumped QVM have been determined, simulation in MBS is performed to compare response of the sprung and unsprung masses. The system response when subjected to a transient road input indicates very similar body and hub/unsprung mass responses. There is a slight variation in the hub/unsprung mass displacement profiles typically due to effect of non-linear elements in the realistic model. Based on calculation, the equivalent vehicle parameters of the lumped mass QVM are as shown in Table 4.3.

Vehicle Parameters	Symbol	Units	2dof QVM
Effective sprung mass	m_b	kg	535
Unsprung mass	m_w	kg	47.75
Suspension stiffness	k_s	N/m	31000
Suspension damping	c	Ns/m	1500
Tyre stiffness	k_t	N/m	239000

Table 4.3: Lumped Mass QVM Vehicle Data [6, 111]

Vehicle body resonance occurs at 1.14 Hz and the wheel hop frequency occurs at 11.97 Hz. The ride rate, K_{eq} and the damping ratio, ζ, are determined as 27.4 kN/m and 0.2, respectively. Gillespie [51] suggests that a comfortable ride can be achieved for a passenger vehicle when the resonance of the sprung mass and the wheel hop fall between 1-1.5 Hz, and 10-15 Hz, respectively. This is true provided the suspension working space is kept within practical limit. Clearly, the MPV model satisfies the general requirement for a typical passenger vehicle. The dynamic characteristics are calculated according to [51] and are available in Appendix III. Additionally, these lumped mass and realistic vehicle models have been previously validated [111] with MATLAB/Simulink, MBS simulation, and MBS cosimulation. Though in this analysis the scope is confined to MBS cosimulation to evaluate the body and the hub/unsprung mass response of the quarter vehicle models.

4.4 Derivation of a Seven-Degree of Freedom Full Vehicle Model

The primary aim of building a lumped mass full vehicle model (FVM) is to evaluate the effect of various semi-active controllers on the suspension components as well as their effect on pitch and roll motions, which will be discussed in the Chapter 5. The study of the FVM in this chapter focuses on validating the responses of the vehicle models against published results [6], and examining the dynamic responses of the sprung and unsprung masses.

A schematic diagram of the MBS cosimulation of an unladen FVM is illustrated in Figure 4.2. The FVM is allowed to move in the vertical direction at all four corners of the unsprung mass, but the unsprung mass is restrained in both lateral and longitudinal directions. The constraint on the sprung mass allows translational motion in the

vertical axis and rotational motions around the lateral and longitudinal directions.

Vehicle Parameters	Symbol	Units	7DOF FVM
Effective sprung mass (front)	m_{bf}	kg	535
Effective sprung mass (rear)	m_{br}	kg	400
Unsprung mass (front and rear)	m_w	kg	47.8
Suspension stiffness (front and rear)	k_s	N/m	31000
Suspension damping (front and rear)	c	Ns/m	1500
Tyre stiffness (front and rear)	k_t	N/m	239000
Pitch Inertia	I_{xx}	kgm^2	1761.3
Roll Inertia	I_{yy}	kgm^2	465.3

Table 4.4: Lumped Mass FVM Vehicle Data

Figure 4.2: MBS Cosimulation of FVM

4.5 Analysis Procedure

In order to fully evaluate the dynamic behaviour of a selected vehicle model, the analysis examines the vehicle responses under transient and random road excitations. This includes responses from sprung and unsprung masses of the QVM and the FVM, and specifically to the lower suspension arm where the load histories will be utilized in durability calculations. The dynamic analysis includes:

a. Time domain displacement response for a transient bump and pothole input.
b. Time domain and frequency domain representation from a random road input.
c. RMS acceleration from a random input

4.5.1 Power Spectral Densities

When a vehicle traverses a road surface, it generates broadband vibrations. These vibrations resulting from the vehicle dynamic response, can be classified into two frequency ranges according to Gillespie [51] and Blundell and Harty [15]. Ride occurs in the range of 0-25 Hz. Within this range, most machines and structures vibrate producing low frequency and non-directional sound. At these low frequencies, passengers tend to feel rather than to hear the sound. Above 25 Hz, these vibrations become more audible as the wavelengths grow shorter, in which range, the passengers hearing tend to be more sensitive. The maximum frequency limit of human hearing is about 20 kHz. The sources for these vibration and noise originate from the interaction between the tyres contact patches and the roughness of the road surfaces, engine and transmission, as well as from the vehicle aerodynamics.

Human perception of vibration and noise in vehicles is subjective. In the context of this study, the vehicle ride response occurs when the tyre interacts with the unevenness of the road surface. Variation in amplitude of the road surface over which the vehicle traverses defines the road roughness [51]. The roughness can be described as a function of road length or as statistical properties generally represented as a power spectral density (PSD) function. Here, the road irregularities emulate a random signal. Inman [110] describes a stationary random signal, $x(t)$ as one that occurs when its statistical properties are time invariant. Thus, the average (mean) of a random input,

x_{avg} can be written as:

$$x_{avg} = \lim_{T\to\infty} \frac{1}{T}\int_0^T x(t)dt \qquad \textbf{Eq 4.2}$$

Finding the mean value of the square of *x(t)* defines variance. It is the average of the square of each data point of *x(t)* from the mean and for zero mean values is denoted as:

$$x_{avg}^2 = \lim_{T\to\infty} \frac{1}{T}\int_0^T x^2(t)dt \qquad \textbf{Eq 4.3}$$

Square rooting Eq 4.3 yields the root mean square (RMS) of the signal *x(t)*. It quantifies the fluctuation of the time history data and in this case, it is used as indication of the severity of vibration subjected to random road input.

$$x_{rms} = \sqrt{x_{avg}^2} \qquad \textbf{Eq 4.4}$$

For random excitation, it is often important to know how fast the time series changes. This can be determined by applying the autocorrelation function, $R_{xx}(\tau)$ expressed as the product of the time signal sampled at different points in time.

$$R_{xx}(\tau) = \lim_{T\to\infty} \frac{1}{T}\int_0^T x(t).x(t+\tau).dt \qquad \textbf{Eq 4.5}$$

where, τ is the time difference at which the time signal is sampled.

The time series can be converted into the frequency domain using Fourier transform. Generally, it decomposes a complex random signal into a discrete set of sine waves of varying amplitudes, wavelengths and phase angles denoted as:

$$X(\omega) = \frac{1}{2\pi}\int_{-\infty}^{\infty} x(t).e^{-j\omega t}.dt \qquad \textbf{Eq 4.6}$$

in which, $X(\omega)$ is the signal in the frequency domain.

Transforming the autocorrelation of the random signal in time series of Eq 4.5, to a function of frequency defines the power spectral density (PSD).

$$S_{xx}(\omega) = \frac{1}{2\pi}\int_{-\infty}^{\infty} R_{xx}(\tau).e^{-j\omega\tau}.d\tau \qquad \textbf{Eq 4.7}$$

It describes the amount of power per unit of frequency as a function of the frequency. PSD indicates the strength of the variance as a function of frequency. It is measured as magnitude squared per frequency and the magnitude within a specific frequency range can be identified by integrating PSD within that frequency range. In evaluating dynamic response of vehicle subjected to random road input, PSD and RMS values are utilised throughout Chapter 4 and 5.

PSD can be calculated using the periodogram function in MATLAB. This is a function in the MATLAB Signal Processing Toolbox. Here, PSD, P_{xx} is calculated using sampling frequency, f_s in Hz, of the response, x. The syntax is given as:

$$[Pxx, f] = periodogram(x, window, nfft, f_s) \qquad \textbf{Eq 4.8}$$

The frequency range, f is determined by the length of the FFT, $nfft$, f_s and response vector, x. A sample calculation and MATLAB commands containing the calculations is available in Appendix IV. The corresponding RMS acceleration is determined by calculating the area under the PSD and is given as:

$$RMS\ Acceleration = \sqrt{\int_{f_1}^{f_2} p_{xx}.df} \qquad \textbf{Eq 4.9}$$

where, f_1 and f_2 are the lower and upper frequency limits

4.5.2 Road Surface Modelling

Generally, vehicles are driven over a variety of road surfaces. Accurate representation of these surfaces is vital, as it plays a significant role in suspension designs [83], and in the context of this research, a reliable fatigue life prediction. The process of modelling road surface starts using measurement techniques either by surveying, using a wheeled profilometer, or with non-contact probes [30]. This is followed by digitising the measured road data into the form of displacement or frequency. In displacement, the road models are then converted into a time domain by dividing the distance travelled with a constant velocity. This form of road representations is employed in this research, and is explained later in this section.

In frequency domain, the road models can be described mathematically using a spectral density function as reported in [30].

$$S(n) = G.n^{-p} \qquad \textbf{Eq 4.10}$$

where *S(n)* is the spectral density as a function of wavenumber, *n* (in cycle/m), *G* is the road roughness coefficient, and *p* is the slope of the spectral density curve (in log-log scale). The surface roughness coefficients typically range from 1 x 10^{-7} for smooth road (motorway) to 5 x 10^{-6} for a rough road (minor road). Figure 4.3 illustrates the spectral density of an average motorway, principal road, and minor road according to the values given in [30]. For normal use, value of *p* of 2.5 is applied in Eq 4.10.

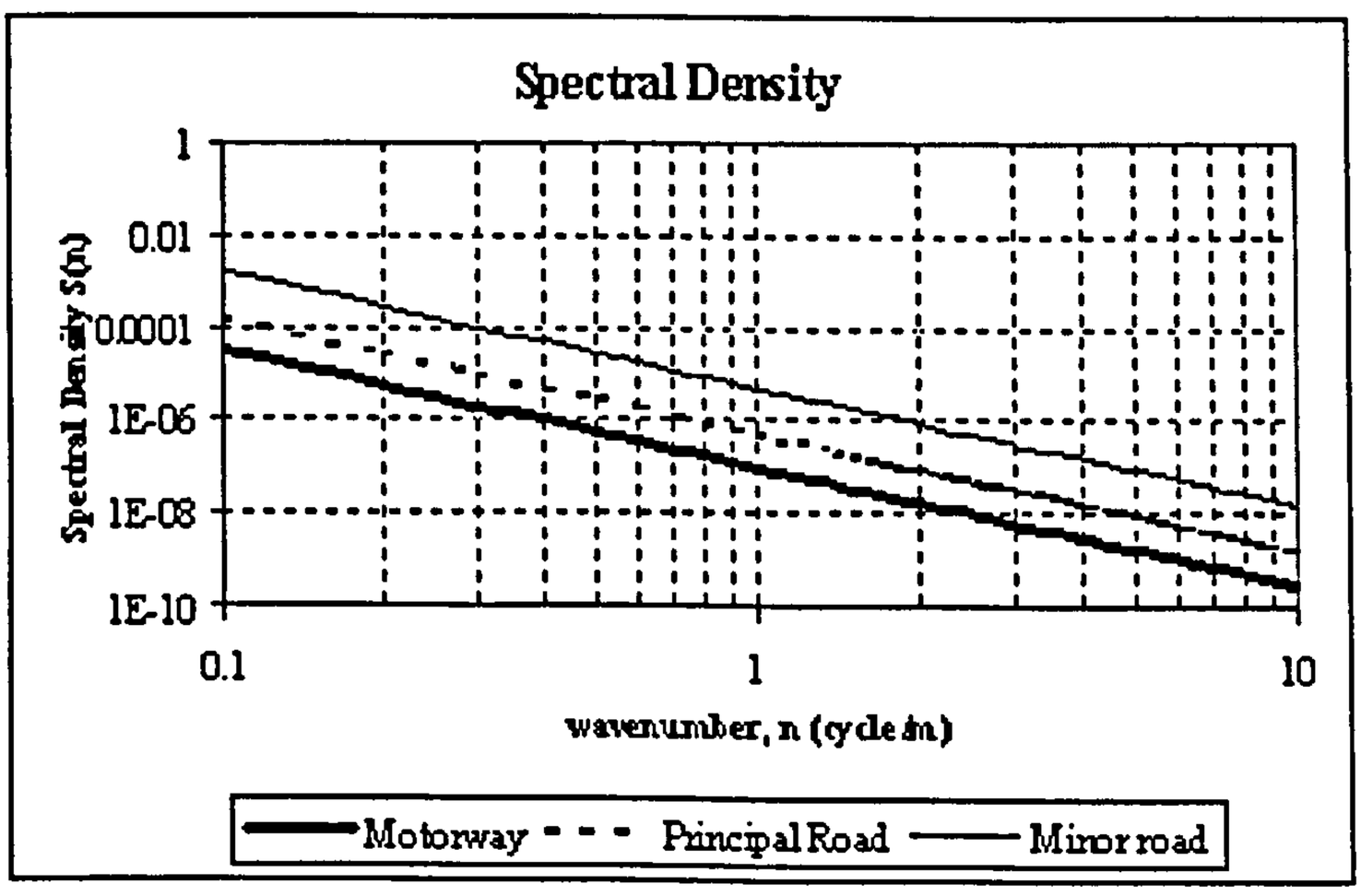

Figure 4.3: Spectral Density of Typical Road Surface [30]

Two categories of road input are used throughout this research. A bump and pothole input for evaluation of transient events and random road inputs for evaluation of ride dynamics. In durability analysis, these road models impose different forms of loading on the components. While, there are many studies involving durability under the influence of random road excitations, very few reported in the literature have examined durability due to transient events. In this research, the transient road input in Figure 4.4 combines a bump profile from Blundell and Harty [15] and a pothole profile from Sui and Hirschey [106] while Figure 4.5 shows the profiles at 34 km/h, built in MATLAB/Simulink which is employed as an input in the MBS cosimulation.

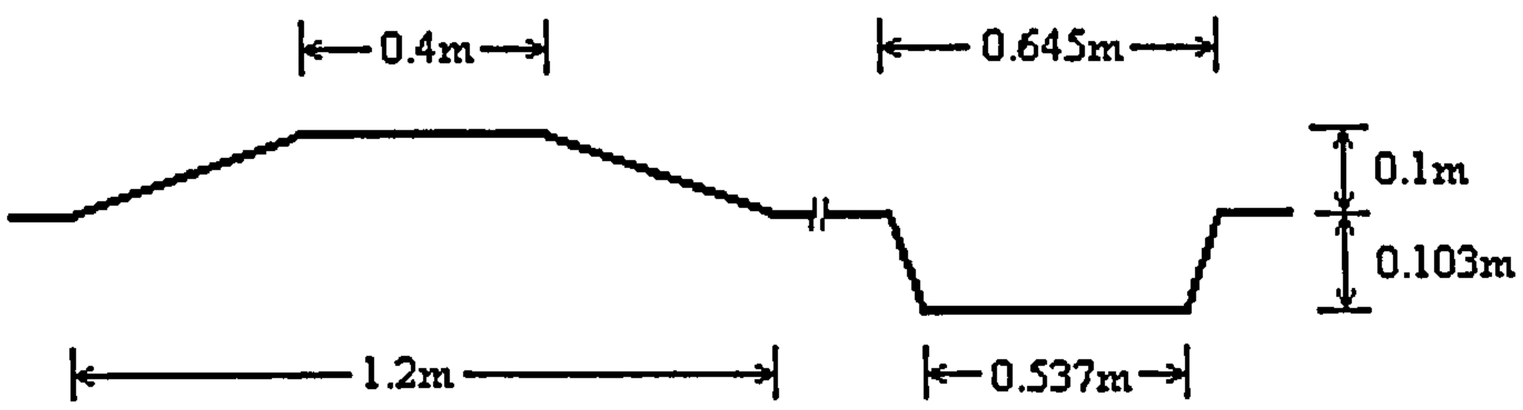

Figure 4.4: Bump and Pothole Road Profile

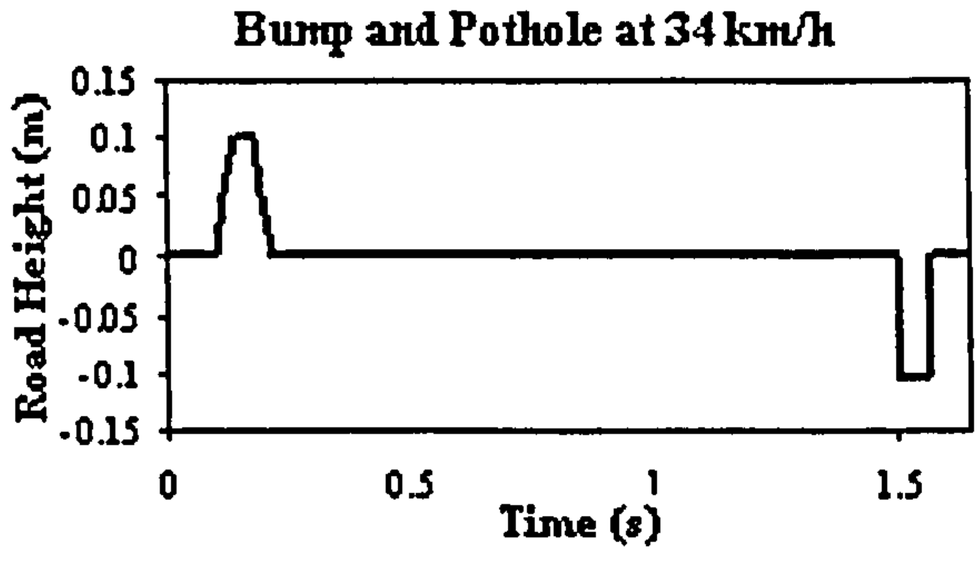

Figure 4.5: Bump and Pothole at 34 km/h (9.44 m/s)

In order to examine the ride dynamics of the selected vehicle models, two forms of virtual random road surfaces are adopted throughout this chapter and the next. They are:

a. Smooth tracks (courtesy of MIRA Ltd) as shown in Figure 4.6(a) and (b). The smooth road tracks are used to represent normal driving conditions mainly to determine the performance of the MR damper in the semi-active applications in Chapter 5.

b. The rough road surfaces (courtesy of Leyland Technical Centre, LTC Ltd.) as illustrated in Figure 4.7(a) and (b). These surfaces, also known as durability tracks, are utilised for fatigue life prediction in Chapter 6. They are also used for investigating the effect of road roughness on the performance of semi-active systems. These durability road profiles are built such that accelerated durability tests can be conducted since general road surfaces inflicted insignificant damage to vehicle components over short durations. They consist of specifically designed track elements that would simulate extreme driving

conditions [1]. Each of the wheels will have its distinctive displacement along the tracks inducing the vehicle body to bounce, pitch and roll. This imposes severe loading to vehicle components. These 350 meters virtual pavé tracks are measured at a constant forward velocity of 34 km/h and digitised in the form of road height as a function of distance. In MBS cosimulation, the digitised road profiles are converted from the numerical format in Microsoft Excel and stored in MATLAB as a 2D array. This method is simpler to develop unlike the method by [1] where the numerical road data are modelled as road surface using a CAD package.

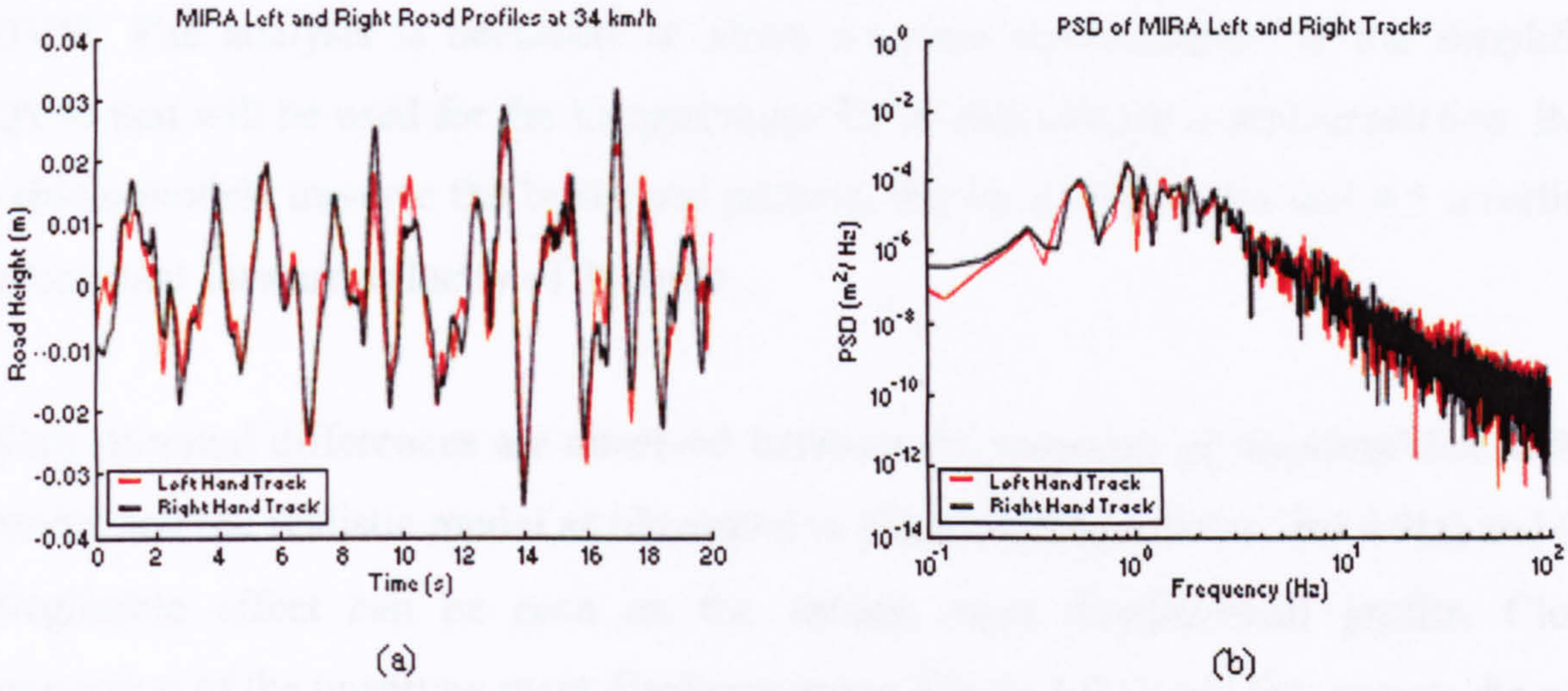

Figure 4.6: MIRA Tracks Left and Right Hand at 34 km/h (Smooth Road)
(a) Time Domain; (b) Frequency Domain (PSD)

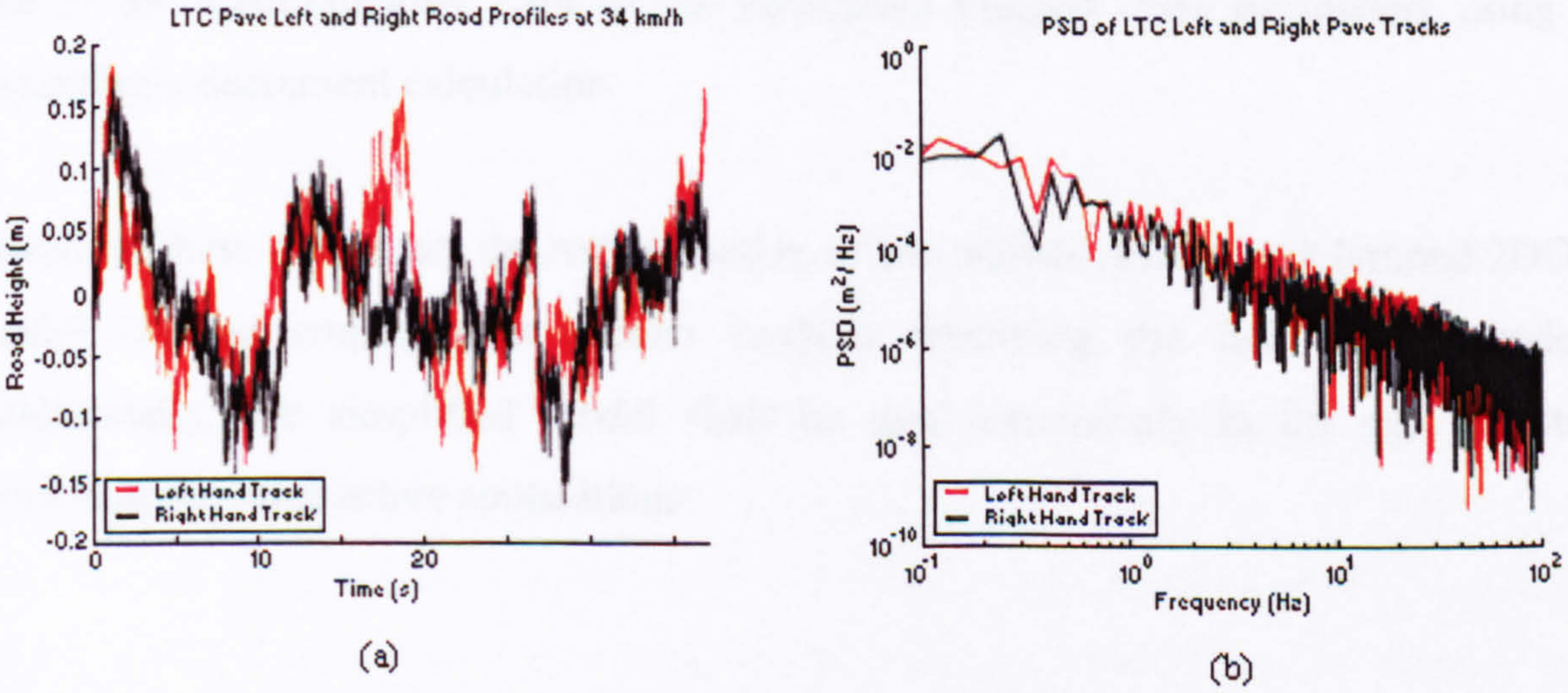

Figure 4.7: LTC Pavé Left and Right Hand Tracks at 34 km/h (Rough Road)
(a) Time Domain; (b) Frequency Domain (PSD)

4.6 Results and Analysis

Observations made in this chapter are centred on the dynamic ride response of an MPV with passive suspension, modelled as a lumped mass 2DOF QVM, a realistic QVM, and a lumped mass 7DOF FVM in an unladen state. The findings will be used as benchmarks in the following two chapters.

4.6.1 Dynamic Simulation of MPV Quarter Vehicle Models

The first analysis involves correlation between the lumped mass 2DOF QVM derived from the logarithmic decrement calculation and the reference model of the realistic QVM. The analysis is necessary to attain accurate representation of the simplified QVM that will be used for the lumped mass 7DOF full vehicle model simulation. Both vehicle models traverse the bump and pothole, shown in Figure 4.4 and 4.5 travelling at constant forward velocity of 34 km/h.

Very minimal differences are observed between the response of the simplified 2DOF model and the realistic model as illustrated in Figure 4.8(a) and (b), and 4.9(a) and (b). Negligible effect can be seen on the sprung mass displacement profile. Closer inspection of the unsprung mass displacement in Figure 4.9(a) and (b), reveals the peak value for the lumped mass model slightly overestimates those of the realistic model. It is apparent that, it entails slightly longer settling time than those from the realistic model. Minor variations between the unsprung mass response of the two models are due to the approximation error of the equivalent lumped mass parameters using a logarithmic decrement calculation.

Based on these outcomes, the representation of the realistic model as a lumped 2DOF model can be employed in further analysis involving the full vehicle model. Additionally, the simplified model shall be used extensively in the next chapter involving the semi-active applications.

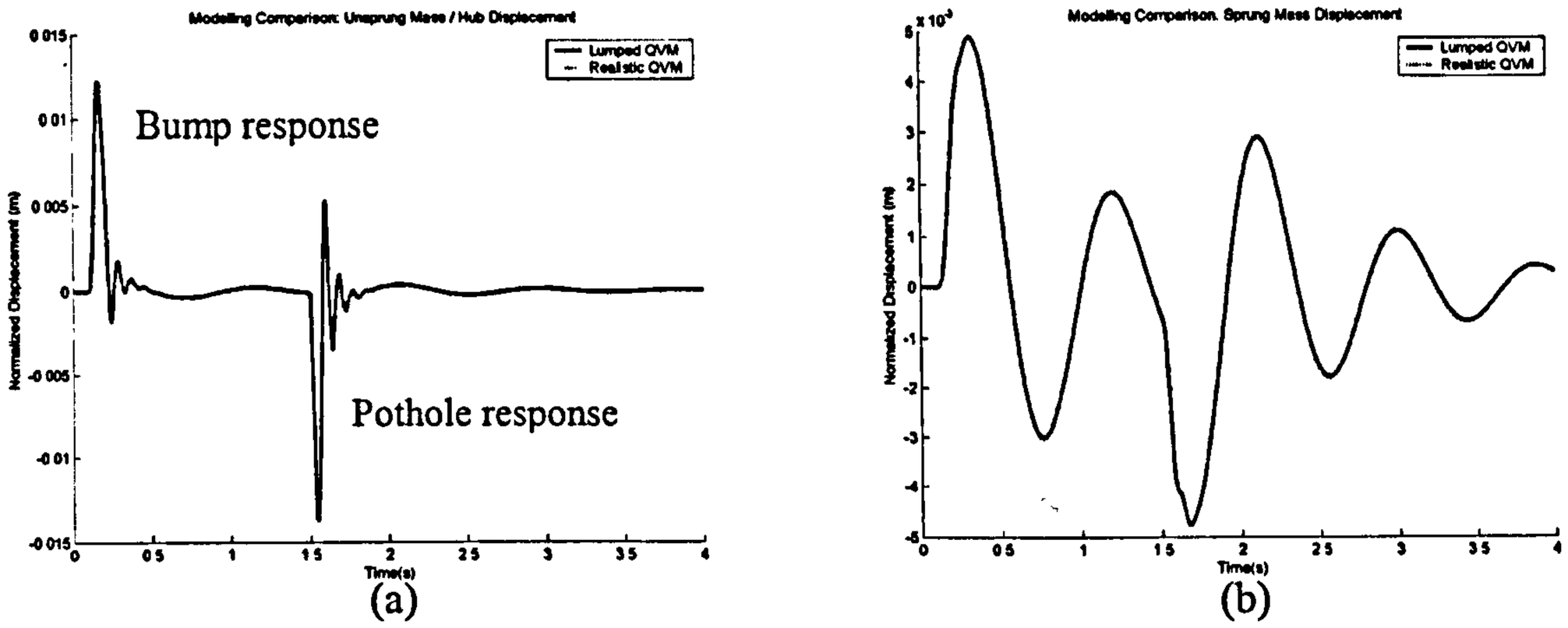

Figure 4.8: Bump and Pothole Response (a) Unsprung Mass; (b) Sprung Mass

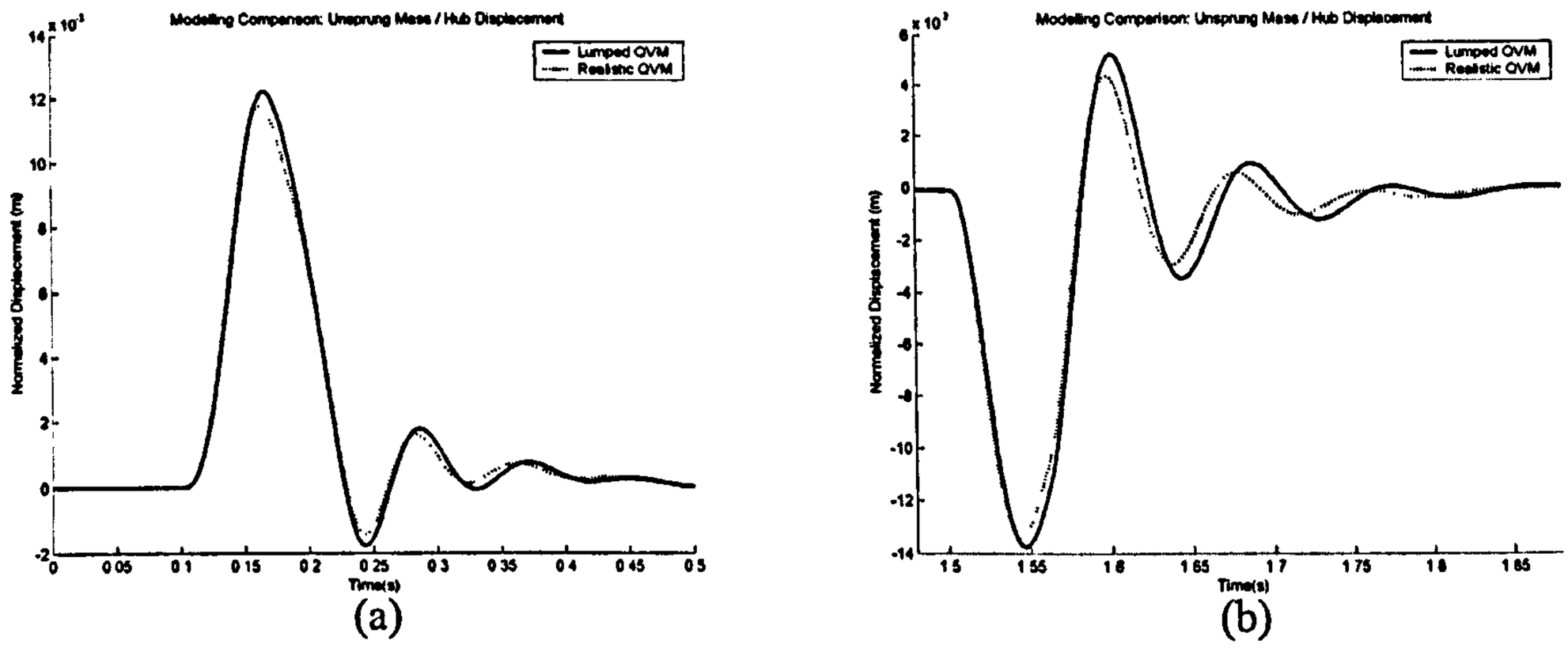

Figure 4.9: Close-up of Unsprung Mass Response (a) Bump; (b) Pothole

4.6.2 Dynamic Simulation of MPV Realistic Suspension Model

In this analysis, the MPV with realistic suspension model is driven over the right hand side of the LTC pavé track at a constant forward velocity of 34 km/h. It attempts to establish and evaluate the response of MPV suspension components subjected to random excitation. The response is recorded in three principal directions, namely longitudinal (X), lateral (Y) and vertical (Z) with respect to the vehicle centreline from front to rear. Each signal is sampled every 2 milliseconds for the entire 350 m track length for 37 s. Analysis centres on the acceleration response in the time domain and expressed as PSD as illustrated in Figure 4.10(a) and (b) to Figure 4.13(a) and (b). RMS acceleration is calculated in a range from 0 to 20 Hz and is tabulated in Table 4.5

The time and spectral plots suggest that most of the dynamic response is concentrated in the vertical direction compared to the longitudinal and lateral directions. This is true for all suspension components and the sprung mass since the road undulations are defined along the same direction. The longitudinal and lateral vibrations appear to be relatively small in comparison with the magnitude in vertical direction. Lateral vibrations at the suspension components register higher levels mainly due to the suspension system hitting the bump stop while the response in longitudinal direction is associated with the forward motion of the vehicle traversing road irregularities.

Closer inspection of the RMS vertical acceleration indicates a gradual decrement in vibration energy as it progresses from the hub to the vehicle body. Most of this energy is generated by resonance of the vehicle and its components resulting from the random road excitation. PSD accelerations of the suspension components shown in Figure 4.10(b)-4.12(b) illustrate the influence of the wheel hop frequency. Similar representation of the vehicle body as shown in Figure 4.13(b) demonstrates the dominance of lower frequencies originating from the natural frequency of the vehicle body. However, a clearer indication of the wheel hop frequency from the PSD plots could not be obtained. This is due to the periodogram function employed for this analysis which did not consider other signal processing functions such as overlapping process [102]. To account for a long span of time signal as the vehicle traverses the track, a rectangular window is selected. Rectangular window or no window is suitable for analysing pseudo-random signals that generate no leakage when transforming the time domain signal into the frequency domain using the FFT process. As a result, the PSD plots register all disturbances along the track as the vehicle passes through. There are other forms of windowing functions such as Flattop and Hanning windows which are generally utilised for periodic signals.

During actual driving conditions, the time histories obtained with data acquisition are passed through signal processing sequences so that the PSDs provide meaningful representations of the wheel hop and body bounce frequencies. For example the overlapping process uses a segment of the time signal to calculate the PSD which not only will reduce the time of FFT computation but also improve the PSD representation.

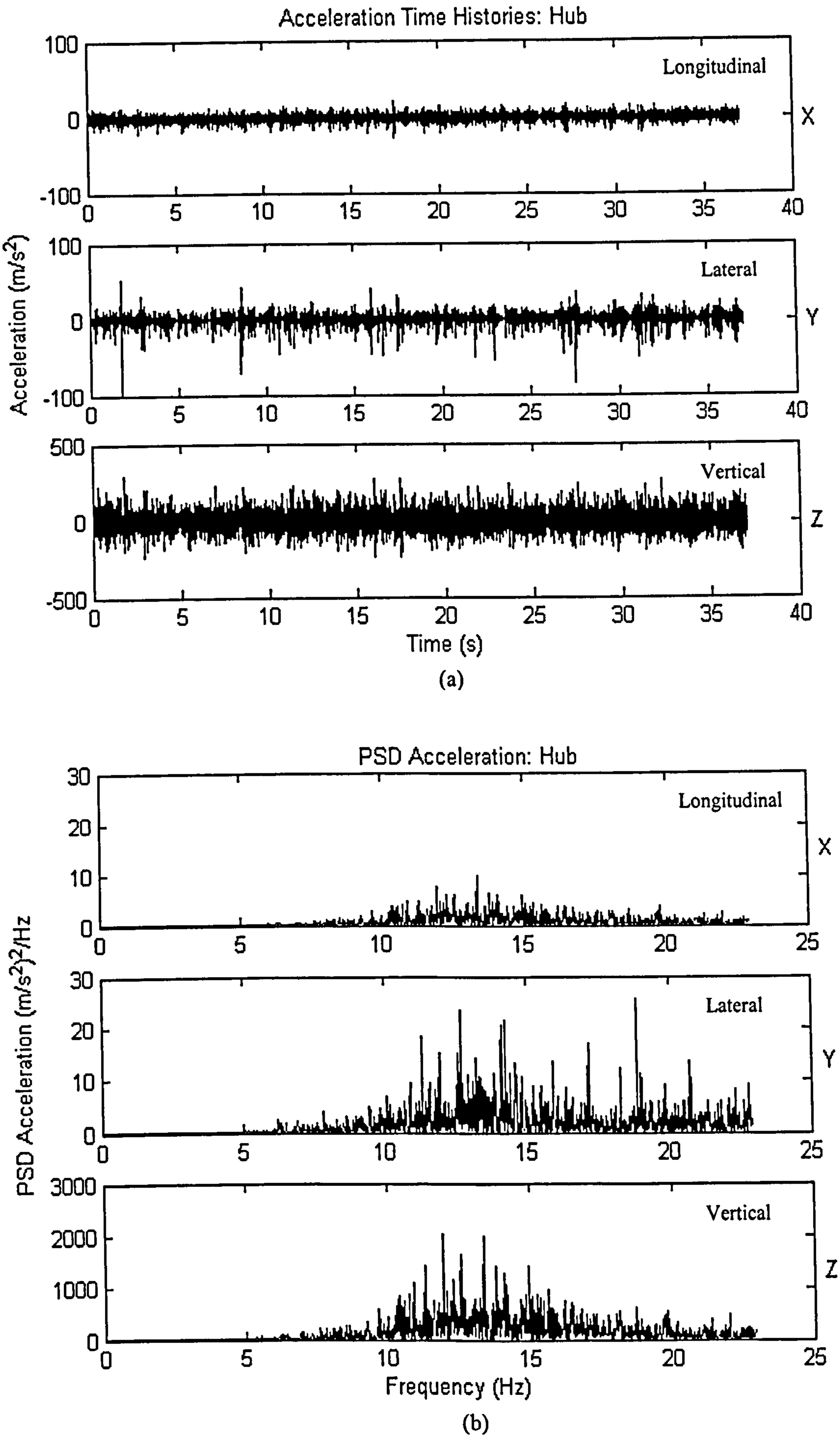

(a)

(b)

Figure 4.10: Hub Acceleration; (a) Time Histories and (b) PSD

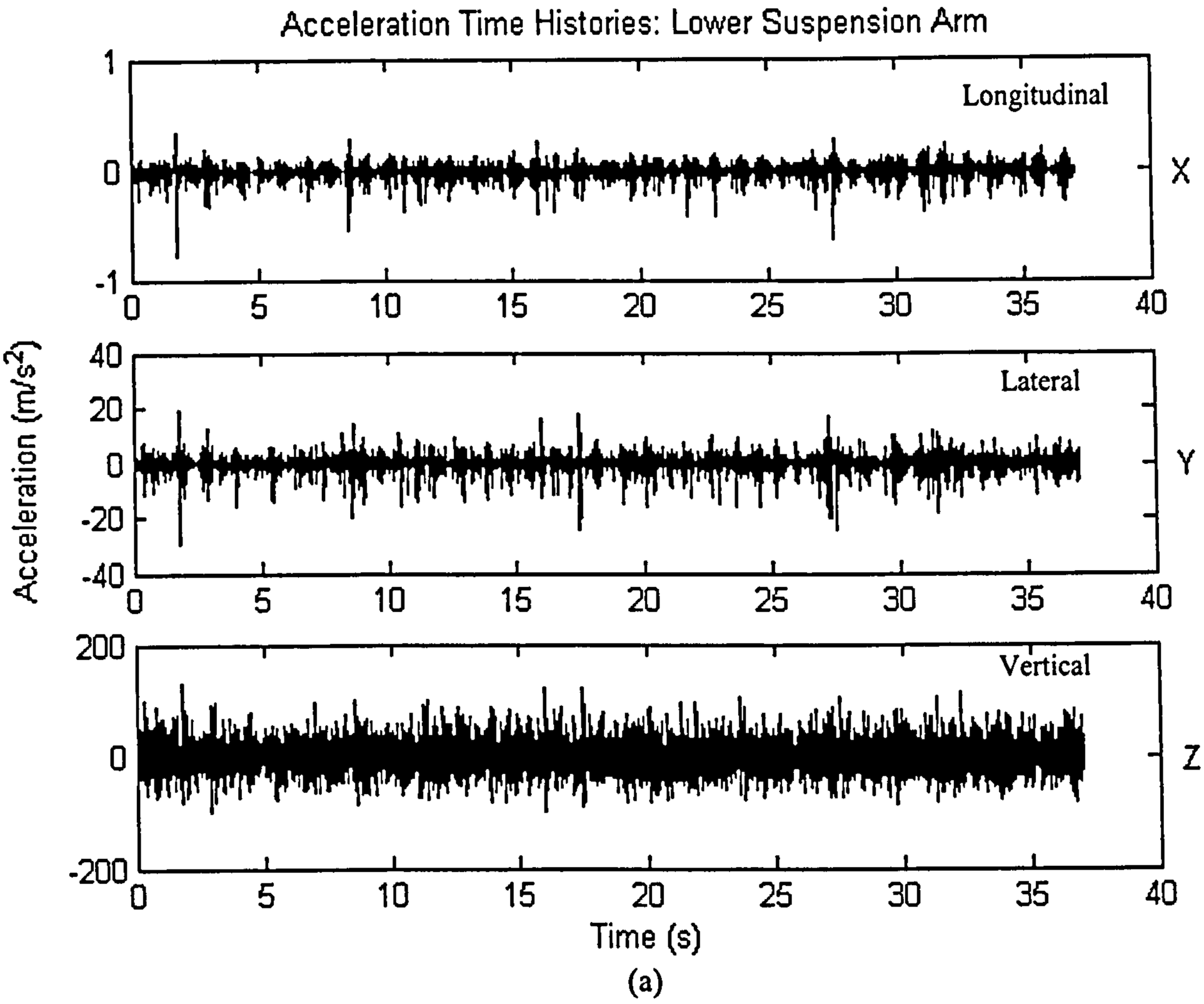

Figure 4.11: Lower Arm Acceleration; (a) Time Histories and (b) PSD

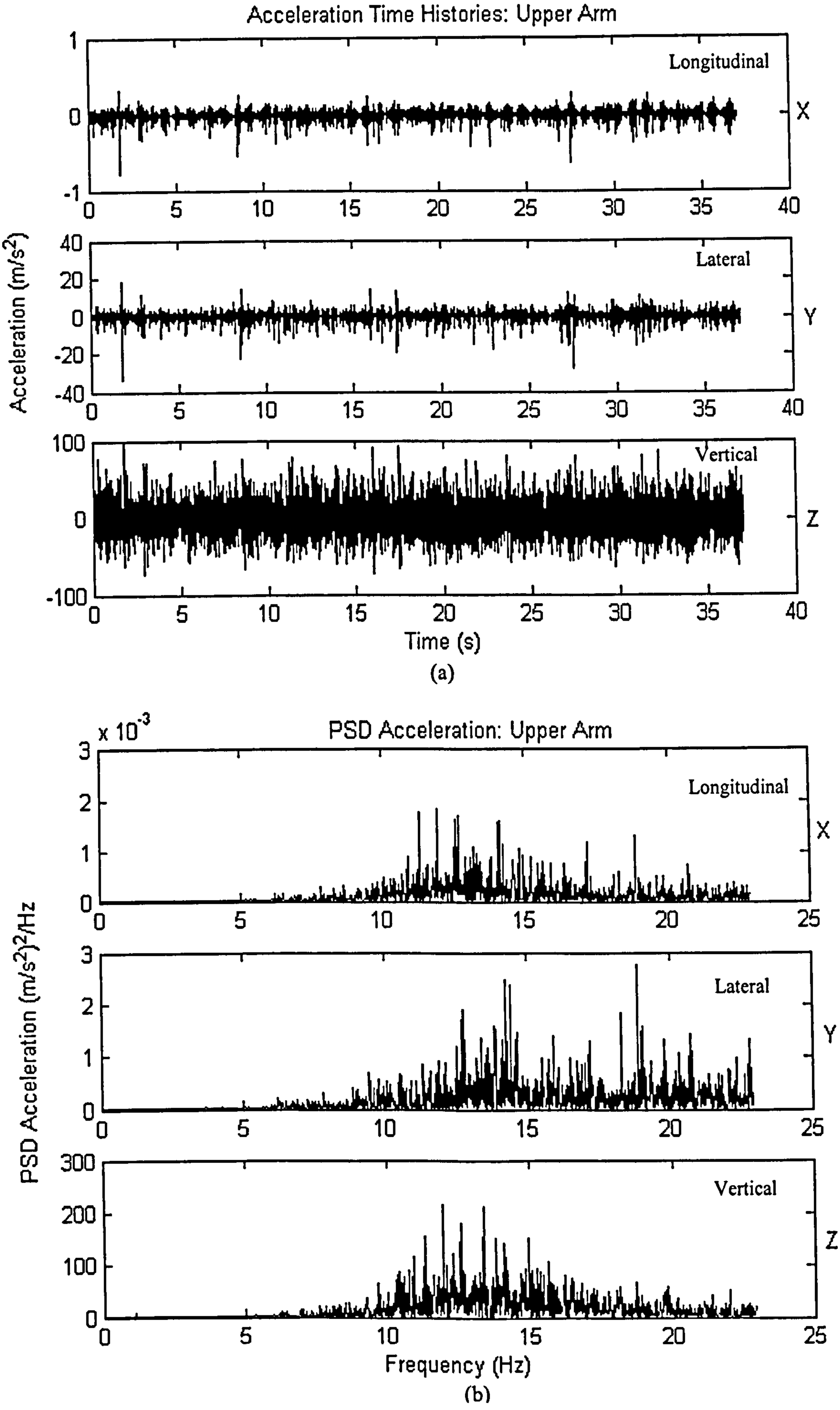

Figure 4.12: Upper Arm Acceleration; (a) Time Histories and (b) PSD

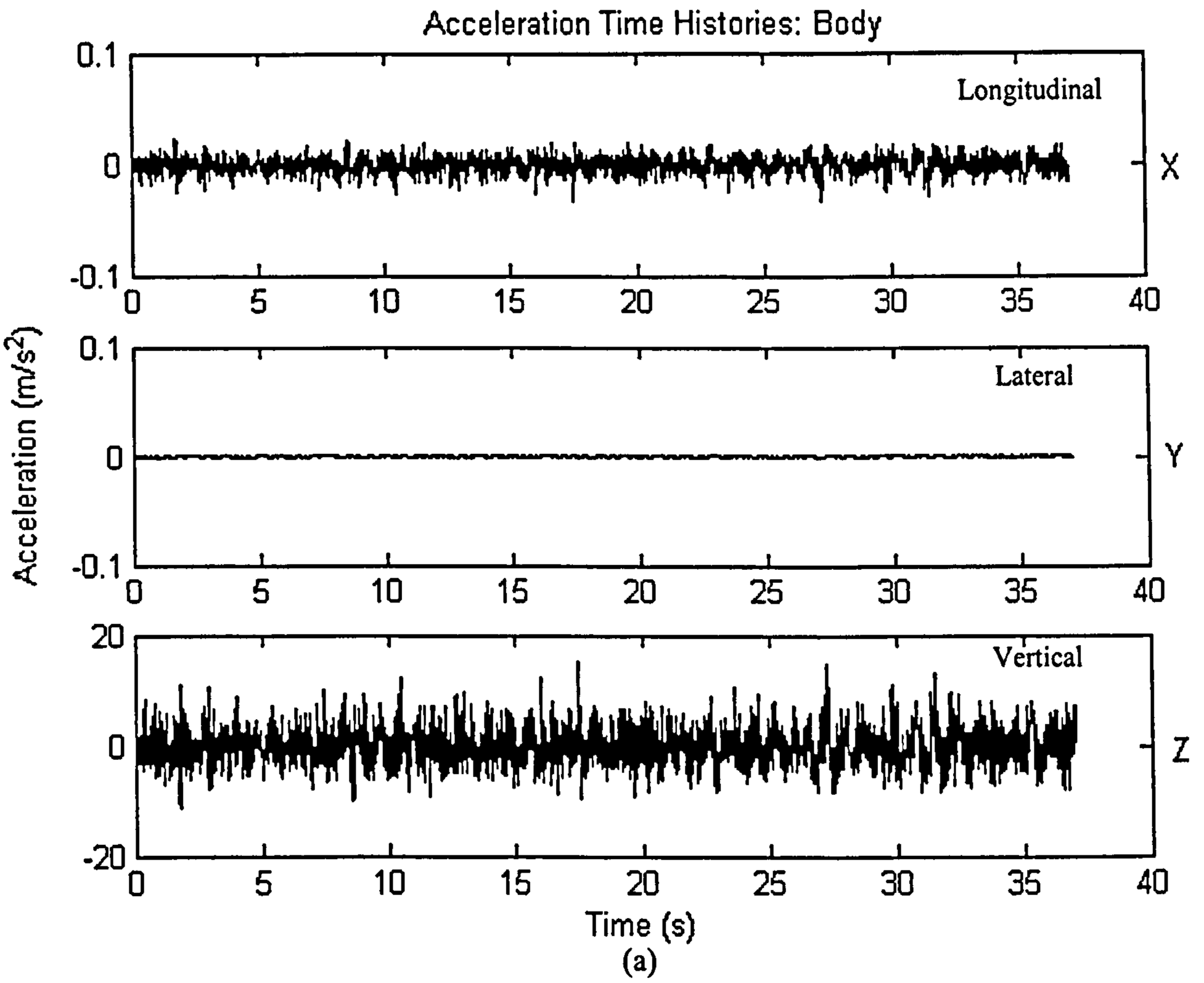

Figure 4.13: Body Acceleration; (a) Time Histories and (b) PSD

Directions		RMS Acceleration in m/s^2 (0-20 Hz)			
		Hub	**Lower Arm**	**Upper Arm**	**Body**
X	Longitudinal	4.0869	0.05188	0.00538	0.00689
Y	Lateral	6.1954	2.4169	2.0212	0.00011
Z	Vertical	59.216	25.683	19.376	3.2274

Table 4.5: RMS Acceleration of the Realistic QVM Suspension Components

4.6.3 Dynamic Simulation of a Full Vehicle Model

To evaluate any significant differences in dynamic behaviour between a full and a quarter vehicle response, the analysis continues by investigating the dynamic response of a full vehicle ride model subjected to a transient road input. This is essential particularly when assessing semi-active systems where most of the control algorithms are developed based on quarter vehicle models. Implementing such a system in a full vehicle model may or may not produce the desired results as in a QVM application. As the degrees of freedom increase, the vehicle body is not only confine to move vertically as in a QVM application, but also is influenced by rotational motions around the vehicle centre of gravity.

Constructing a full vehicle model in MSC.visualNastran can be done either with a distributed sprung mass or using lumped masses at each corner of the vehicle. The difference between the two models in terms of dynamic response is negligible as reported by Hudson [103]. He provides a comprehensive analysis on a typical saloon car with a passive suspension system. The vehicle models include a QVM, HVM, and FVM subjected to sinusoidal and step inputs. Hence, in this research, an FVM with lumped mass is adopted. This is to allow sprung mass response at each corner to be utilised as a feedback input to the damper force when the MBS cosimulation approach is employed. The suspension system is assumed to be independent so that the effect of body motions can be thoroughly assessed.

The lumped mass FVM of the MPV (Figure 3.1), is driven over the bump and pothole profile shown in Figure 4.4 and Figure 4.5 at a constant forward velocity of 34 km/h. To aid analysis, the simulation is simplified by having only the front right hand side of the FVM allowed to strike the pothole. Generally, for a vehicle travelling on a straight path, the rear section will eventually hit the obstacle at a certain time delay that can be calculated as:

$$v = \frac{d_{wb}}{t_d} \qquad \textbf{Eq 4.11}$$

where, v denotes constant forward velocity, d_{wb} is the wheelbase distance, and t_d represents the corresponding time delay between the front and the rear wheel.

Figure 4.14 – Figure 4.19 show the displacement response of FVM due to the transient excitation. Evaluating the FVM response at each corner and the QVM response for the sprung and unsprung mass reveal the following characteristics:

a. The FVM unsprung mass responses clearly indicate that the assumption of a fully independent suspension remains valid. It can be observed that there is minimal impact at the other three suspension corners as the front right wheel strikes the bump and pothole (Figure 4.14 and 4.15). Additionally, comparing the FVM and the QVM show nearly similar responses when the wheel hits the bump and pothole, as illustrated in Figure 4.14 and Figure 4.15, although slight differences in the signatures was observed when encountering the pothole.

b. Even though the amplitudes of the lateral (Figure 4.18) and the longitudinal (4.19) motions are much smaller than that of in the vertical direction, these roll and pitch motions of the vehicle body have provided some damping effect to the vertical motion. This can be seen by observing the vertical response between the FVM and QVM as illustrated in Figure 4.17.

c. Observing the sprung mass vertical response in Figure 4.17 clearly suggests that, with the absence of body lateral and longitudinal motions, QVM overestimates the displacement response. The FVM displacement signatures

show higher damping than those from the QVM. This can be seen with a shorter settling time in which the successive peaks produce greater attenuation. Similar findings are observed by Ramli *et al.* [99] and Levesley *et al.* [6]. However, in both papers only a single transient event was employed in which the residual effect of the latter excitation was not realized.

These outcomes are expected to significantly influence the dynamic behaviour when semi-active control systems are employed. Two key elements will be ascertained. Firstly, to assess the effect of implementing semi active control derived from a QVM, on the FVM, as finding suggests the QVM dynamic response considerably overestimates those of the FVM. Secondly, to evaluate how much pitch and roll motions in the FVM affect the performance of semi-active control based on a QVM. This will be studied in detail in Chapter Five, focussing on the aspect of dynamic load prediction. Ultimately, these assessments will provide valuable insight to the load histories, which will eventually be used to evaluate fatigue life of a given suspension component.

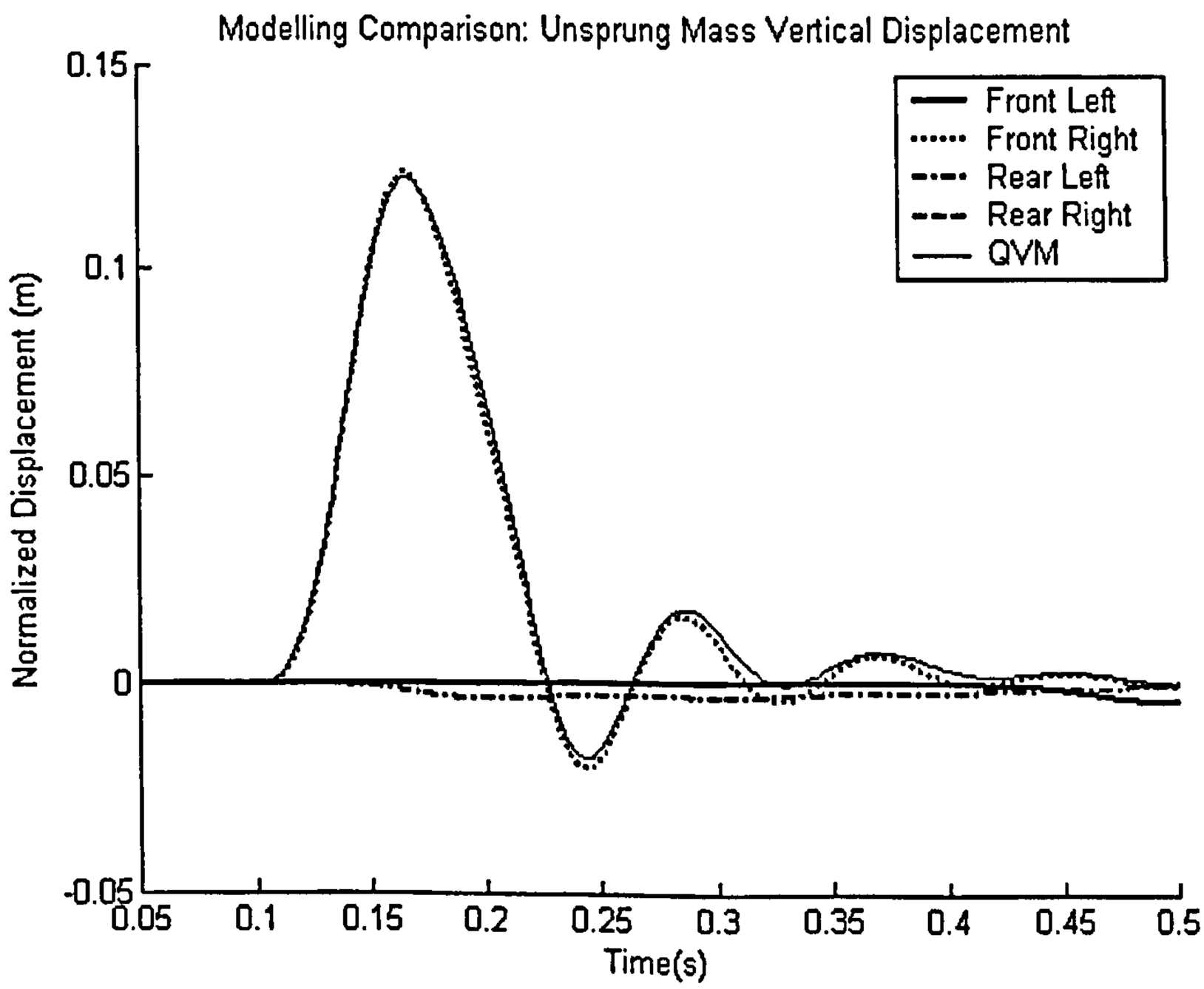

Figure 4.14: Close-up of Unsprung Mass Response – Bump

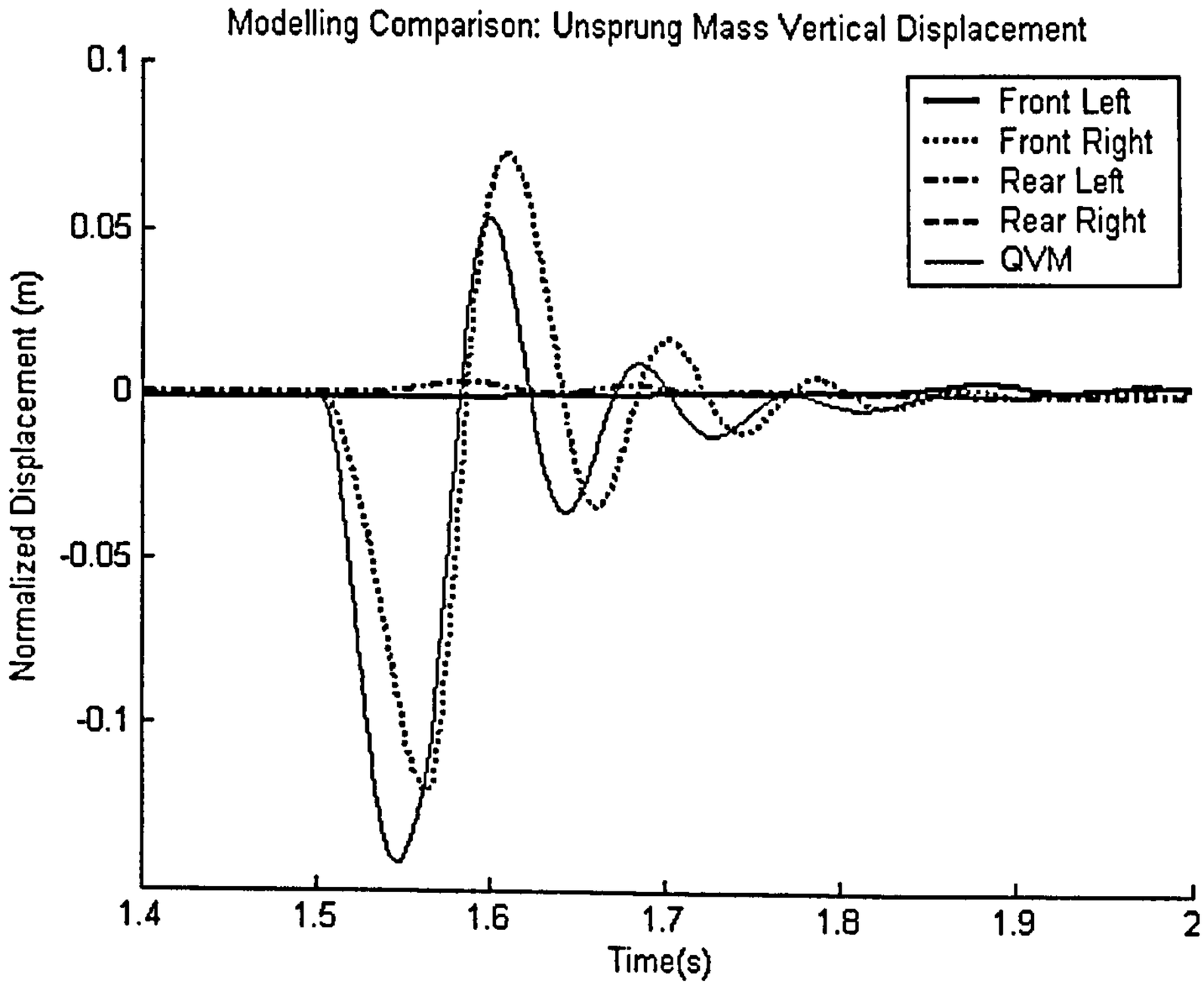

Figure 4.15: Close-up of Unsprung Mass Response – Pothole

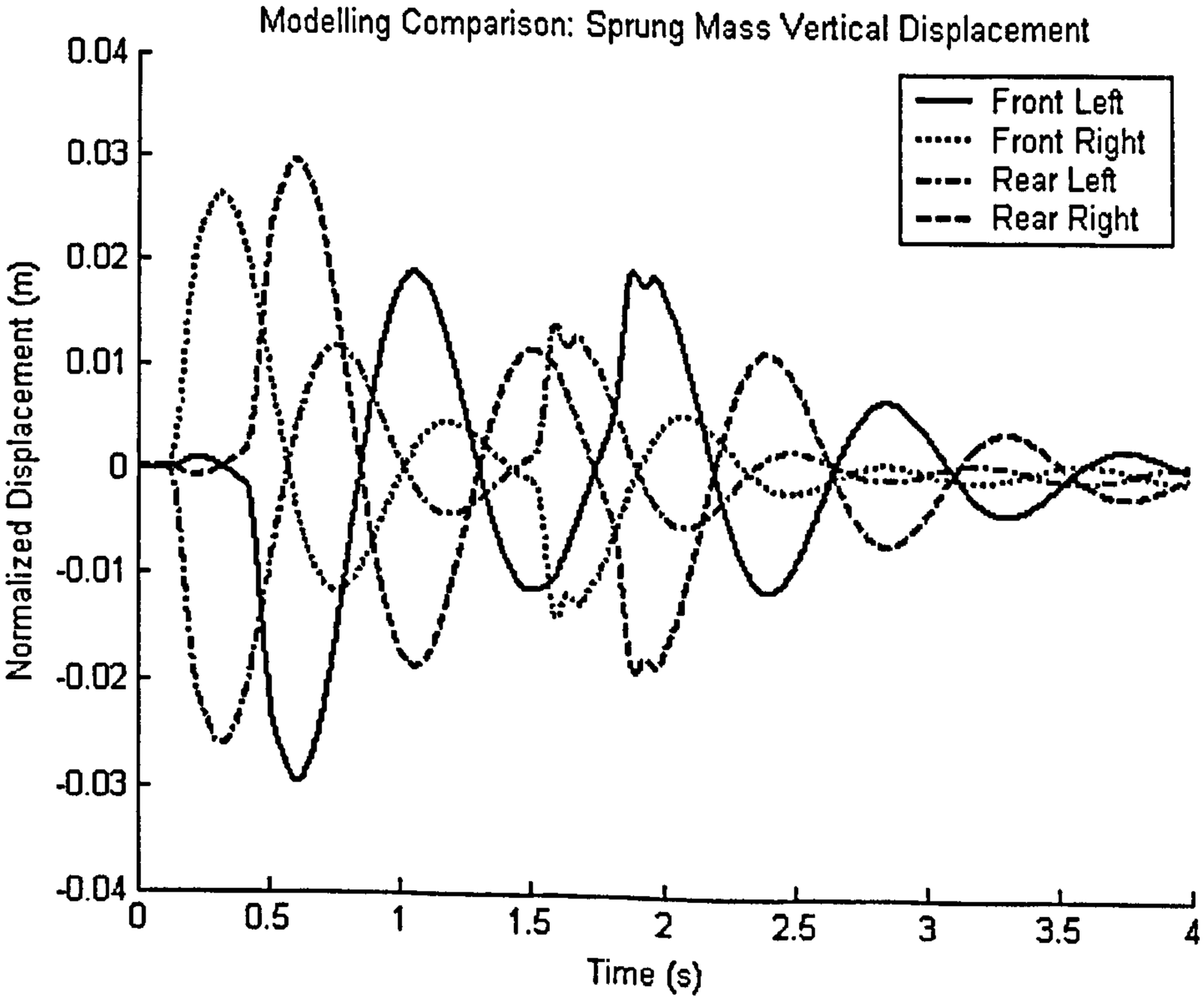

Figure 4.16: Sprung Mass Response of Lumped Mass FVM at All Corners

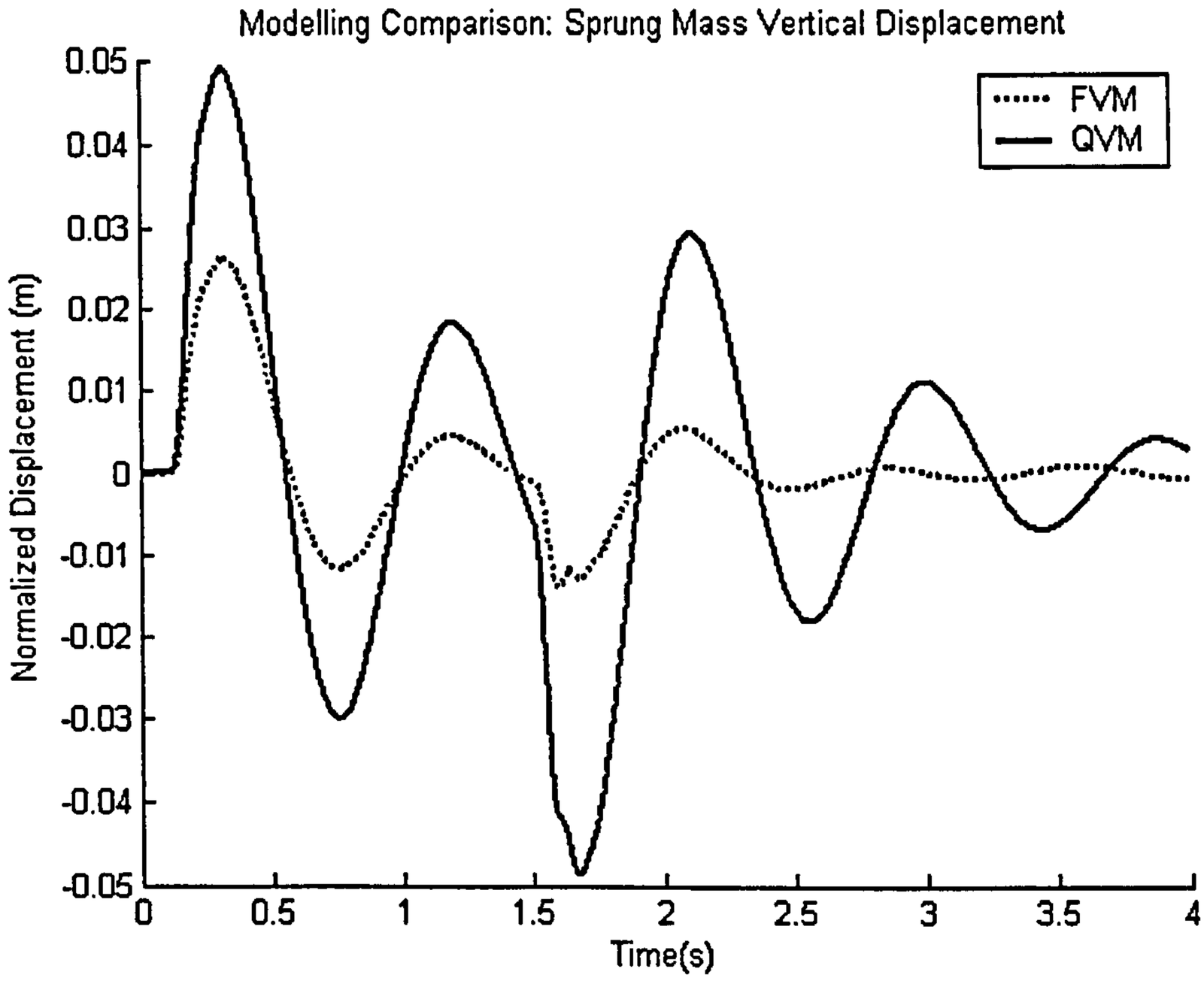

Figure 4.17: Sprung Mass Response between FVM (Front Right) and QVM

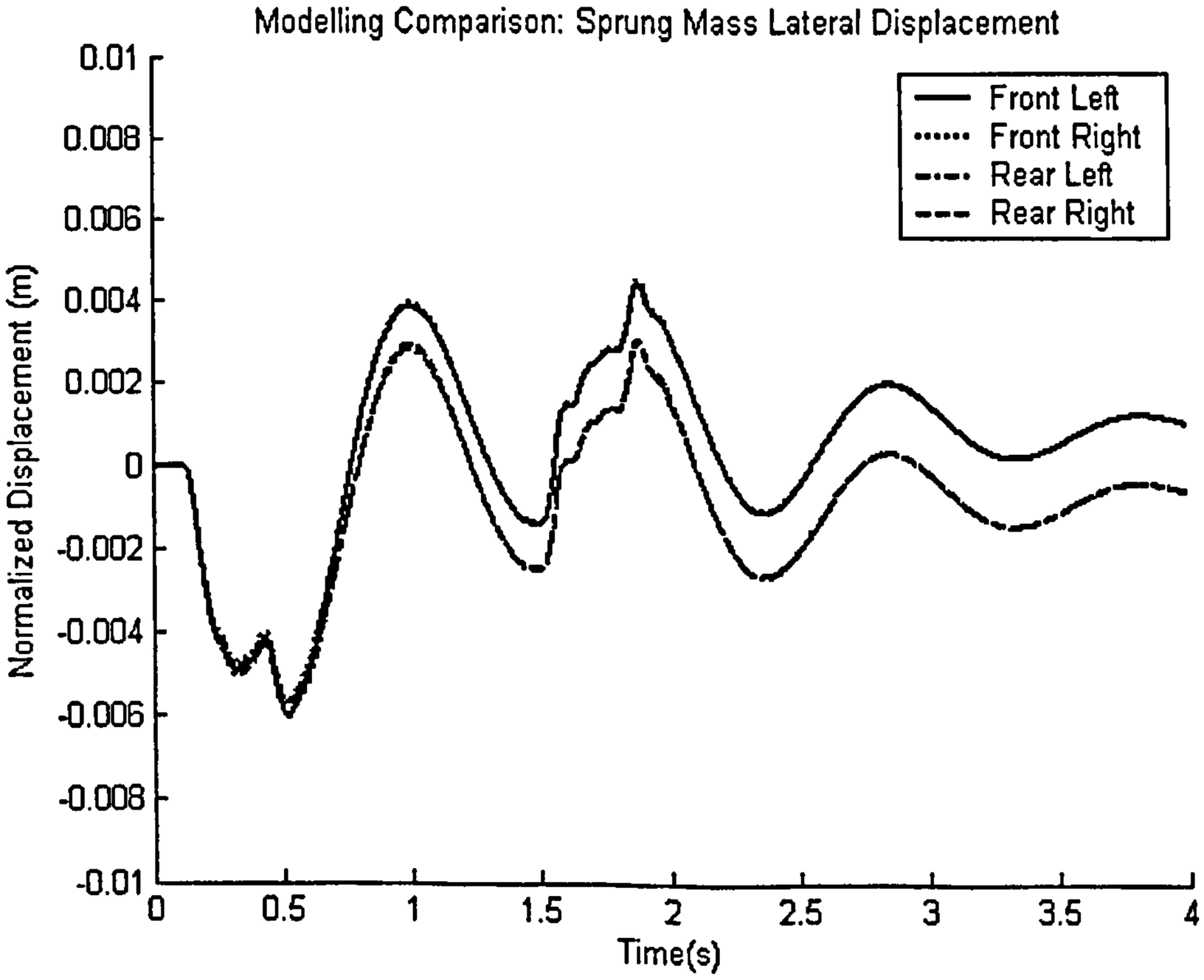

Figure 4.18: Sprung Mass Lateral Response of Lumped FVM

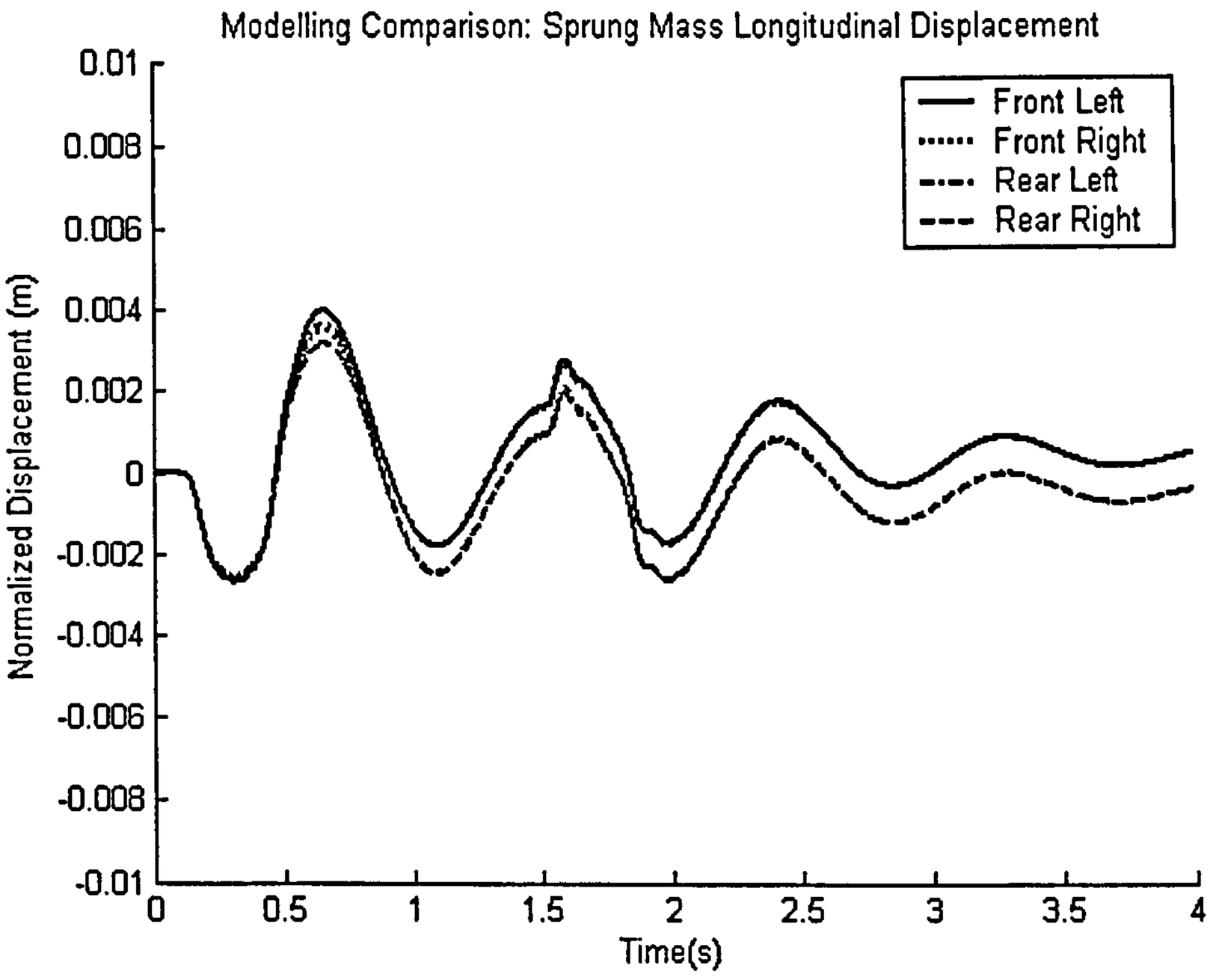

Figure 4.19: Sprung Mass Longitudinal Response of Lumped FVM

4.7 Conclusions

This chapter has described important aspects of modelling vehicles with increasing complexity and its relation with the dynamic response when subjected to potentially damaging road inputs. In general, the QVM simulation response overestimates displacements when compared to those from FVM particularly for the sprung mass. The vehicle body pitch and roll motions of the FVM appear to have dampening effects on the body vertical response. This would impinge on the vehicle dynamic responses when semi-active control systems are applied, as many semi-active controller theories are derived based on a QVM. However, the usage of quarter vehicle models remains vital for supporting evaluation of existing semi-active control theories.

The MBS cosimulation approach has again demonstrated a degree of flexibility when building complex vehicle models, unlike a purely mathematical approach or a purely MBS approach. Lengthy and complicated derivation of equations of motions using the mathematical method can be replaced with geometric models within an MBS. Previously, the representation of road surface in an MBS environment requires

conversion of the digitised road data into a 3D surface modelled in a CAD package. This process can be tedious and time consuming if a variety of road surfaces are to be considered. Alternatively, MBS cosimulation allows the digitised road data to be used in its original form, where only minimum effort is required to convert the data into the format recognisable by the mathematical code. The only drawback to this approach is that it requires longer simulation time than the other approaches.

CHAPTER FIVE

Dynamic Analysis of Semi-Active Control Systems

5.1 Introduction

The work presented in the last two chapters focuses entirely on dynamic analysis of vehicle with passive suspension systems. Some of the findings will be used as benchmarks involving dynamic analysis and fatigue life assessment of semi-active control systems. This chapter examines the effects of selected local and global semi-active control strategies on the vehicle dynamic response. This includes analysis of load histories of a suspension component that will be employed later in the next chapter on fatigue life prediction. Local and global control laws are developed and analysed. The local control strategies consist of two-state switchable (TSS) semi-active systems that adopt skyhook control theory, and control algorithms for an MR damper model derived from experimental data. Inclusion of an MR damper model attempts to demonstrate the ability and limitations of MBS cosimulation to produce load histories based on realistic semi-active applications. The effects of global control strategies on the dynamic response are evaluated based on implementation of a semi-active algorithm that includes pitch and roll motions of a full vehicle model. The vehicle models are subjected to transient and random road inputs with a simple point contact tyre model.

5.2 MR Damper Model

In recent years, the use of magnetorheological (MR) dampers has received increasing interests as an affordable and reliable semi-active device [61, 68, 85, 112, 113]. It works principally by manipulating the viscosity of MR fluid when it is exposed to a magnetic field. The fluid consists of very small iron particles submerge in a carrier

liquid such as mineral oil, synthetic oil, water or glycol. When a control current is passed through the coils located at both ends of the fluid, a magnetic field is induced. The fluid modifies its rheological behaviour according to the changes in magnetic polarization induced by the control current, effectively altering the damping characteristics of the damper. The changes from free-flowing state to semi-solid are reversible and occur almost instantaneously.

This study utilizes the Carrera Magneshock™ MR damper model. Fluid damping characteristics are varied according to the coil current which generates an electromagnetic field within the fluid. The fluid characteristics of the Carrera Magneshock™ are shown in Figure 5.1, expressed as experimental force-velocity data [114]. With zero control current, the MR damper acts like a conventional passive damper. As control current is passed through the coil the fluid characteristics change in accordance to the applied current. The dependency on current flow can be simplified using a Bingham plastic flow model as describe by Peel and Bullough [115]. Generally, fluid that complies with the Bingham plastic model shown in Figure 5.2(a) requires a minimum shear stress, τ to initiate flow. It displays a linear shear-stress and shear-rate behaviour after reaching the stress at threshold and can be expressed as the following equation [116].

$$\tau = Y_p + PV(\gamma) \qquad \textbf{Eq 5.1}$$

where, τ is shear stress, Y_p is the fluid plastic viscosity or the stress at threshold, PV is the slope of the Bingham fluid model , and γ is shear rate (1/sec).

In developing a control model, the discontinuity of the Bingham fluid model (finite yield force, F_y at zero velocity) creates modelling difficulties and is not suitable when adopting MBS cosimulation approach. Alternatively, a bi-viscous model as shown in Figure 5.2(b) introduced by John and Wereley [117] and Sims *et al.* [113], assumes a pre-yield and a post yield damping states. Pre-yield damping, C_{pre} exhibits a very high damping value at very low velocity and a post-yield C_{post} damping is similar to the Bingham model. The bi-viscous model can be expressed mathematically as the following equation.

$$c(\dot{z}_w - \dot{z}_b, I) = \begin{cases} C_{pre}(\dot{z}_w - \dot{z}_b) & \text{if } (\dot{z}_w - \dot{z}_b) \le F_y C_{pre} \\ C_{post}(\dot{z}_w - \dot{z}_b) + F_y \operatorname{sgn}(\dot{z}_w - \dot{z}_b) & \text{if } (\dot{z}_w - \dot{z}_b) \ge F_y C_{pre} \end{cases} \quad \textbf{Eq 5.2}$$

where, c_{pre} is the pre-yield damping, c_{post} is the post yield damping and F_y is the yield force.

Table 5.1 shows the values of C_{pre}, C_{post}, and F_y derived from experimental data [111, 114]. Without the discontinuity as in the Bingham model, the controller model can be implemented within MBS cosimulation environment.

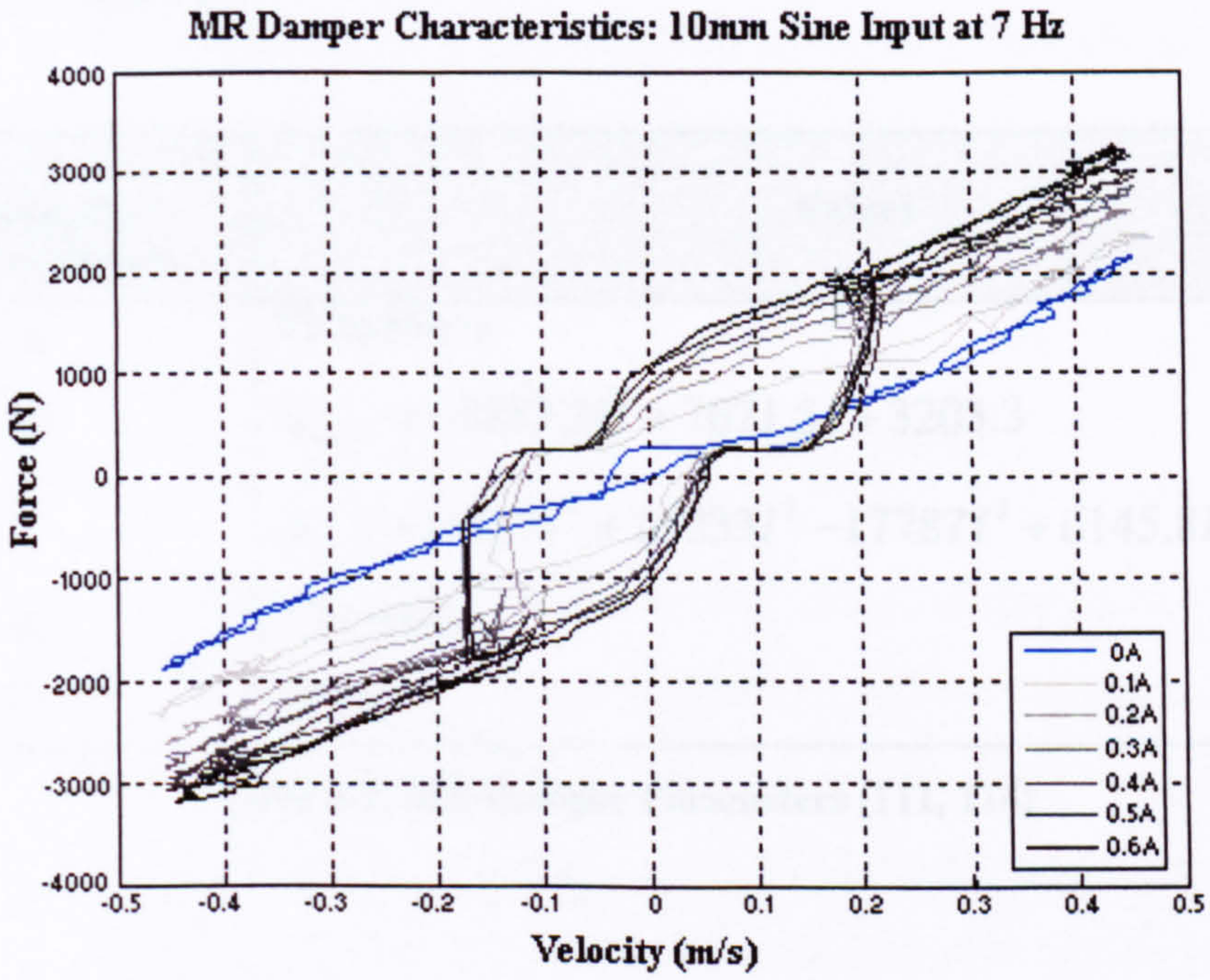

Figure 5.1: MR Damper Experimental Characteristics [111, 114]

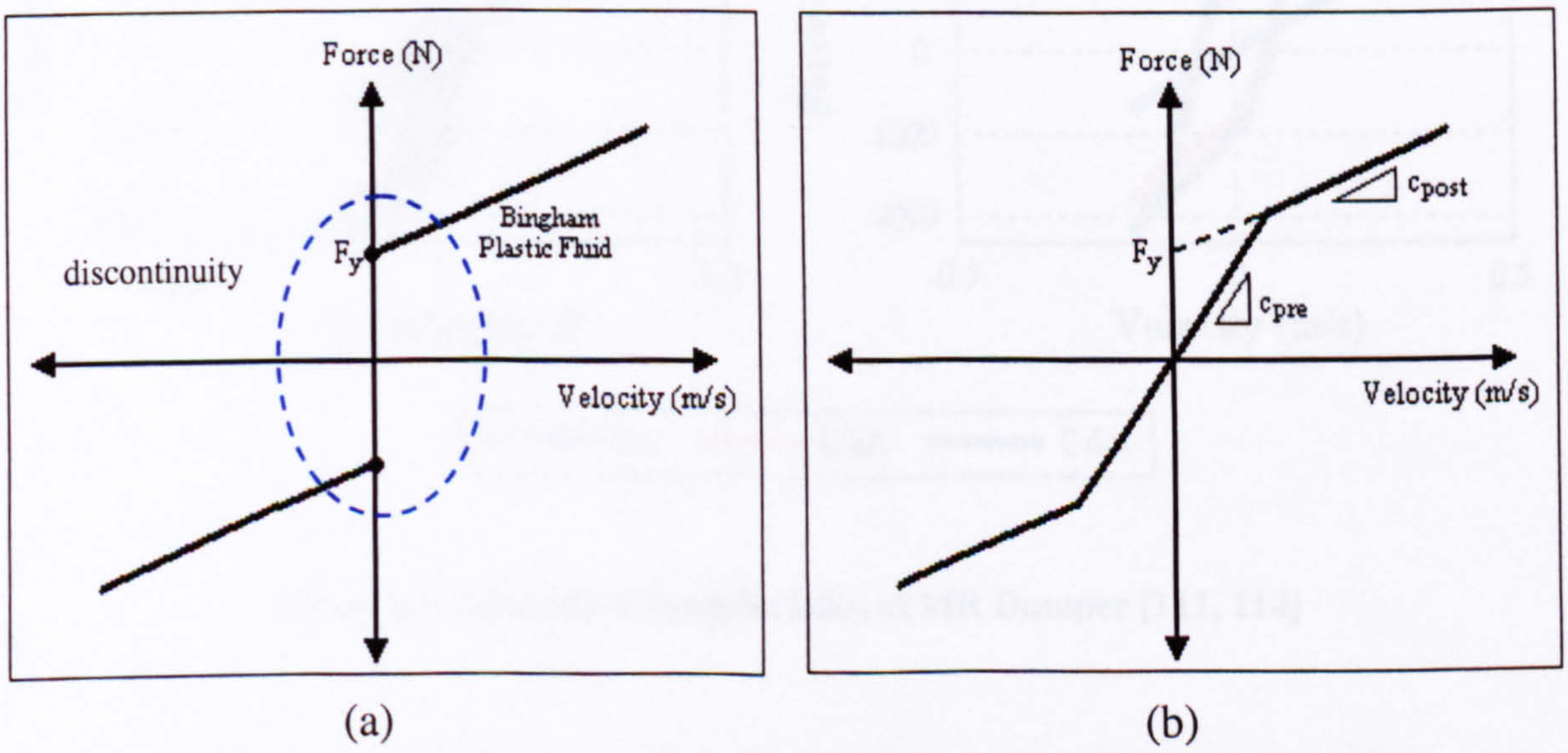

Figure 5.2: (a) Bingham Plastic Model [116]; (b) Bi-viscous Model [111, 114]

The dynamic characteristics of the MR damper are made up of the fluid stiffness, K_f and its mass M_f and can be predicted as described by Sims *et al.* [113]. MR fluid is compressible and its compressibility behaves like a spring where the stiffness is derived from the experimental data. The fluid mass represented by the fluid inertia can be approximated from the density and volume of the fluid inside the damper as shown in Table 5.1. It is worth noting that the values for C_{post}, and F_y depends on the amount of control current passed through the fluid while other parameters remain constant. The difference in MR damper characteristics between the experimental and the simulation is illustrated in Figure 5.3.

MR Damper Model Parameters	**Values**
C_{pre}	55.76 kNs/m
C_{post}	$C_{post} = -5257.3I^2 + 7671.5I + 3203.3$
F_y	$F_y = -13417I^4 + 25233I^3 - 17787I^2 + 6145.8I + 1.33$
K_f	1.29 MNm
M_f	1.5 kg

Table 5.1: MR Damper Parameters [111, 114]

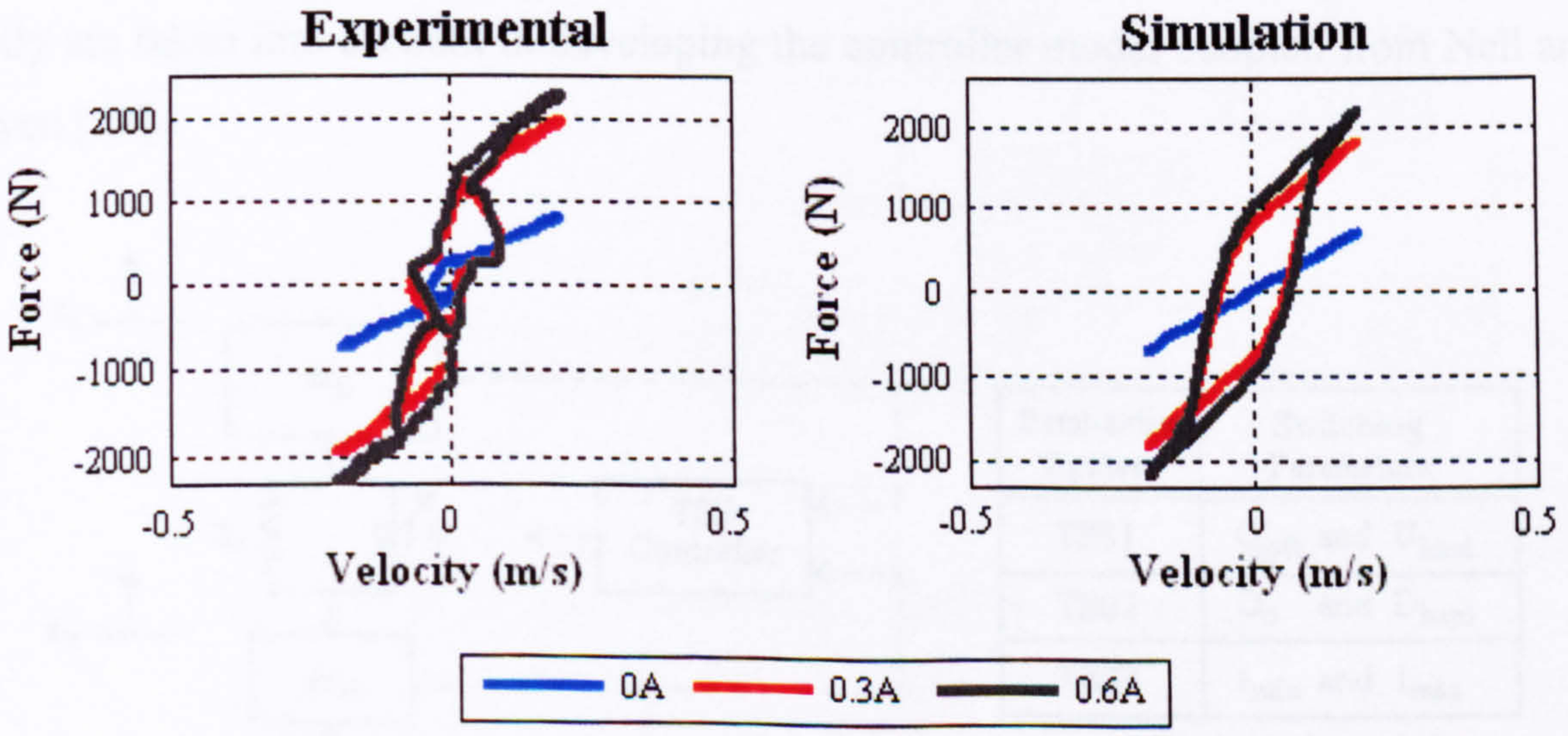

Figure 5.3: Dynamic Characteristics of MR Damper [111, 114]

5.3 Vehicle Models, Road Input and Tyre Model

The vehicle models employed in this chapter include a lumped mass 2DOF QVM, a realistic QVM and a lumped mass 7DOF FVM of the MPV. Vehicle parameters for the realistic and the lumped mass QVM are available in Chapter 4, Table 4.2 and 4.3, respectively, and the parameters for the lumped mass FVM are shown in Table 4.4. In this chapter, the capability of MBS cosimulation technique is demonstrated by increasing the complexity of the vehicle models and integrating these with the realistic semi-active control models. Ultimately, a realistic QVM is used with the realistic semi-active controller models to evaluate the load histories of the suspension arm. Similar transient and random road input are applied to all vehicle models as in Chapter 4 except for in evaluating semi-active control strategies for a full vehicle model where rougher road profiles are utilized.

5.4 Two-State Switchable Semi-Active Control Systems

This section evaluates several two-state-switchable (TSS) semi-active control systems based on local and global controls. The local control system refers to the derivation of the control algorithm from a two-degree of freedom model. Variations of the skyhook control models are introduced in the form of an ideal model and those from the MR damper models (Figure 5.4). In global control, pitch and roll motions of the vehicle body are taken into account in developing the controller model adopted from Nell and Styen [20].

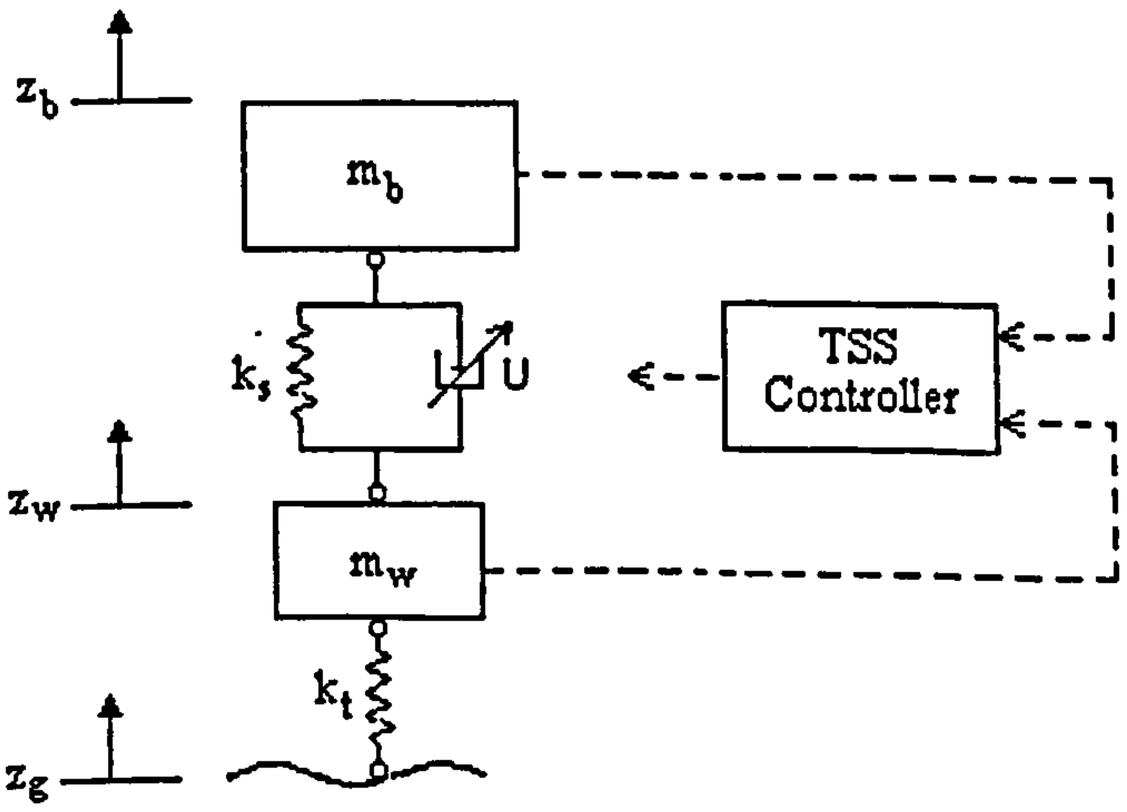

Semi-active System	Switching Parameters
TSS1	C_{soft} and C_{hard}
TSS2	D_o and D_{hard}
TSS3	I_{min} and I_{max}

TSS Controller

Figure 5.4: Schematic of Two-State Switchable with Switching Parameter [111]

5.4.1 Two-State Switchable with Damping Coefficient Switching (TSS1)

This control strategy was introduced by Karnopp *et al.* [39] for a single-degree-of freedom (SDOF) model. Moline *et al.* [44] extend the method for a 2DOF QVM model and is given as:

$$\begin{aligned} &if\ \dot{z}_b(\dot{z}_b - \dot{z}_w) > 0; && \text{switching parameter} = C_{hard} \\ &else && \text{switching parameter} = C_{soft} \end{aligned} \qquad \textbf{Eq 5.3}$$

It evaluates the product of sprung mass absolute velocity and the relative velocity between the sprung and unsprung mass. If the sprung mass velocity is greater than the velocity of the unsprung mass, the damper will switch to a hard setting to minimise the response. Otherwise, the controller switches to the soft setting equivalent to the passive damper since it cannot provide a negative force to oppose the unsprung mass response. Modelling the control algorithm in MATLAB/Simulink requires an on/off logic controller that switches between two linear damping coefficients, namely the hard, C_{hard} and the soft, C_{soft} setting as shown in Figure 5.5. TSS1 serves as an ideal case which subsequent MR controller models such as TSS2 try to emulate.

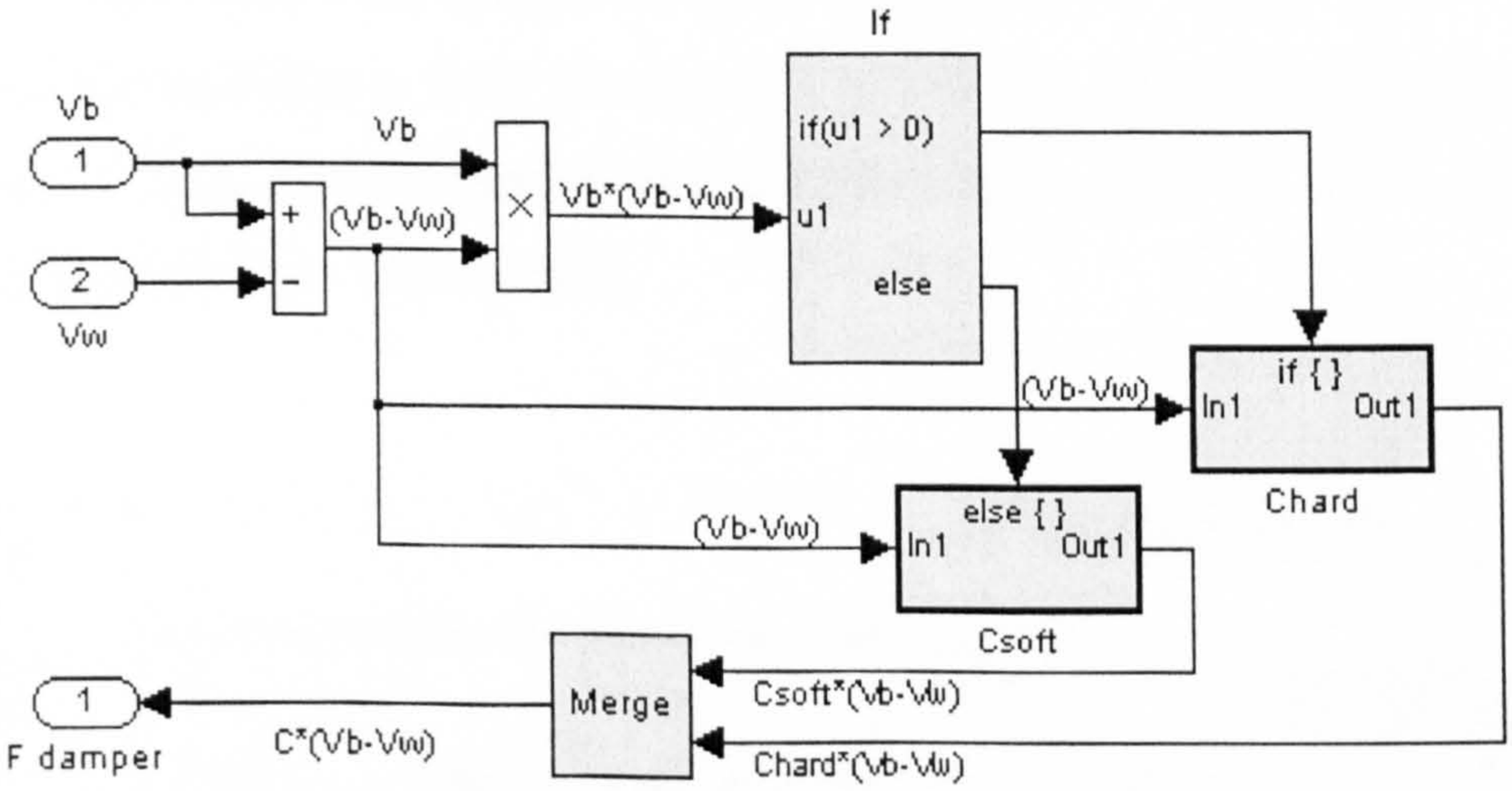

Figure 5.5: TSS1 with Damping Coefficient Switching

The hard and soft damping constants are approximated from the experimental MR damper force velocity characteristics. The soft setting is when zero control current is given to the MR damper which is equivalent to a passive setting of 3800 Ns/m, as shown in Figure 5.3. The hard setting is estimated at 6000 Ns/m. The damping

coefficients are applied to the realistic QVM at an oblique angle. For the equivalent damping coefficients in a lumped 2DOF model, the values are scaled down to 1500 Ns/m and 2368 Ns/m respectively.

5.4.2 Two-State Switchable with Damper Force Switching (TSS2)

The second TSS employs an MR damper model that relies on damper force switching. It is based on control scheme develop by Sims *et al.* [118] that uses a linear feedback control as shown in Figure 5.6, in order to achieve a linear response from a non-linear response of the MR damper. It compares the actual damping force with the one produced from TSS1 until the error between the two forces is minimised. The optimized controller gains are B = 0.8 and G = 0.001 as reported by Levesley *et al.* [111].

In MBS cosimulation, MR damper models for the TSS2 and TSS3 are treated as a subsystem represented in a "black box" as shown in Figure 5.7(b), which requires the absolute velocities of the sprung mass, v_2 and unsprung mass, v_1. The input velocities to the subsystem are taken from the MBS vehicle model and the damper force, F_d goes back to the vehicle model as a force actuator. By setting the control current to zero as shown in Figure 5.7(a), the MR damper acts as passive system and is used as reference when comparing with other TSS models.

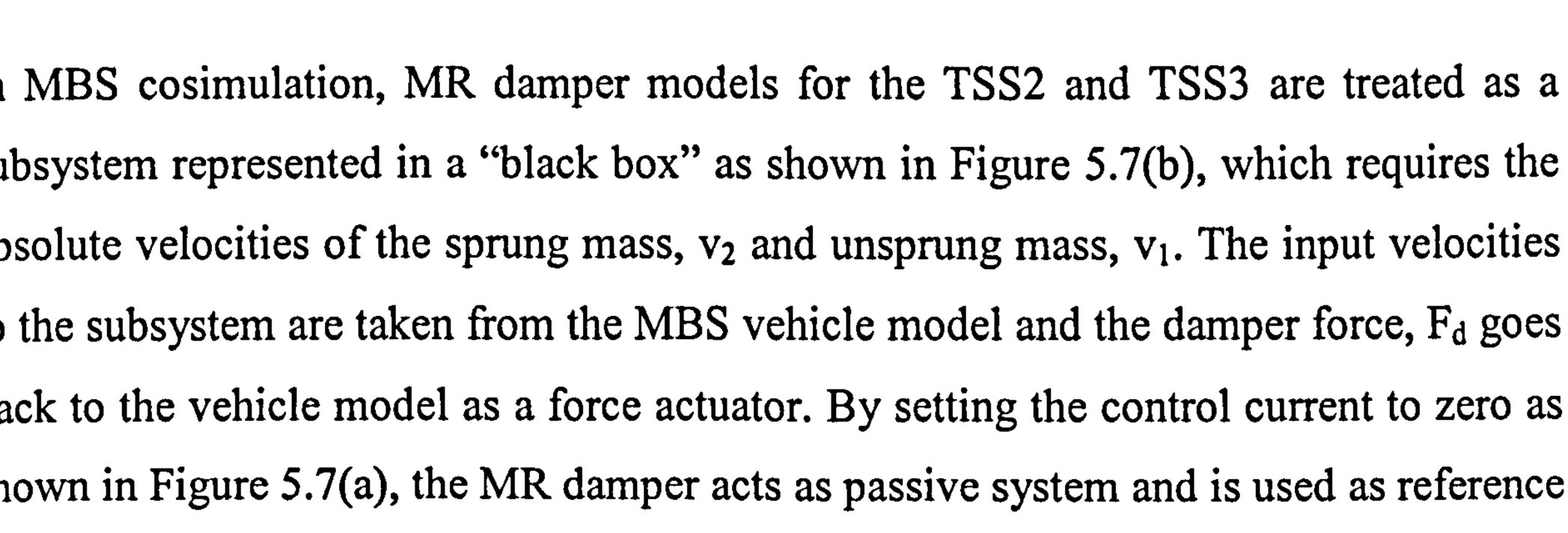

Figure 5.6: MR Damper Feedback Control of TSS2 [111]

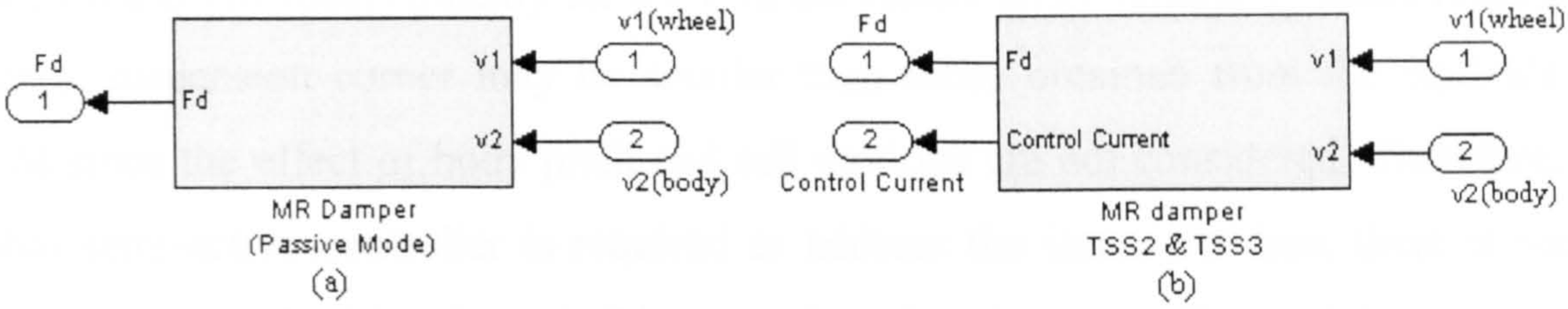

Figure 5.7: MR Damper Subsystems (a): Zero Current; (b) TSS2 and TSS3

5.4.3 Two-State Switchable with Control Current Switching (TSS3)

In a similar fashion to TSS2, the two-state switching parameter can be replaced with a maximum I_{max} and a minimum current, I_{min} control currents, where I_{max} and I_{min} are 0.6 A and 0A, respectively. This semi-active strategy is defined as TSS3. The switching to zero control current resembles the soft setting similar to TSS1 and TSS2. The only difference is that when the controller selects the hard setting in which a maximum control current of 0.6A is exerted, the MR damper displays its non-linear characteristics. The difference between TSS2 and TSS3 can be observed from the signature of their respective control currents that will be discussed later in this chapter. The representation in MATLAB/Simulink is illustrated in Figure 5.7(b), but the details of the block diagrams are not included in this thesis due to confidentiality issues. As far as the author's objective is concerned, the intention of incorporating realistic semi-active controllers within the MBS cosimulation is one of the key research objectives.

5.4.4 Two-State Switchable with Pitch and Roll (TSS1 PnR)

Generally, semi-active controller models have been developed based on quarter vehicle models. Applying such a model in a full vehicle model assumes all suspension corners are independent. Effects of vehicle body motions are generally not taken into account. Levesley *et al.* [6] analyse a lumped 7DOF FVM with independent passive suspension having only one wheel striking a pothole. They demonstrate that the other three wheels and body positions exhibit some response suggesting a strong influence of body rotational motions during the simulation. They conclude that the differences in response might be induced by the body pitch and roll motions. Similar conclusions were obtained by Ramli *et. al* [99] using MBS cosimulation of the MPV traversing a bump and a pothole. It is predicted that by applying semi-active control systems

based on a QVM independently for a FVM, the reduction in vehicle dynamic response at each suspension corner may be smaller than those obtained from the equivalent QVM since the effect of body pitch and roll motions are not considered. Therefore, a global semi-active controller is required to address the issue. To date, there is very limited number of publications on this type of semi-active controller model.

Among the first to implement semi-active suspension with pitch and roll control was Venhovens *et al.* [19]. They introduced both attitude and vibration control, primarily aimed at reducing pitch and roll motions resulted from acceleration and braking. This is achieved by determining the wheel loads as a function of lateral, longitudinal and yaw accelerations. The control strategy determines vertical force at each wheel station while maintaining the suspension working space as constant at a given load transfer, thus the vehicle body will only rotate due to the tyre deflections. This strategy was developed using a PID controller but was unsuitable to be adopted for the present work due to hardware limitations.

A similar control strategy was investigated by Ieluzzi *et al.* [25], implemented on a 10-wheeled truck. The controller model consists of a skyhook control law to improve ride comfort, a lateral control for reducing roll motion caused by driving inputs (cornering and lane-change), and a longitudinal control to manage pitch motion resulted from braking. However, no details are provided for the lateral and longitudinal controls. The controller model is capable of controlling both ride and handling behaviours and demands that the tyre model incorporates lateral and longitudinal dynamics, which is outside of the scope of this research.

Another interesting controller model in this category was developed by Nell and Styen [20]. This global two-state switchable semi-active controller was implemented to improve ride performance for a heavy off-road vehicle using a simplified three-degree of freedom vehicle model considering roll, pitch, and bounce motions of the sprung mass. To reduce body acceleration, the controller strategy calculates the combination of damper states that would generate the largest acceleration opposing the sprung mass motion, or a minimum acceleration in the direction of the sprung mass movement. The outcomes suggested that by incorporating pitch and roll motions in the semi-active controller algorithm, showed improve performance in ride comfort. Greater reduction

in body acceleration was observed when the vehicle was examined on rougher road profiles.

Based on the survey, the control law from [20] is suitable for implementation in this study. However, some modification to the algorithm is required to suit the 7DOF FVM of the MPV. The main improvement lies with the relative velocity measurement, which is measured between the sprung mass and the corresponding unsprung mass, whilst the original controller measures relative velocity between the sprung mass and the corresponding velocity at ground position.

Several assumptions have been made when adopting this controller strategy. The vehicle body is allowed to rotate about the lateral (pitch) and longitudinal (roll) axes with respect to the vehicle centre of gravity with no rotation about the vertical (yaw) axis. Vertical translational motion is caused by forces from the suspensions and translational motions along the lateral and longitudinal directions are constrained. It was reported [119] that rotational motions produce more discomfort than the translational motions.

Developing the controller model begins by comparing the pitch acceleration, $\ddot{\Theta}_x$, against the roll acceleration, $\ddot{\Theta}_y$. The pitch acceleration is defined as the difference in vertical body acceleration between the front left hand side, $\ddot{z}_{F\_LHS}$ and the rear left hand side, $\ddot{z}_{R\_LHS}$ divided by the distance between the two measurement locations, α. Similarly, the roll acceleration is obtained by taking the difference of the vertical body acceleration between the front left side, $\ddot{z}_{F\_LHS}$ and the front right side, $\ddot{z}_{F\_RHS}$ divided by the distance of the two points, β. The distance α and β can be regarded as the wheelbase and wheel track, respectively measured from the wheel centres. The two expressions are shown in the following equations.

$$\ddot{\Theta}_x = \frac{\ddot{z}_{F\_LHS} - \ddot{z}_{R\_LHS}}{\alpha} \quad \text{(Pitch Acceleration)} \qquad \textbf{Eq 5.4}$$

$$\ddot{\Theta}_y = \frac{\ddot{z}_{F\_LHS} - \ddot{z}_{F\_RHS}}{\beta} \quad \text{(Roll Acceleration)} \qquad \textbf{Eq 5.5}$$

Next, the algorithm compares the two angular accelerations from Eq 5.4 and Eq 5.5. In Eq 5.6, if the value of pitch is larger than those of the roll, then the product of the damper forces and the pitch acceleration will be chosen to calculate the damper forces (Eq 5.7). Otherwise, the damper forces will be computed from the product of the damper force and the roll acceleration (Eq 5.8). The representation of the equations in MATLAB/Simulink block diagram is shown in Figure 5.8.

$$if \ |\ddot{\Theta}_x| > |\ddot{\Theta}_y| \qquad \textbf{Eq 5.6}$$

$$then; (d_{F\_LHS} + d_{F\_RHS} - d_{R\_LHS} - d_{R\_RHS})_{n=1:16} \times \ddot{\Theta}_x \qquad \textbf{Eq 5.7}$$

$$else; (d_{F\_LHS} + d_{R\_LHS} - d_{F\_RHS} - d_{R\_RHS})_{n=1:16} \times \ddot{\Theta}_y \qquad \textbf{Eq 5.8}$$

Where, d_{F_LHS}, d_{F_RHS}, d_{R_LHS}, d_{R_RHS} are the damper forces on the front left, front right, rear left, and rear right hand side of the vehicle body, respectively. For a two-state switchable strategy, each of these damper forces is capable of switching between a soft and a hard setting. With four suspension units, there are 16 possible combinations of damping forces for each unit, denoted as subscript "*n*". Out of the 16 possibilities, the combination from the four dampers that produces the minimum product (MP) with either the pitch or the roll accelerations will be chosen as the output damper forces to the MBS suspensions. The damper forces are determined by multiplying the damping coefficients with the relative velocities across the damper, as shown in Eq 5.9 to Eq 5.12.

$$d_{F\_LHS} = C_{soft/hard} \cdot \dot{z}_{rel\ F\_LHS} \qquad \textbf{Eq 5.9}$$

$$d_{F\_RHS} = C_{soft/hard} \cdot \dot{z}_{rel\ F\_RHS} \qquad \textbf{Eq 5.10}$$

$$d_{R\_LHS} = C_{soft/hard} \cdot \dot{z}_{rel\ R\_LHS} \qquad \textbf{Eq 5.11}$$

$$d_{R\_RHS} = C_{soft/hard} \cdot \dot{z}_{rel\ R\_RHS} \qquad \textbf{Eq 5.12}$$

Table 5.2 shows the switching logic combinations (denoted as MP1 to MP16) and the damping coefficient values approximated from the lumped mass vehicle model with the MR damper.

No.	Damping Coefficients for All Four Suspensions			
	Front Left (FL)	**Front Right (FR)**	**Rear Left (RL)**	**Rear Right (RR)**
MP 1	C_{soft}	C_{soft}	C_{soft}	C_{soft}
MP 2	C_{soft}	C_{soft}	C_{soft}	C_{hard}
MP 3	C_{soft}	C_{soft}	C_{hard}	C_{soft}
MP 4	C_{soft}	C_{soft}	C_{hard}	C_{hard}
MP 5	C_{soft}	C_{hard}	C_{soft}	C_{hard}
MP 6	C_{soft}	C_{hard}	C_{soft}	C_{hard}
MP 7	C_{soft}	C_{hard}	C_{hard}	C_{soft}
MP 8	C_{soft}	C_{hard}	C_{hard}	C_{hard}
MP 9	C_{hard}	C_{soft}	C_{soft}	C_{soft}
MP 10	C_{hard}	C_{soft}	C_{soft}	C_{hard}
MP 11	C_{hard}	C_{soft}	C_{hard}	C_{soft}
MP 12	C_{hard}	C_{soft}	C_{hard}	C_{hard}
MP 13	C_{hard}	C_{hard}	C_{soft}	C_{soft}
MP 14	C_{hard}	C_{hard}	C_{soft}	C_{hard}
MP 15	C_{hard}	C_{hard}	C_{hard}	C_{soft}
MP 16	C_{hard}	C_{hard}	C_{hard}	C_{hard}
$C_{soft} = 1500$ Ns/m; $C_{hard} = 2368$ Ns/m				

Table 5.2: Damping Coefficients Combinations

In MATLAB/Simulink, a logic operator is used to determine the minimum value. Representation of the selection procedure is shown in Figure 5.9. Finally, the selected damper forces are sent back to MBS in the form of actuator forces. This procedure is executed for each time step defined by the MBS cosimulation.

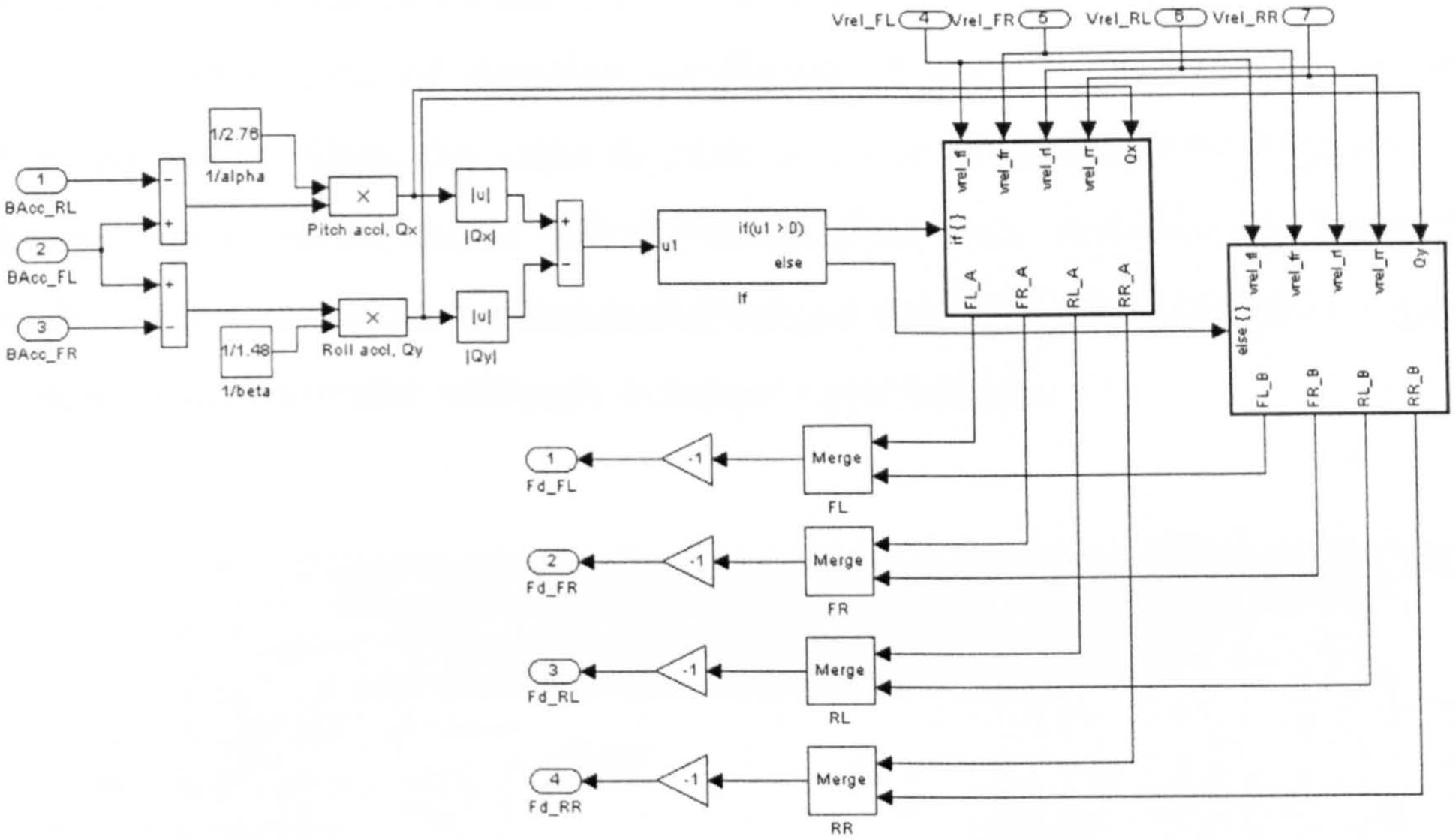

Figure 5.8: Two-State Switchable with Pitch and Roll Controller Model

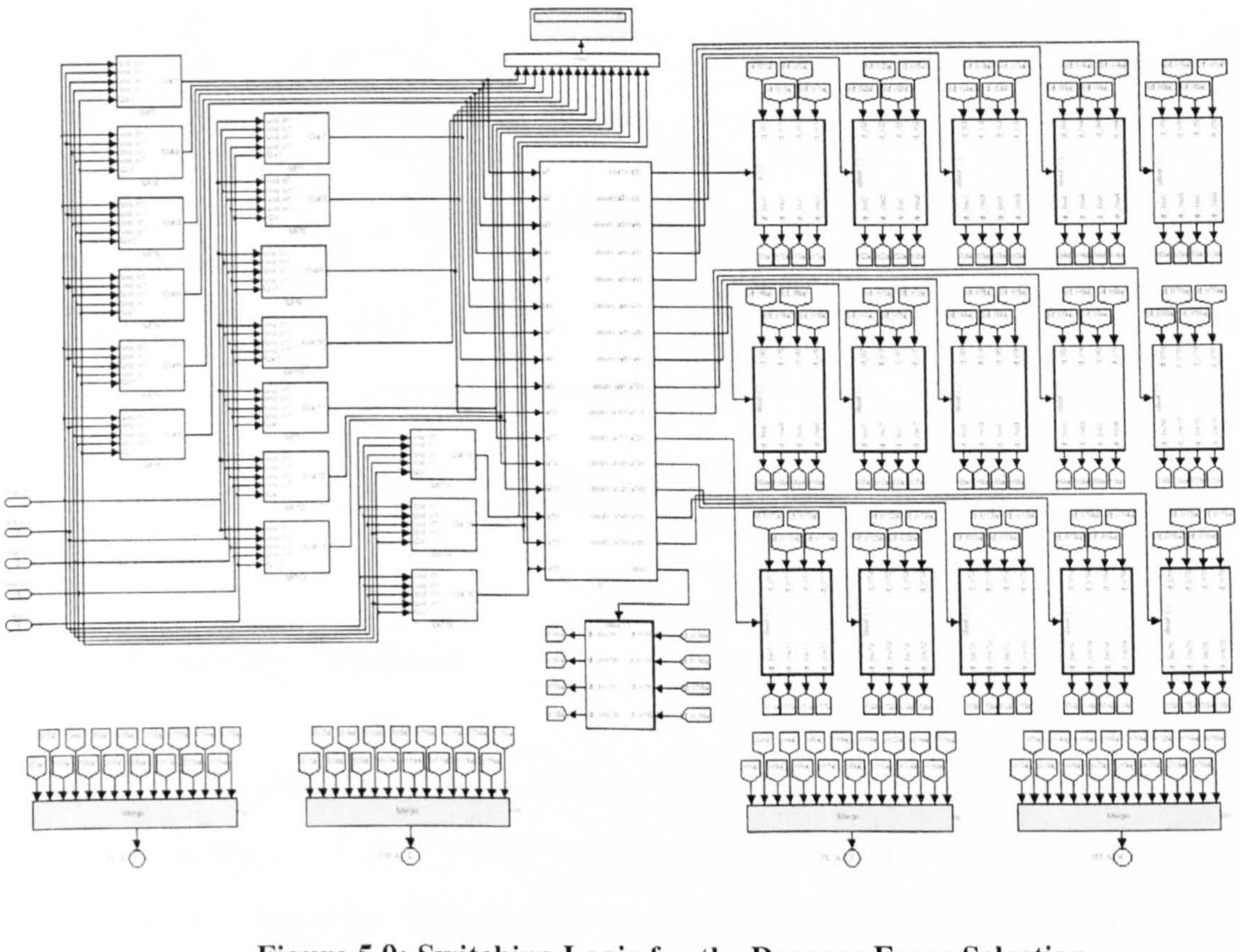

Figure 5.9: Switching Logic for the Damper Force Selection

5.4.5 Verifying Two-State Switchable with Pitch and Roll Controller Model

The controller model is analysed to confirm that the selected damper force combination satisfies the minimum product of acceleration. This is done by manually

assigning known values for the relative velocities. These velocities are multiplied with the 16 combinations of damping coefficient of hard and soft setting to produce damping forces. Then, the value of pitch or roll acceleration is multiplied by the 16 damper force combinations. MATLAB/Simulink then searches for the minimum product and produces the corresponding damper forces. Figure 5.10 shows a simplified version of the controller with only 4 damper combinations.

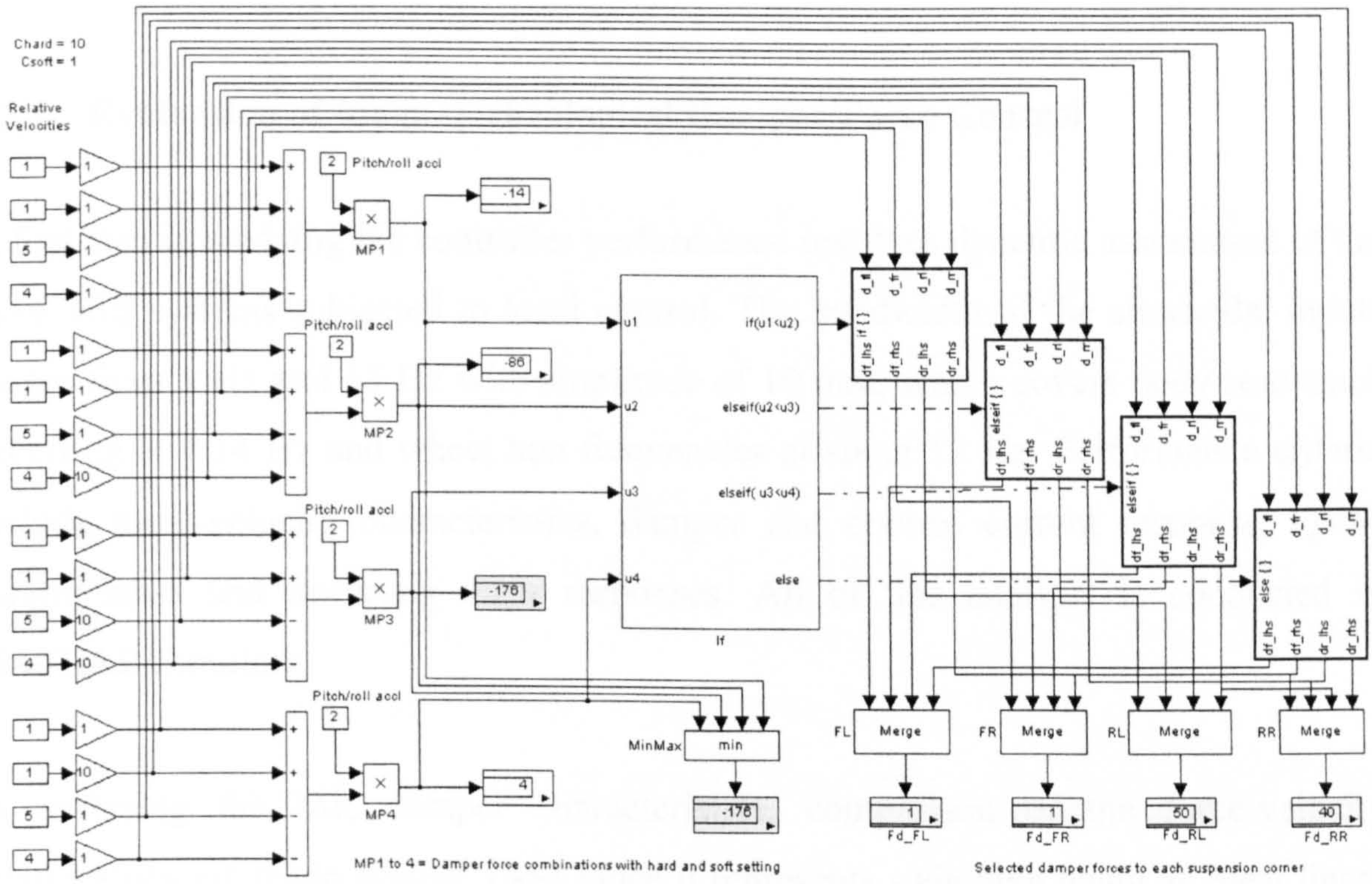

Figure 5.10: Validating the Damper Selection Logic

5.5 Results and Analysis

The focus of analysis in this section examines the dynamic characteristics and responses when local and global semi-active controller strategies are applied to the selected vehicle models. Ultimately, it aims at generating service load histories such that the durability of a suspension component can be predicted and compared. The analysis begins by evaluating the MR damper force performance applied using TSS2 and TSS3. Successful implementation of a realistic semi-active controller model in MBS cosimulation would confirm the suitability of the method to be used in a future study concerning controllable suspension systems. This is followed by dynamic analysis of the three participating semi-active strategies on a QVM of the MPV

subjected to transient and random road inputs. The study continues, using all suspension systems, to examine the response of the lower suspension arm from the realistic QVM. The extent of the study will provide indication of the load histories that will be utilised in fatigue analysis. Final analysis in this chapter centres on assessing local and global semi-active controllers on a full vehicle model of the MPV. The evaluation includes ride performance of the sprung and unsprung masses subjected to different random road surfaces, traversing at various constant forward velocities.

5.5.1 Evaluation of Magnetorheological Damper Force Control

A first step in studying the controller performance involves dynamic assessment of the three TSS systems subjected to local control. The bandwidth of the sinusoidal inputs ranges from 1 Hz and 15 Hz with amplitude of 10 mm, which covers body resonance occurring at 1.14 Hz and wheel hop frequencies at about 12 Hz. Performance criteria include force-velocity characteristics, damper and control current response, QVM sprung mass and unsprung mass responses. All of this analysis is conducted in MATLAB/Simulink.

In analysing the MR damper characteristics, comparison of the force-velocity relationships are made against TSS1 since it represents switching using an ideal linear damper. Figures 5.11(a) to (f) illustrate the force-velocity relationships for the TSS2 and TSS3 controllers against TSS1. It can be observed that TSS2 closely emulates TSS1 throughout the input frequency range. In contrast, TSS3 at low input frequencies presented in Figure 5.11(a) to (c) shows a complex signature, resulting from the non-linear nature of the damper. The patterns significantly improve at higher frequencies as depicted in Figure 5.11(d) to (f) as they more closely resemble TSS1. This demonstrates that the current switching of TSS3 is not as efficient as TSS2 which results in excessive damper forces produced at low frequencies.

This complex behaviour is mainly caused by the nature of TSS3 that switches between only the minimum and the maximum control currents. Clearly, Figure 5.12(a) to (f) demonstrates the discrete switching pattern of TSS3 when compared to TSS2. Unlike TSS3, the feedback control loop of TSS2 continuously adjusts the control current for the hard setting to match the ideal Karnopp law. At low frequencies, less control

current is required in TSS2 compared to TSS3 where maximum current of 0.6 A is demanded as illustrated in Figure 5.12(a) to (c). It can be observed that, as the input frequencies are increased, the amount of control current required by TSS2 is relatively similar to the control current of TSS3 (Figure 5.12(d) to (f)).

Next, the study examines the dynamic response of damper force, sprung mass and unsprung mass accelerations as shown in Figure 5.13(a) to (f), Figure 5.14(a) to (f), and Figure 5.15(a) to (f), respectively. In this analysis, the response from the passive damper is used as a benchmark for the three semi-active strategies. The response signatures from all three figures demonstrate an interesting finding. Sharp transient forces appeared in all competing semi-active systems even though sinusoidal inputs were used. These erratic patterns are not present for the passive damper. At low bandwidth between 1 Hz to 5 Hz, the damper force response from TSS3 is significantly greater than the other systems as the frequency increases, its performance is more closely matched with those from TSS1 and TSS2. This sharp transient response is known as jerk, as mentioned earlier in Chapter 2, and it is a common event in switchable semi-active systems where conventional skyhook control is used. According to Ahmadian *et al.* [49], the jerk minimises the benefit of the switchable strategy. It can be seen that, even with an ideal linear semi-active damper as in TSS1, jerk still occurs particularly at peak amplitudes and registers higher amplitudes than from the passive damper. In fatigue analysis, the effect of this sharp transient response on the suspension components' durability could inflict greater damage, thus shortening the service life of components. This issue will be addressed in the next chapter.

Figure 5.16 and 5.17 illustrate RMS accelerations of the sprung and unsprung masses plotted against the input frequencies. In both figures, the highest RMS accelerations are measured at the wheel hop resonance occurring approximately at 12 Hz. For the sprung mass response (Figure 5.16), all semi-active systems perform much better below 3 Hz where TSS3 produces the smallest RMS value. Above this frequency, the performance deteriorates for the semi-active systems, with the worst from TSS3. In contrast, the unsprung mass response in Figure 5.17, demonstrates higher RMS accelerations for the semi-active systems than from the passive system, at frequencies below 6 Hz. Beyond this frequency, the semi-active systems perform better than the passive. The RMS accelerations of the semi-active systems gradually reduce, with

TSS3 showing the best response. Around the wheel resonance frequencies, all semi-active systems show significant overall RMS reduction compared to the passive. Based on these analyses, it shows that the switchable semi-active systems might contribute less damage to the suspension components.

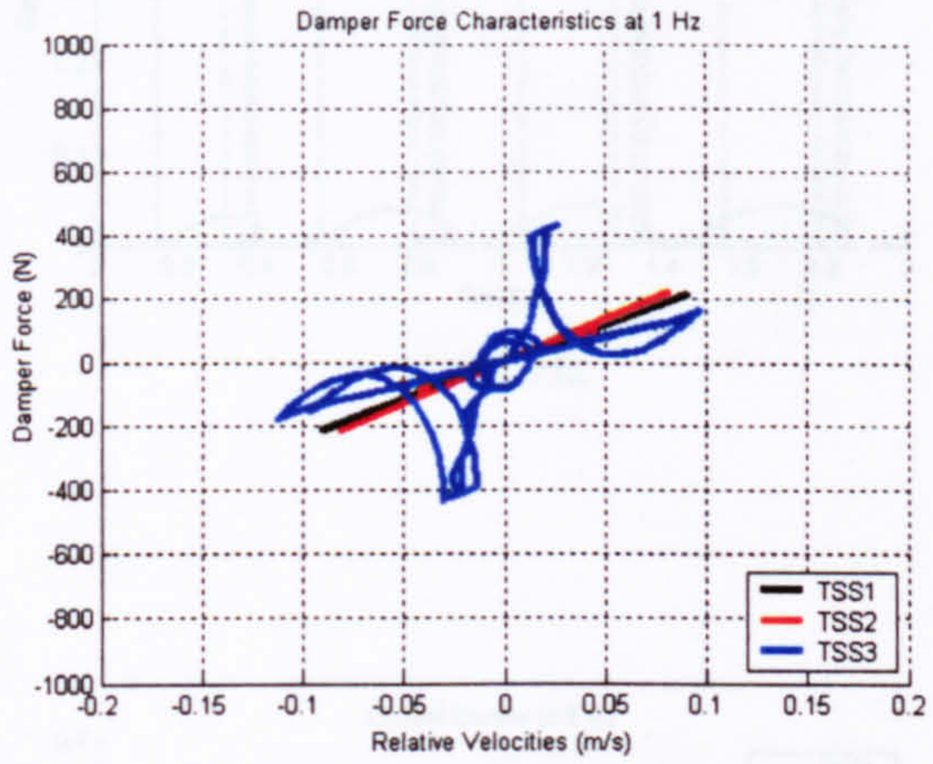

(a) 1 Hz

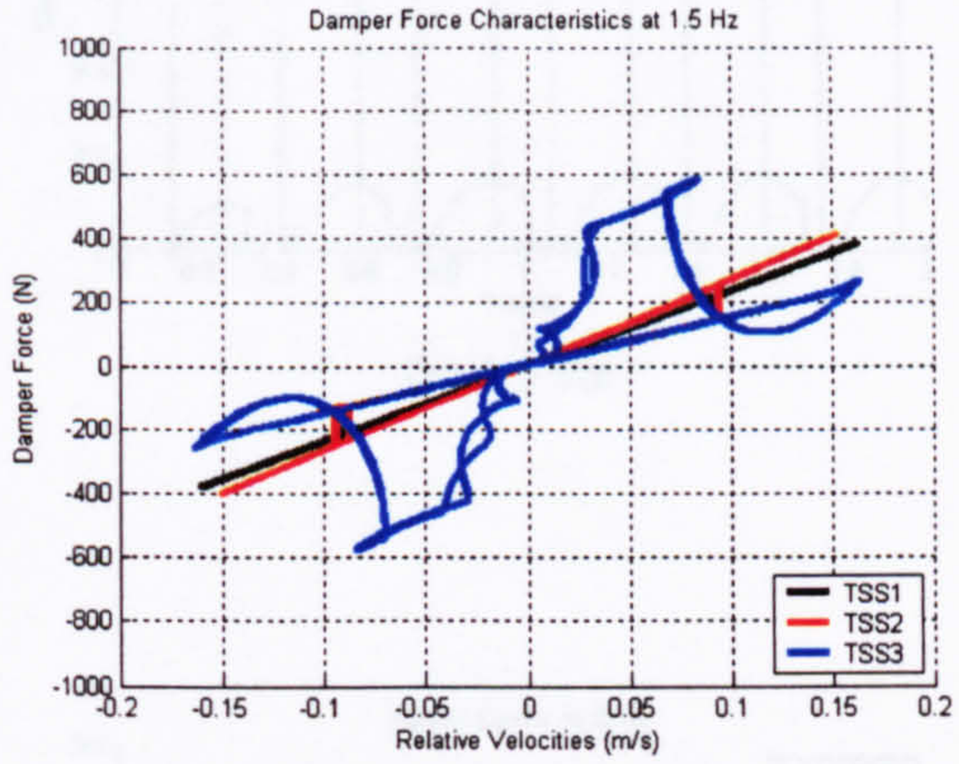

(b) 1.5 Hz

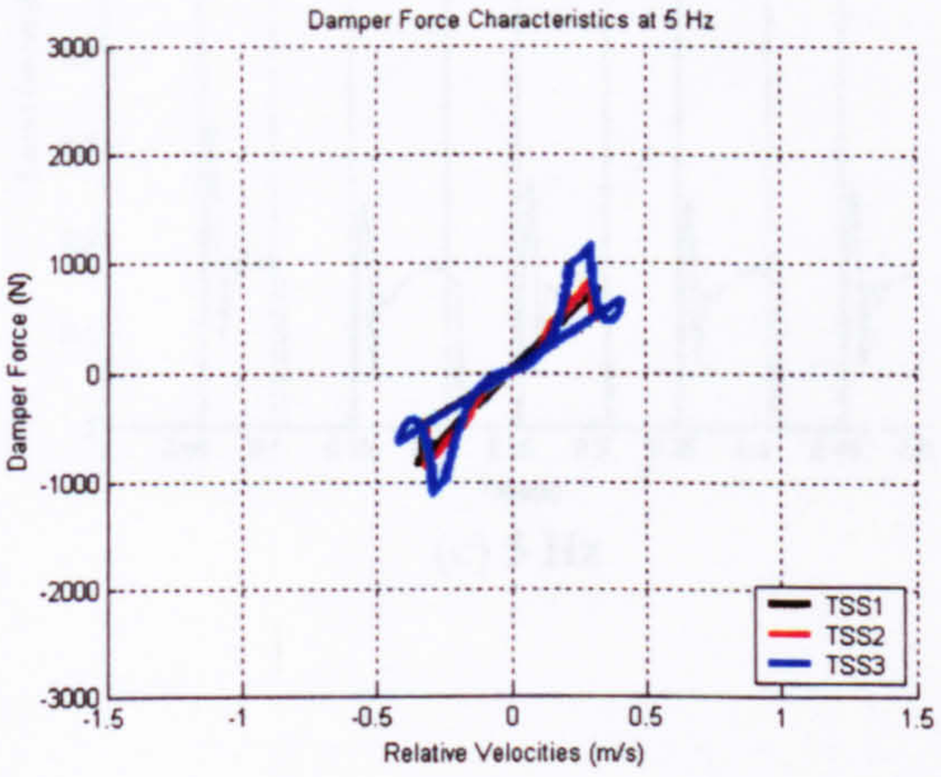

(c) 5 Hz

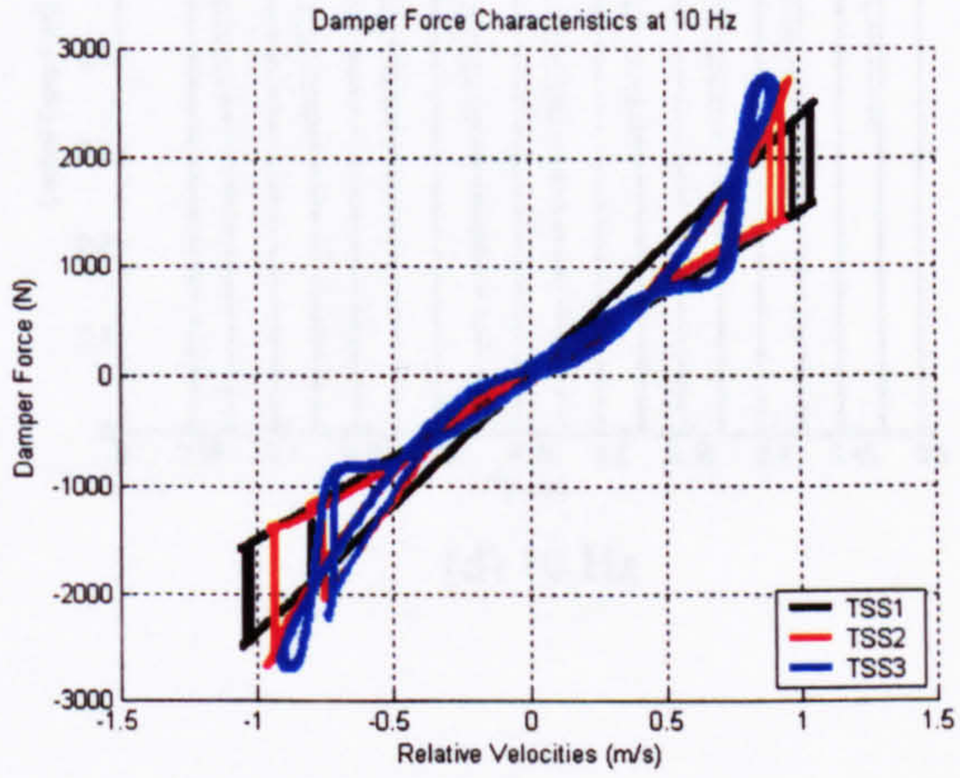

(d) 10 Hz

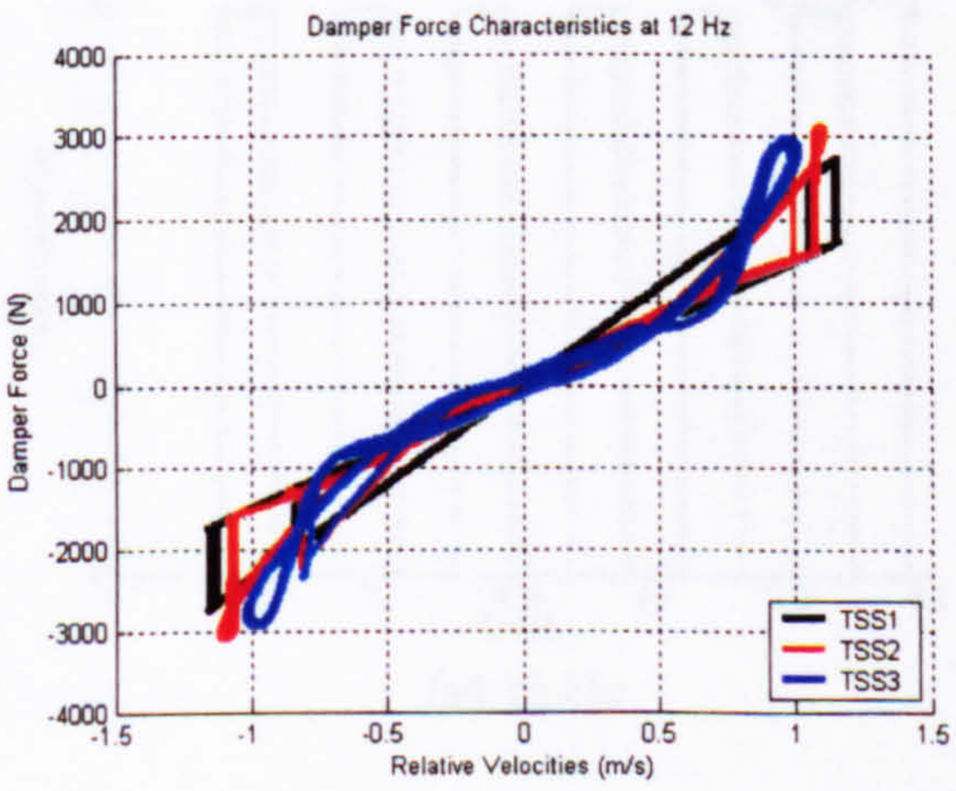

(e) 12 Hz

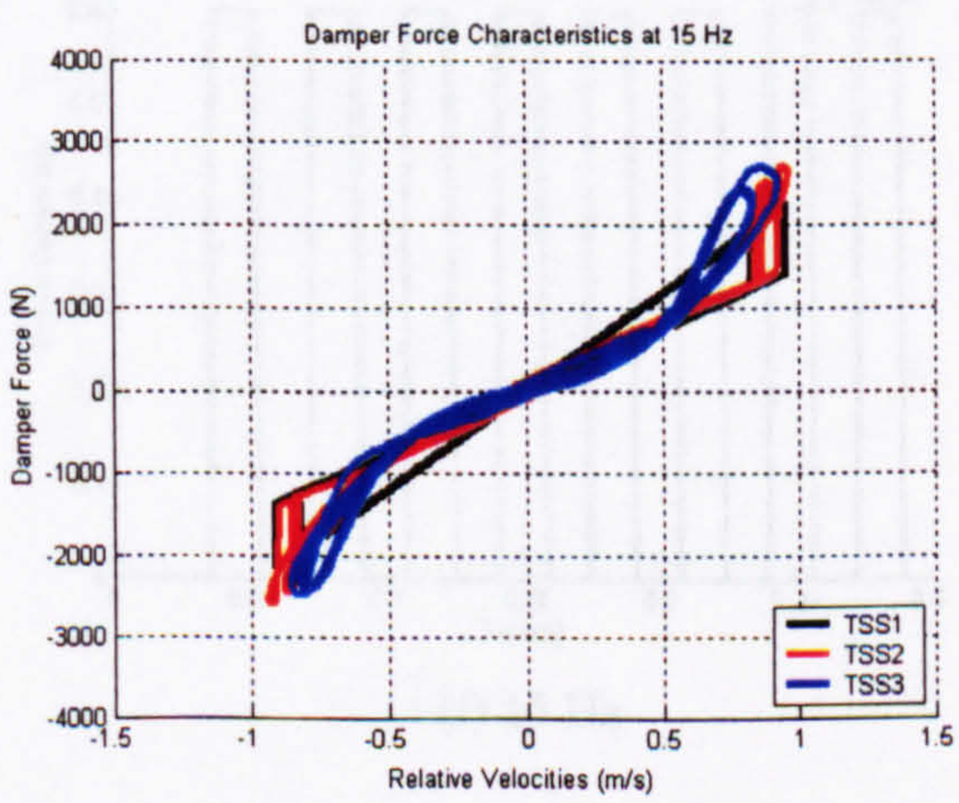

(f) 15 Hz

Figure 5.11 (a) to (f): Force-Velocity Characteristics

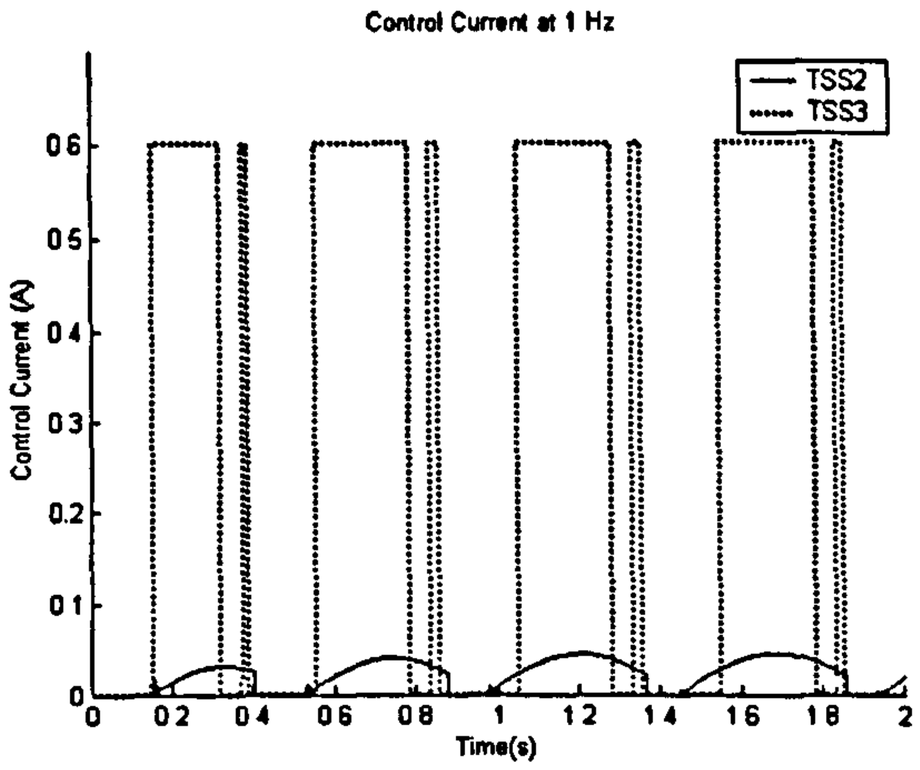

(a) 1 Hz

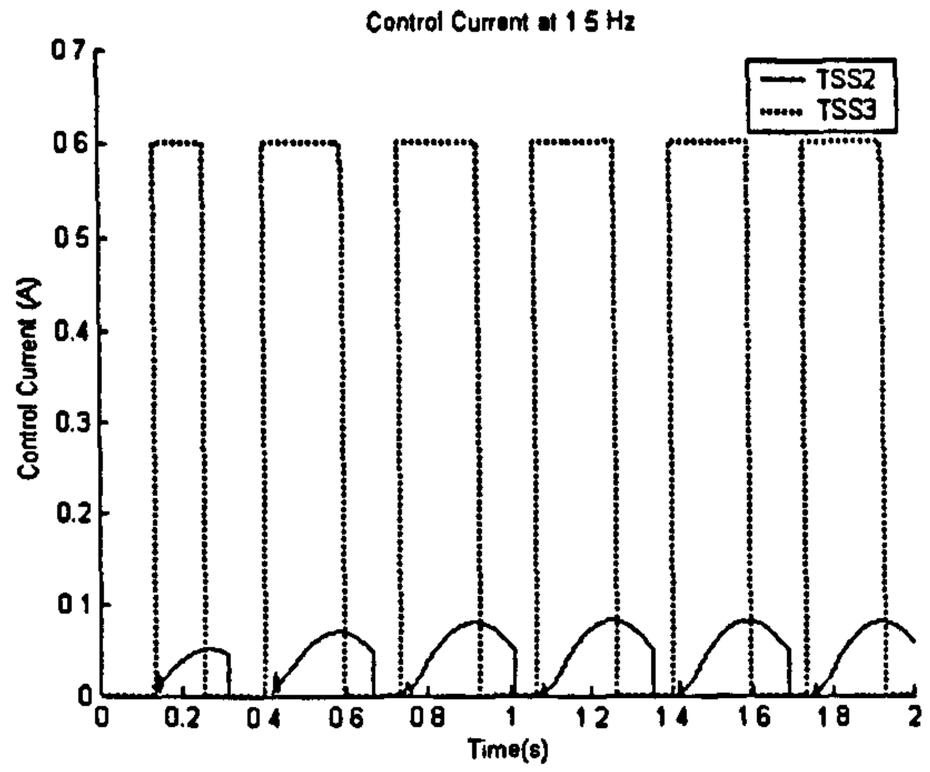

(b) 1.5 Hz

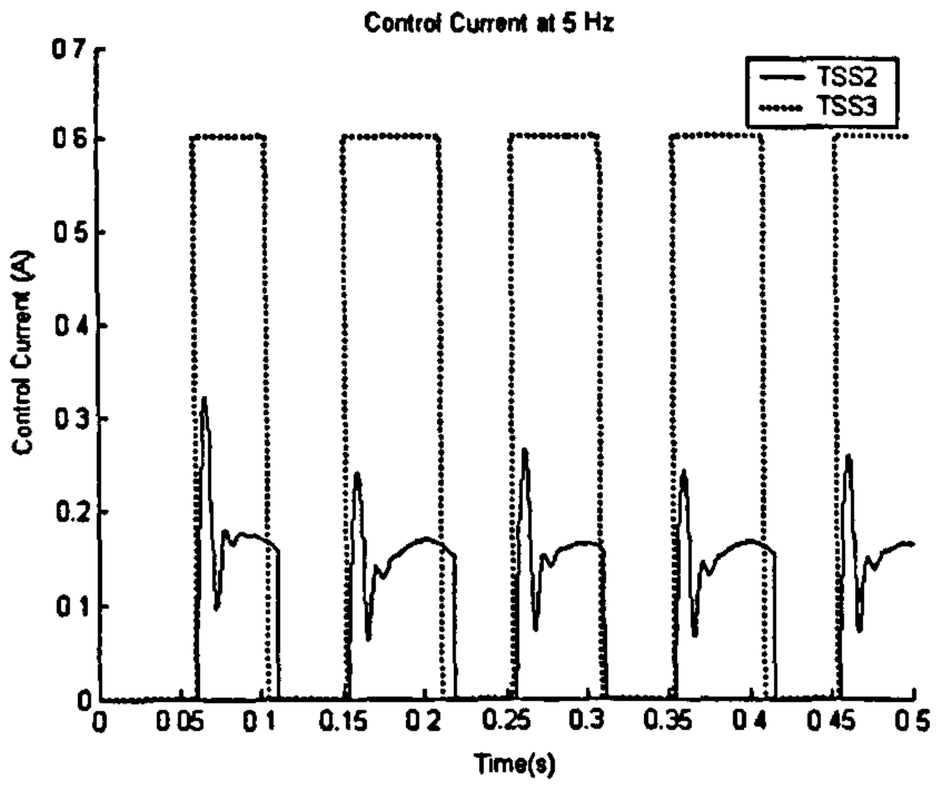

(c) 5 Hz

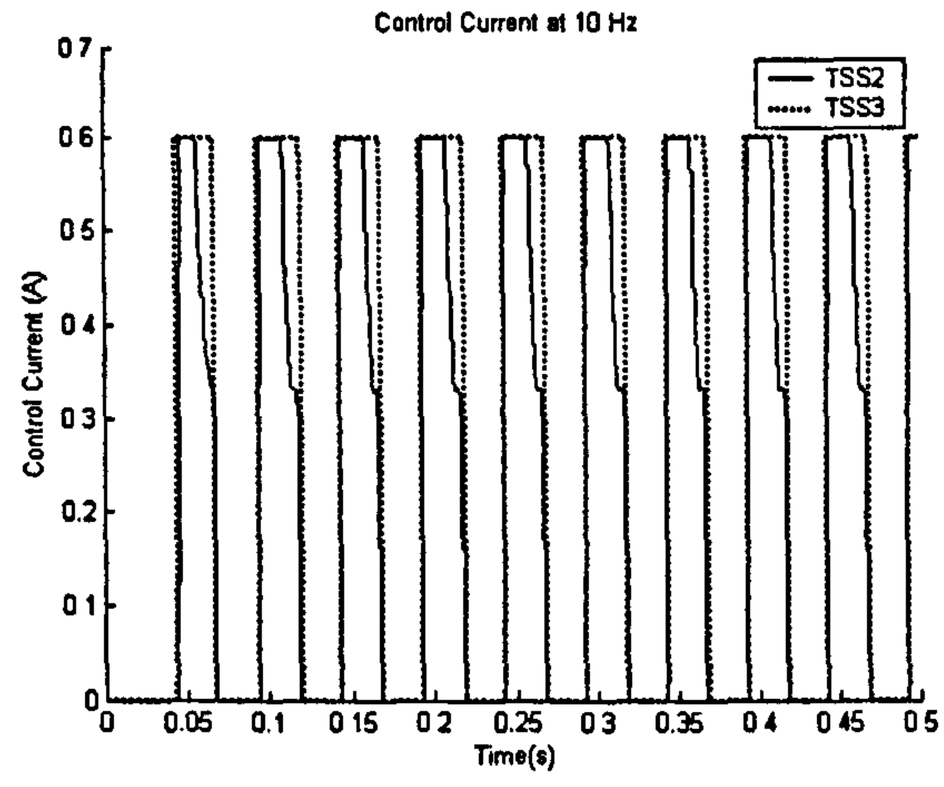

(d) 10 Hz

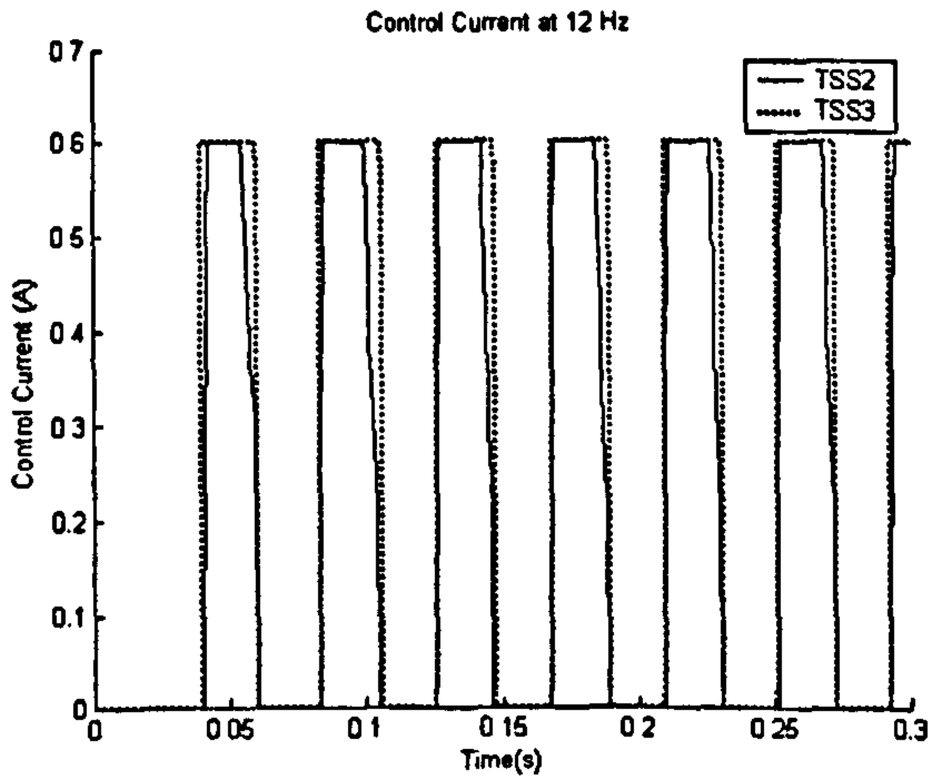

(e) 12 Hz

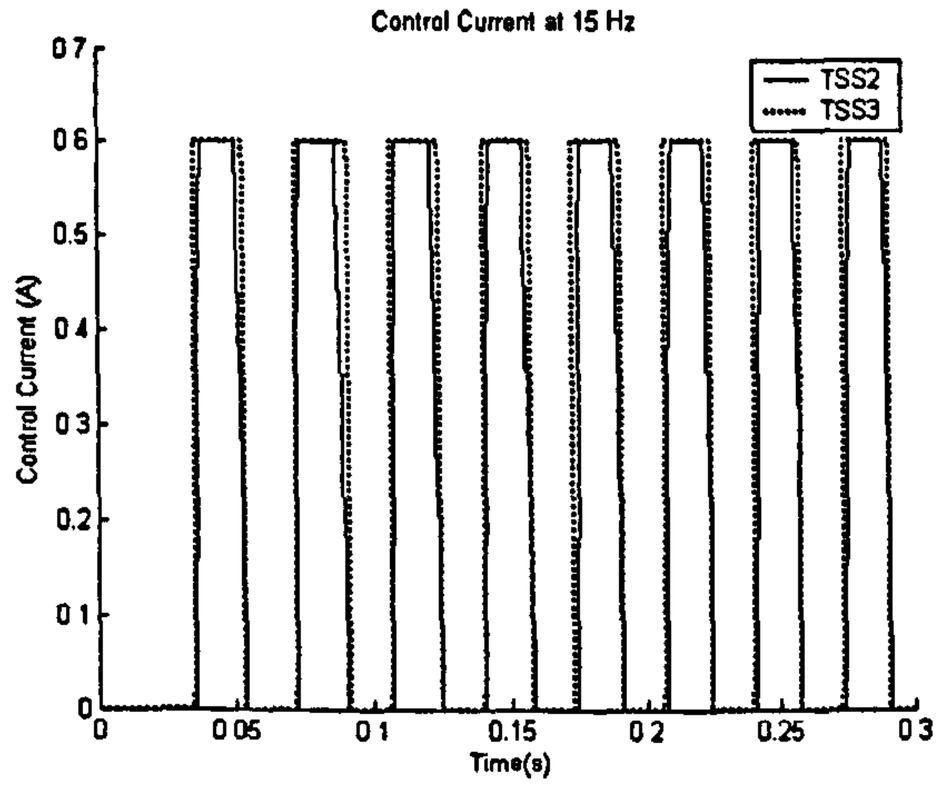

(f) 15 Hz

Figure 5.12 (a) to (f): Control Current between TSS2 and TSS3

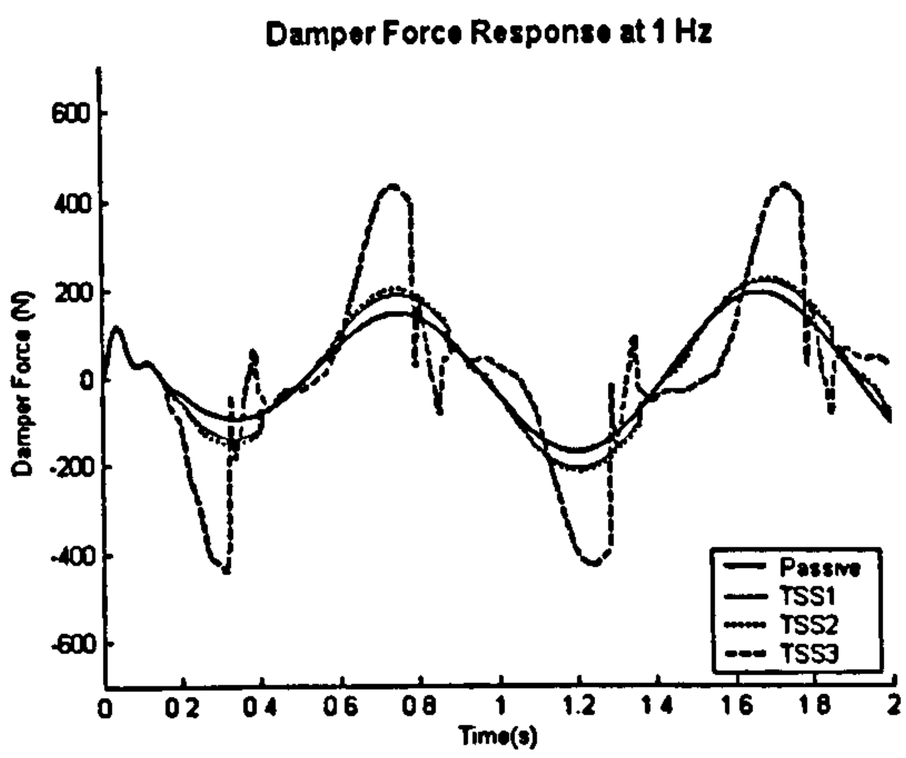

(a) At 1 Hz

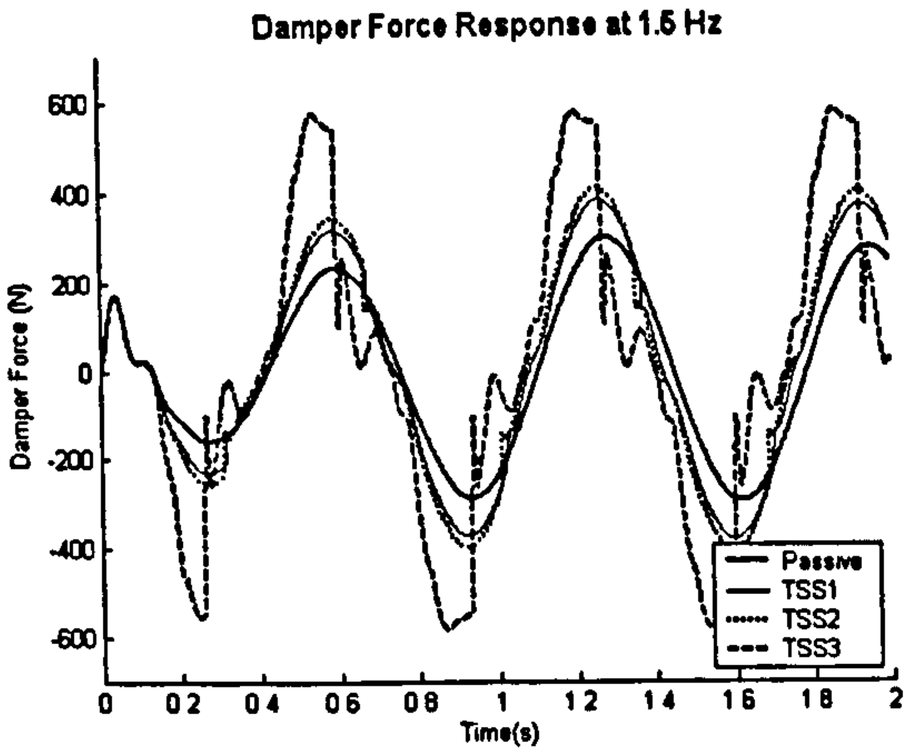

(b) At 1.5 Hz

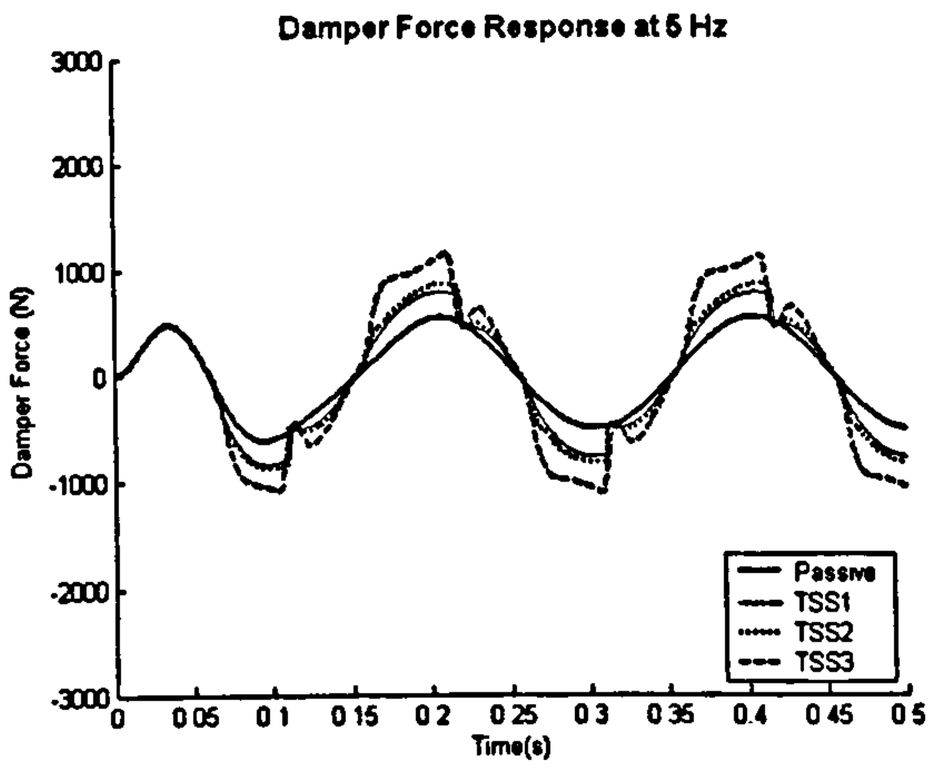

(c) At 5 Hz

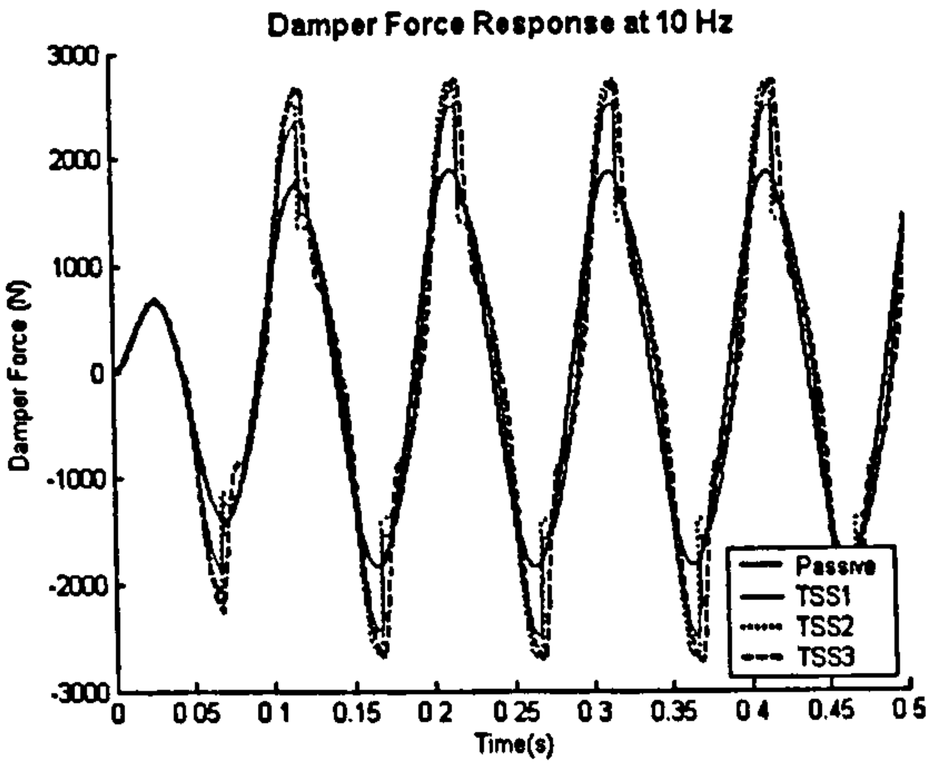

(d) At 10 Hz

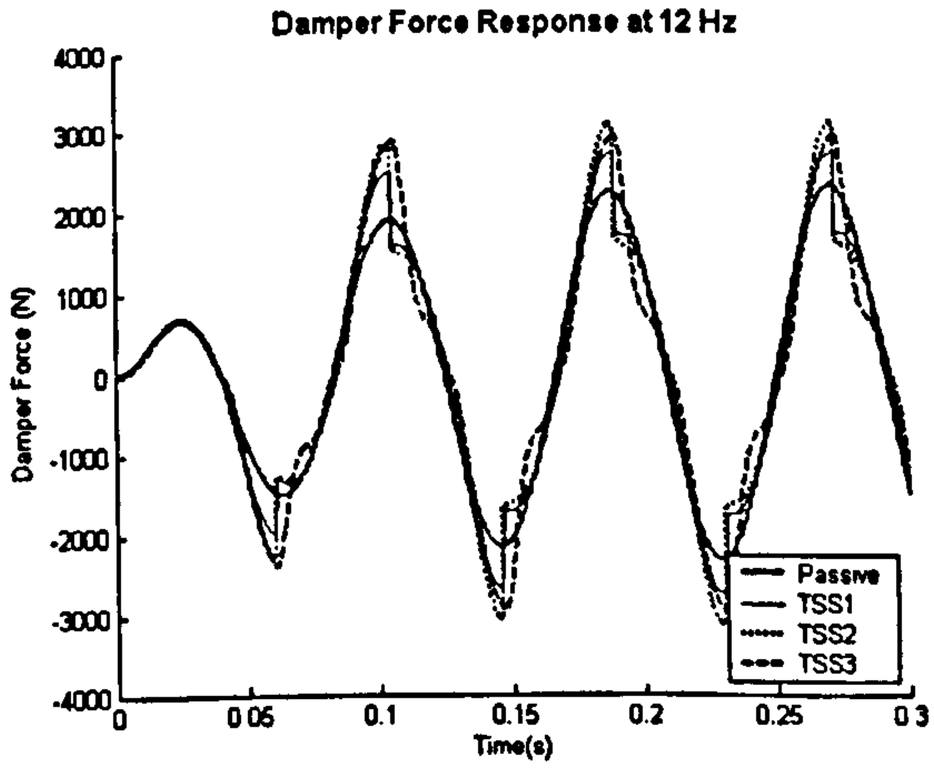

(e) At 12 Hz

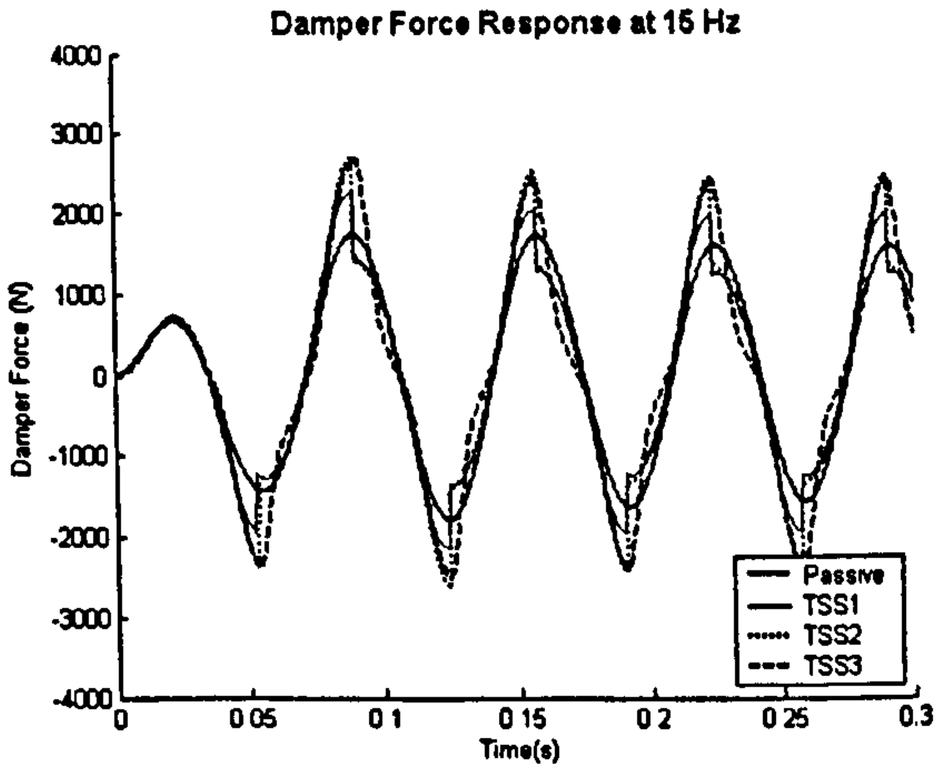

(f) At 15 Hz

Figure 5.13 (a) to (f): Damper Force Response

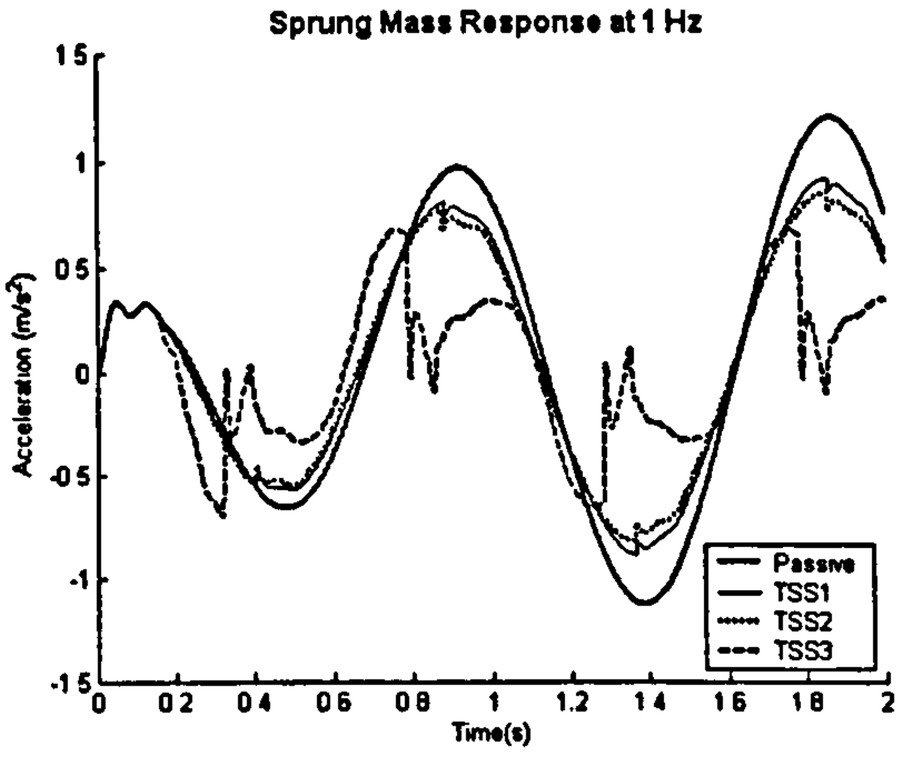

(a) At 1 Hz

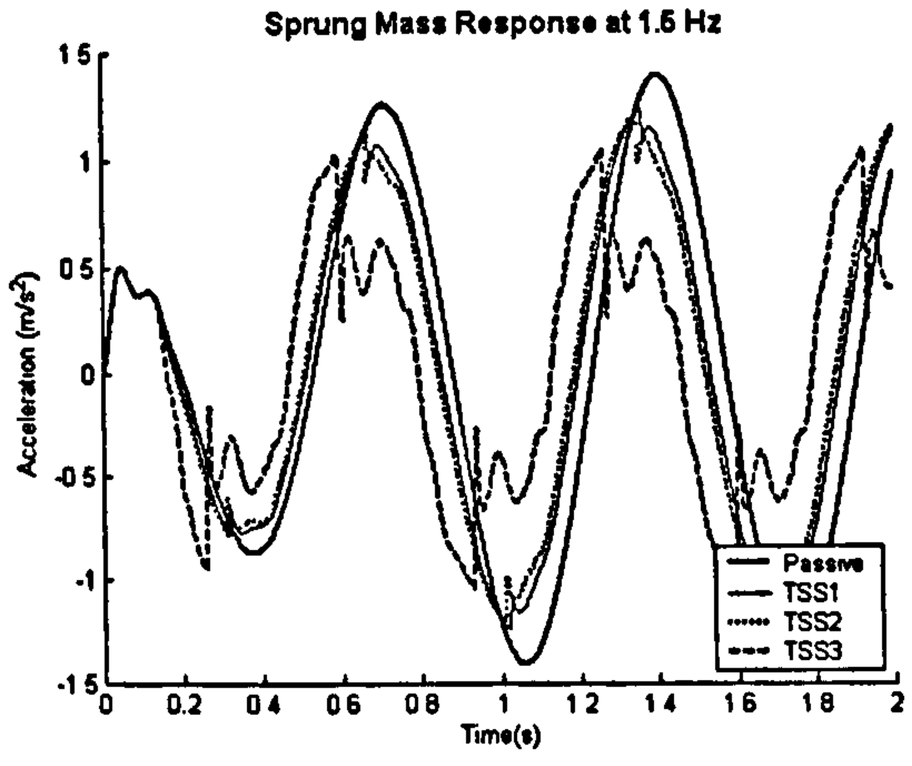

(b) At 1.5 Hz

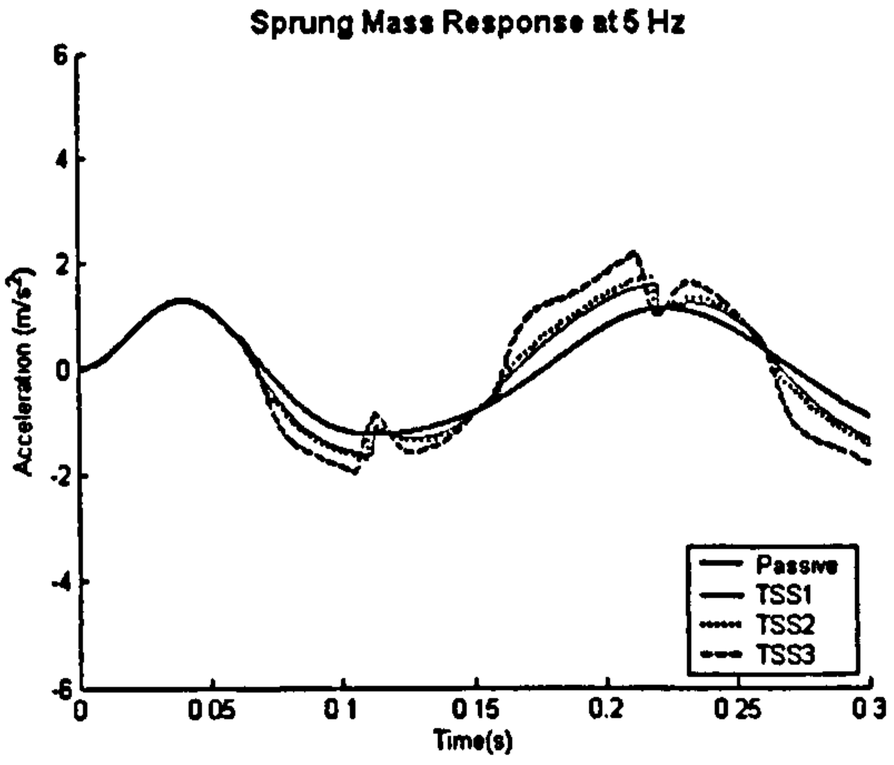

(c) At 5 Hz

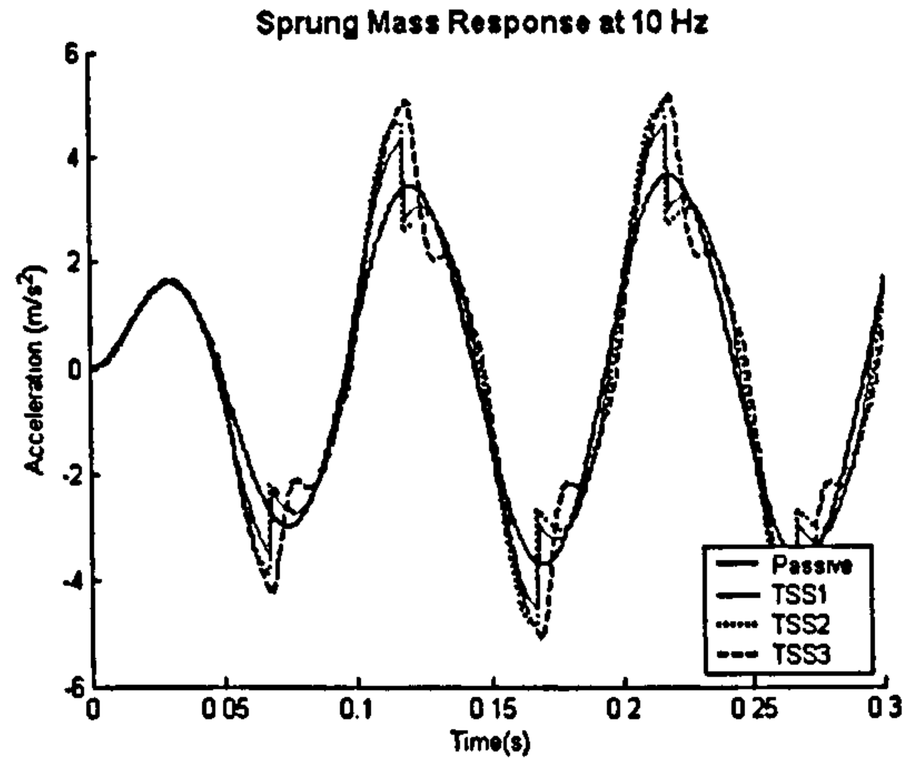

(d) At 10 Hz

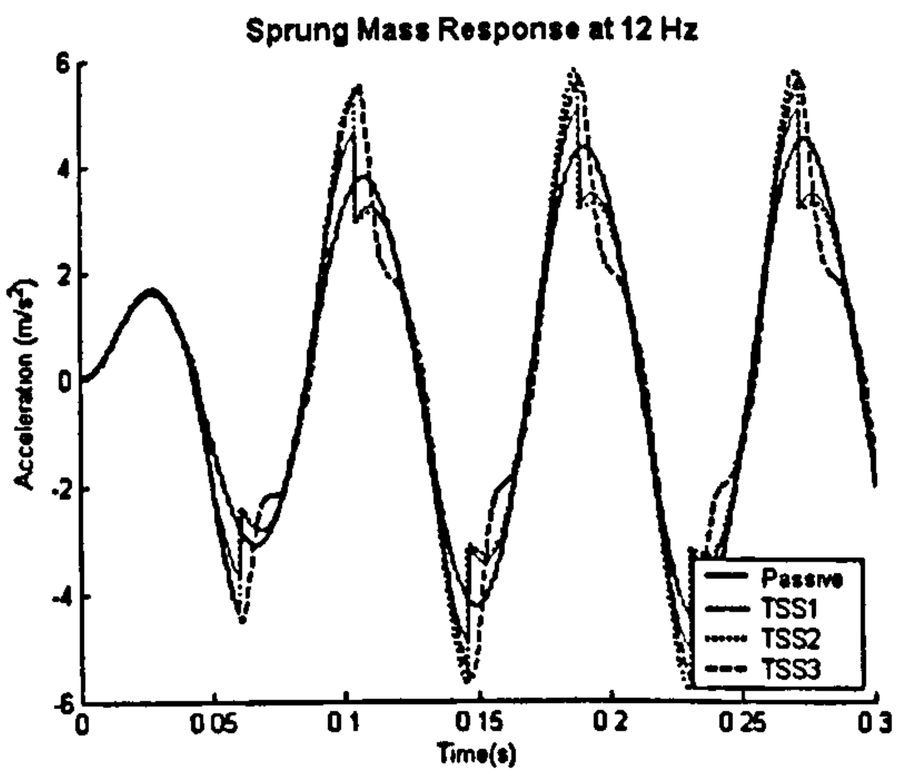

(e) At 12 Hz

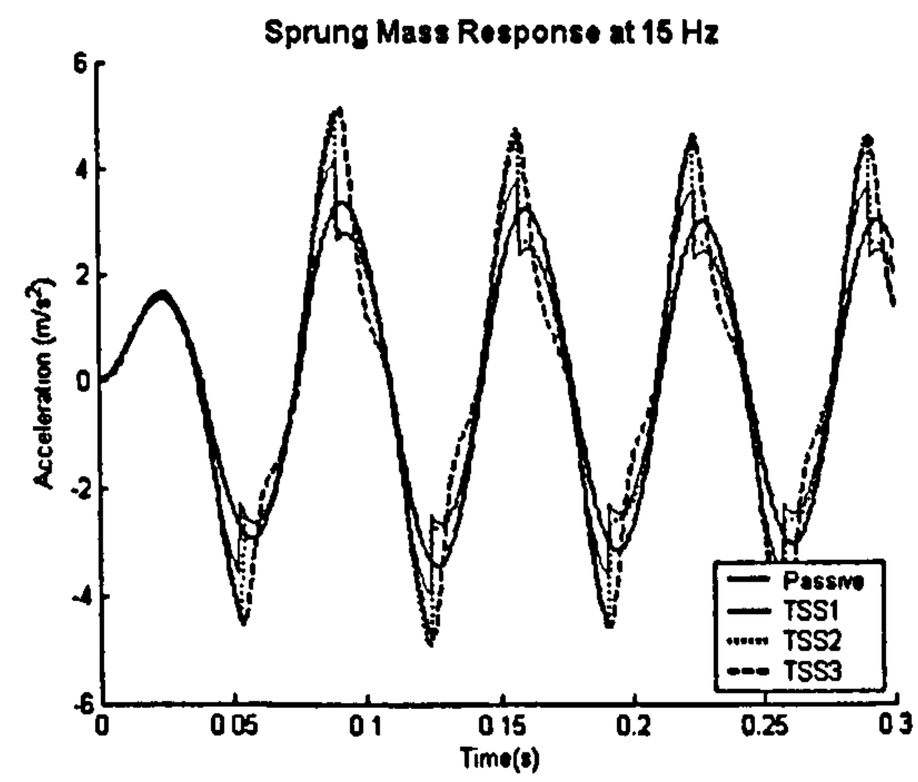

(e) At 15 Hz

Figure 5.14 (a) to (f): Sprung Mass Response

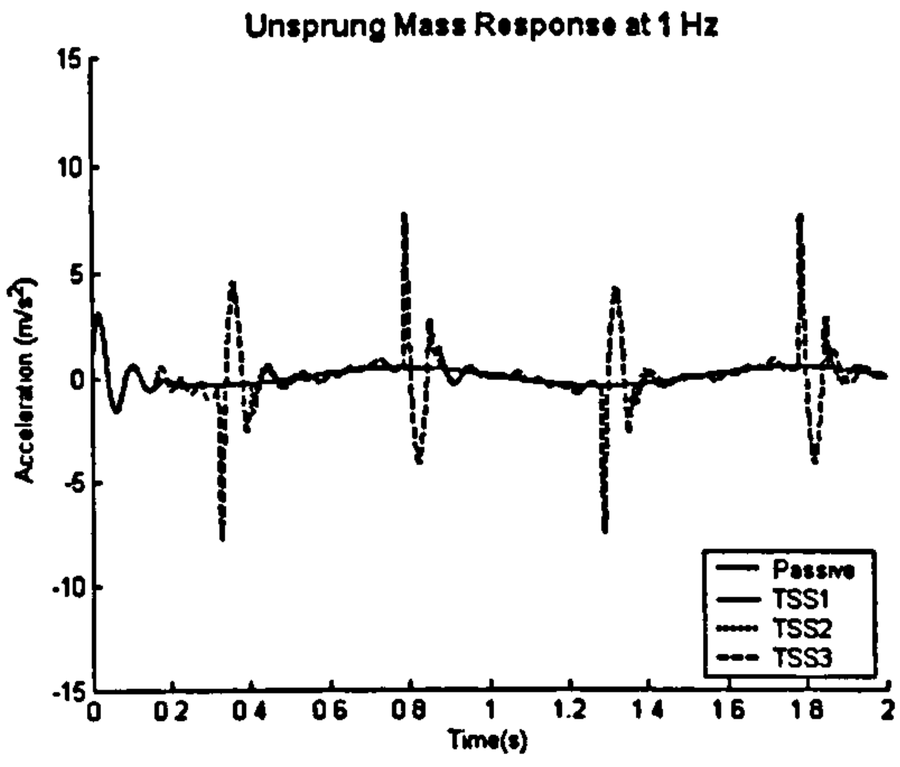

(a) At 1 Hz

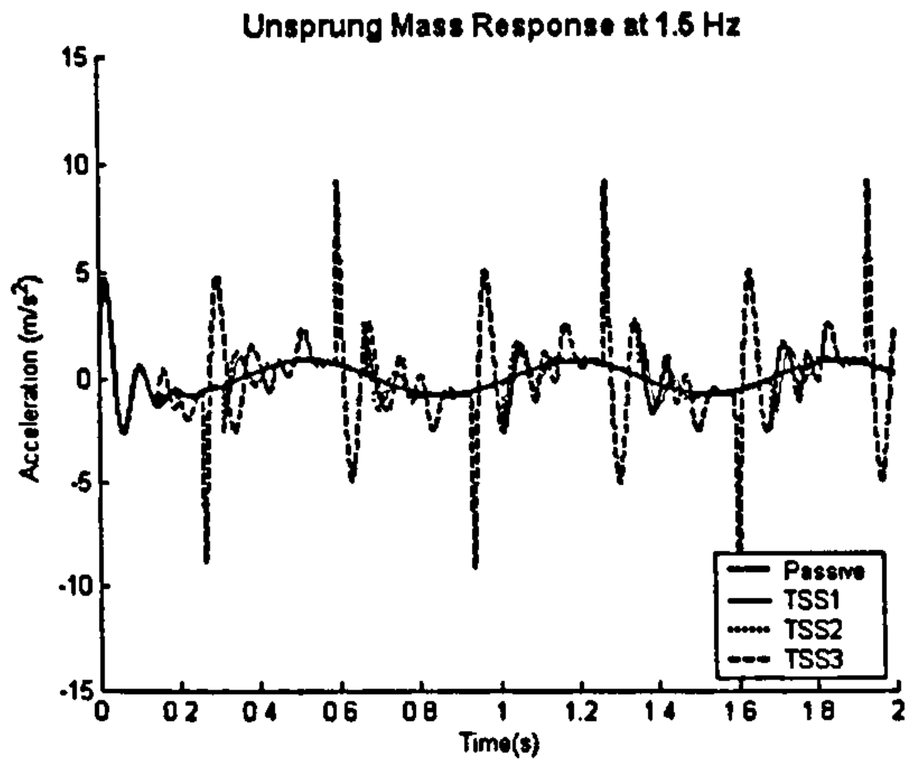

(b) At 1.5 Hz

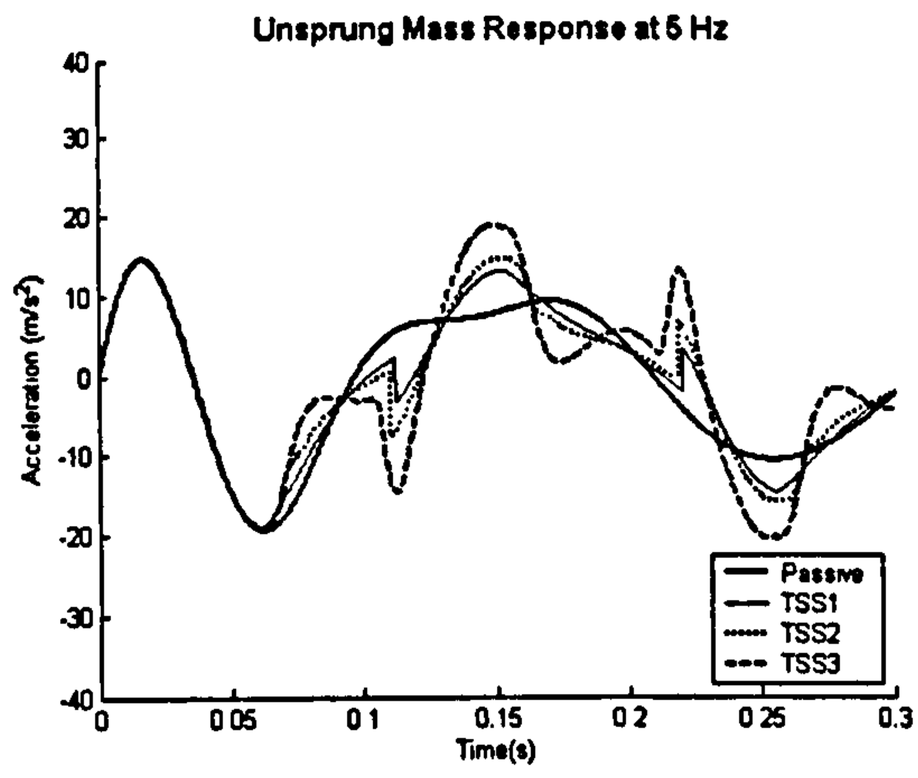

(c) At 5 Hz

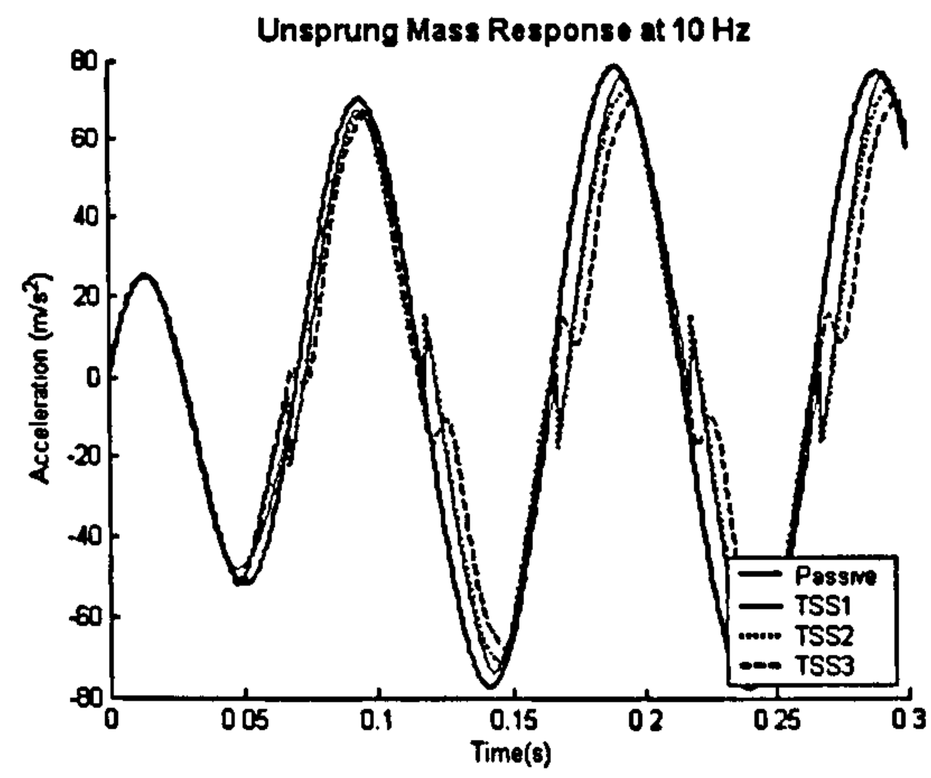

(d) At 10 Hz

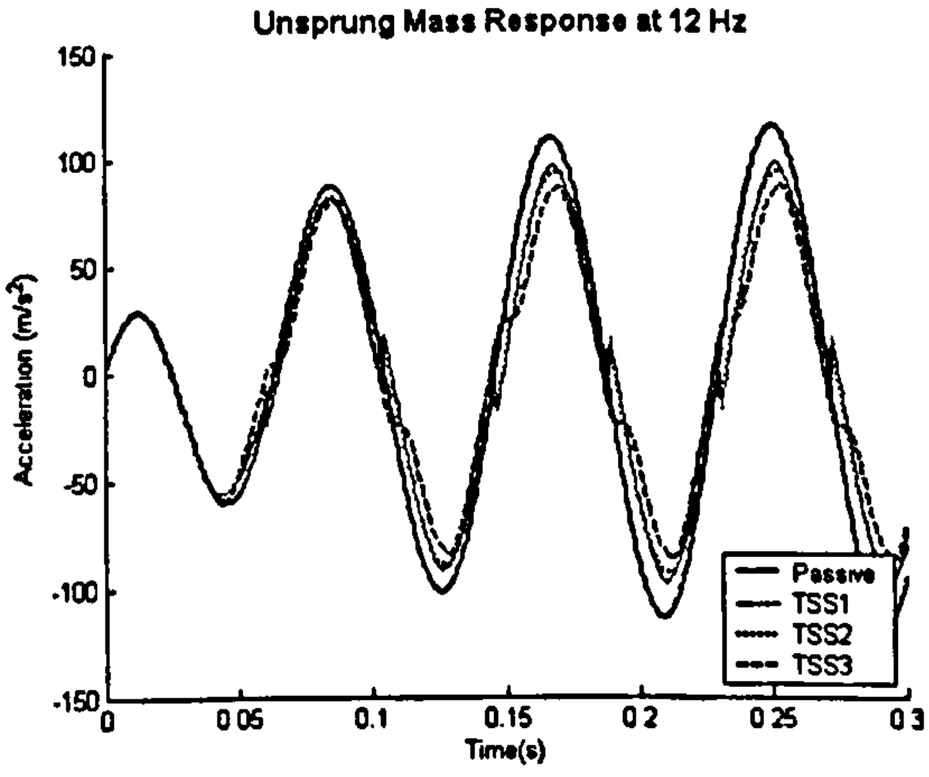

(e) At 12 Hz

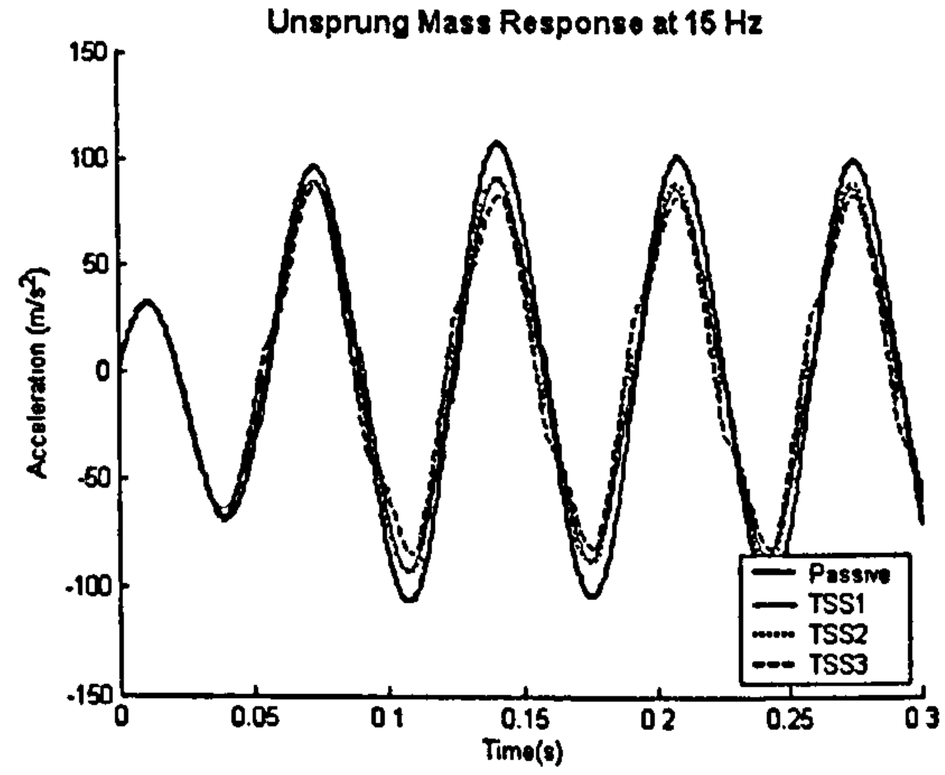

(f) At 15 Hz

Figure 5.15(a) to (f): Unsprung Mass Response

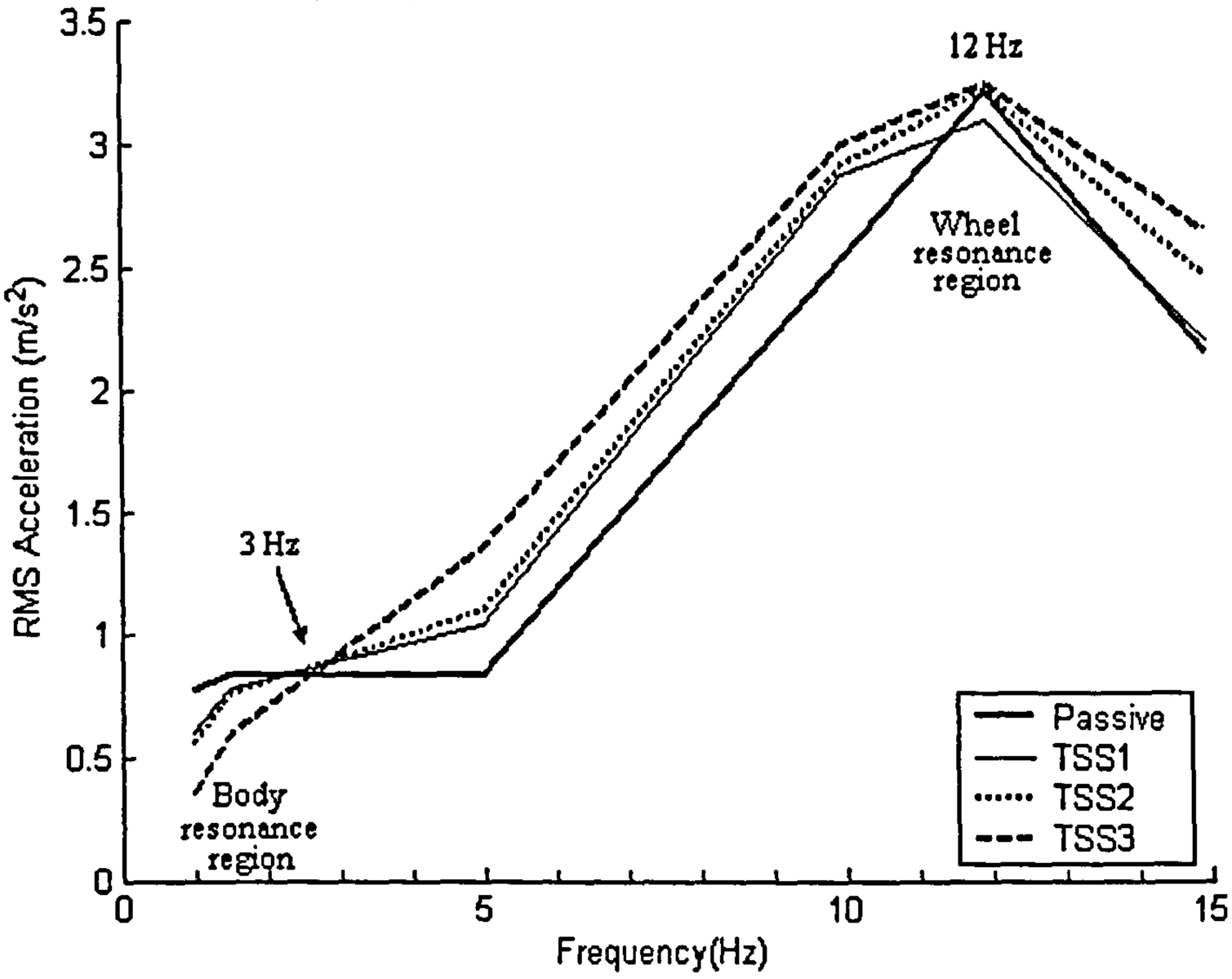

Figure 5.16: Sprung Mass RMS Acceleration

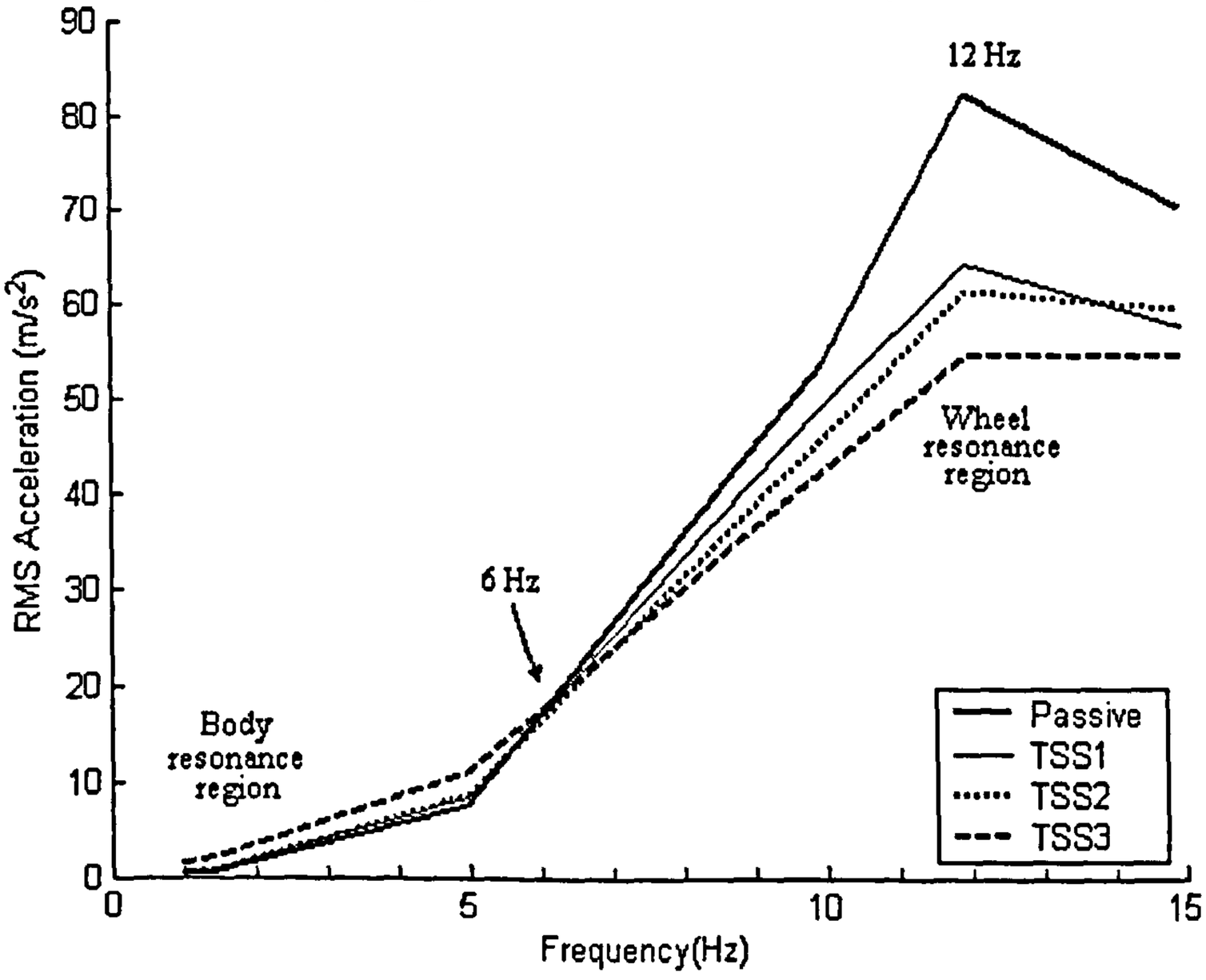

Figure 5.17: Unsprung Mass RMS Acceleration

5.5.2 Dynamic Simulation of Vehicle Models with Semi-active Systems

In the previous section, the two-state switchable strategies were analysed based on sinusoidal inputs at frequencies covering the sprung and unsprung mass resonances, using MATLAB/Simulink. The following assessment involves implementing these strategies on the MPV with realistic and lumped suspension models employing the MBS cosimulation approach. Here, the vehicles traverse a bump and pothole, as well as a random road input, used in Chapter 4, at a constant forward velocity, with the aim of examining the effect of various suspension systems on large transient and random road inputs. The study begins by evaluating the dynamic response of quarter vehicle models (a lumped mass model and a realistic model) under the influence of bump and pothole road input. Next, the two vehicle models are assessed based on the sprung and unsprung mass responses subjected to random road input.

Figure 5.18 and 5.19 show dynamic response comparison of the competing suspension systems from a lumped mass QVM. Observing sprung and unsprung mass displacement response from bump and pothole indicate TSS3 outperforms other semi-active strategies. Closer inspection of Figure 5.19 reveals TSS3 generates the smallest response and lowest oscillations for both the bump and pothole excitations compared to the other suspension systems. Since all the controller strategies implement skyhook control, significant improvement can be observed from the sprung mass response compared to the passive model. The three controller strategies provide, on average, 10 percent reduction in peak amplitudes from the passive system. Additionally, the control current switching of the TSS3 seems to perform better for transient events where it exhibits the smallest residual oscillations than from TSS1 and TSS2. This is primarily due to a larger damper force produced by TSS3 compared to TSS1 and TSS2 at low frequencies. It can be observed from the sprung mass acceleration in Figure 5.16 that TSS3 showed the best RMS acceleration reduction, among all competing systems, below 3 Hz.

Similar displacement signatures can be observed from the realistic QVM analysis illustrated in Figure 5.20 and 5.21, although there is variation in terms of amplitudes. A large reduction in sprung mass displacement response is measured for TSS3, principally due to a large damper force produced at low bandwidth compared to other

systems. Analysing the response between the lumped mass model and the realistic model, in Figure 5.19(a) and 5.21(a), shows different displacement signatures. When the vehicle travels over the bump, the lower suspension arm moves upwards until it strikes the bump stop, indirectly restricts the upward motion of the hub. This non-linear response is not present in the simulation. Referring back to Figure 4.8 and 4.9 in Chapter 4, the responses from the two vehicle models were almost similar. This was due to the application of low amplitude of the bump and pothole so that the movements of the suspension components were not affected by the non-linear element in the realistic model when the two models were compared for validation purpose.

Following on the findings from the transient excitation, the study continues by examining the semi-active strategies subjected to random road input. A right hand side of the MIRA track is used for the simulation of a lumped and a realistic QVM. Results from the sprung mass RMS acceleration in Table 5.3, indicate a reduction of at least 20 percent can be achieved from all three semi-active systems when compared with the passive case. TSS1 registers about 20 percent reduction, TSS2 registers 22 to 25 percent, and lastly TSS3 produces the most reduction at around 30 to 38 percent. Time and frequency domain representations in Figure 5.22 to 5.23 show similar trends of the competing suspension systems. Of the two vehicle models, response from the realistic QVM is generally slightly smaller that of the lumped mass model with the exception of TSS3, possibly be due to the influence of non-linear elements within the realistic model such as the bump stop.

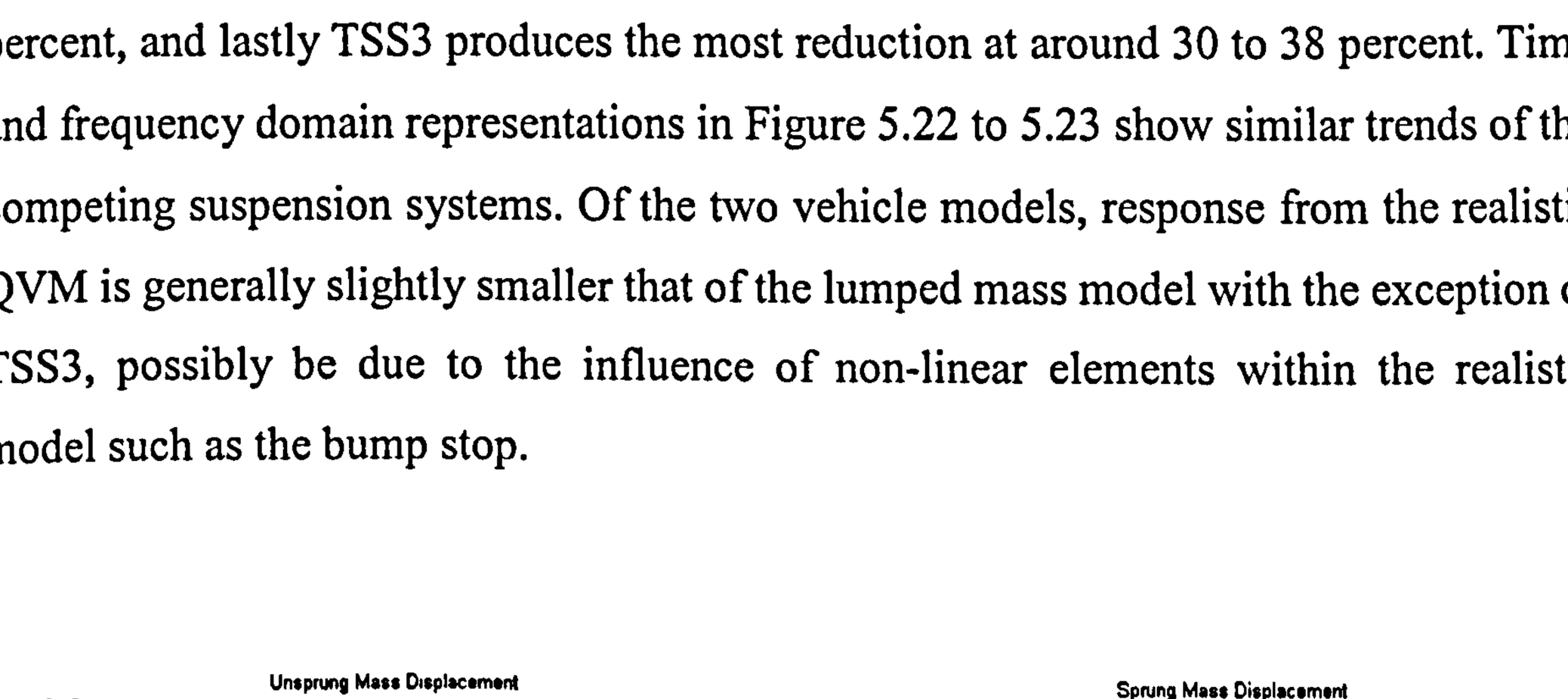

Figure 5.18: Lumped QVM Response (a) Unsprung Mass; (b) Sprung Mass

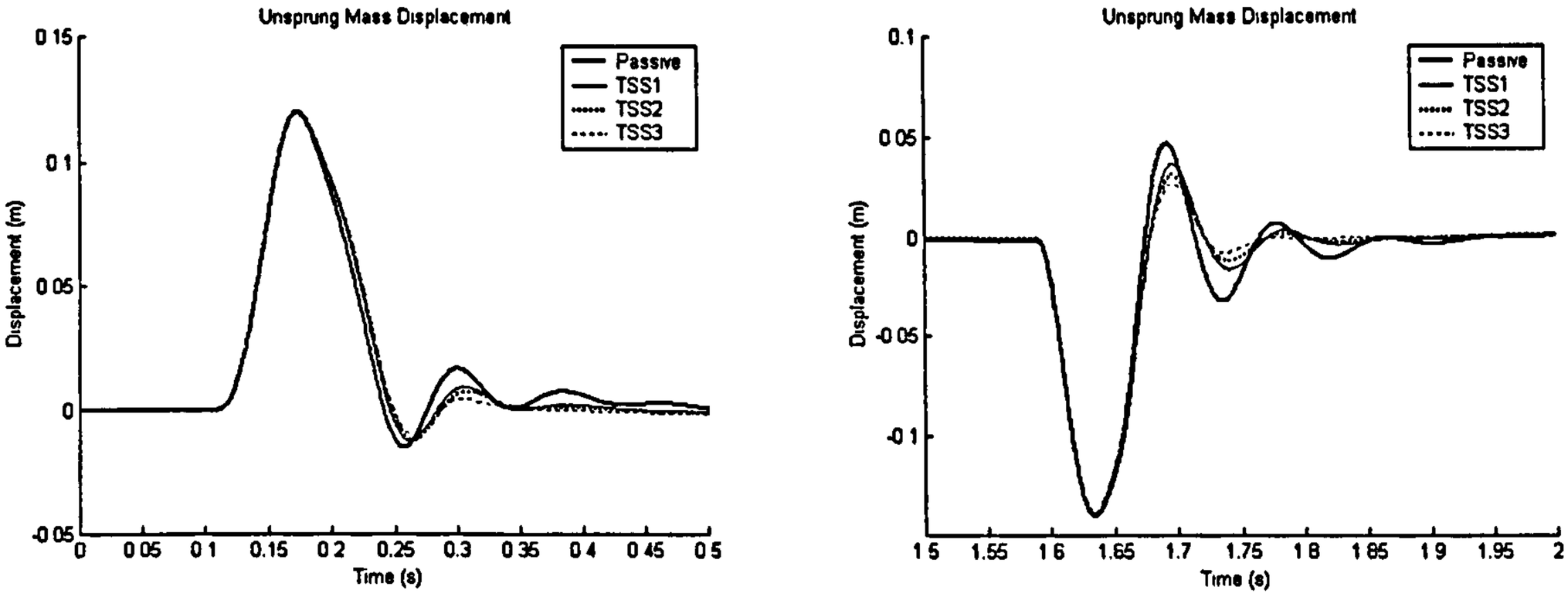

Figure 5.19: Close-up of Unsprung Mass Response (a) Bump; (b) Pothole

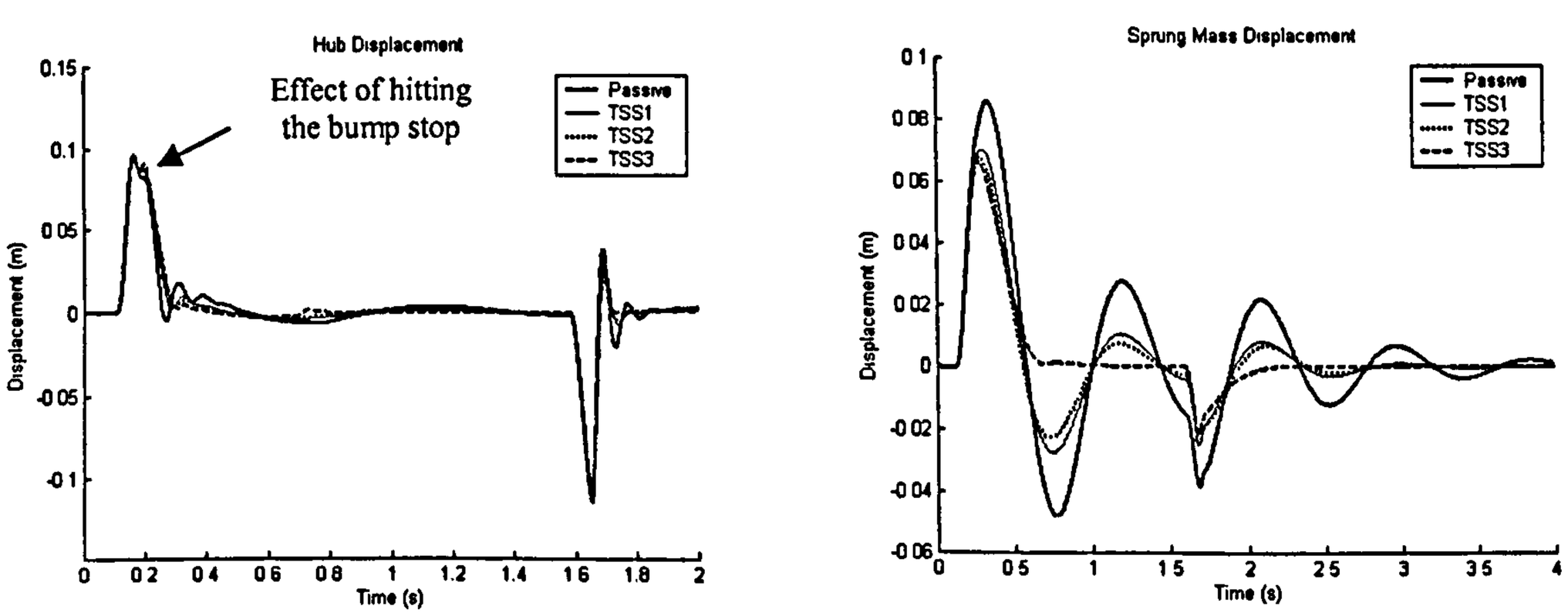

Figure 5.20: Realistic QVM Response (a) Hub; (b) Sprung Mass

Figure 5.21: Close-up of Hub Response (a) Bump; (b) Pothole

Suspension Types	Sprung Mass RMS Acceleration (in m/s^2)		% difference (based on lumped mass QVM)
	Lumped mass QVM	Realistic QVM	
Passive	0.8981	0.8336	7.2
TSS1	0.7112	0.6720	5.5
TSS2	0.6752	0.6452	3
TSS3	0.5528	0.5815	-5.2

Table 5.3: RMS Acceleration Comparison due to Random Road Input

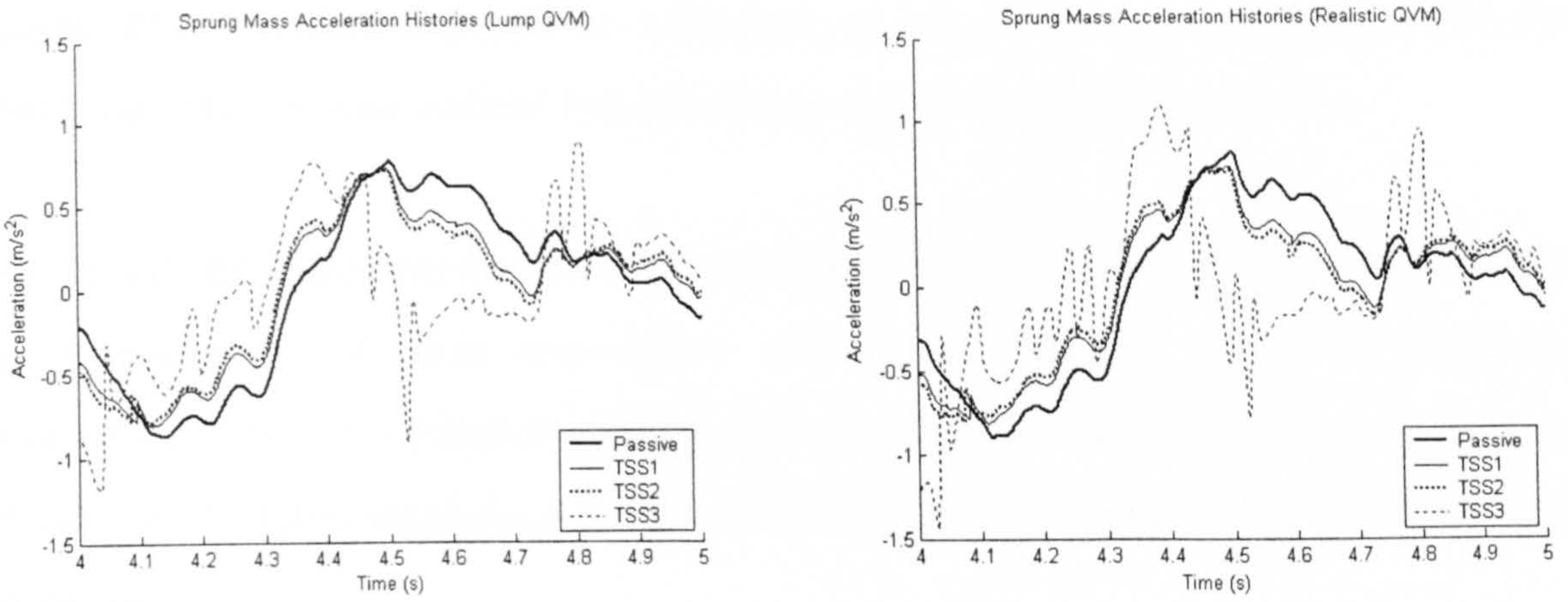

(a) (b)

Figure 5.22: Acceleration Histories (a) Lumped QVM; (b) Realistic QVM

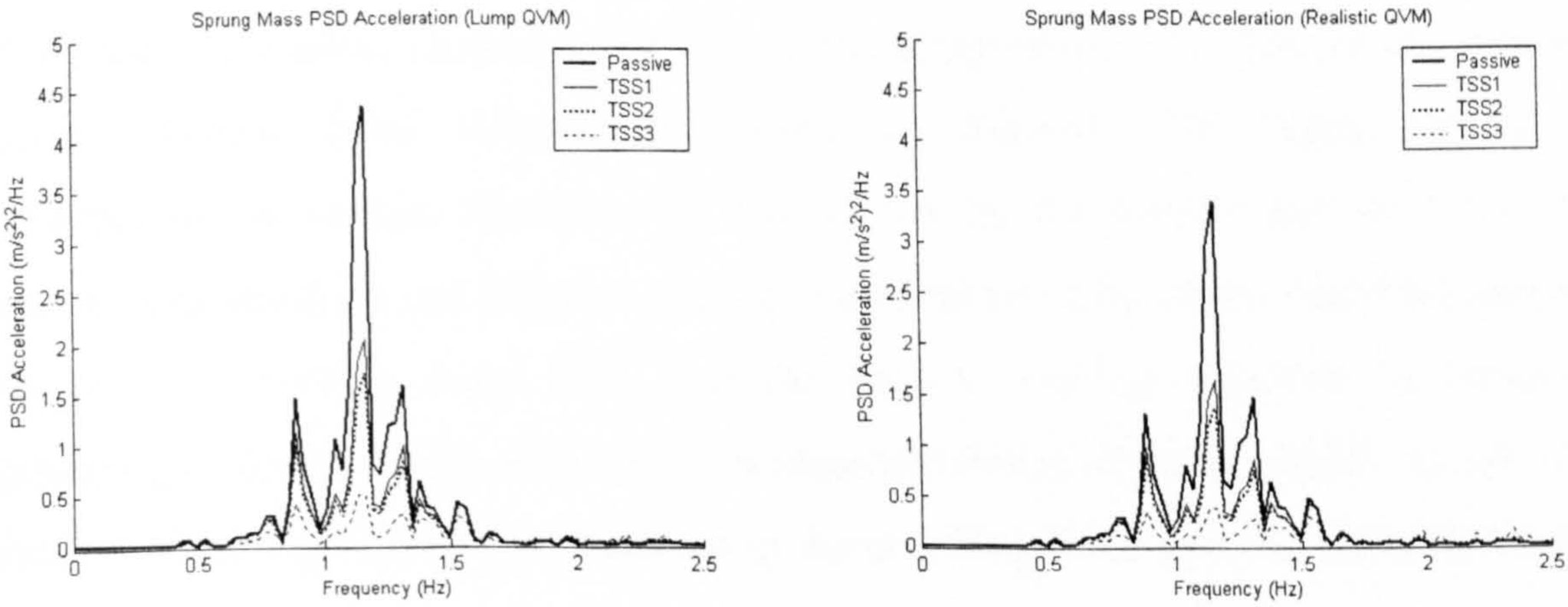

(a) (b)

Figure 5.23: Acceleration PSD (a) Lumped QVM; (b) Realistic QVM

5.5.3 Dynamic Response of a Suspension Component

Assessment in this section centres on attaining dynamic loads from the competing suspension systems. It considers the lower suspension arm from the realistic QVM and evaluates three TSS semi-active models against the passive system. The vehicle is driven over a numerical representation of the MIRA right hand track using MATLAB/Simulink at a constant forward velocity of 34 km/h (9.44 m/s). This generates a dynamic response measured as acceleration histories recorded along the arm. The analysis focuses on measurement at the centre of gravity and at two other locations, namely Loc1 and Loc2, as illustrated in Figure 5.24. Results are presented as overall RMS accelerations and as a function of acceleration power spectral densities (PSD) recorded in longitudinal (x), lateral (y), and vertical (z) directions.

The overall RMS accelerations of the suspension arm are tabulated in Table 5.4. Here, the performance of each semi-active strategy is assessed based on percentage improvement from the passive system [20] expressed in Equation 5.13. A positive sign of the overall value indicates a reduction in vibration level and a negative sign shows otherwise.

$$\%\ improve \;=\; \frac{ACC_{RMS}(passive) - ACC_{RMS}(semi-active)}{ACC_{RMS}(passive)} \qquad \textbf{Eq 5.13}$$

Of all three principle measurement directions, longitudinal (x) records the smallest overall vibration level, followed by lateral (y) direction. The highest levels are registered in the vertical direction (z). This is true for the passive and the three TSS systems. Longitudinal and lateral movements are restricted by constraints adjoining the arm with the vehicle body, hub, and the tie-rod. Vertical vibration is dominant particularly near the hub (Loc1) due to its close proximity of the excitation source. The vibration energy gradually decreases along the arm from Loc1 to Loc2 (near the body).

Comparing the semi-active strategies, TSS2 produces a maximum reduction in overall vibration. On average the system provides a reduction of between 15 and 25 percent from the passive system except in vertical direction at the arm centre of gravity, where

only a drop of 10 percent is observed. TSS1 records a similar yet smaller reduction when compared to TSS2. In contrast, TSS3 performs poorly at the lower suspension arm with most of the vibration levels exceeding that of the passive system. The highest level is registered at Loc1 in the vertical direction, and can be observed in the PSD plots illustrated in Figure 5.25(a) and (b) to 5.27(a) and (b).

Due to the characteristics of the TSS systems, the PSD plots in the longitudinal, lateral and vertical directions are described in terms of two frequency ranges, namely (a) at low bandwidth (0–5 Hz), and (b) at higher bandwidth (5–50 Hz). At low frequency in the region of body (0.5–1.5 Hz), TSS3 appears to exhibit the lowest response in all principal directions (see Figure 5.25(a), Figure 5.26(a), and Figure 5.27(a)). However, above these frequencies (around the wheel hop region, from 10–15 Hz, TSS3 performance deteriorates drastically influencing the overall vibration levels (Figure 5.25(b), Figure 5.26(b), and Figure 5.27(b)). Further evidence is highlighted in Figure 5.28(a) to (d), which examines the hub and body acceleration response. Vertical vibration energy for TSS3 extends well above the wheel hop frequency to about 50 Hz in the proximity of the hub and the arm at Loc1 (5.28 (a) and (b), respectively). It can be concluded that even though TSS3 has excellent performance in ride comfort with significant reduction in body acceleration, it has adverse effects on loads at component levels which could be detrimental to fatigue life. In general, TSS2 exhibits the best performance not only with respect to ride comfort but generates smaller loads on the suspension components as well. This is achieved by means of linearising the MR damper response.

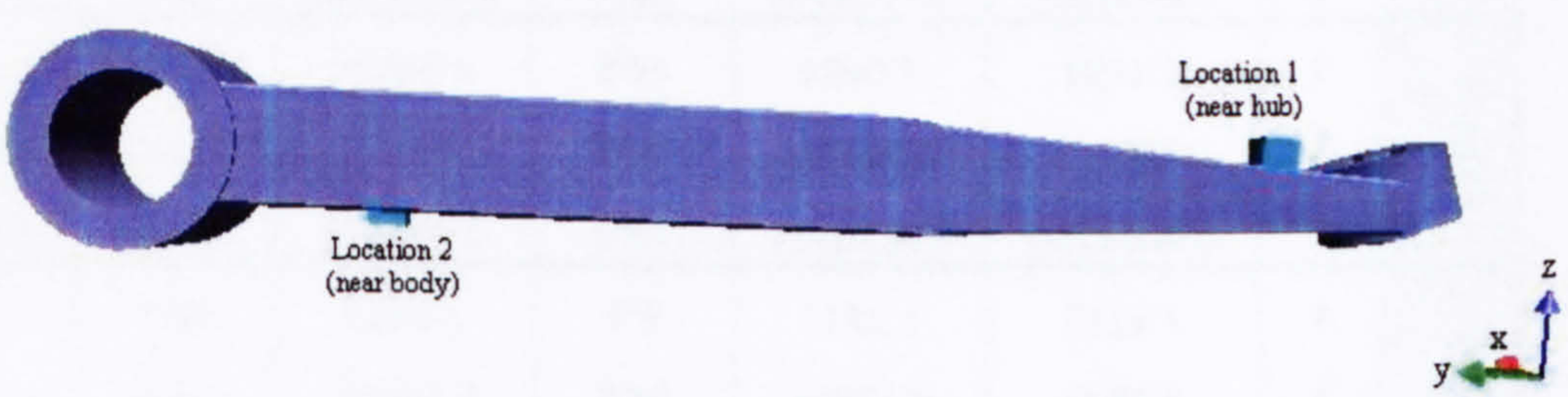

Figure 5.24: Lower Suspension Arm Measurement Positions

		Passive	TSS 1		TSS 2		TSS 3	
Dir.		Acc RMS (m/s^2)	Acc RMS (m/s^2)	% improve	Acc RMS (m/s^2)	% improve	Acc RMS (m/s^2)	% improve
C of G Loc 1	x	0.0024727	0.001965	**20.5**	0.00187	**24.4**	0.0022779	**7.9**
	y	0.1853	0.15859	**14.4**	0.14102	**23.9**	0.27384	**-47.8**
	z	1.8712	1.7111	**8.6**	1.5827	**15.4**	3.0176	**-61.3**
	x	0.0021199	0.0017912	**15.5**	0.001743	**17.8**	0.0023929	**-12.9**
	y	0.062426	0.049574	**20.6**	0.048729	**21.9**	0.080131	**-28.4**
	z	1.1184	1.0064	**10.0**	0.99714	**10.8**	1.6461	**-47.2**
Loc 2	x	0.0022736	0.0020336	**10.6**	0.0019187	**15.6**	0.0031968	**-40.6**
	y	0.073985	0.064739	**12.5**	0.060339	**18.4**	0.10828	**-46.4**
	z	0.79274	0.67123	**15.3**	0.64311	**18.9**	0.77377	**2.4**

Table 5.4: Lower Suspension Arm RMS Acceleration Comparison

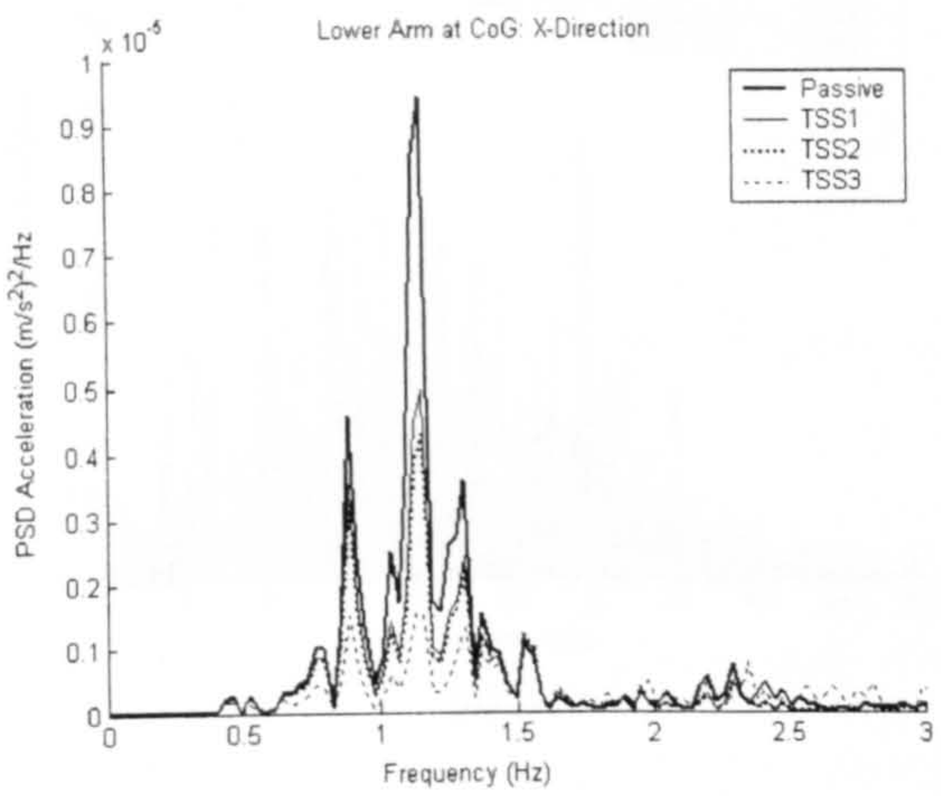

(a) At Low Frequency

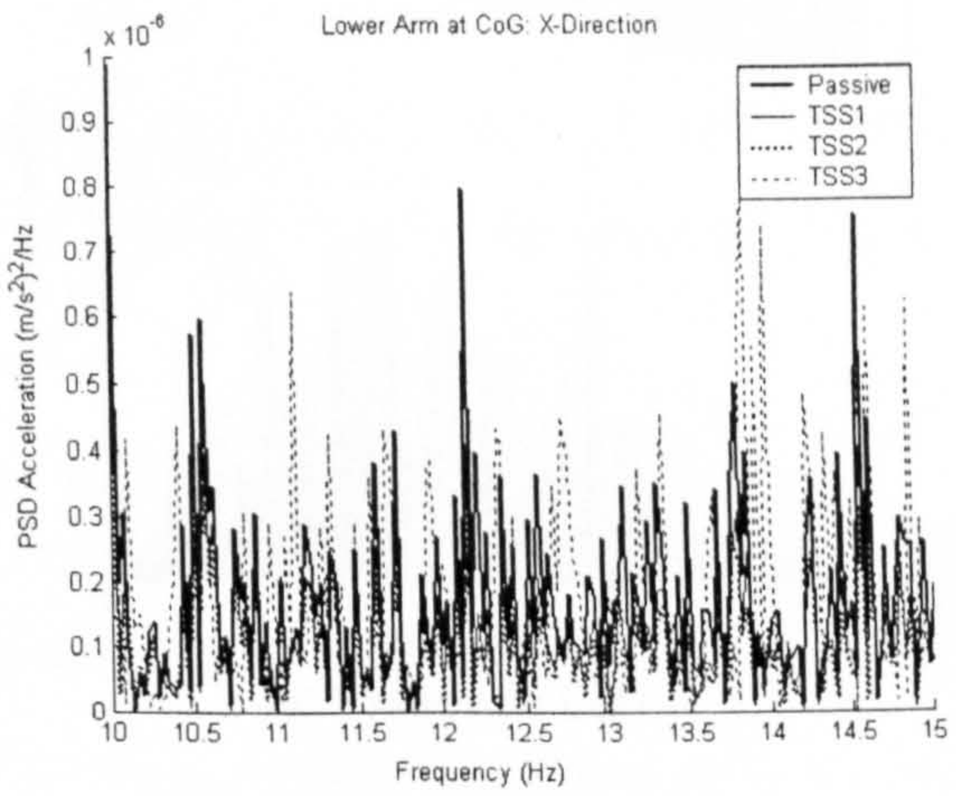

(b) At High Frequency

Figure 5.25 (a) and (b): PSD Accelerations in Longitudinal (x) Direction

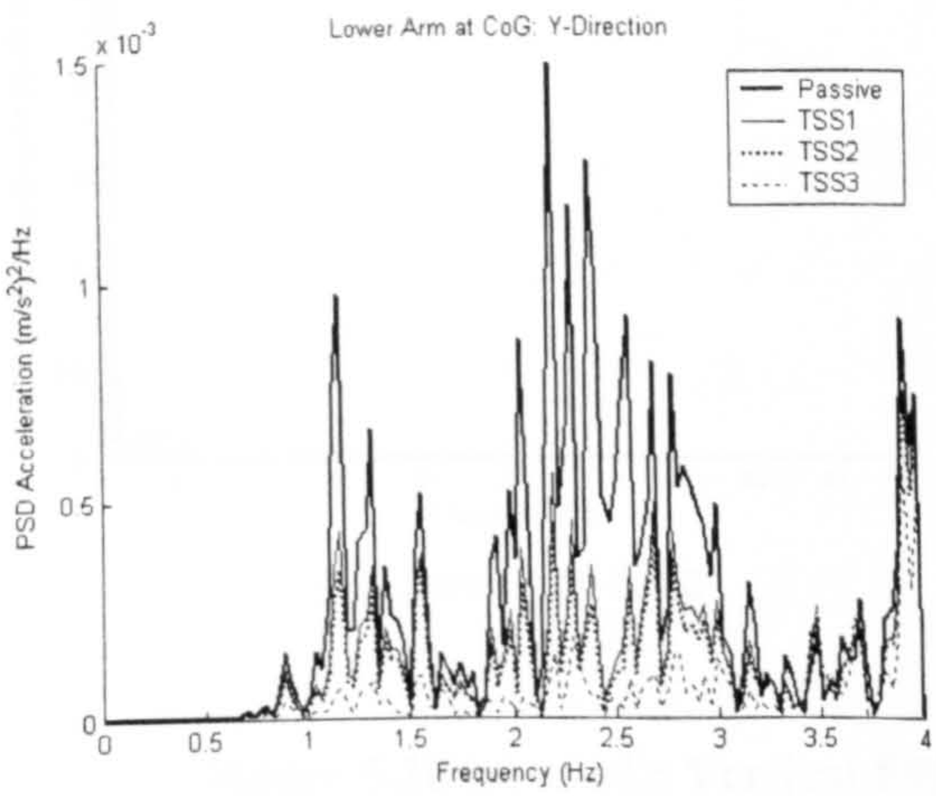

(a) At Low Frequency

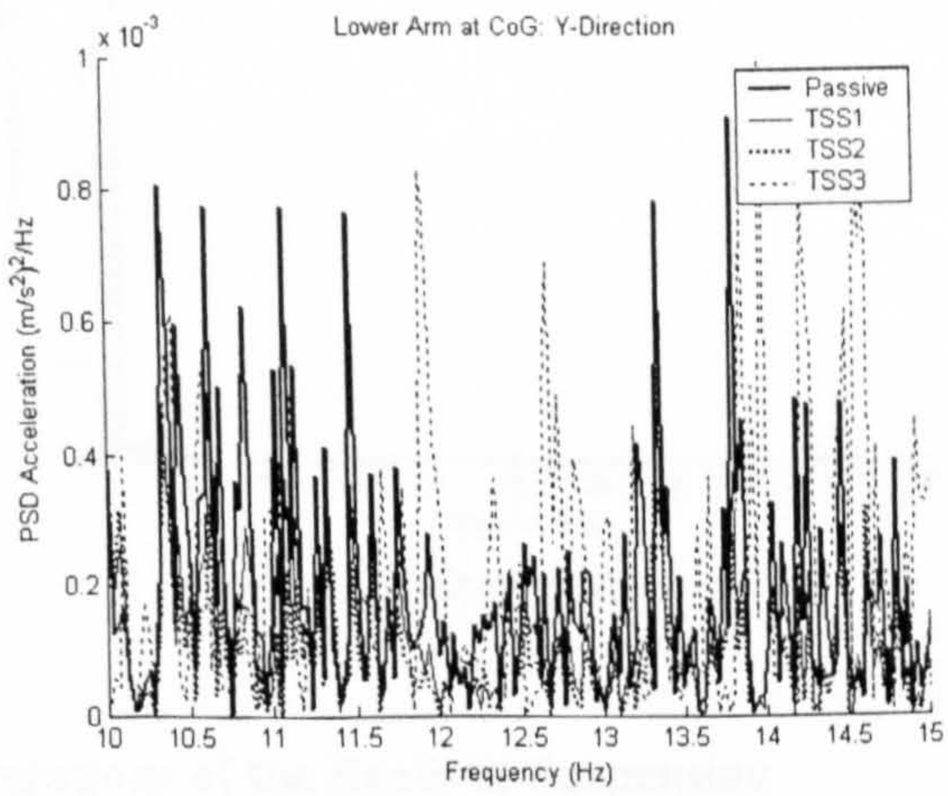

(b) At High Frequency

Figure 5.26 (a) and (b): PSD Accelerations in Lateral (y) Direction

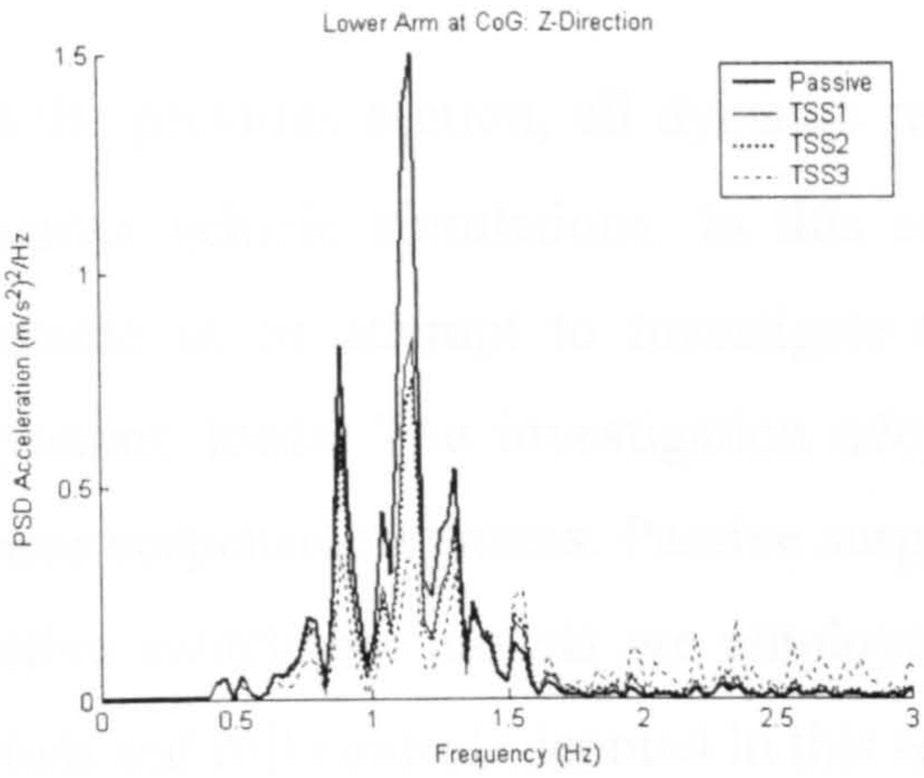

(a) At Low Frequency

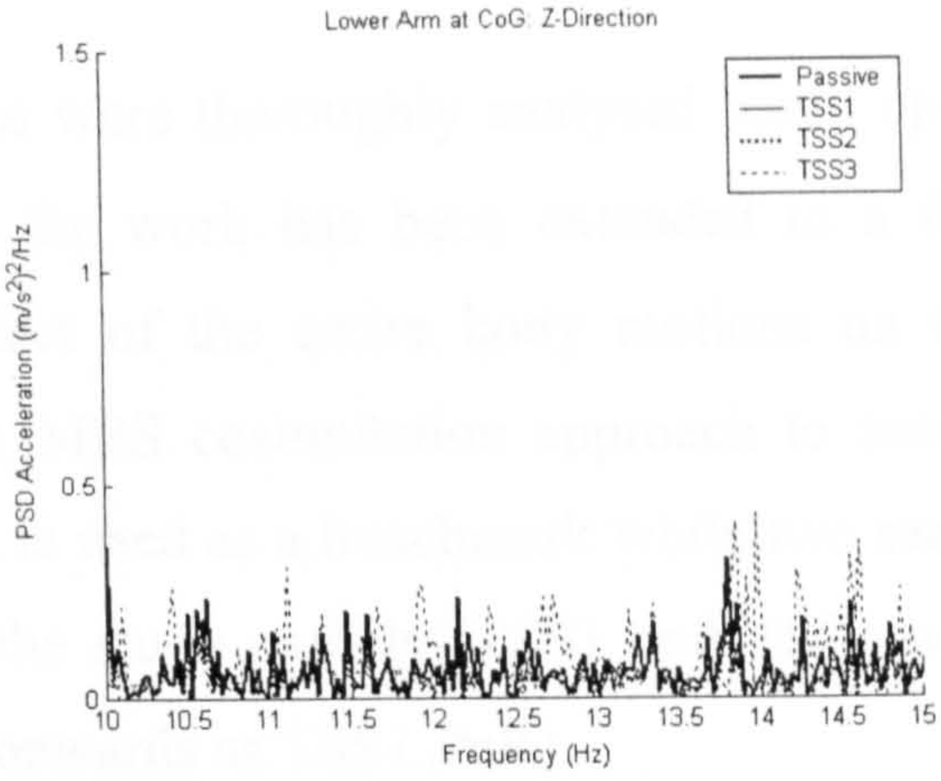

(b) At High Frequency

Figure 5.27 (a) and (b): PSD Accelerations in Vertical (z) Direction

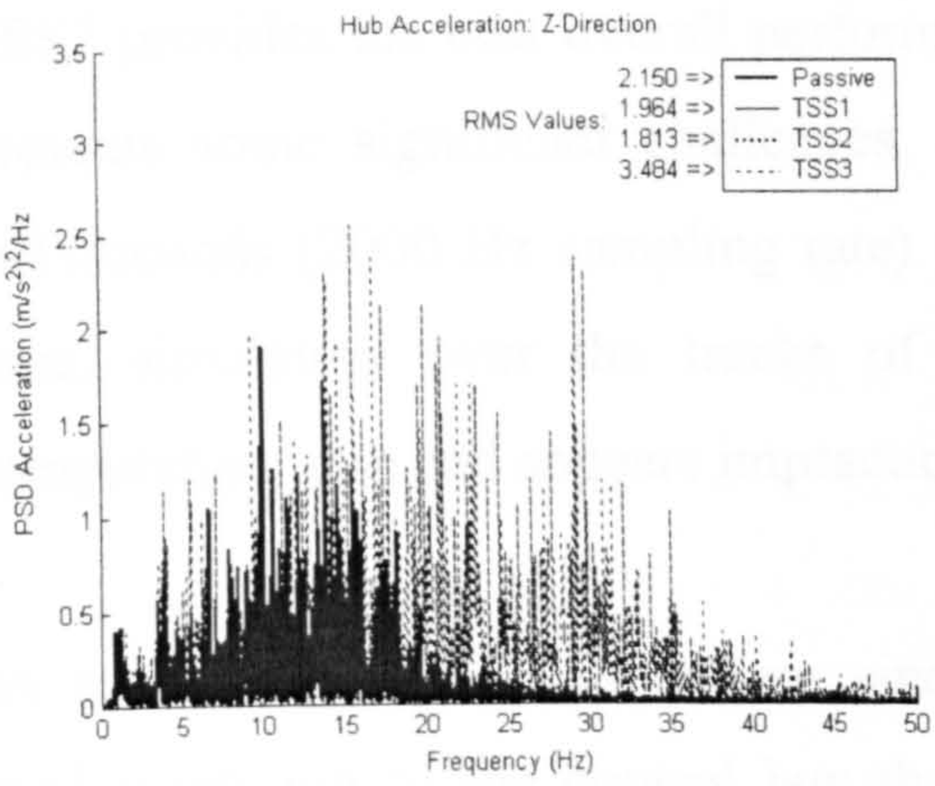

(a) Hub

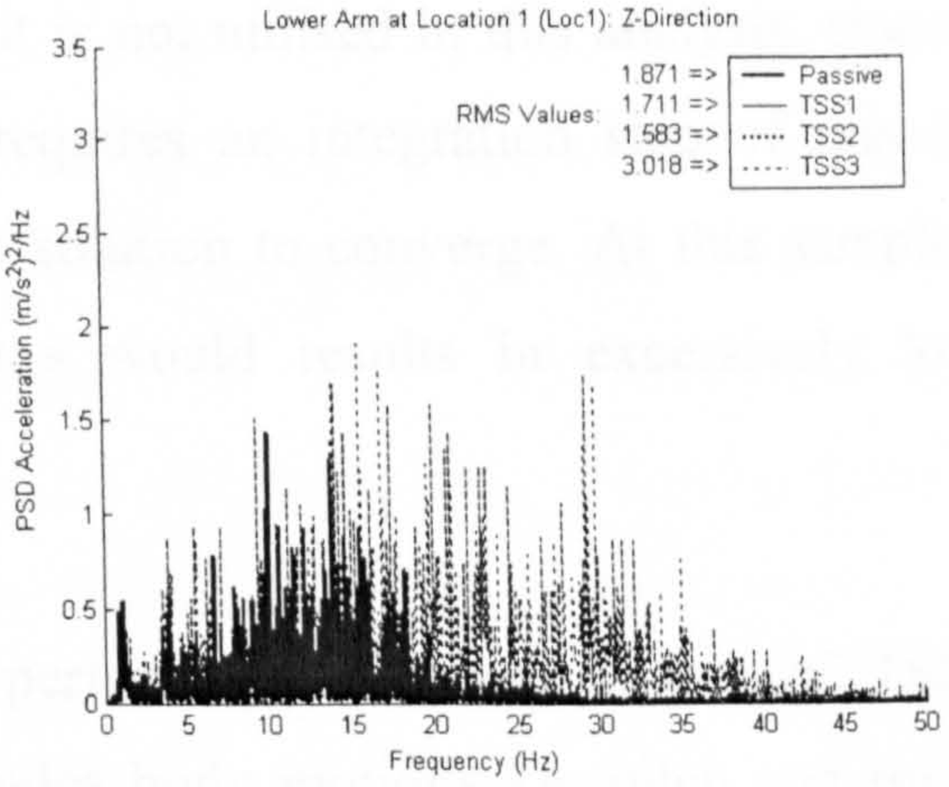

(b) Lower Arm Loc1

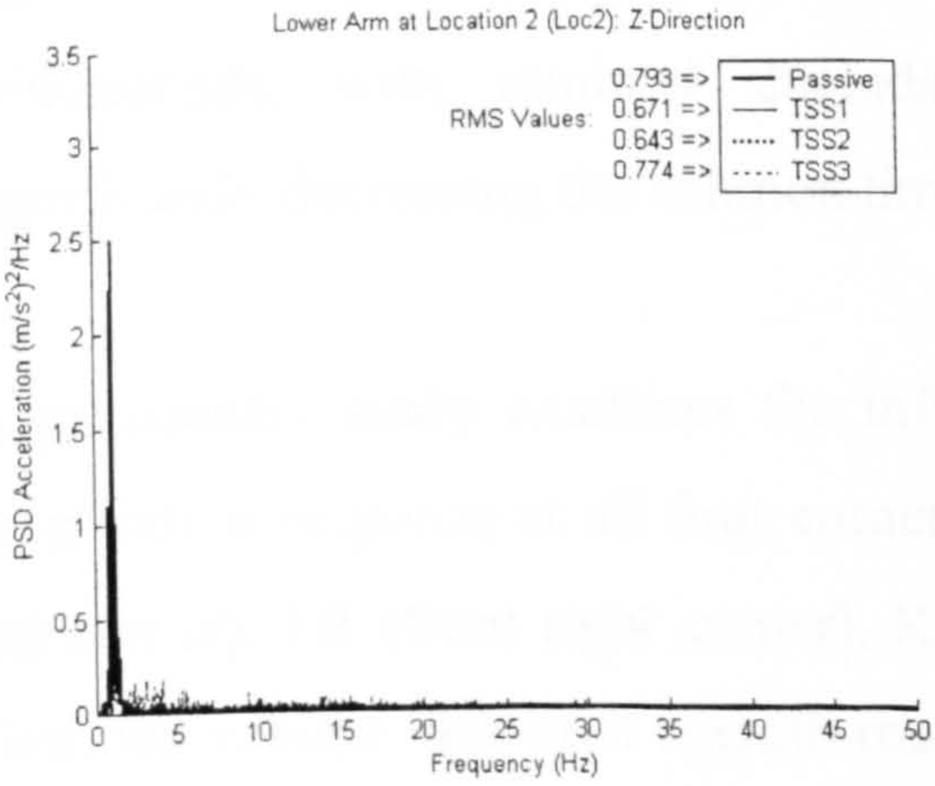

(c) Lower Arm Loc2

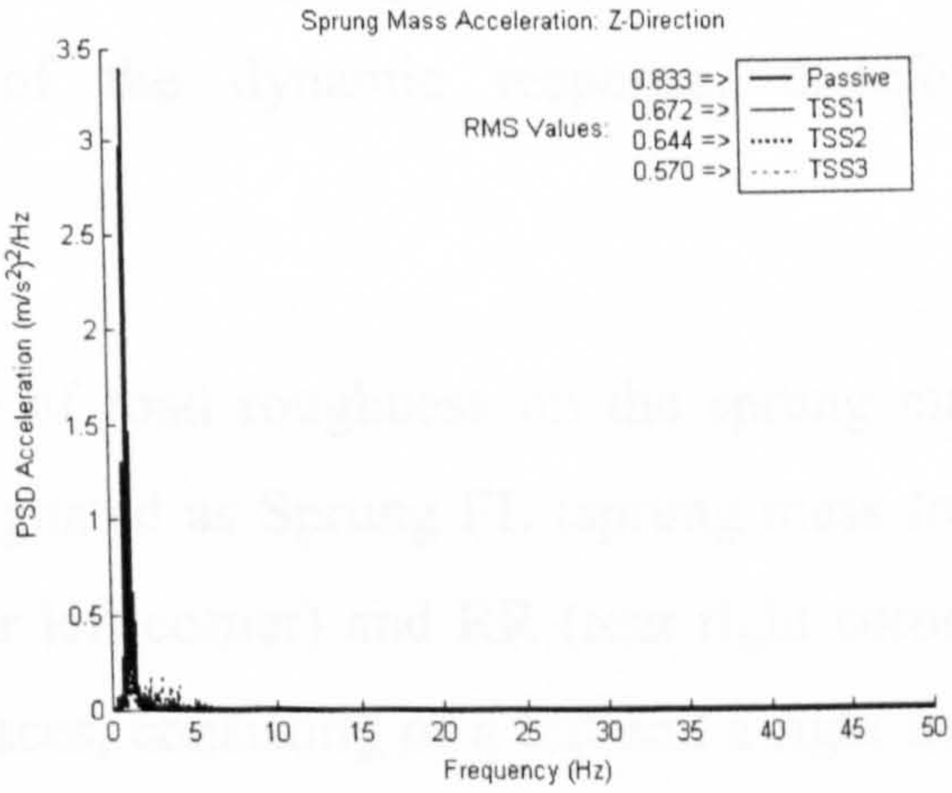

(d) Sprung Mass

Figure 5.28 (a) to (d): Vertical PSD Accelerations of the Realistic Suspension

5.5.4 Suspension Control Strategies for a Lumped Mass FVM

In the previous section, all dynamic responses were thoroughly analysed based upon quarter vehicle simulations. In this section, the work has been extended to a full vehicle in an attempt to investigate the effect of the entire body motions on the dynamic loads. The investigation adopts the MBS cosimulation approach to assess three suspension systems. Passive suspension is used as a benchmark while two semi-active switchable models are employed for the study namely, TSS1 and TSS1 with pitch and roll control (denoted in this section onwards as TSS1 PnR).

Passive and TSS1 suspension models emulate totally independent suspension. Here, each corner is allowed to move independently, neglecting the influence of body motions. TSS1 PnR considers these effects as described in section 5.4.4. Although TSS2 provides the best overall performance, it is not utilised in this analysis, since it presents some significant challenges, as it requires an integration step of just 0.5 milliseconds (2000 Hz sampling rate) for the solution to converge. At this sampling time, simulation over the tracks of 30-40 s would results in excessively long computation time and appears impractical.

As a substitute, TSS1 is chosen since its performance is close to that of TSS2. Implementation of the control law that includes body motions i.e. pitch and roll is much simpler since it only considers two damping states (hard and soft damping coefficients). Additionally, TSS1 allows a lower sampling rate of 500 Hz or 2 milliseconds, with minimal degradation of the dynamic response, therefore, significantly decreasing the solution time.

A preliminary study examines the influence of road roughness on the sprung mass acceleration response at all four corners designated as Sprung FL (sprung mass front left corner), FR (front right corner), RL (rear left corner) and RR (rear right corner). First, the vehicle runs on a smooth road surfaces, consisting of a left and a right track of a virtual representation of MIRA road as shown in Figure 4.6(a) and (b), at a constant forward velocity of 34 km/h for 20 s. Then the procedure is repeated for a rough road surface, also known as durability track, that comprises of a numerical representation of the left and the right hand side of Leyland Technical Centre (LTC)

pavé as illustrated in Figure 4.7(a) and (b) at the same forward velocity. The analysis is conducted for an unladen full vehicle model.

Table 5.5 summarizes the overall RMS acceleration for the vehicle sprung mass at all four corners subjected to road input from the MIRA tracks. On average switchable semi-active systems reduces body acceleration between 15–20 percent over the passive system. It shows that TSS1 with independent suspension performs marginally better than those from TSS1 PnR. Minimal improvement of TSS1 PnR might be due to lack of pitch and roll motions when travelling on this surface. According to Nell and Styen [20] the performance of this type of controller performs better on rough road profiles. Levesley *et al.* [111] suggest continuing the study on a durability road sections at various constant velocities to assess the pitch and roll strategy.

Examining the results in Table 5.6 indicates the performance of TSS1 PnR significantly deteriorates on rough road profiles. RMS acceleration values on two corners slightly exceed those from the passive system while the other two corners show relatively small improvement. In contrast, TSS1 with independent suspension appears to generate improvement in ride comfort with an average reduction between 13–20 percent. The reduction is consistent with the results from the suspension arm presented for the realistic QVM, in which the maximum possible reduction of 20 percent can be achieved with TSS1.

For the TSS1 PnR, it can be concluded that the strategy does not work as expected. The original application [20] was intended for an off-road commercial vehicle in which the vehicle was modelled in three degrees of freedom consisting of body bounce, pitch and roll motion only. The relative velocities were measured between the vehicle body and the ground in which the unsprung masses were assumed negligible with respect to the vehicle body mass. At present, the application of TSS1 PnR has been modified to suit a small size multi-purpose vehicle. Here, the relative velocities are recorded between the vehicle body and the corresponding unsprung mass. In this case, the response from the unsprung mass must be considered since it significantly affects the overall vibration levels.

RMS Acceleration at 34 km/h	Passive (m/s^2)	TSS1 (m/s^2)	% improve	TSS1 PnR (m/s^2)	% improve
Sprung Mass FL	0.8427	0.6756	19.8	0.6734	20.1
Sprung Mass FR	0.8836	0.6999	20.8	0.7276	17.7
Sprung Mass RL	0.8432	0.6953	17.5	0.7284	13.6
Sprung Mass RR	0.8465	0.6899	18.5	0.6742	20.3

Table 5.5: Vertical RMS Acceleration on Smooth Road (MIRA Track)

RMS Acceleration at 34 km/h	Passive (m/s^2)	TSS1 (m/s^2)	% improve	TSS1 PnR (m/s^2)	% improve
Sprung Mass FL	1.4633	1.2744	12.9	1.5234	-4.1
Sprung Mass FR	1.4348	1.152	19.7	1.4216	1
Sprung Mass RL	1.4338	1.1517	19.7	1.4205	1
Sprung Mass RR	1.46	1.2698	13	1.5186	-4

Table 5.6: Vertical RMS Acceleration on Rough Road (LTC Pavé)

To further verify the performance of TSS1 PnR, the FVM is tested on the LTC pavé at various constant forward velocities. Analysis focuses on sprung mass acceleration response at all four corners in three principal directions i.e. lateral (x), longitudinal (y), and vertical (z). Table 5.7 to 5.10 provide the summary of overall RMS accelerations calculated from 0 to 16 Hz. General trends remain similar to previous finding where vertical vibrations dominate overall levels for all competing suspension systems. It can be observed that as the velocity increases, the overall vibration gradually increases. Again, it shows that this type of semi-active controller does not perform as good as the independent TSS1. Figures 5.26 (a) to (d) reveal sprung mass acceleration from TSS1 PnR exhibits a higher response than the passive systems while TSS1 with independent suspension appears to generate a more consistent reduction at all corners.

FL Sprung Mass RMS Acc (m/s^2)		34 km/h	40 km/h	60 km/h	80 km/h
X	Passive	0.5113	0.5317	0.5689	0.5837
	TSS1	0.5181	0.5286	0.5672	0.6391
	TSS1 PnR	0.5256	0.5499	0.5899	0.6369
Y	Passive	0.3609	0.3805	0.4664	0.5339
	TSS1	0.333	0.3467	0.3979	0.4565
	TSS1 PnR	0.363	0.3873	0.4697	0.5442
Z	Passive	2.2382	2.3231	2.6384	2.9071
	TSS1	2.1833	2.2485	2.458	2.7894
	TSS1 PnR	2.3187	2.4218	2.7331	3.0611

Table 5.7: RMS Accelerations at Front Left Body

FR Sprung Mass RMS Acc (m/s^2)		34 km/h	40 km/h	60 km/h	80 km/h
X	Passive	0.5114	0.5425	0.5716	0.6123
	TSS1	0.5213	0.5433	0.5769	0.6307
	TSS1 PnR	0.529	0.5617	0.5958	0.6332
Y	Passive	0.3665	0.3834	0.458	0.5127
	TSS1	0.3374	0.3489	0.3942	0.4302
	TSS1 PnR	0.3707	0.3913	0.4641	0.52
Z	Passive	2.2355	2.384	2.6986	2.9605
	TSS1	2.1116	2.2177	2.425	2.6347
	TSS1 PnR	2.2497	2.4199	2.7279	2.9734

Table 5.8: RMS Accelerations at Front Right Body

RL Sprung Mass RMS Acc (m/s^2)		34 km/h	40 km/h	60 km/h	80 km/h
X	Passive	0.5055	0.5314	0.5605	0.5758
	TSS1	0.5103	0.5264	0.5541	0.5787
	TSS1 PnR	0.5234	0.5503	0.5831	0.5903
Y	Passive	0.3522	0.3733	0.4398	0.4728
	TSS1	0.3237	0.3403	0.3773	0.4083
	TSS1 PnR	0.3559	0.3819	0.4444	0.4856
Z	Passive	2.2312	2.3812	2.6893	2.9615
	TSS1	2.108	2.2166	2.4204	2.6359
	TSS1 PnR	2.2456	2.4171	2.7187	2.9743

Table 5.9: RMS Accelerations at Rear Left Body

RR Sprung Mass RMS Acc (m/s^2)		34 km/h	40 km/h	60 km/h	80 km/h
X	Passive	0.51	0.5467	0.5704	0.6082
	TSS1	0.518	0.5459	0.5705	0.6171
	TSS1 PnR	0.5314	0.5672	0.5957	0.628
Y	Passive	0.3621	0.3813	0.4387	0.4843
	TSS1	0.3316	0.3469	0.3803	0.4132
	TSS1 PnR	0.3681	0.3908	0.4454	0.4915
Z	Passive	2.2331	2.3139	2.6257	2.7993
	TSS1	2.1764	2.2392	2.4474	2.6162
	TSS1 PnR	2.3119	2.4122	2.7198	2.9165

Table 5.10: RMS Accelerations at Rear Right Body

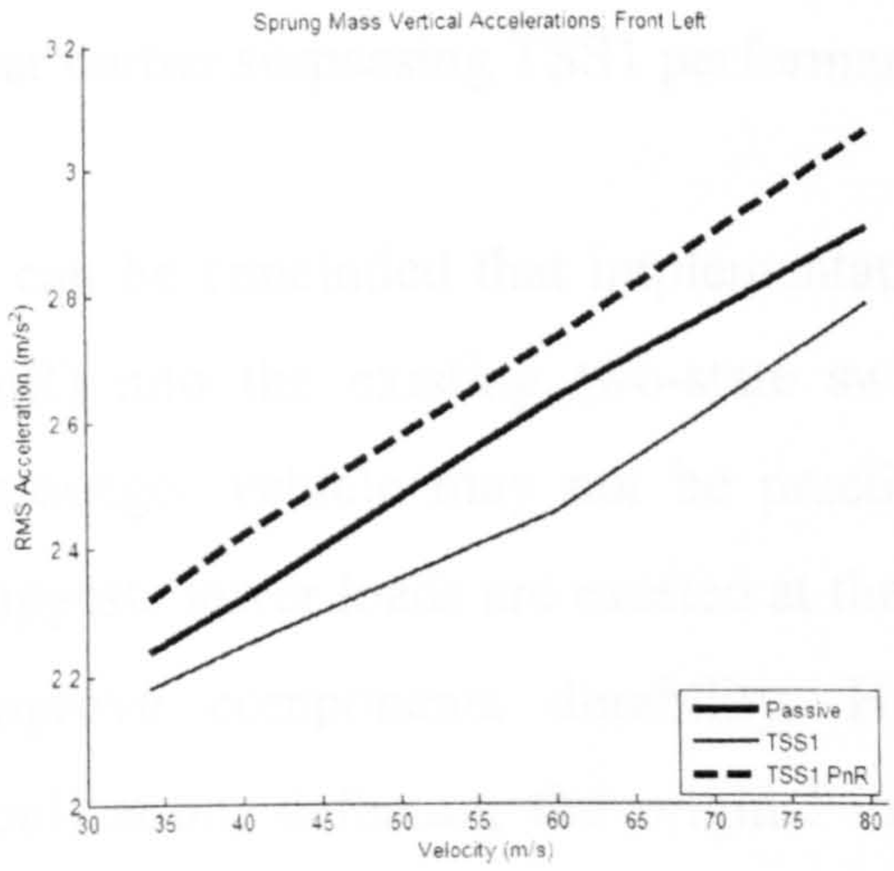

(a) Front Left

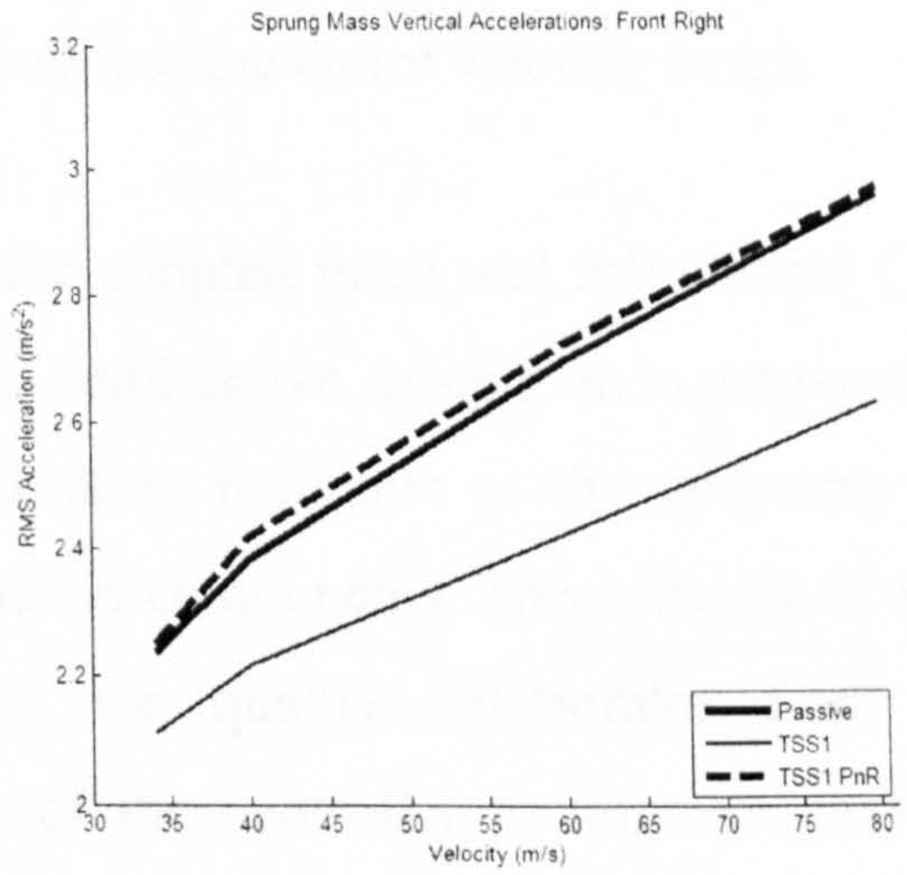

(b) Front Right

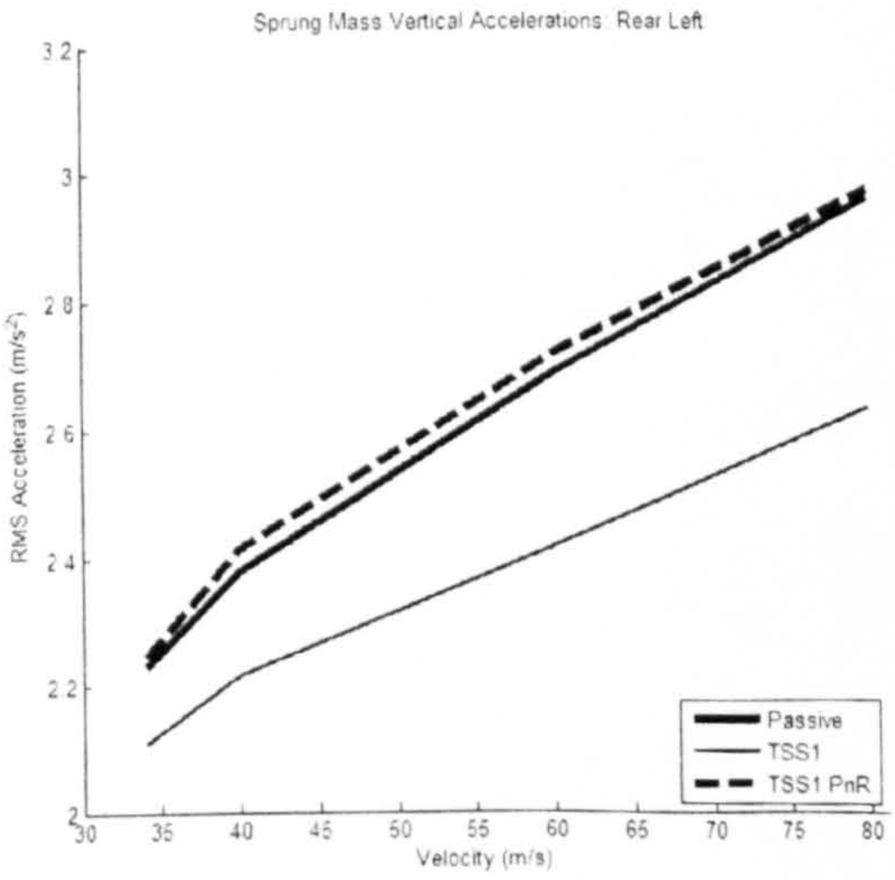

(c) Rear Left

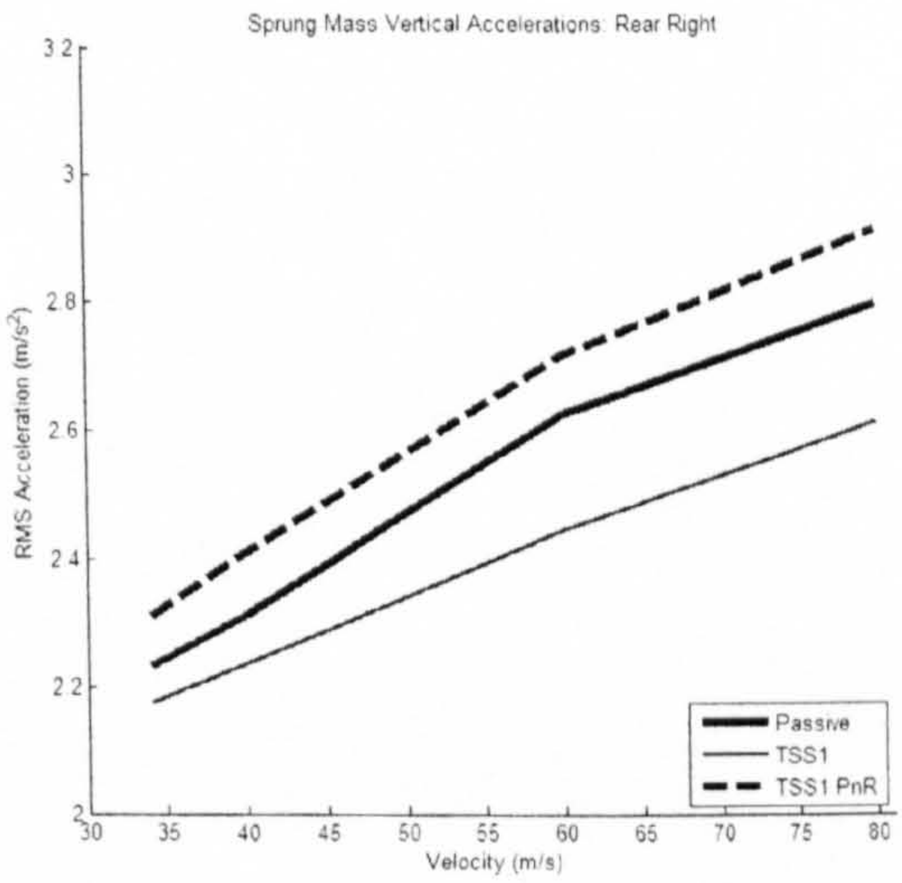

(d) Rear Right

Figure 5.29 (a) to (d): FVM Sprung Mass Vertical RMS Accelerations

To further investigate the TSS1 PnR controller, the unsprung mass responses resulted from the implementation of the competing suspension systems are examined. Table 5.11 shows tabulated vertical vibrations at various constant velocities. The unsprung mass recorded dramatically increased levels, as the forward velocity increases implying higher loads experienced by the suspension components.

Figure 5.30 (a) to (d) provide a graphical comparison of vibration level against forward velocity. Clearly, TSS1 with independent suspension shows consistent reduction in overall RMS accelerations at all suspension corners. In contrast, TSS1 PnR provides mixed results. It recorded marginal improvement at the front suspensions. Greater reduction is observed at the rear suspensions, with the highest reduction recorded at the rear corner surpassing TSS1 performance throughout the entire velocity range.

It can be concluded that implementation of the adopted pitch and roll control (TSS1 PnR) into the existing two-state switchable semi-active system in a conventional passenger vehicle may not be practical. Vibration reduction at the unsprung mass suggests lower loads are exerted at the suspension components. Theoretically, it would improve components durability. However, ride quality deteriorates from such application, defeating the original intention of the controller to improve passenger comfort.

Unsprung Mass RMS Acc (m/s^2)		34 km/h	40 km/h	60 km/h	80 km/h
FL	Passive	55.301	59.15	64.713	70.3
	TSS1	45.234	47.894	52.433	56.66
	TSS1 PnR	55.08	59.067	64.531	69.8
FR	Passive	57.631	58.544	61.018	64.151
	TSS1	46.561	47.911	50.029	53.25
	TSS1 PnR	55.815	56.702	59.564	62.7
RL	Passive	53.3	56.871	61.448	65.854
	TSS1	43.703	46.62	51.051	54.21
	TSS1 PnR	46.37	47.767	52.459	55.86
RR	Passive	55.284	55.052	58.238	61.625
	TSS1	44.9036	45.424	48.551	50.7
	TSS1 PnR	41.389	40.93	43.524	46.8

Table 5.11: Vertical RMS Accelerations of Unsprung Mass at All Corners

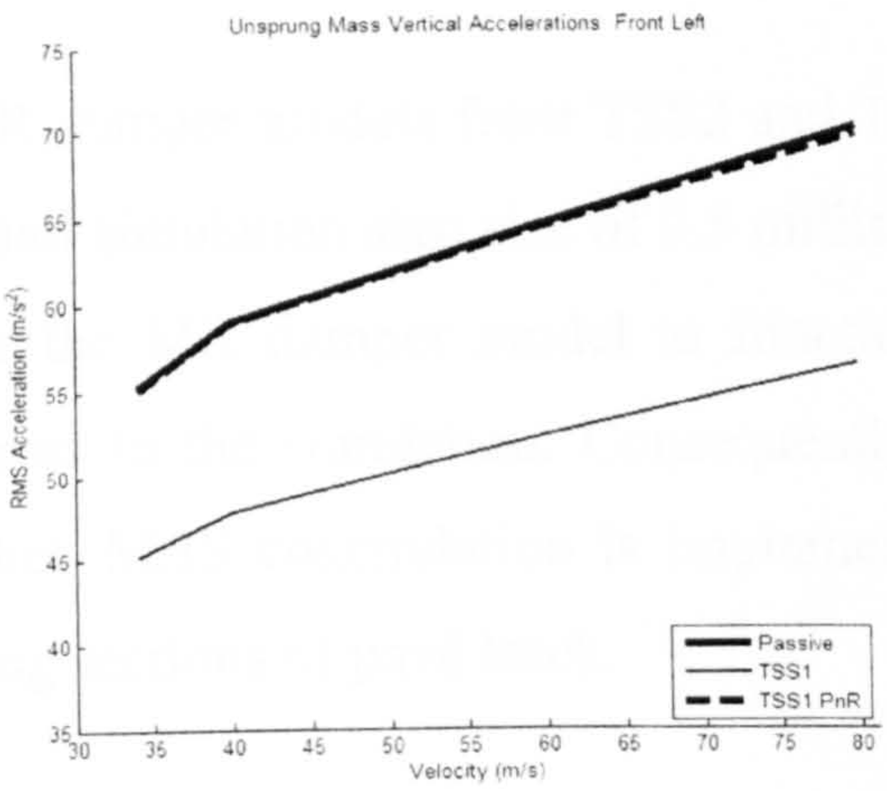

(a) Front Left

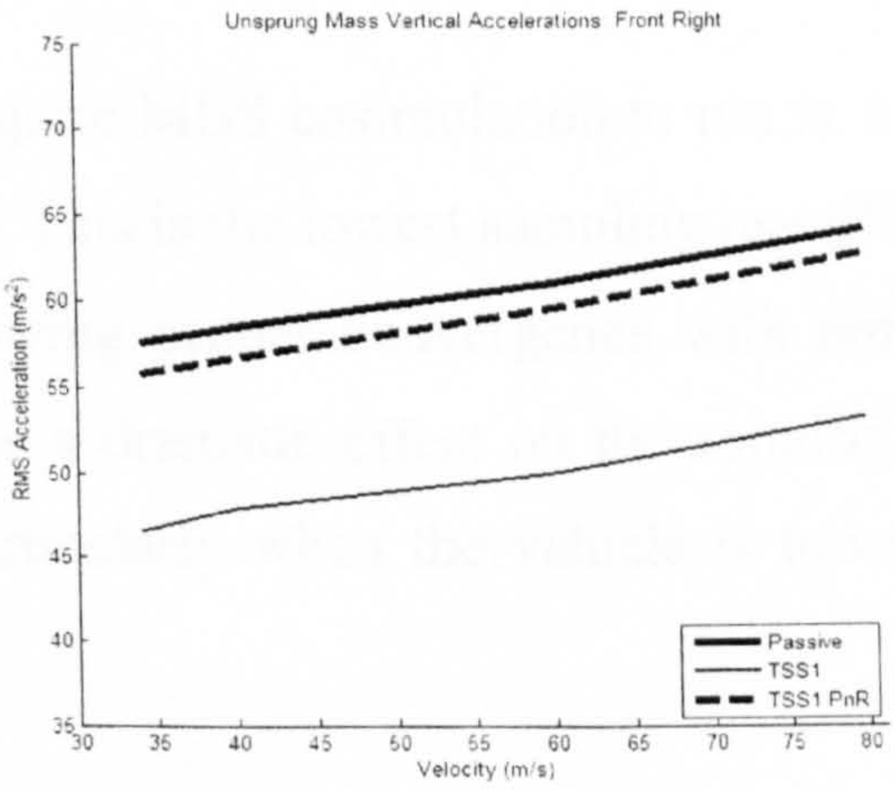

(b) Front Right

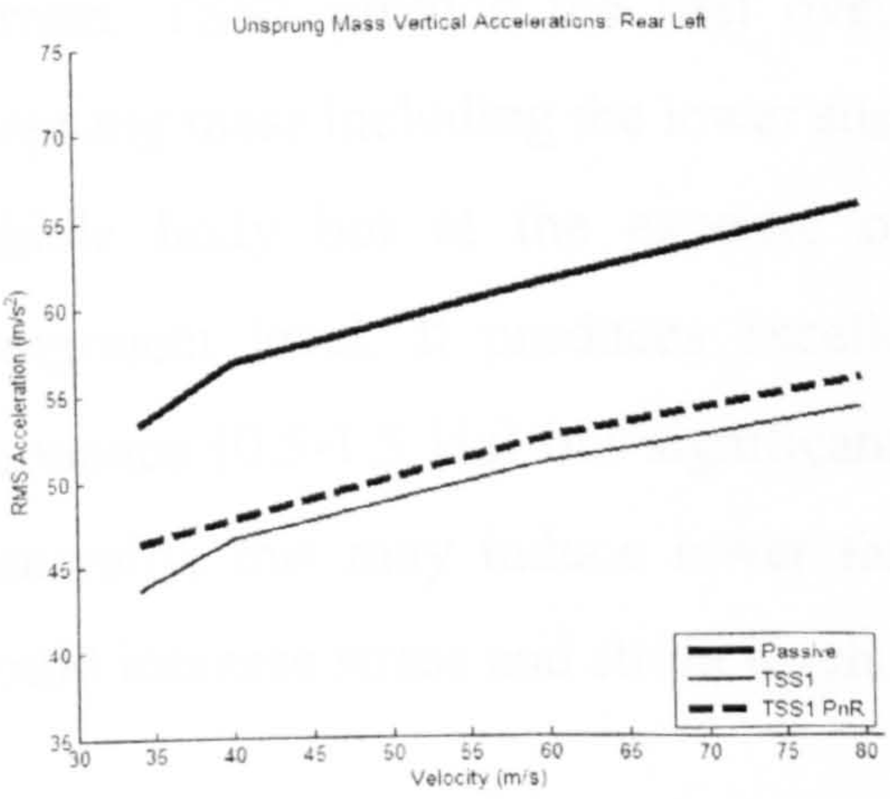

(c) Rear Left

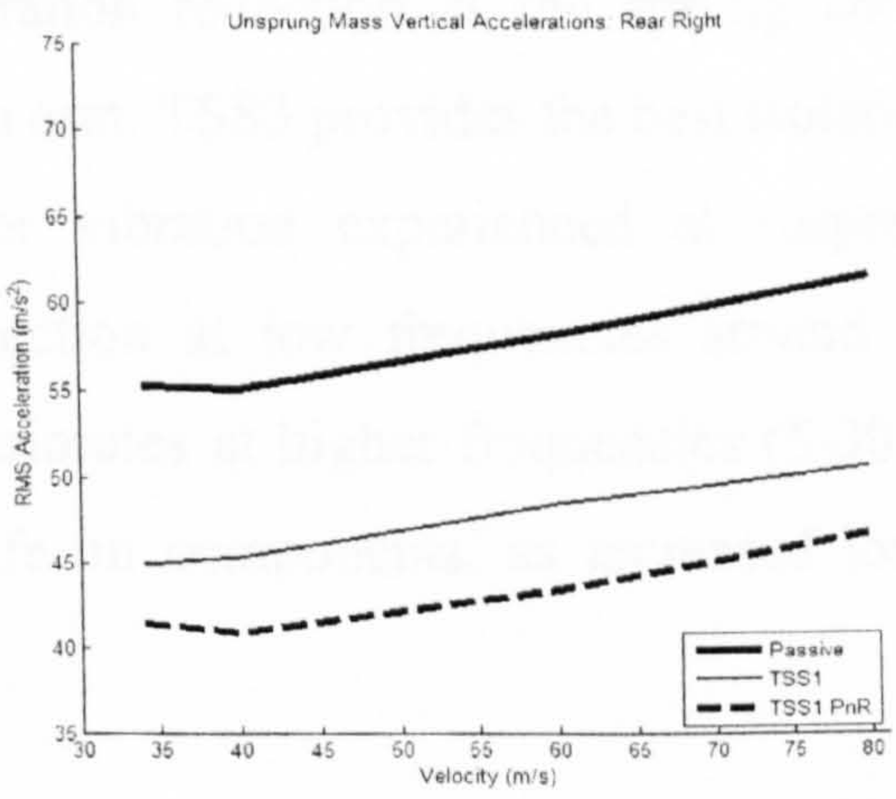

(d) Rear Right

Figure 5.30 (a) to (d): FVM Unsprung Mass Vertical RMS Accelerations

5.6 Conclusions

It has been demonstrated that MBS cosimulation can be utilised as a tool in readily obtaining load histories for vehicles with semi-active suspension systems. Simple and realistic subsystems describing controller functions can be separately analysed and easily substituted into the simulation scheme. This is shown by firstly, employing TSS1 that uses a simple damper coefficient switching to a lumped QVM. Next, two realistic controller models (TSS2 and TSS3), where the damper characteristics, derived experimentally from an MR damper, are implemented to a lumped QVM. Once the dynamic response has been established, the two-state semi-active controller models are applied to a realistic suspension quarter vehicle model. MBS cosimulation determines the load histories of a suspension arm from the competing suspension systems. These results will be used in Chapter Six to evaluate the effect of implementing these control strategies on the suspension arm durability.

MR damper models from TSS2 and TSS3 require MBS cosimulation to run at a very small simulation step size of 0.5 milliseconds. This is the lowest sampling rate (2 kHz) for the MR damper model to function, allowing proper convergence with minimal errors to the simulation. Consequently, it has a dramatic effect on the solution time when MBS cosimulation is implemented particularly when the vehicle is traversing long sections of pavé track.

MR dampers employing two-state switchable strategies are dependent on control current. TSS2 provide the best overall vibration reduction at the sprung and the unsprung mass including the lower suspension arm. TSS3 provides the best isolation to vehicle body but at the expense of higher vibration experienced at suspension component level. It produces excellent reduction at low frequencies around body resonance (0.5-1.5 Hz) but significantly deteriorates at higher frequencies (5-30 Hz). Generally, this may induce lower fatigue life on components, as increased loading would increase stress and strain levels.

Implementing the two-state switchable with pitch and roll control strategy derived from an off-road semi-active application has not improved the ride comfort for a multi-

purpose passenger vehicle. Employing existing semi-active control derived from QVM to FVM appears to be adequate. Unlike for off-road vehicles, the effect of pitch and roll is less on passenger vehicle with shorter wheelbase and track width. Additionally, an MPV is typically designed to perform on smooth road surfaces rather than on roads with large undulations. Therefore, incorporating pitch and roll control strategy based on an off-road vehicle [20] into the multi-purpose passenger vehicle does not seem to be beneficial. Nevertheless, the study has again highlighted the capability of MBS cosimulation approach, which can be readily extended to evaluate dynamic response of a full vehicle model.

CHAPTER SIX

Durability Analysis of the MPV Suspension Arm

6.1 Introduction

In this chapter, the durability of a suspension component that is subjected to several semi-active control systems is evaluated. To achieve this, necessitates the use of a finite element (FE) method and a fatigue solver. According to Halfpenny [86], implementing fatigue life prediction using FE methods has been limited, until recently, with improved computing capability and resources, this method has received wider attention from researchers and analysts alike. The degree of accuracy in fatigue prediction is far superior than the load based and location based durability analysis but at the expense of increase solution time, as reported by Pompetzki [2]. As suggested in Chapter 2, quasi-static durability analysis is selected as an accurate and reliable method in predicting fatigue for the lower arm used in this study. Here, the FE method provides a set of static stress or strain solutions at each node or element in the form of load cases that correspond to the load histories obtained from MBS cosimulation models described in Chapter 5. Using a fatigue solver, the product of each load case and its equivalent load histories is linearly combined producing a total dynamic stress or strain history at each node of the suspension arm. Then, the fatigue solver calculates the number of cycles for the stress or strain range of the dynamic stress histories using rainflow cycle counting. Finally, utilising Miner's rule the fatigue life of the suspension arm can be estimated by summing the damage for each stress range. The assessments are based on relative distribution and relative estimates of the life, rather than on exact values, measured in repeats of the distance of a virtual durability track, and the nodal life distributions of the suspension arm.

However, the usage of the quasi-static durability analysis has some limitations. The strategy does not account for stress or strain where the structure is influenced by local and global vibrations. It means that if there exists structural natural frequencies within the calculation range of the stress, then the predicted results will be inaccurate at the affected region. In a previous study [1], the suspension arm's lowest flexural mode occurred in a frequency region higher than the frequencies of the durability road input, suggesting that the effect of the global and local vibration can be ignored. Consequently, this allows the quasi-static strategy to be implemented. In order to perform the durability analysis for the suspension lower arm, a new model has to be created. Additionally, this requires modal analysis to be repeated to validate the new model against the previous one. With no previous FE model or the geometric details available, the process of creating the model is done by approximating the dimensions from a half-scale physical model of the suspension arm.

For this research, ANSYS 9.0 is utilised for the finite element modelling of the lower suspension arm. ANSYS is a computer-aided-engineering (CAE) tool for solving multi disciplinary problems. It consists of many products such as multiphysics, structural, mechanical, fluid dynamics, electromagnetics, etc., capable of producing linear and non-linear solutions. The present study employs an ANSYS structural module to determine the arm's resonance frequencies and to establish the static load cases.

Once, the static load cases have been obtained, a fatigue solver, FE-Fatigue from nCode is used to calculate the minimum fatigue life and the corresponding damage distributions. nCode provides a comprehensive package for fatigue solutions ranging from data acquisitions to virtual design analysis software. This includes a fatigue module known as FE-Fatigue. The module is a CAE fatigue prediction package that can be integrated into many leading CAE codes, for example MSC.Nastran, ANSYS, ABACUS, LS-DYNA, etc. In this study, the FE-Fatigue program is utilised to predict the minimum life by applying the static load cases from ANSYS and multiplying them with the corresponding load histories obtained from MSC.visualNastran, to establish the dynamic stress histories. Then, the program computes the stress range cycles from the dynamic stress histories, and finally calculates the accumulated damage. Fatigue life prediction of the lower suspension arm, described in this chapter, will be based on the implementation of ANSYS and nCode software which is explained in the

following sections.

6.2 Finite Element Modelling of the Lower Suspension Arm

The first step in creating the geometric representation of the suspension arm begins with constructing a 3D solid model as illustrated in Figure 6.1(a). It is defined as a volume with isotropic mechanical properties. Then, the volume is meshed into solid elements. Shown in Figure 6.1(b), the model consists of about 1980 solid elements, where 1845 elements are meshed as 3D solid bricks, and 135 elements as 2D solid beams. For the solid brick element, a 20-node element is utilised instead of the standard 8-node element, where each node on the element, has three translational degrees of freedom [120]. Unlike the 8-node element, this higher order quadratic element has additional midside nodes, suitable for irregular-shaped models or curved boundaries and is capable of providing better convergence for the solutions. The solid beam elements represent the joints/constraints in MBS. In order to prevent localised bending and localised resonance, the beam elements are defined to have high stiffness with low density with large sectional geometries.

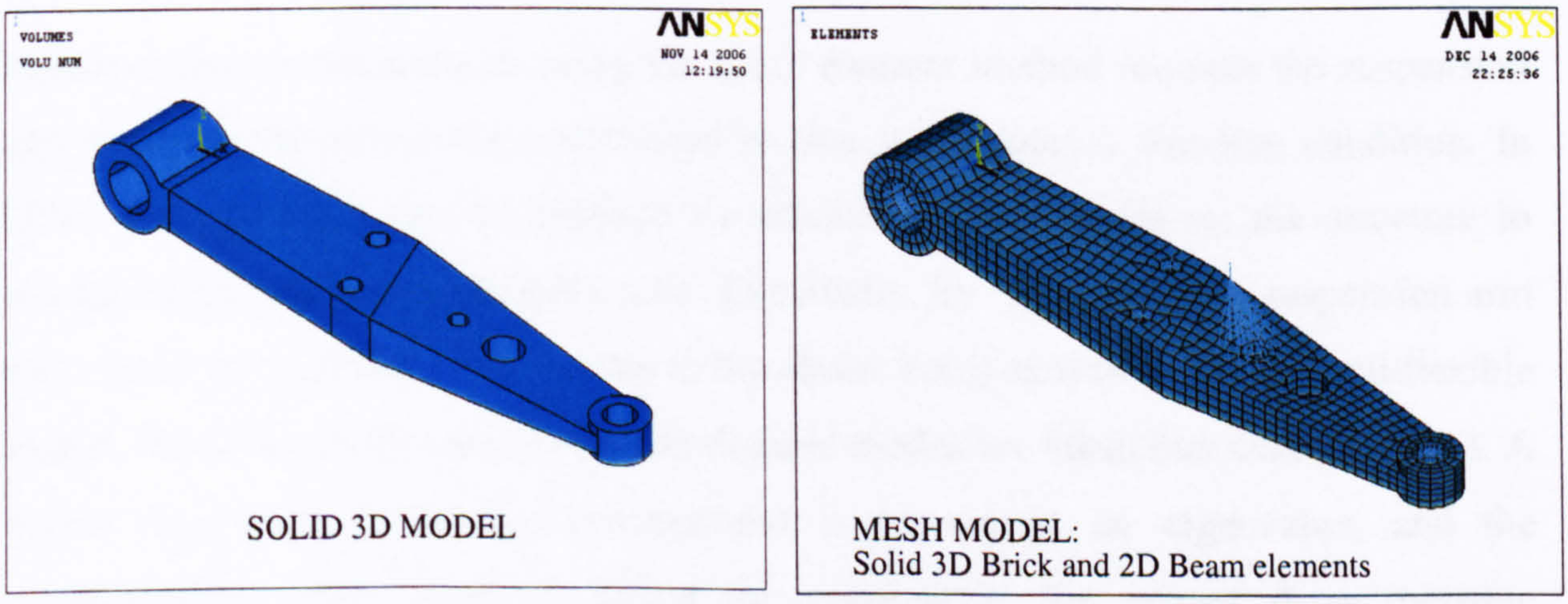

Figure 6.1: Lower Suspension Arm FE Model (a) Solid 3D Model; (b) With Mesh

6.2.1 Performing Modal Analysis on the Lower Suspension Arm

Since quasi-static stress method does not consider the effect of local and global vibrations, modal analysis must be performed on the lower suspension arm in order to identify the lowest resonance frequencies. If the fundamental resonant frequency falls

within the range of the excitation frequencies (0-60 Hz), then the quasi-static method may not be accurate in predicting the stresses. In this present work, modal analysis is performed to validate the suspension arm model against results obtained from earlier studies.

Modal analysis is a method of determining dynamic properties of a mechanical system, namely the natural frequencies, the mode shapes and the modal damping. A natural frequency or a resonant frequency occurs when the stiffness force and the inertia force of the structure, are equal, and are acting in the opposite directions [14]. The stiffness force attempts to restore structural response to its equilibrium position once an imbalance force is exerted on the structure. In contrast, the inertia force is the force acting on the structure due to the unbalance force, and it is proportional to acceleration. At resonance, these forces cancel out, and the frequency at which it occurs is called the natural frequency. Consequently, the structure looses its ability to resist external load and the resultant vibration is balanced by the damping force. The mode shape of the structure at each resonance frequency can be in the form of rigid body or flexible body modes. In this context, only flexible modes are considered since they produce stresses and strains on the elements.

Implementing modal analysis using the finite element method requires the suspension arm model to be minimally constrained so that it emulates a free-free condition. In FEM, this condition can be realised by attaching a few nodes on the structure to ground nodes with a low stiffness cord. Eventually, by doing this, the suspension arm will consist of rigid body modes (due to the elastic cord) as well as the flexural/flexible modes. However, in this study only the flexural modes are taken into considerations. A natural frequency in an FE environment is known as an eigenvalue, and the corresponding mode shape is called its eigenvector. To extract these dynamic characteristics, the block Lanczos method is employed. The method is suitable and generally accurate for most structures and is used as a default in many FE codes. Furthermore, the same method was adopted in earlier studies to produce the natural frequencies, allowing comparison with the present model.

6.2.2 Lower Arm Natural Frequencies and Mode Shapes

Modal analysis results summarised in Table 6.1 compares the first six of the flexible modes of the suspension arm with those obtained from Haiba [1]. The findings indicate that the natural frequencies do not match well with those produced in [1]. The differences in natural frequencies may be attributable to different geometrical details and boundary conditions applied to the model.

Mode shapes comparison is not possible since no eigenvectors were provided from earlier work. Further modifications on the applied boundary conditions failed to show any similarity with previously obtained frequencies, since information on the boundary conditions and the mode shapes from previous studies, were not available. The first three flexible modes of the current model are presented in Figure 6.2 and can be described as the fundamental vertical bending, twisting, and lateral bending.

Though exact values of the natural frequencies differ, the analysis confirms that the lowest flexural mode is significantly above the excitation frequencies. Hence, the lower arm's stresses and strains will not be affected by local and global vibrations, allowing implementation of the quasi-static durability method.

Model Descriptions	Mode 1	Mode 2	Mode 3	Mode 4	Mode 5	Mode 6
Lower arm (current model)	362.3	430.1	1047	1372	1378	1401
Lower arm (Haiba's model)	420.5 *	589.5 *	1129 *	1809 *	1891 *	2227 *
* Based on tabulated results. No descriptions on mode shapes and boundary conditions						

Table 6.1: Comparison of the First Six Natural Frequencies (in Hz)

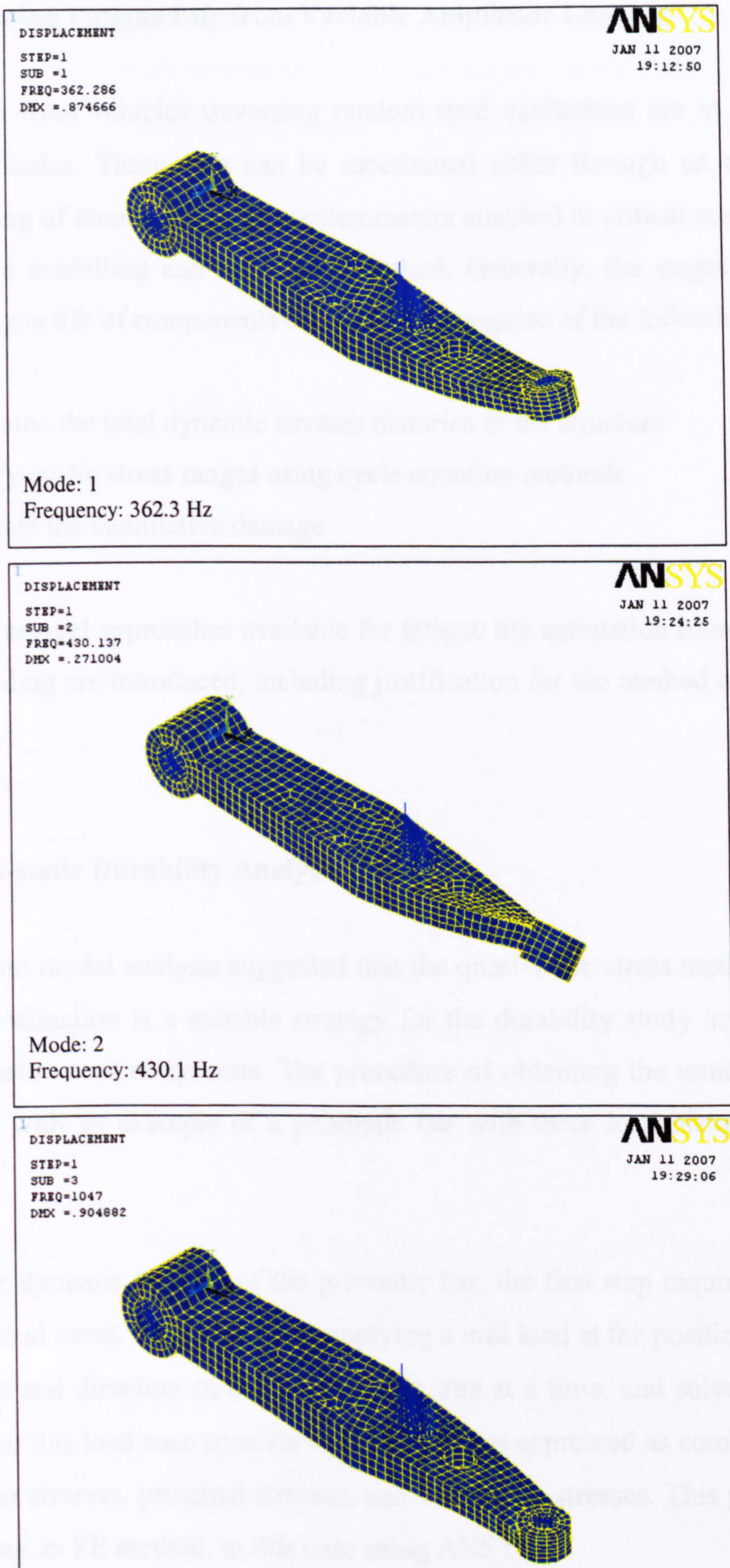

Figure 6.2: Modal Analysis of the First Three Flexural Modes

6.3 Estimating Fatigue Life from Variable Amplitude Loading

Load histories from vehicles traversing random road excitations are in the form of variable amplitudes. These data can be ascertained either through an experimental setup, consisting of strain gauges or accelerometers attached at critical components, or by means of a modelling and simulation method. Generally, the stages involved in predicting fatigue life of components or structures comprise of the following:

a. Determine the total dynamic stresses histories of the structure
b. Identify cyclic stress ranges using cycle counting methods
c. Calculate the cumulative damage

In Chapter 2, several approaches available for fatigue life estimation based on variable amplitude loading are introduced, including justification for the method adopted in the current study.

6.3.1 Quasi-static Durability Analysis

Outcomes from modal analysis suggested that the quasi-static stress method with time domain life estimation is a suitable strategy for the durability study involving semi-active suspension control systems. The procedure of obtaining the minimum life can be explained with an example of a prismatic bar with three load histories shown in Figure 6.3.

To obtain the dynamic stresses of the prismatic bar, the first step requires calculation of the static load cases. This is done by applying a unit load at the position, in the same line of action and direction of the load history, one at a time, and solve for the static stress. Each of this load case consists of nodal stresses expressed as component normal stresses, shear stresses, principal stresses, and von Mises stresses. This process can be executed using an FE method, in this case using ANSYS.

Then, these static load cases are multiplied by the corresponding load histories to ascertain dynamic stress histories. The total stress histories can be determined by applying the superposition principle to the dynamic stress histories, in which stresses

of all load cases for the entire time interval are added. For example, the component stresses for a 3D stress analysis contain normal and shear stresses in the form of σ_x, σ_y, σ_z, τ_{xy}, τ_{yz} and τ_{zx}. The solutions for the dynamic stress histories can be calculated as:

$$\sigma_x(t) = \sigma_{x_1} F_1(t) + \sigma_{x_2} F_2(t) + \sigma_{x_3} F_3(t) + \cdots + \sigma_{x_n} F_n(t)$$
$$= \sum_{i=1}^{n} \sigma_{x_i} F_i(t) \qquad \textbf{Eq 6. 1}$$

$$\sigma_y(t) = \sigma_{y_1} F_1(t) + \sigma_{y_2} F_2(t) + \sigma_{y_3} F_3(t) + \cdots + \sigma_{y_n} F_n(t)$$
$$= \sum_{i=1}^{n} \sigma_{y_i} F_i(t) \qquad \textbf{Eq 6. 2}$$

$$\sigma_z(t) = \sigma_{z_1} F_1(t) + \sigma_{z_2} F_2(t) + \sigma_{z_3} F_3(t) + \cdots + \sigma_{z_n} F_n(t)$$
$$= \sum_{i=1}^{n} \sigma_{z_i} F_i(t) \qquad \textbf{Eq 6. 3}$$

$$\tau_{xy}(t) = \tau_{(xy)_1} F_1(t) + \tau_{(xy)_2} F_2(t) + \tau_{(xy)_3} F_3(t) + \cdots + \tau_{(xy)_n} F_n(t)$$
$$= \sum_{i=1}^{n} \tau_{(xy)i} F_i(t) \qquad \textbf{Eq 6. 4}$$

$$\tau_{yz}(t) = \tau_{(yz)_1} F_1(t) + \tau_{(yz)_2} F_2(t) + \tau_{(yz)_3} F_3(t) + \cdots + \tau_{(yz)_n} F_n(t)$$
$$= \sum_{i=1}^{n} \tau_{(yz)i} F_i(t) \qquad \textbf{Eq 6. 5}$$

$$\tau_{zx}(t) = \tau_{(zx)_1} F_1(t) + \tau_{(zx)_2} F_2(t) + \tau_{(zx)_3} F_3(t) + \cdots + \tau_{(zx)_n} F_n(t)$$
$$= \sum_{i=1}^{n} \tau_{(zx)i} F_i(t) \qquad \textbf{Eq 6. 6}$$

where,

i is the number of load case, σ_{xi}, σ_{yi}, σ_{zi}, $\tau_{(xy)i}$, $\tau_{(yz)I}$, $\tau_{(zx)i}$ correspond to the stress components, and $F(t)$ is the load history.

This process can either be computed using a MATLAB program (Appendix V) or using nCode FE-Fatigue file translation.

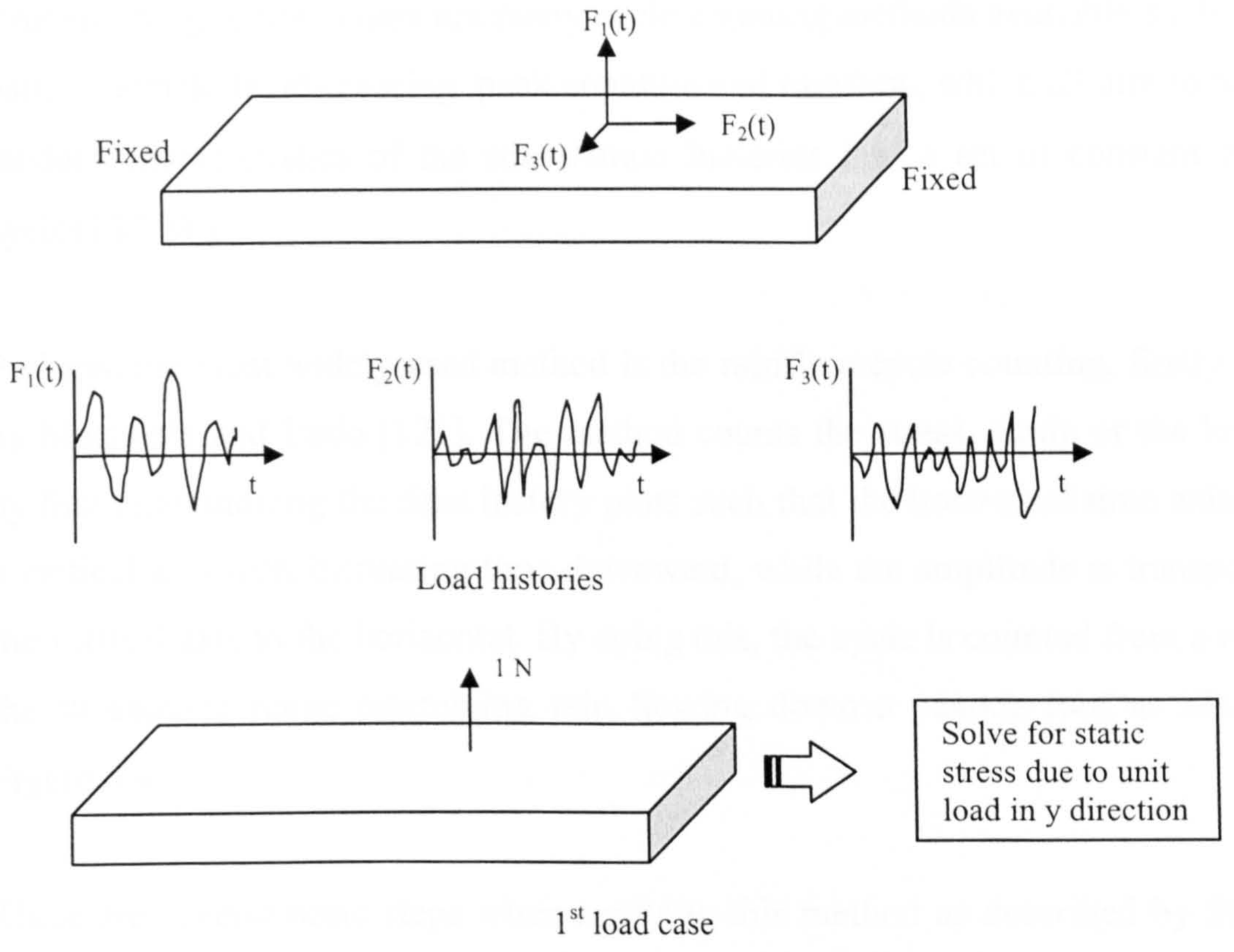

Figure 6.3: Obtaining Static Load Cases using Quasi-Static Method

Once the total dynamic stress/strain histories have been obtained, the results have to be quantified into a set of constant amplitude cycles using a cycle counting method. The purpose of cycle counting is to compare the contributions of the varying amplitudes to the fatigue obtained from a constant amplitude cycle [90]. This is necessary because the stresses or the strains histories are of varying amplitudes. Cycle counting methods are designed to extract equivalent constant amplitude cycles from the random stress and strain histories so that the linear cumulative damage calculation can estimate the

structure fatigue life. There are many cycle counting methods available such as range-pair, racetrack, level-crossing, peak counting and rainflow, which all aim to reduce the random characteristics of the stress/strain histories into a set of constant amplitude cycles [87, 90].

Perhaps, the most widely used method is the rainflow cycle counting, firstly proposed by Matsuishi and Endo [121]. The method counts the stress, strain or the load cycles by first repositioning the time history plots such that the horizontal time axis becomes a vertical axis with increasing time downward, while the amplitude is transposed from the vertical axis to the horizontal. By doing this, the cycle is counted from a reversal to the subsequent range resembling rain flowing down a pagoda roof as illustrated in Figure 6.4.

There are several basic steps when applying this method as described by Stephens *et al.* [90]. First, the time history must begin either from the highest peak or the lowest valley. This is necessary to avoid counting of half cycles. Then, the rainflow continues until the next reversal is encountered, where it reaches a peak or a valley in which the magnitude is equal or greater than the previous ones. Additionally, the counting is stopped when it encounters the previous rainflow. The step is repeated for the following reversal until the end of the history. For example, in Figure 6.4, the rainflow can be described as follows:

a. The flow begins from a local minimum at point A and continues at the next reversal at point B to B′. Since the subsequent local minimum point at C is larger than point A, the flow continues to another reversal at point D until the end of the time history.

b. Rain flows from a local maximum at point B continues at point C and stops at point D since the subsequent local maximum is equal or greater than point B.

c. The rainflow from a local minimum at C stops at point B′ because it encounters the previous flow from ABB'D.

d. Rain flows from a local maximum at point D continues to the next reversal at

point E followed by another reversal at point G, and continues until the end of the time history as no succeeding local maximum is greater or equal to point D.

e. The flow starts at a local minimum E continues at the next reversal at F and terminates at the following local minimum point G since it is smaller or equal to point E.

f. Rainflow from point F ends at E′ when it meets the earlier rainflow from DEE′G.

g. The rainflow begins at a local minimum at point G to point H and continues until the end of the time history since the conditions to stop the rainflow have not been satisfied.

Based on this description, the cycles can be counted. Two full cycles are present i.e. from BCB′D and EFE′G, and the remaining are half cycles. This rainflow counting method can be performed manually for a short time history. For a long and complex history, the method can be executed using computer programs. Several rainflow counting algorithms are available, in the American Society for Testing and Materials (ASTM), for this purpose [87]. The rainflow algorithm adopted by nCode is based on the extension of the ASTM standard (a 4-point method), that allows the cycle counting to start at the beginning of the time history [122]. A sample of cycle counting using this method is available in Appendix V.

Finally, the damage produced by these set of constant amplitude cycles can be approximated with cumulative damage calculation from the Palmgren-Miner Linear Damage rule as explained in Chapter Two. Alternatively, the fatigue calculation and estimation can be evaluated using commercially available software. FE-Fatigue software from nCode is capable of providing detailed fatigue analysis using the quasi-static method or random vibration method depending on the load histories and FE results. Since this study involves a linear stress/strain analysis, the former method is employed.

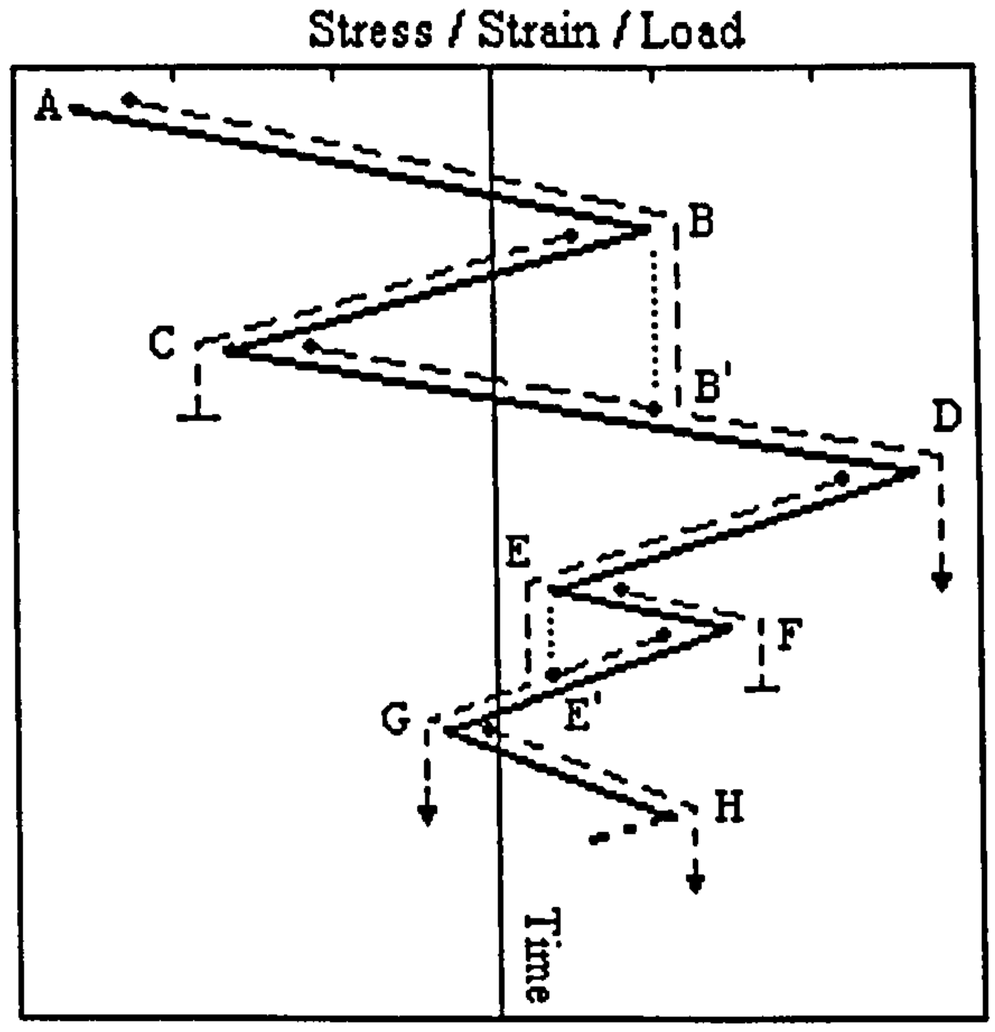

Figure 6.4: Rainflow Cycle Counting Method

6.3.2 Durability Analysis of the Lower Suspension Arm

To examine the effect of semi-active control systems on the durability of suspension components, the lower suspension arm is selected as a case study. The motives behind this selection are based on the following:

a. To allow fatigue life comparison between the present lower arm model with earlier results. Indirectly, it can also be used to validate the cosimulation approach against those previously obtained from pure MBS simulation.

b. The lower suspension arm has the most loading, in comparison with the hub, upper arm, tie-rod, and the vehicle body. In addition, it has a direct contact with the bump stop when a large transient event is encountered.

c. Due to lack of geometrical details for other suspension components, the lower arm is the only available component for the durability analysis. As previously mention, the geometric details are manually approximated from a half-scale model. As a result, the current representation of the suspension arm is not as detailed as the one produced in earlier studies. However, this limitation offers another perspective in this durability study. By comparing fatigue results with the previous study, some appreciation of the effect that geometrical details have

on the fatigue life estimation and its distribution can be gained.

The lower suspension arm consists of twenty one load histories in the form of forces and moments, at the constraints as depicted in Figure 6.5. These load histories are obtained from MBS cosimulation for four competing suspension systems, namely the passive system, and three semi-active systems with a two-state switchable control strategy, denoted as TSS1, TSS2, and TSS3. An example of the load histories is illustrated in Figure 6.6.

In order to ascertain the static load cases, the suspension arm has to be statically solved with a finite element code. These load cases represent the MBS constraint interfaces. Since a unit force or moment is applied at the nodes, some of the load histories have to be divided according to the number of nodes representing the constraint. For instance, the revolute joint connecting the arm to the vehicle body is represented by 2 nodes (A and B in Figure 6.7). Therefore, the load histories for the revolute joint have to be divided by two, so that the resultant dynamic stress histories will be the equivalent of a single load case applied at the centre between A and B.

Inertia relief is applied to the arm as shown in Figure 6.8, to account for force or moment imbalance when a unit of load is applied for each load case. It works using the assumption that the structure under consideration is in static equilibrium under minimal constraints. In ANSYS, applying the inertia relief method requires a maximum of 6 constraints where reaction forces are determined due to the applied load. Once these static load cases have been determined, the results files are then translated to nCode FE-Fatigue program where these load cases are combined with the designated load histories. Then the fatigue solver is executed to predict the lower arm minimum life and the nodal distributions.

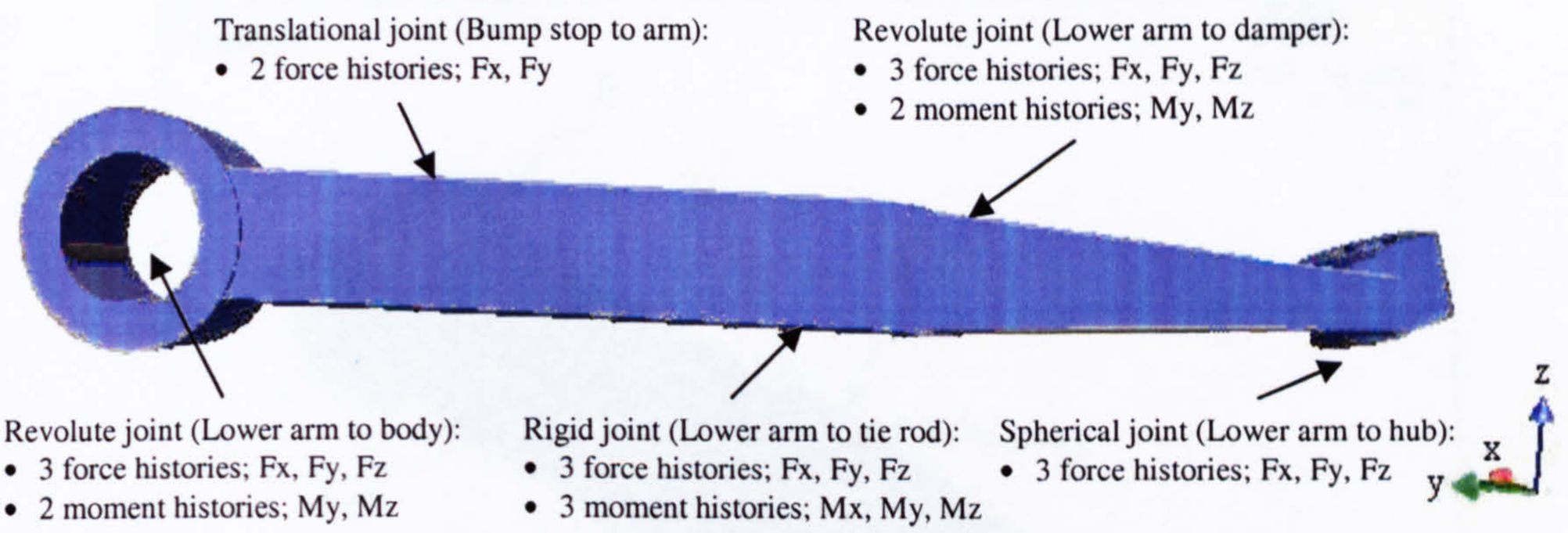

Figure 6.5: Load Histories of Lower Suspension Arm

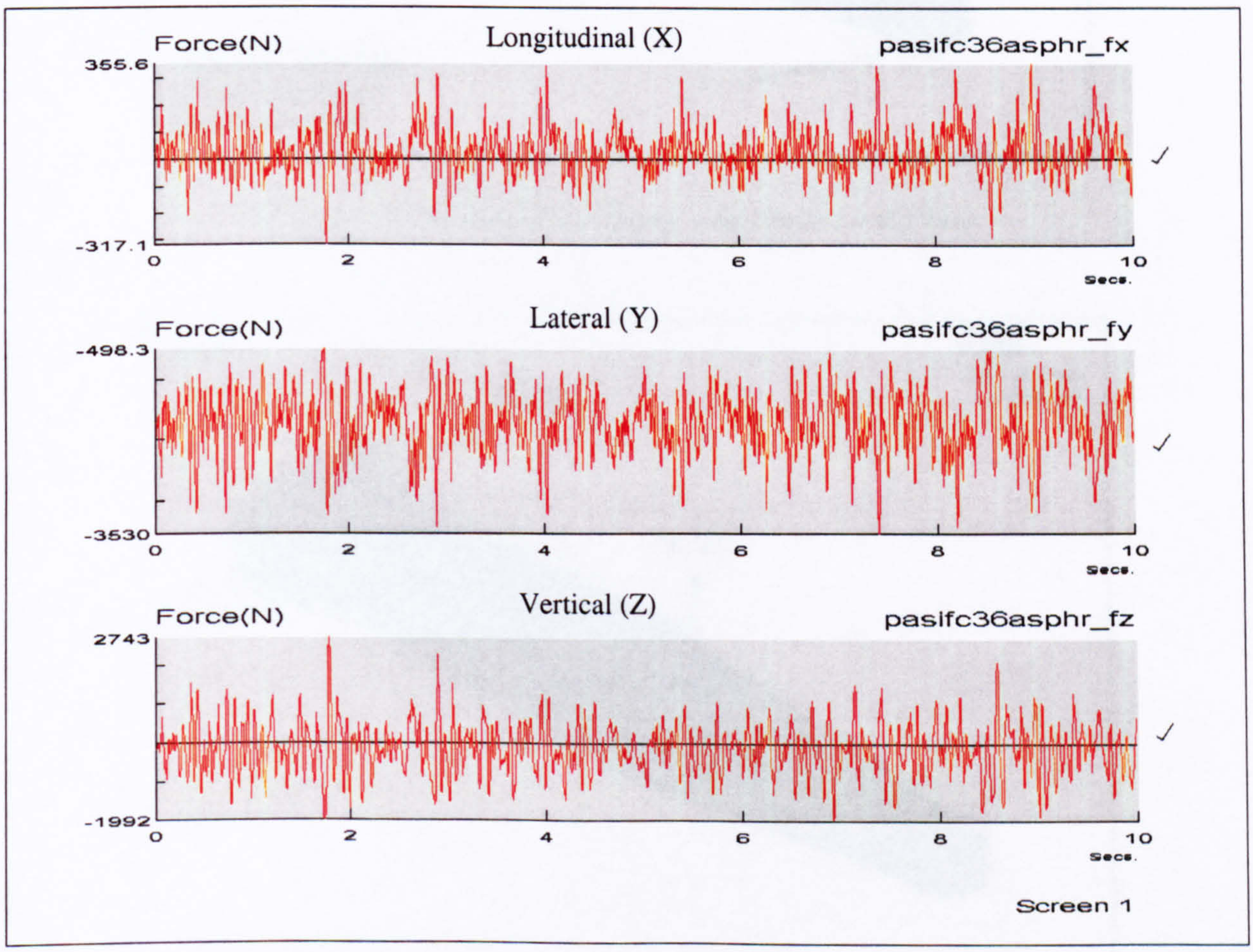

Figure 6.6: Sample of Load Histories at Spherical Joint (Lower Arm to Hub)

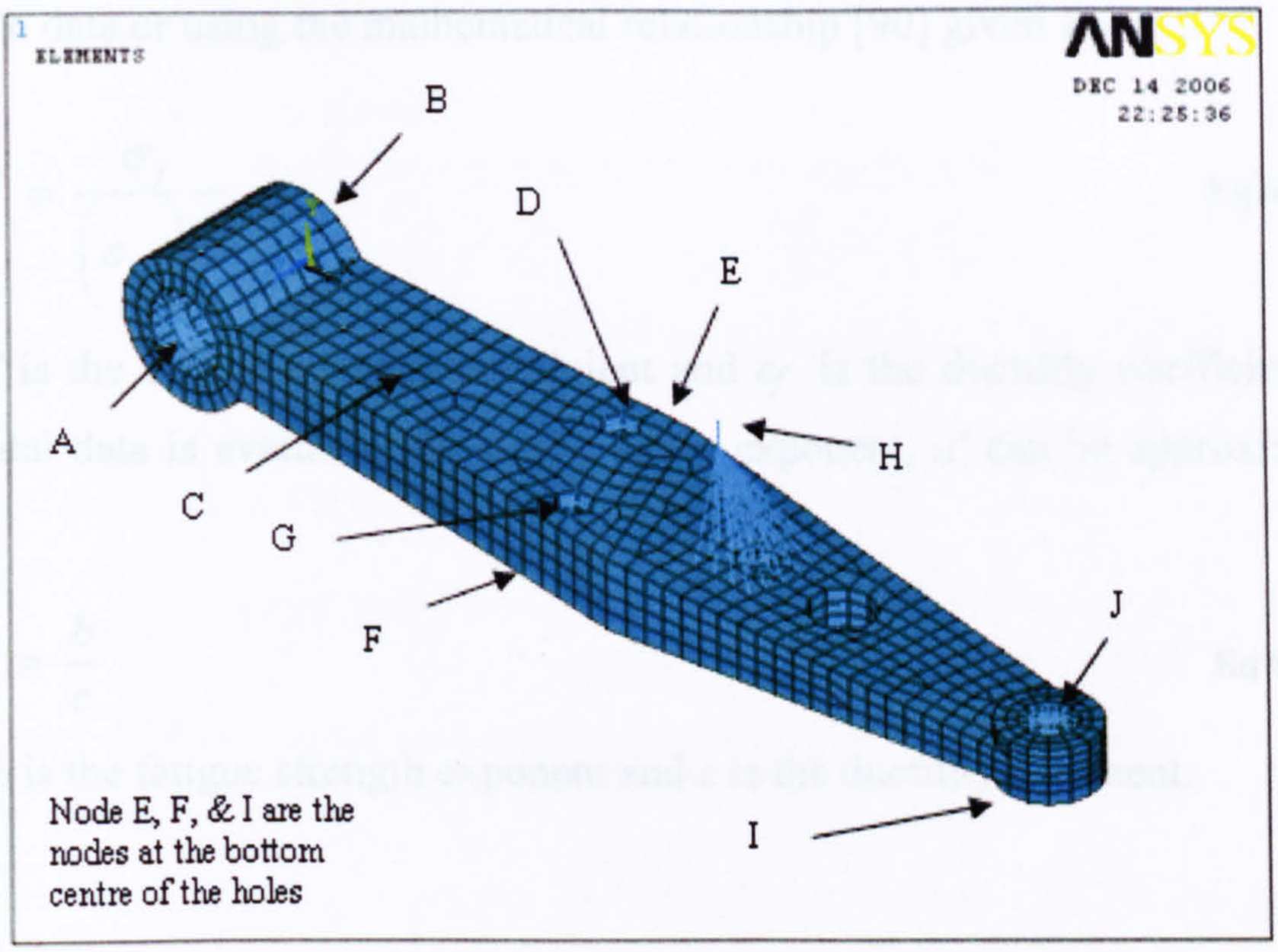

Figure 6.7: Location of the Lower Arm Static Load Cases

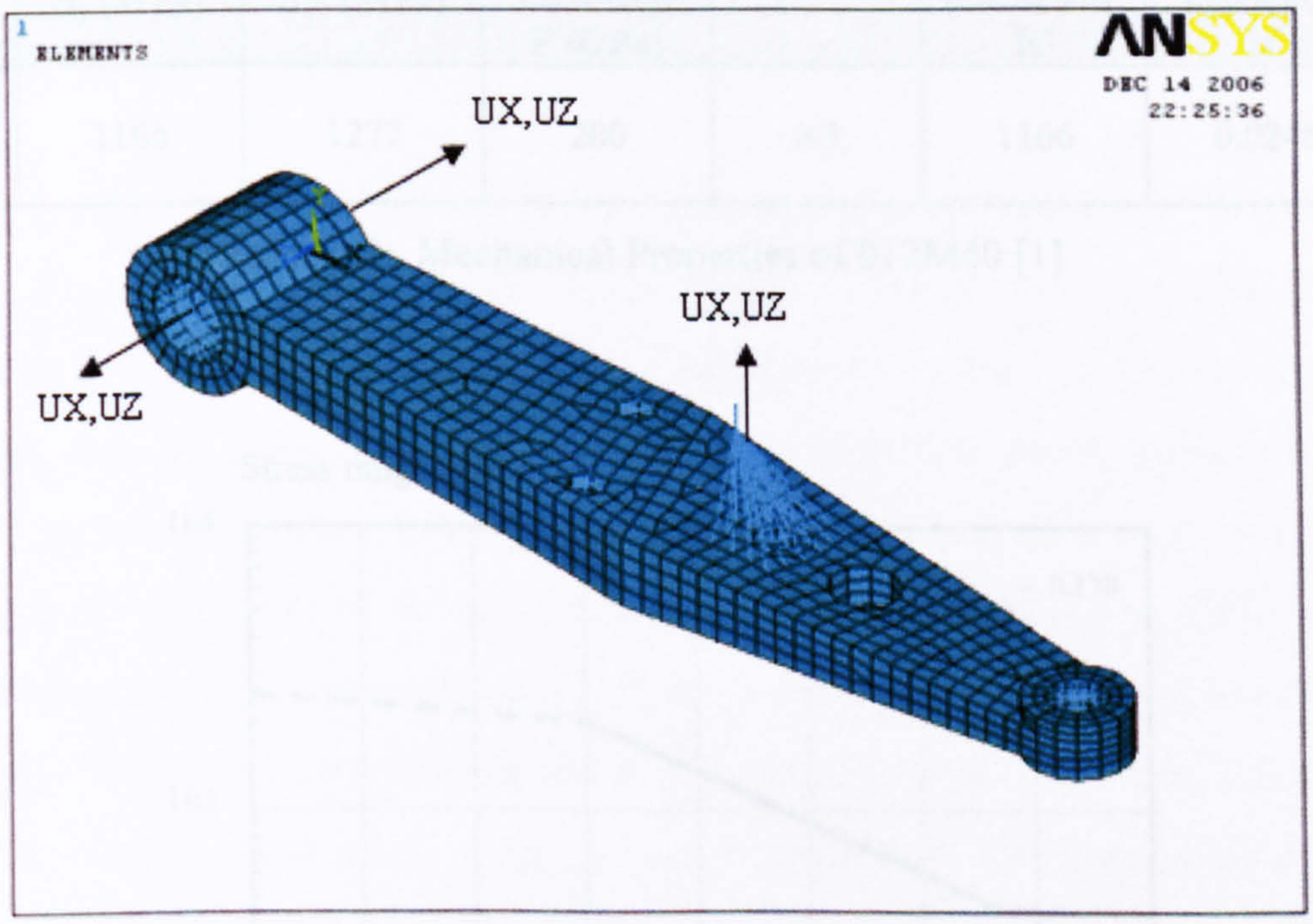

Figure 6.8: Applied Constraints with Inertia Relief

The lower suspension arm is made of hardened and tempered alloy steel, 817M40 and having the following material properties as summarized in Table 6.2. The stress-life and strain-life curves of the alloy steel are as shown in Figure 6.9 and 6.10. The first five material properties can be ascertained from engineering material properties database. When estimating fatigue using the strain-life method, the remaining two properties must be utilised. It can be determined either by curve-fitting the cyclic

stress-strain data or using the mathematical relationship [90] given as:

$$K' = \frac{\sigma_f{}'}{\left(\varepsilon_f\right)^{n'}} \qquad \textbf{Eq 6. 7}$$

where $\sigma_f{}'$ is the fatigue strength coefficient and ε_f is the ductility coefficient. If no experimental data is available, the cyclic strain exponent, n' can be approximated as follows:

$$n' = \frac{b}{c} \qquad \textbf{Eq 6. 8}$$

in which b is the fatigue strength exponent and c is the ductility exponent.

Density, ρ (kg/m^3)	Yield strength, σ_y (MPa)	Ultimate strength, σ_{ult} (MPa)	Modulus of elasticity, E (GPa)	Poisson's ration, υ	Cyclic strength coefficient, K'	Cyclic strain exponent, n'
7800	1166	1277	200	0.3	1166	0.0246

Table 6.2: Mechanical Properties of 817M40 [1]

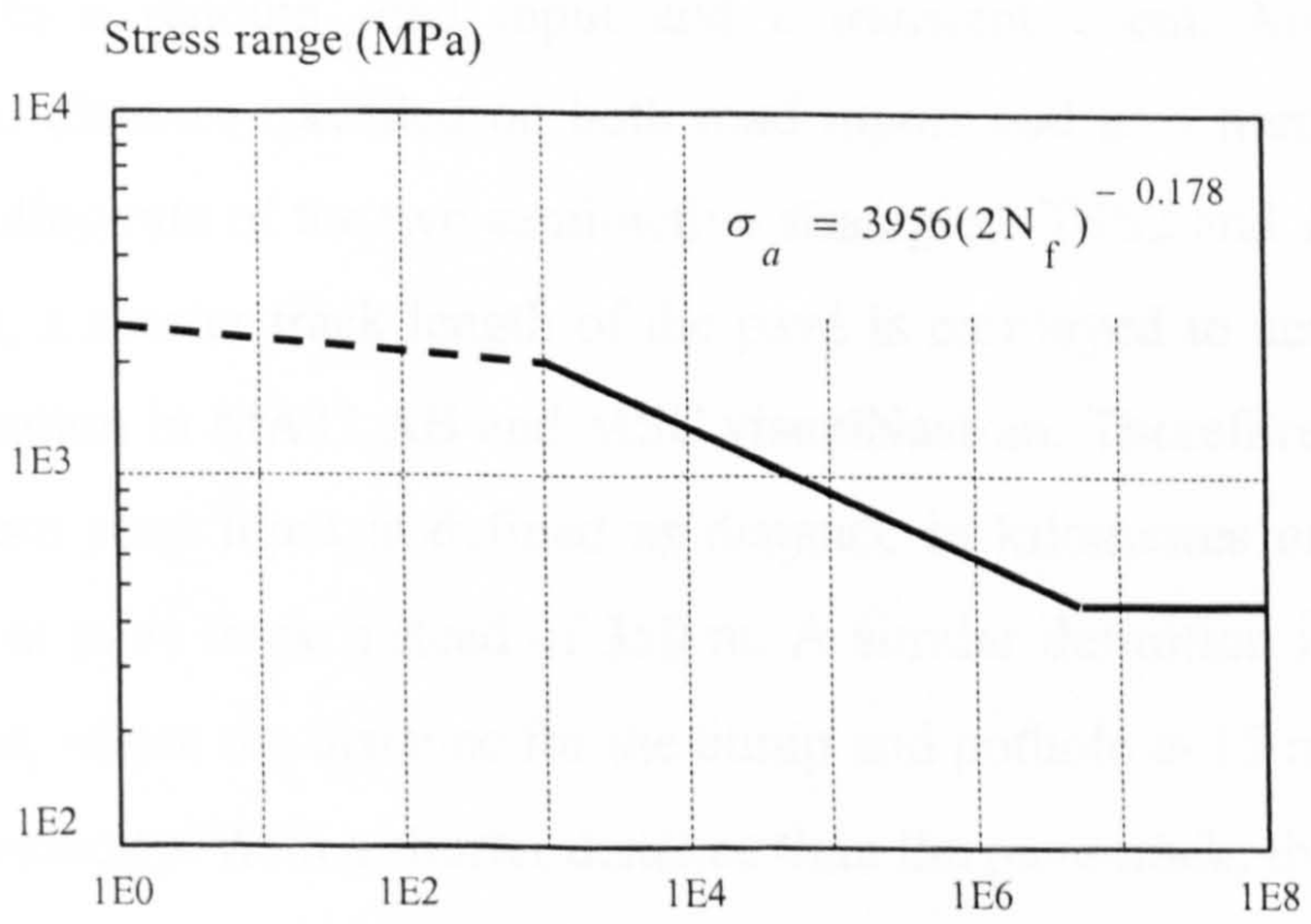

Figure 6.9: Stress-Life (S-N) Curve for 817M40 Alloy Steel [1]

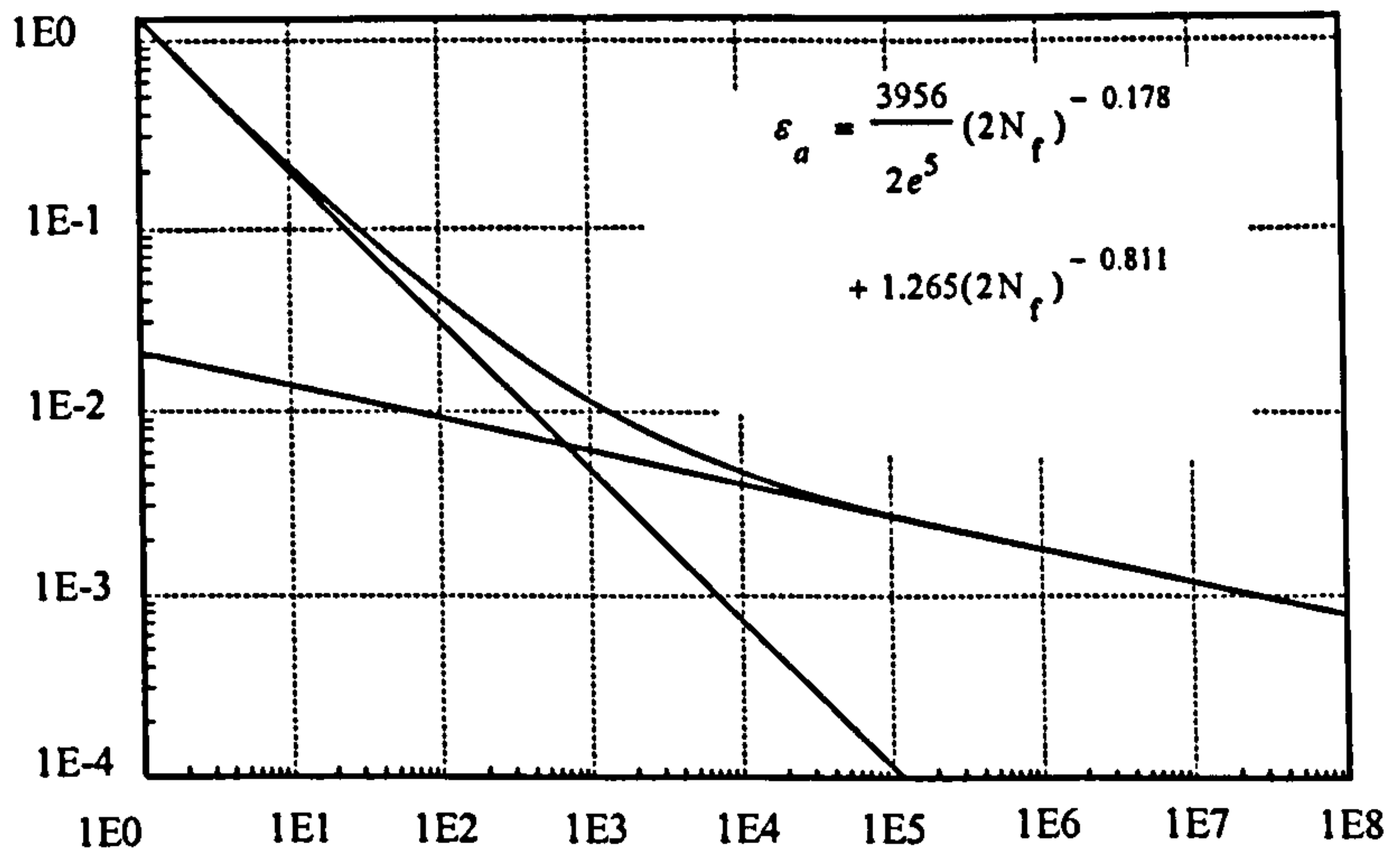

Figure 6.10: Strain-Life (E-N) Curve for 817M40 Alloy Steel [1]

6.4 Results and Analysis

With the method for ascertaining fatigue life established, the study examines the influence of semi-active strategies on the durability of the lower suspension arm. This includes the prediction of minimum fatigue life and the nodal life distributions of the component due to a random road input and a transient event. Minimum life is quantified as total distance travelled on both road inputs and as a number of repeats. Due to high sampling rate of the two semi-active strategies (TSS2 and TSS3) to obtain the load histories, a shorter track length of the pavé is employed to accommodate the data storage limitation in MATLAB and MSC.visualNastran. Therefore, the minimum life for the random road input is defined as distance in kilometres or as number of repeats of a 100 m pavé track instead of 350 m. A similar definition is employed for the transient input, where the distance for the bump and pothole is 15 m with the same vehicle forward velocity. With a shorter distance than the pave track, the minimum life is expressed as distance in metres and as repeats of the bump and pothole length.

6.4.1 Fatigue Life Assessment due to Random Road Input

This evaluation begins with the comparison of the predicted minimum life among the competing suspension systems based on relative estimates of the life and its distribution rather than as exact values. The results presented in Table 6.3 and 6.4 show the first 4 of the most damaged nodes. These nodes are consistent in terms of severity from all suspension systems that contribute to shorter service life. Generally, it can be concluded that, the implementation of semi-active system with switchable skyhook damping control technique will produce a more than 50 percent reduction in service life of the suspension component, when compared to a conventional passive suspension system. TSS1, TSS2 and TSS3 register reductions of 48, 68, and 96 percent, respectively, in minimum fatigue life in comparison with passive suspension. The worst of the 3 semi-active systems came from the implementation of TSS3, with the shortest life of about 52 km or 522 repeats traversing the pavé track. This poor fatigue life performance is most likely due to the influence of the sharp transient events or the jerks, as illustrated in Figure 5.13(a)-(f) to Figure 5.15(a)-(f), originating from semi-active systems with a conventional skyhook damping control, implemented in this study. Additionally, the minimum life of TSS3 further deteriorates as a result of the high frequency content from the constant current switching algorithm.

Even though dynamic analysis of TSS2 in previous chapter suggested improvement of the sprung mass, unsprung mass, and lower arm responses, it appears that this semi-active strategy has a detrimental effect on the arm's fatigue life. Similarly, it is true for TSS1 but its minimum life is 20 percent longer than that of TSS2.

Node No.	Passive	TSS1	TSS2	TSS3
217	1279	620	393	52.2
533	1579	911	543	53.2
1436	1704	982	586	56.4
1417	2182	1038	622	64

Table 6.3: Comparison of Minimum Life Prediction (in km)

Node No.	Passive	TSS1	TSS2	TSS3
217	12786	6204	3926.6	522.17
533	15785	9110.2	5428.1	531.77
1436	17037	9816.9	5863.6	563.89
1417	21825	10379	6221.2	639.99

Table 6.4: Comparison of Minimum Life Prediction (in Repeats of Pavé Track)

The nodal life distributions of the suspension arm in Figure 6.11 and 6.12 indicate regions of high stress concentration near the notched area. With all life contours plotted with the same minimum and maximum ranges, TSS3 can be seen to produce the highest fatigue damage followed by TSS2 and then TSS1. The least damage is generated from the passive suspension system. Additionally, damage contours between the top and the bottom surface of the lower arm indicate similarity in distribution for all suspension systems especially at the critical area around the notch. Figure 6.13 and 6.14 display some of the nodes at potentially damaging locations. The effect of the bump stop on the suspension arm can be observed in the region shown in Figure 6.13, represented by node 2131, 2612, 2142, and node 2219.

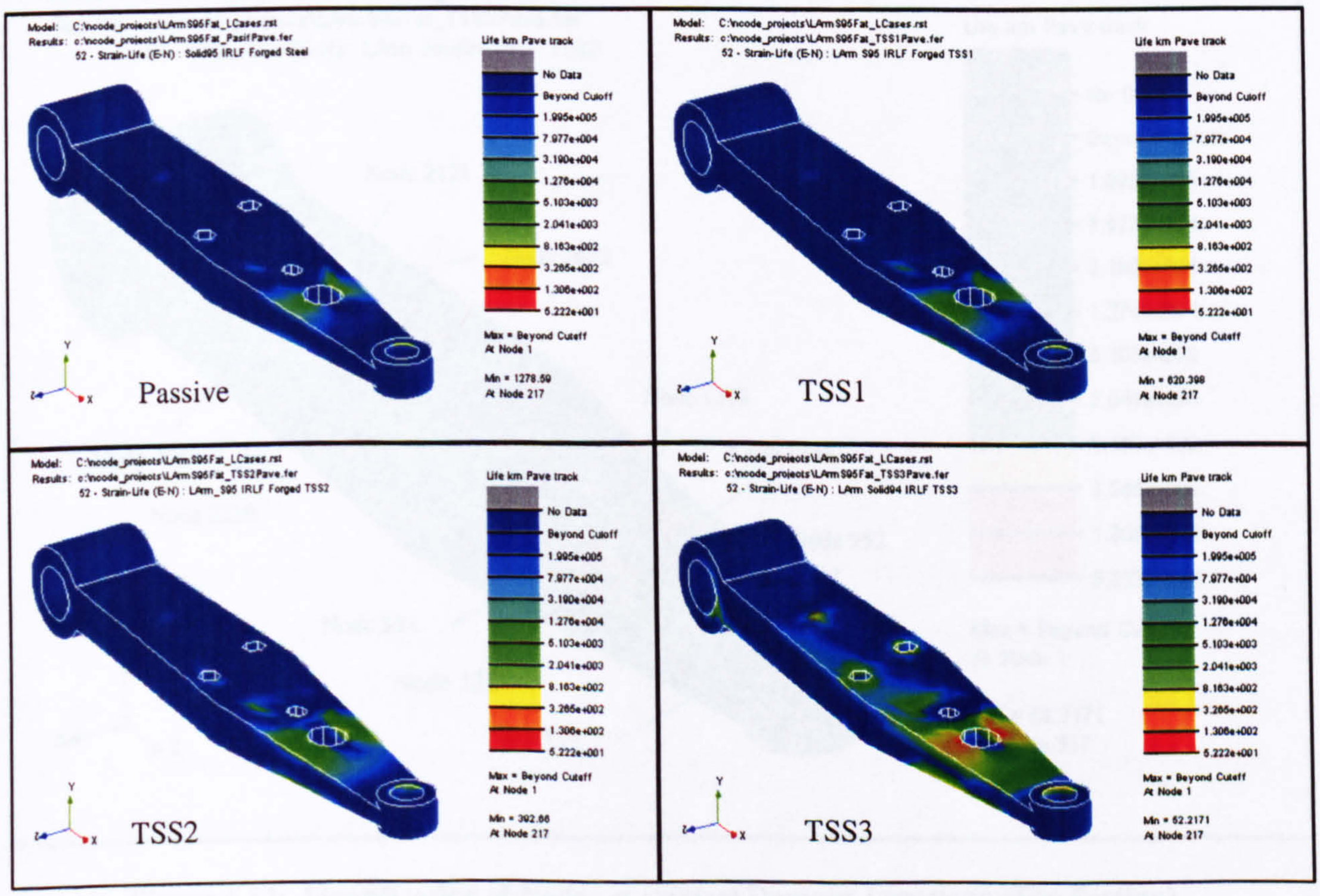

Figure 6.11: Fatigue Life Distributions due to Random Input (Top Section)

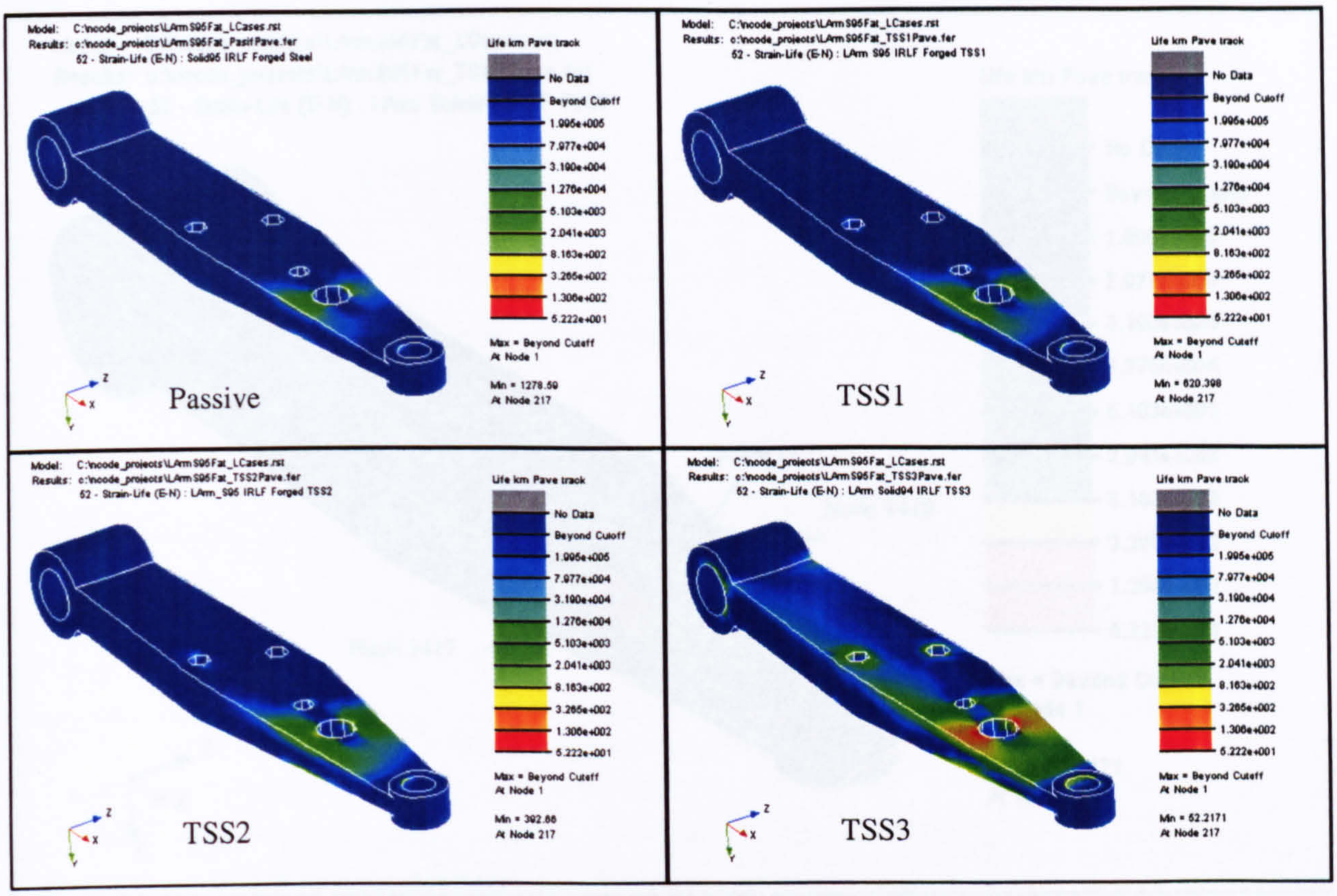

Figure 6.12: Fatigue Life Distributions due to Random Input (Bottom Section)

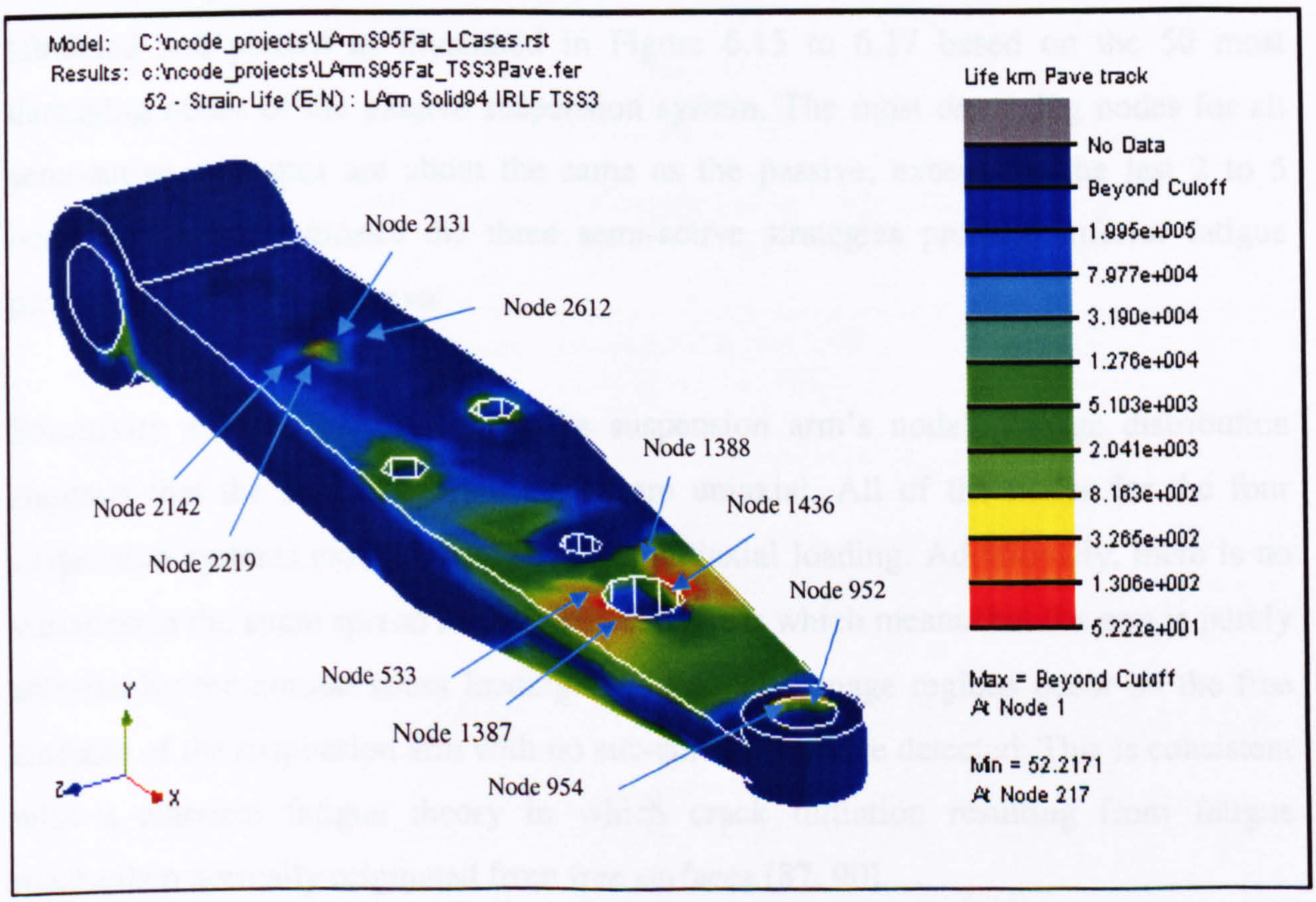

Figure 6.13: Identification of Nodes at Critical Damage Locations (Top Section)

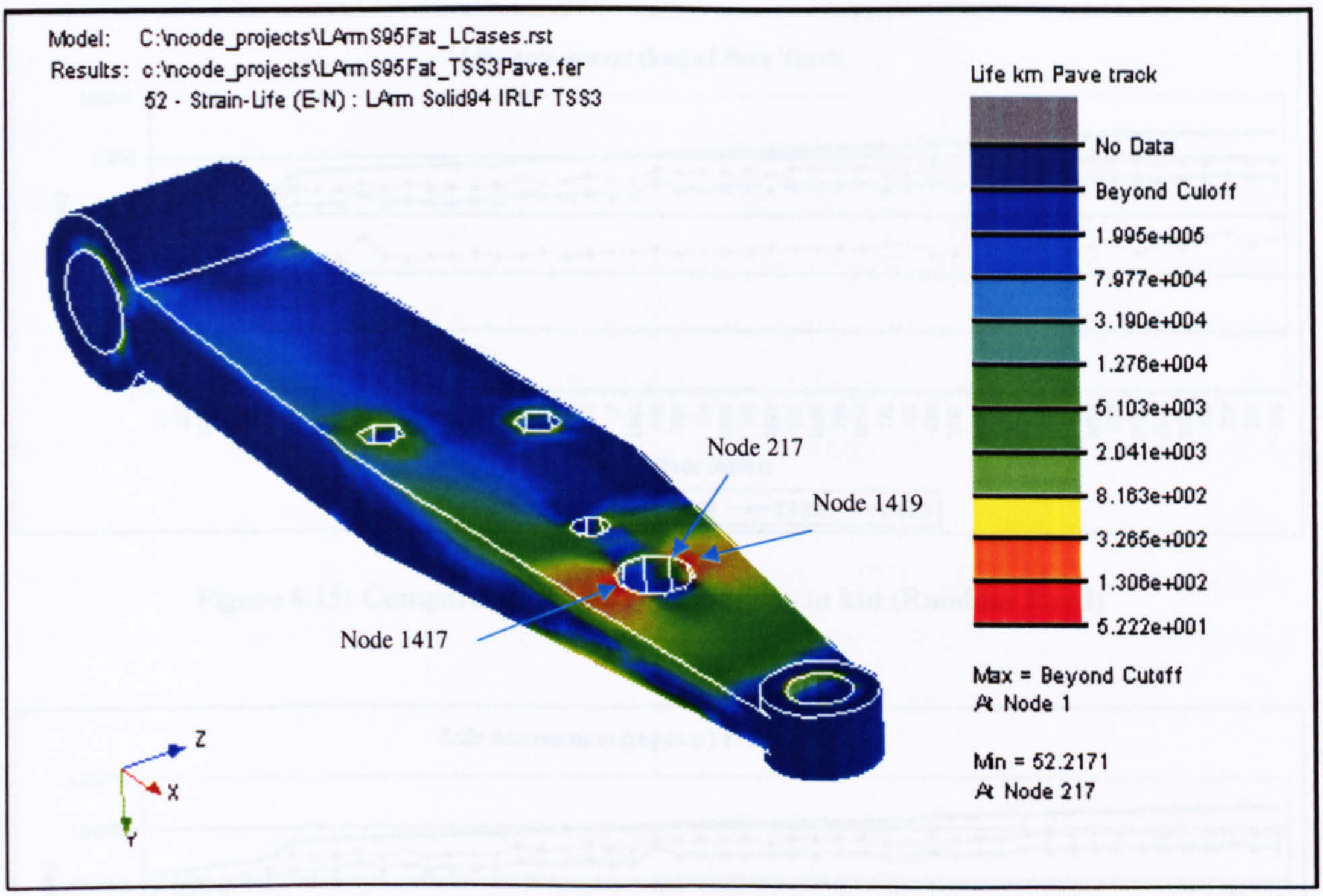

Figure 6.14: Identification of Nodes at Critical Damage Locations (Bottom Section)

The fatigue prediction and nodal distributions of the most damaging nodes are tabulated and plotted as illustrated in Figure 6.15 to 6.17 based on the 50 most damaging nodes of the passive suspension system. The most damaging nodes for all semi-active strategies are about the same as the passive, except for the last 2 to 5 nodes. It clearly indicates the three semi-active strategies produce inferior fatigue performance than the passive.

Sensitivity analysis performed for the suspension arm's nodal damage distribution suggests that the stress or strain cycles are uniaxial. All of the nodes for the four suspension systems exhibit no biaxial or multiaxial loading. Additionally, there is no variation in the angle spread for the principal stress which means that the arm is purely affected by the normal stress loading. The critical damage regions occur on the free surfaces of the suspension arm with no sub-surface damage detected. This is consistent with a classical fatigue theory in which crack initiation resulting from fatigue mechanism normally originated from free surfaces [87, 90].

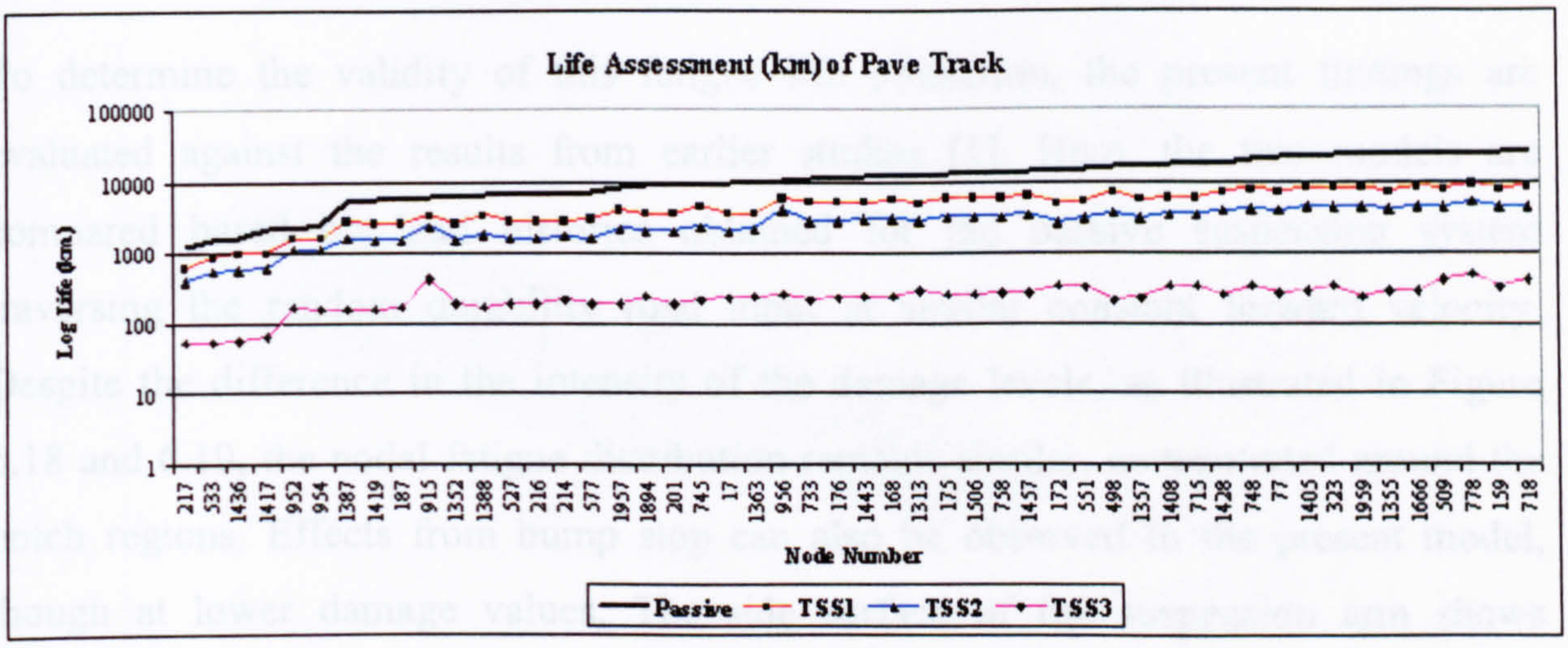

Figure 6.15: Comparison of Life Distributions in km (Random Road)

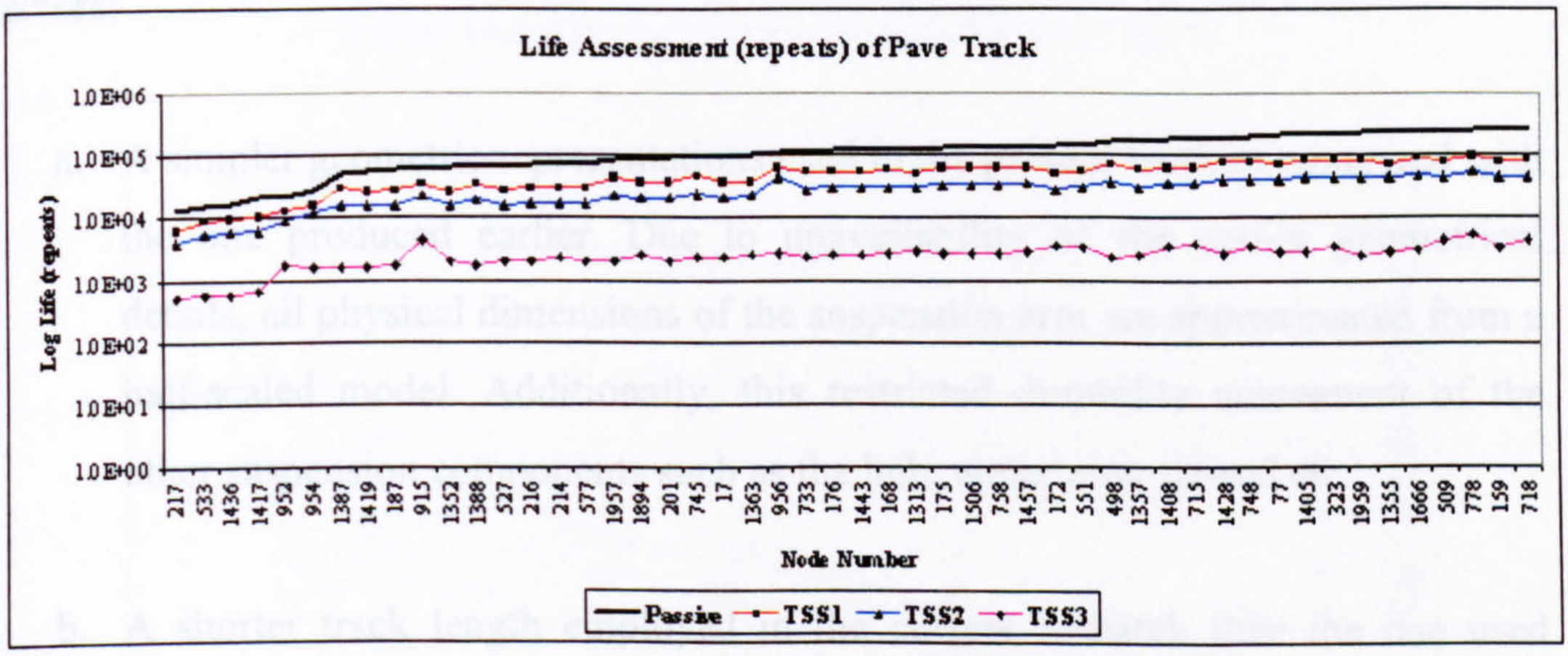

Figure 6.16: Comparison of Life Distributions in Repeats (Random Road)

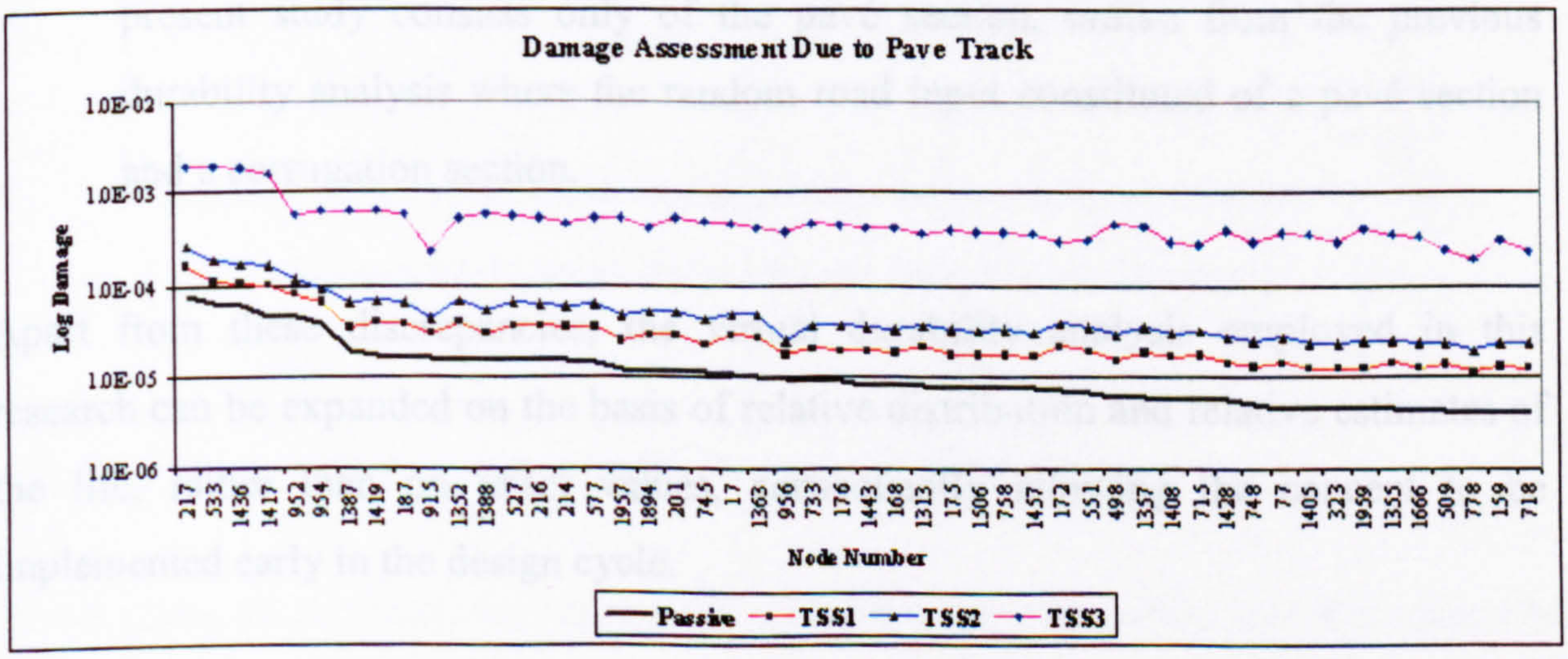

Figure 6.17: Comparison of 50 Most Damaging Nodes (Random Road)

6.4.2 Comparison with Previous Work

To determine the validity of this fatigue life prediction, the present findings are evaluated against the results from earlier studies [1]. Here, the two models are compared based on load histories obtained for the passive suspension system traversing the random durability road input at similar constant forward velocity. Despite the difference in the intensity of the damage levels, as illustrated in Figure 6.18 and 6.19, the nodal fatigue distribution remains similar, concentrated around the notch regions. Effects from bump stop can also be observed in the present model, though at lower damage values. The side surface of the suspension arm shows negligible damage as compared to previous work. The differences in contour intensities and spread between the two models are mainly influenced by the following factors:

a. A simpler geometric representations used in the present work as compared with the one produced earlier. Due to unavailability of the earlier geometrical details, all physical dimensions of the suspension arm are approximated from a half-scaled model. Additionally, this restricted durability assessment of the other suspension components such as the hub, upper arm, tie-rod etc.

b. A shorter track length employed in the current research than the one used previously. This is due to the high sampling rate required by the MR damper, which restricts the data storage capability. Moreover, the available track for the present study consists only of the pavé section, unlike from the previous durability analysis where the random road input constituted of a pavé section and a corrugation section.

Apart from these discrepancies, the virtual durability analysis employed in this research can be expanded on the basis of relative distribution and relative estimates of the life, rather than on exact values, consequently allowing the concept to be implemented early in the design cycle.

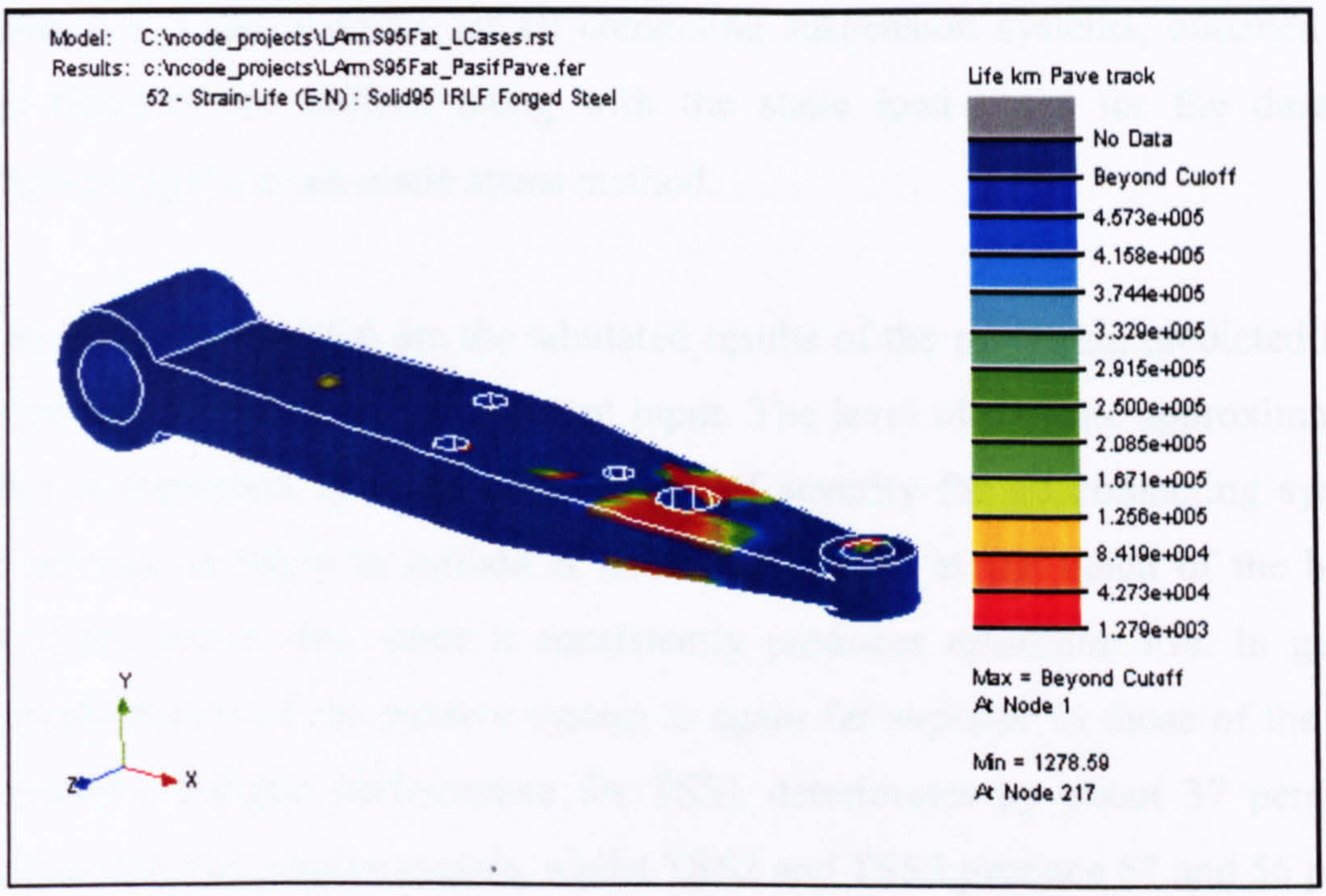

Figure 6.18: Fatigue Life Distribution of Present Work

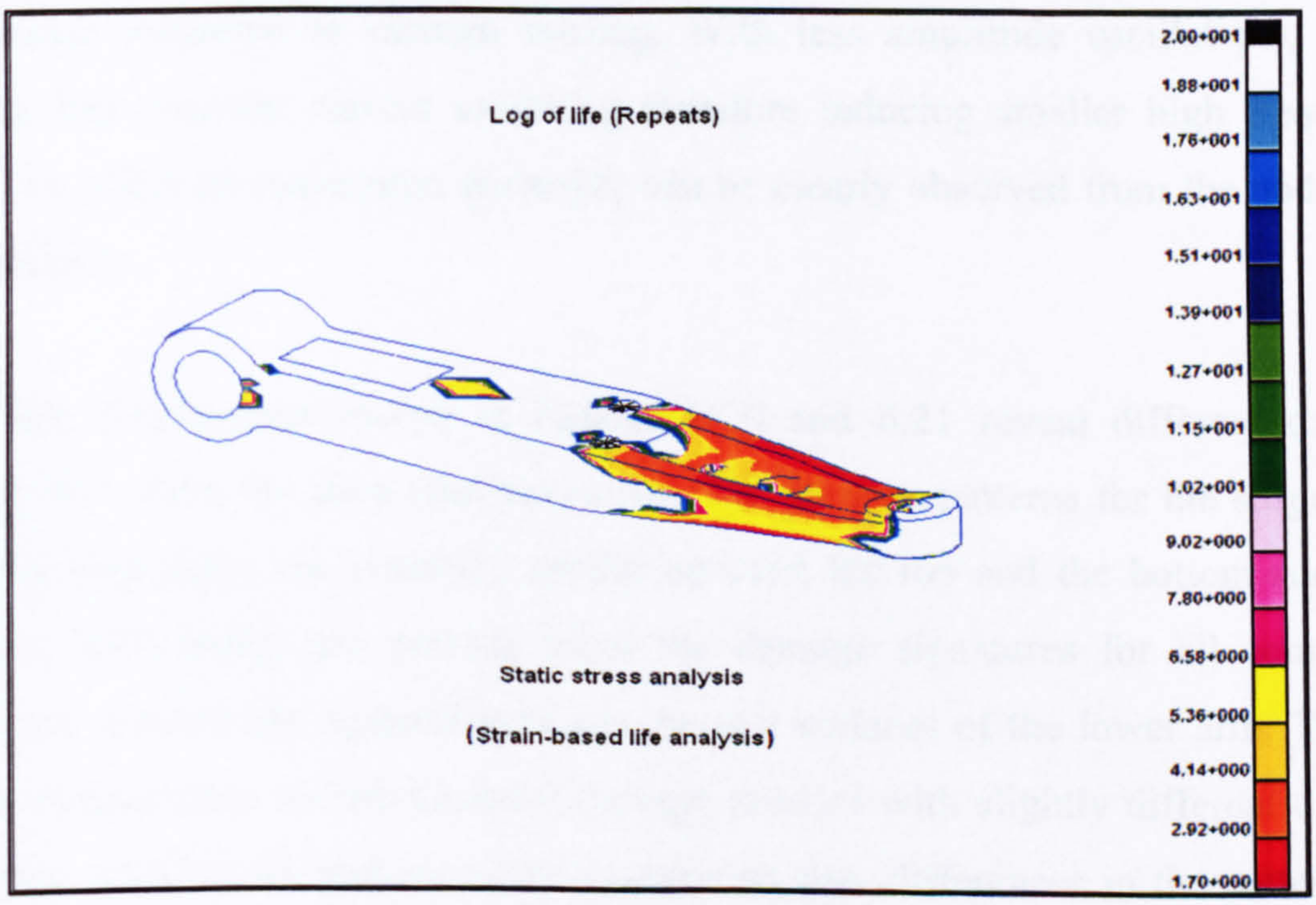

Figure 6.19: Fatigue Life Distribution from Previous Work [1]

6.4.3 Fatigue Life Assessment with Bump and Pothole Input

In the previous two sections, the durability of the lower suspension arm was evaluated under the influence of random road input (pavé track). The work in this section describes fatigue analysis of the suspension arm subjected to potentially damaging transient road excitation in the form of a bump and pothole as illustrated in Figure 4.4

and Figure 4.5. Load histories for all competing suspension systems, obtained from previous chapters are utilised along with the static load cases for the durability calculation using the quasi-static stress method.

Shown in Table 6.5 and 6.6 are the tabulated results of the minimum predicted life in kilometres and in repeats of the transient input. The level of damage approximated at the nodes is consistent in terms of the order of severity for all competing systems. Fatigue damage is likely to initiate at node 217 located at the notch of the bottom section of the lower arm, since it consistently produces minimum life. In general, fatigue performance of the passive system is again far superior to those of the semi-active systems. Fatigue performance for TSS1 deteriorates by about 37 percent in comparison with the passive system, whilst TSS2 and TSS3 produce 57 and 56 percent reduction in fatigue life, respectively, compared to the passive system. TSS3 shows a dramatic improvement in fatigue performance under transient loading compared to its performance subjected to random loading. With less amplitude oscillations, TSS3 produces less constant current switching therefore inducing smaller high frequency energy. Its effect on suspension durability can be clearly observed from the nodal life characteristics.

Nodal life distributions shown in Figures 6.20 and 6.21 reveal different damage contours than from the pavé road excitation. The damage patterns for the suspension arm with pavé input are generally similar between the top and the bottom surfaces. However, with bump and pothole input the damage signatures for all competing suspension systems are different between the two surfaces of the lower arm. The top surface demonstrates almost identical damage profiles with slightly different damage intensities, while at the bottom of the suspension arm, differences in the patterns are more noticeable. The effect of large transient loading seems to contribute to a highly localised damage compared to those caused by the random excitations. This characteristics is further illustrated in Figure 6.22 to 6.24 in which the comparison of the 50 most highly damage nodes showing close resemblance between the values from TSS2 and TSS3.

Nevertheless, the general outcome remains similar to those from the pavé input, where the three switchable semi-active systems produced fatigue damage faster than the

passive system. Again, the cause of this shorter service life is most likely due to the sharp transient events initiated from the conventional skyhook damping control. Unlike, the pavé input, road excitation from a bump and pothole generally produces lower frequency energy. Therefore, the effect of high frequency energy from the constant current switching in TSS3 is not as dominant as in the pavé input.

Node No.	Passive	TSS1	TSS2	TSS3
217	134.8	82.1	58.2	61.1
1417	190.6	118.8	81.6	81.8
952	317.4	208.7	141.6	141.7

Table 6.5: Comparison of Minimum Life Prediction (in km)

Node No.	Passive	TSS1	TSS2	TSS3
217	8986.6	5473.3	3879.3	4076.7
1417	12705	7917.6	5440.8	5450.4
952	21159	13912	9442.2	9446.6

Table 6.6: Comparison of Minimum Life (in Repeats of Bump and Pothole)

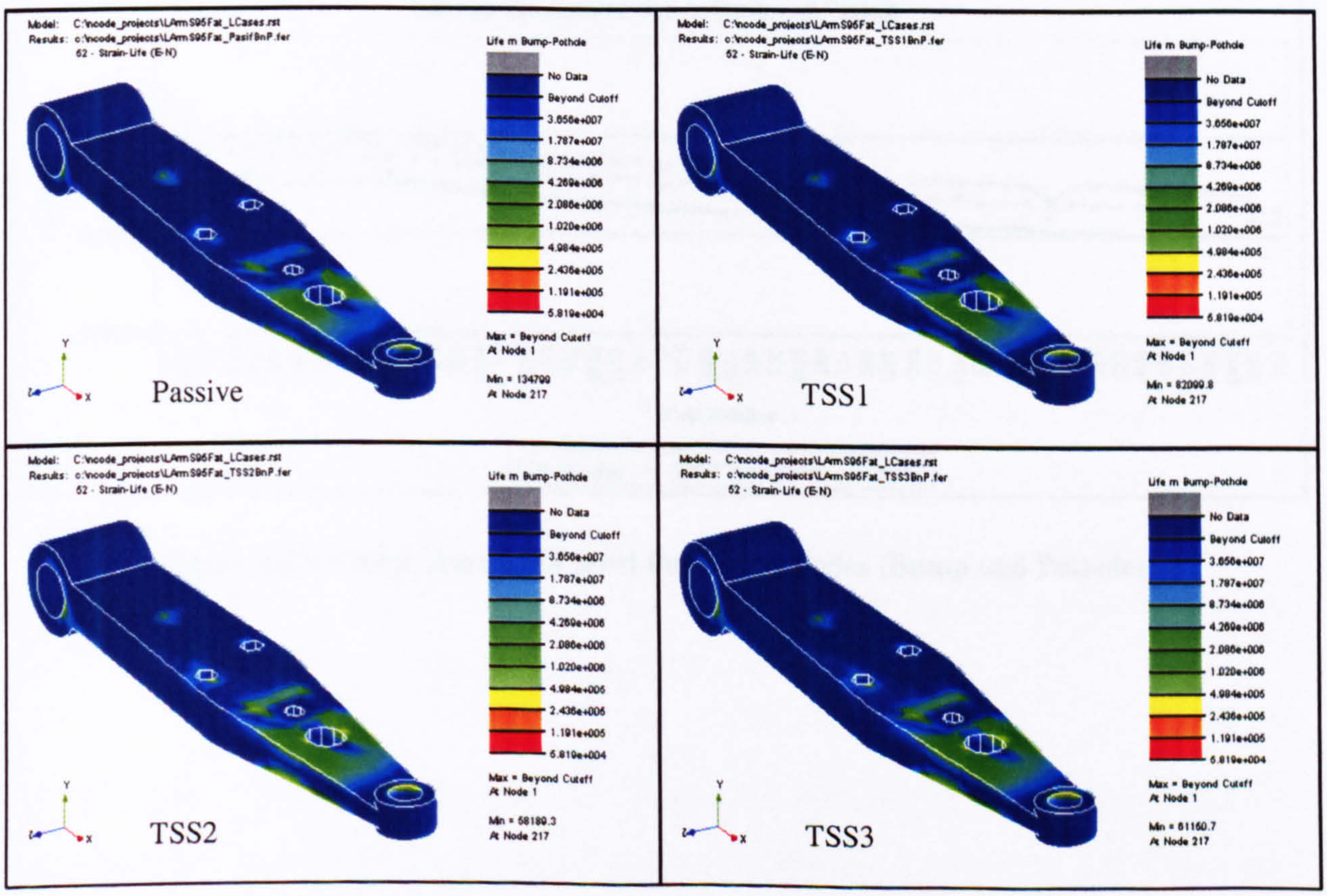

Figure 6.20: Fatigue Life Distributions due to Transient Input (Top Section)

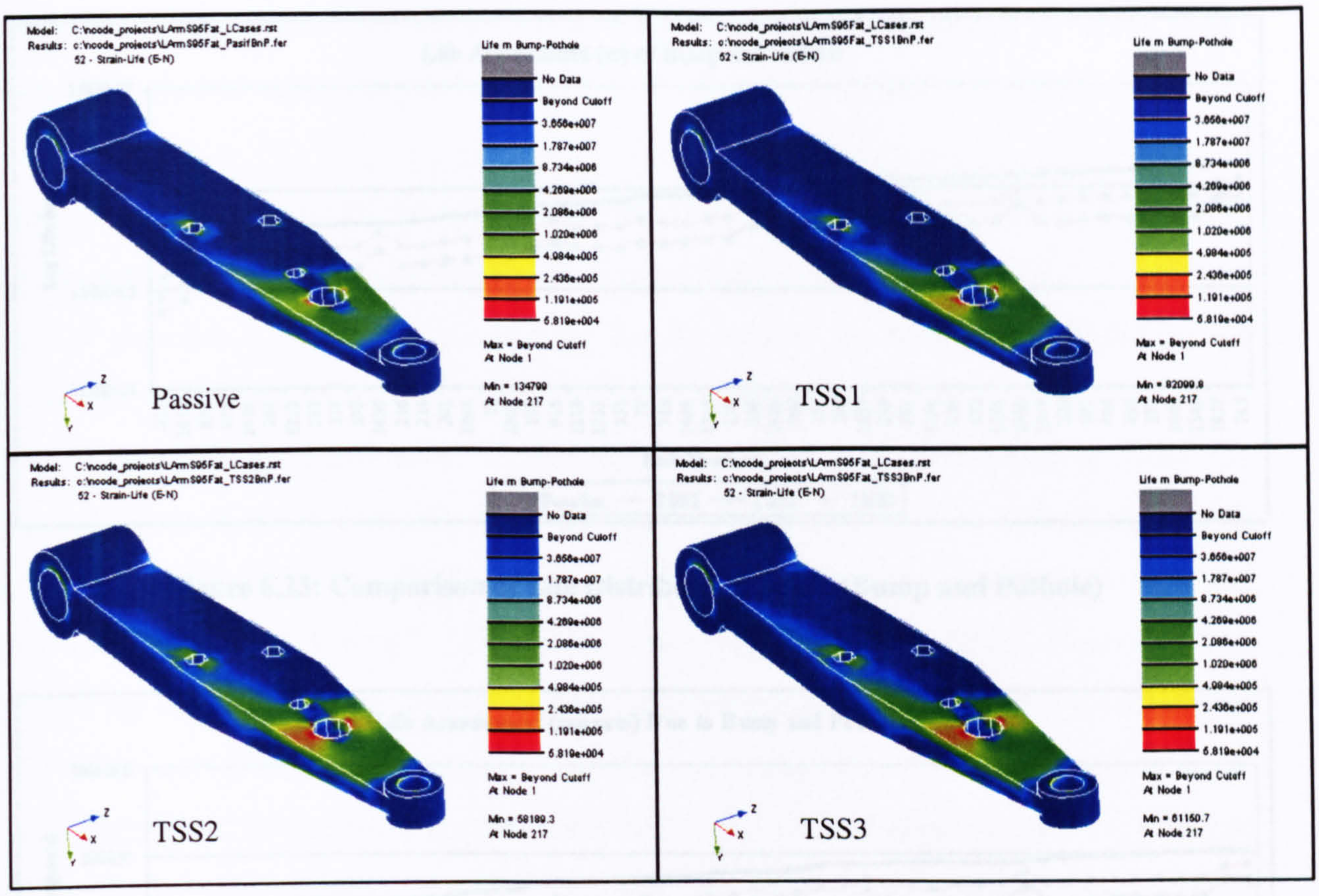

Figure 6.21: Fatigue Life Distributions due to Transient Input (Bottom Section)

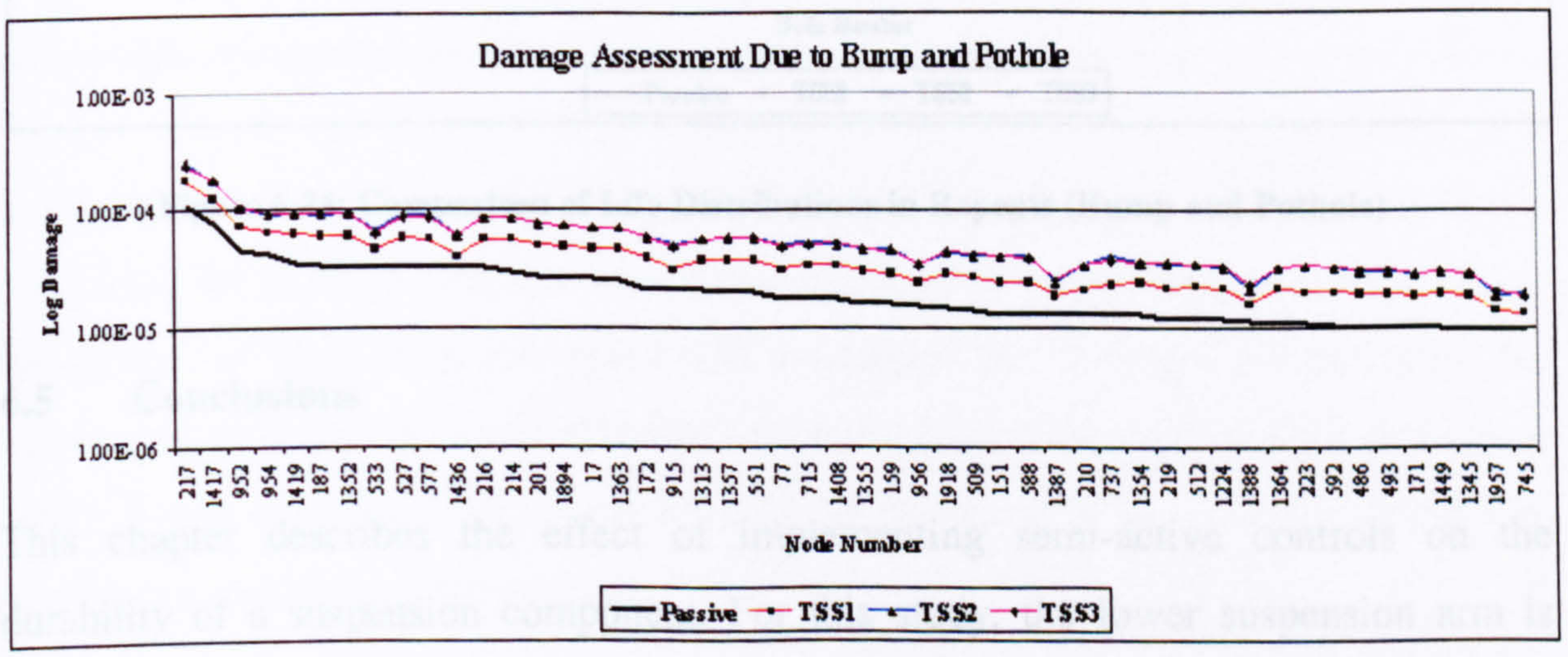

Figure 6.22: Comparison of 50 Most Damaging Nodes (Bump and Pothole)

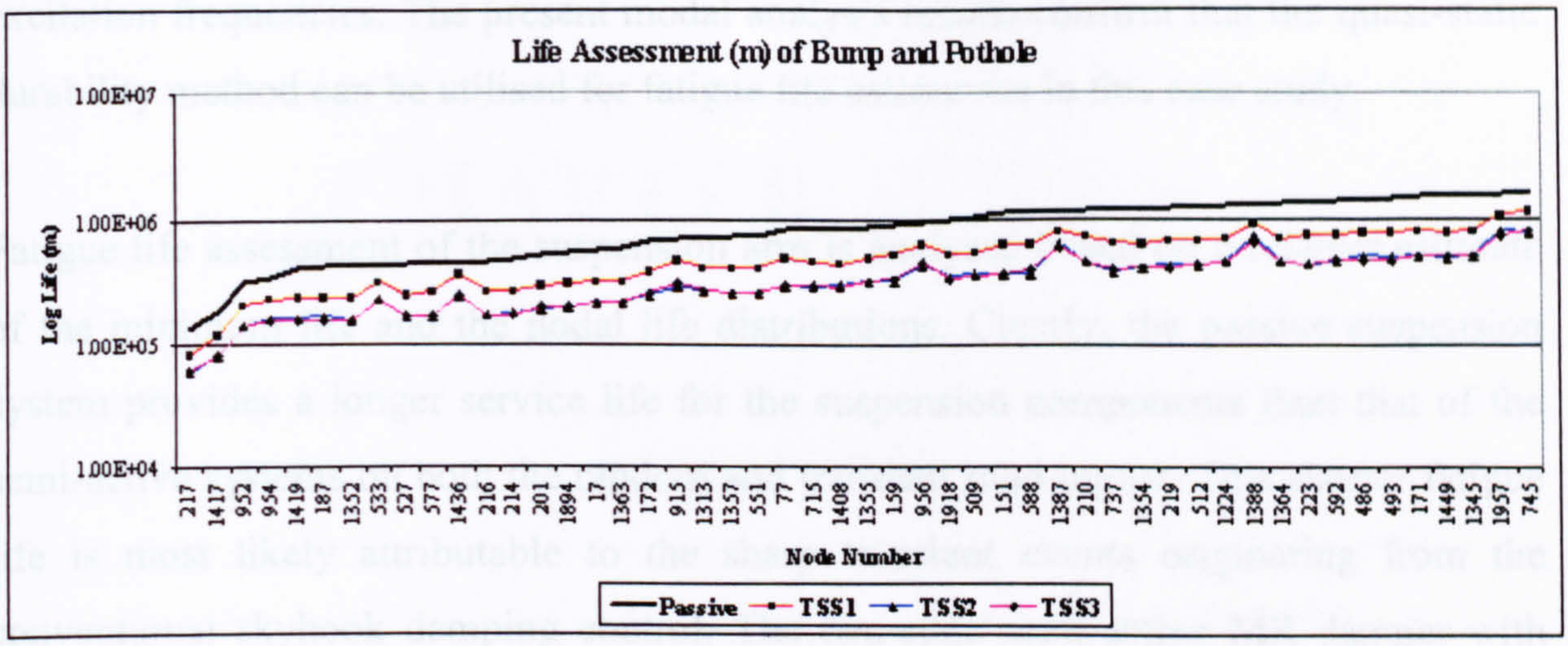

Figure 6.23: Comparison of Life Distributions in km (Bump and Pothole)

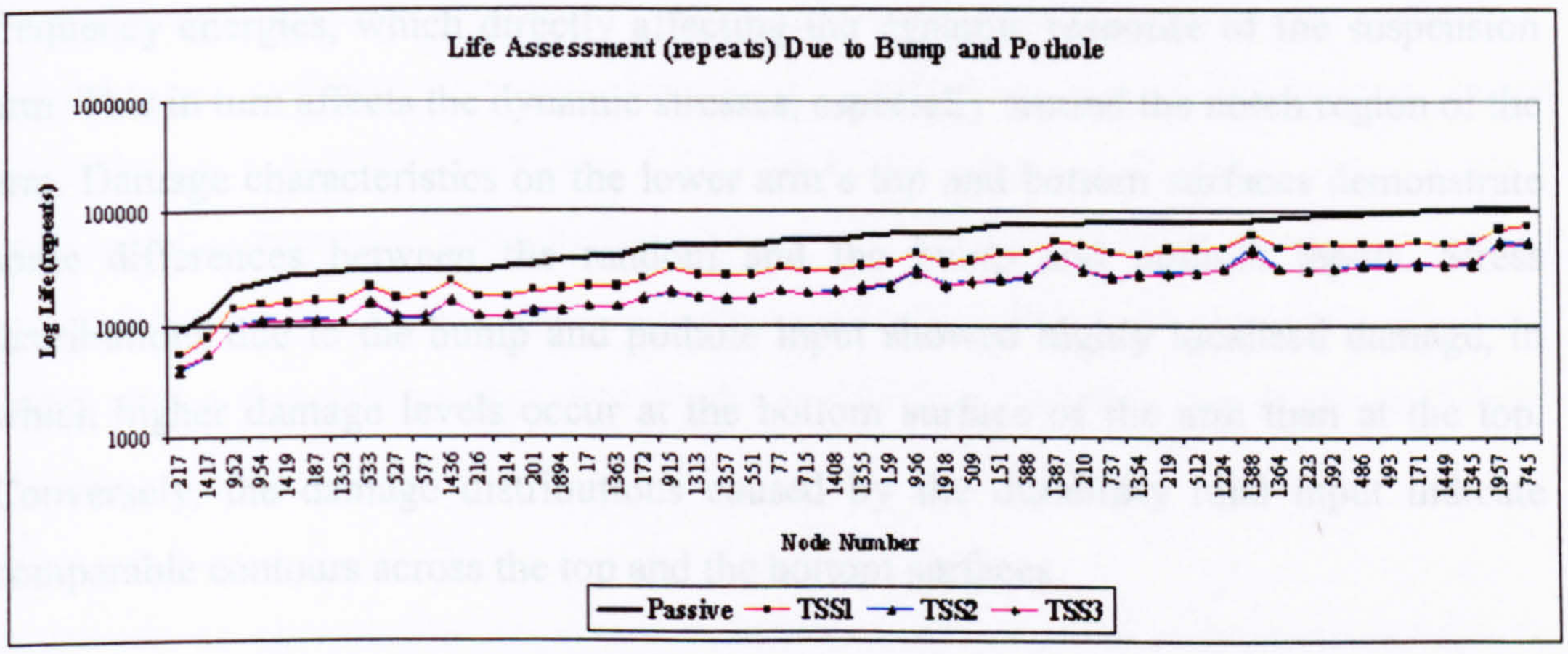

Figure 6.24: Comparison of Life Distributions in Repeats (Bump and Pothole)

6.5 Conclusions

This chapter describes the effect of implementing semi-active controls on the durability of a suspension component. For this study, the lower suspension arm is utilised as a case study to allow verification with previous work. The prediction of the minimum fatigue life and the corresponding nodal distributions are attained using the quasi-static stress method with time domain life estimation.

Determining fatigue performance using quasi-static durability strategy assumes negligible influence from local and global vibrations. Therefore, initially modal analysis is performed to establish the lowest flexural mode of the suspension arm. The finding indicates the lowest flexible mode occurs at 362 Hz, which is far above the

excitation frequencies. The present modal analysis results confirm that the quasi-static durability method can be utilised for fatigue life estimation in this case study.

Fatigue life assessment of the suspension arm is analysed based on a relative estimate of the minimum life and the nodal life distributions. Clearly, the passive suspension system provides a longer service life for the suspension components than that of the semi-active systems on both the random and transient road inputs. This shorter fatigue life is most likely attributable to the sharp transient events originating from the conventional skyhook damping control. The two-state semi-active MR damper with constant current switching (TSS3) produced faster fatigue damage than from the other semi-active systems. Using the durability road input, current switching generates high frequency energies, which directly affecting the dynamic response of the suspension arm. This in turn affects the dynamic stresses, especially around the notch region of the arm. Damage characteristics on the lower arm's top and bottom surfaces demonstrate some differences between the random and the bump and pothole inputs. Stress distributions due to the bump and pothole input showed highly localised damage, in which higher damage levels occur at the bottom surface of the arm than at the top. Conversely, the damage distributions caused by the durability road input indicate comparable contours across the top and the bottom surfaces.

Verification of the durability analysis conducted in this case study, is done by comparing the damage contours with those produced from previous work. Even with limitations on simulation capability and resources, the damage regions from the present research appear to resemble that of the previous work, but with lower damage values. These differences are mainly attributed to the variation in geometric details and road inputs employed in the analysis.

Implementation of the two-state switchable semi-active systems with skyhook control may provide better comfort but this is at the expense of shorter service life of suspension components. Further work can be included by investigating the effect of fully active control systems and semi-active systems with continuously variable dampers, on these suspension components.

CHAPTER SEVEN

Conclusions

7.1 Summary of Thesis

Extensive studies have been done over the last 30 years focussing on developing, testing, and evaluating various semi-active control strategies to achieve better performance in ride and handling. As a result, semi-active suspension systems have been widely accepted as being capable of providing improved performances in vehicle ride and handling over conventional passive systems. However, the effects of applying these semi-active control strategies on the durability of suspension components have received very little attention.

A review of current practice has established that studies pertaining to predicting durability based on fatigue life of suspension components with semi-active control systems are rarely attempted. To address this gap in knowledge, this research examined several semi-active strategies for a passenger vehicle, and their influence on the fatigue life of a suspension component was addressed. To achieve this, a modelling simulation technique capable of generating service load histories was established and evaluated. The approach known as MBS cosimulation allows seamless integration of key vehicle elements such as the tyre models, the damper models, the road models, and the vehicle suspension models, and simulated in a combined environment. Validity of this modular approach has been established by evaluating the accuracy of the dynamic response of vehicle models, in which the proposed method produced comparable results with other modelling techniques. Outcomes from this assessment have been published and presented at an International Symposium of Multi-body Dynamics in July 2004 [108], which focussed on analysing responses from a lumped mass quarter vehicle model.

With the proposed modelling approach validated, this research analysed the response from a variety of vehicle suspension models in terms of increasing the degrees of freedom. It was discovered that the QVM simulation overestimated the response particularly at the sprung mass when compared to a FVM. The FVM responses appeared to be damped by the vehicle body pitch and roll motions raising concerns regarding the validity of semi-active controllers developed on quarter car models. It was proposed that a semi-active controller should take into account these motions when applied to the FVM. Findings from this analysis was presented at the NAFEMS World Congress in May 2005 [99].

The next crucial element in the proposed method involved evaluating the dynamic response and ascertaining the load histories of an MPV with a semi-active suspension system. Linear and non-linear damper models were implemented along with global and local controllers using a skyhook damping approach. The three variants of the discrete two-state-switchable semi-active strategy with local control were a semi-active damper with linear damping coefficients switching (TSS1), an MR damper force switching with linearised feedback control (TSS2), and an MR damper with constant current switching (TSS3). Evaluation of the force characteristics of the selected semi-active systems, revealed that all semi-active systems examined, exhibited sharp transients in their responses compared to the passive system. From the investigation of the local semi-active control systems it was found,

a. TSS2 provided the best vibration reduction at the sprung mass, unsprung mass, and at the lower suspension arm.

b. TSS3 produced exceptional reduction in body acceleration at low frequencies but substantially deteriorated at higher bandwidth.

A global semi-active control (TSS1 PnR), adopting a linear damping coefficient switching that took account of the vehicle body's pitch and roll motions was implemented for the full vehicle model. It was shown that the global controller, which was adopted from an off-road application, resulted in relatively poor ride comfort in comparison with the performance from the fully independent semi-active controller

(using local control). Results from this investigations have been published in a special edition of Part K of the proceedings of the IMechE in January 2007 [111].

With valid load histories from the competing suspension systems established, fatigue life of a particular suspension component was ascertained using a finite element method approach. Quasi-static stress and a time domain life assessment strategy was found to be the most suitable method for the durability calculations, since modal analysis conducted prior to the durability analysis, showed that the lowest flexible mode occurred in a region far above the excitation frequencies. Durability calculations for the lower suspension arm revealed that a shorter service life resulted from all the semi-active systems. It was shown that the switching strategy with skyhook damping control generates sharp transient events, inflicting greater stresses on the suspension arm. TSS3 produced the shortest service life, primarily due to these large transient events but due also to high frequency energies generated from the non-linear characteristics of the MR damper. Verification of the durability analysis with that produced in earlier studies showed some resemblance in terms of damage regions though with less severity, due in part to differences in geometric details.

The major drawbacks of adopting the proposed MBS cosimulation approach to predict the load histories were related to long solution time and software upgrade compatibility. The solution time required to achieve similar accuracy with other modelling and simulation strategies, increased significantly. Therefore, to include MBS cosimulation within an automated structural optimisation framework for example may not be feasible with current computing power despite its ability to seamlessly integrate different modelling methods. Another factor is related to compatibility issues during software upgrade, as each new version is released at different times of the year often affecting communication between programs.

7.2 Statement of Achievement

The ultimate aim of this research was to predict the effect of semi-active control systems on the durability of suspension components. In realizing this objective, the following has been achieved:

a. Comprehensive review of virtual durability analysis comprising of current practice in modelling and simulation techniques, semi-active controls, and durability based on fatigue life.

b. Proposed and validated a modelling and simulation technique that is suitable for semi-active applications.

c. Simulated and evaluated the dynamic response of a multi-purpose passenger vehicle with the proposed MBS cosimulation approach.

d. Simulated a selection of semi-active suspension systems for the MPV that include controllers derived experimentally from an MR damper.

e. Investigated the dynamic response of a full vehicle model when subjected to global semi-active strategies considering the effect of pitch and roll motions.

f. Produced load histories of a suspension component using the MBS cosimulation method for assessing competing suspension systems.

g. Predicted and evaluated the durability of the component by estimating the minimum fatigue life and the damage distributions from the selected suspension systems.

7.3 Original Contributions to Knowledge

To date, research on the durability of suspension components fitted with semi-active systems, specifically involving two-state switchable with skyhook damping controls, has not been published. Additionally, the effect on components fatigue life with the implementation of magnetorheological dampers as a semi-active device has rarely been attempted. The method of predicting load histories for the durability calculations using MBS cosimulation is seldom practiced even though it is capable of producing sufficiently accurate histories but at the expense of increasing solution time. More than

half of the research findings have been presented in international conferences. Recently, results have also accepted for publication in the proceeding of the IMechE. The full papers are available in Appendix I.

7.4 Recommendations and suggestions for future works

This research has provided an important framework for studies involving virtual durability analysis of semi-active suspension components. Further investigations may include the following:

a. To study the effect of driving manoeuvres on suspension component durability for vehicles with semi-active suspension. The same semi-active control laws can be employed however changes in tyre models are necessary to incorporate the lateral and longitudinal loads. Introduction of driving inputs like step steer, lane change, accelerating, and braking can be incorporated to assess the influence of transient driving states on the components' loads.

b. To evaluate the dynamic response of suspension components using a flexible multi-body cosimulation approach. The modelling method chosen for this study assumed the vehicle suspension components as rigid bodies, since the suspension component involved for the durability analysis has natural frequencies far above the road excitation frequencies. If the components in particular those with high mass and low stiffness, having natural frequencies within the bandwidth of the excitation frequencies, then resonance would occur. In durability calculations, effects from resonance are crucial since they have direct influence on the dynamic response, affecting stress and the predicted fatigue life. In these cases, a flexible multi-body approach is required to accurately obtain the load histories. Simulation codes such as MSC.ADAMS and SIMPACK have recently introduced this feature enabling better prediction but none has been applied using a cosimulation approach.

c. To examine the effects of alternative semi-active control strategies such as groundhook or a hybrid fully active suspension control systems.

d. To further investigate the causes of slow simulation speed of the proposed method and to find ways to rectify the problem.

REFERENCES

[1] M. Haiba, "Efficient Algorithms for Structural Optimisation Based on Fatigue for Automotive Chassis Components", PhD thesis, *School of Mechanical Engineering*, University of Leeds, UK, 2002.

[2] M. Pompetzki, "Combining Durability with Multibody Dynamics", *International ADAMS User Conference*, Orlando, U.S.A., 2000.

[3] W. M. Kyoung, J. W. Jeon, and S. G. Joo, "Durability Analysis of a Suspension Part by Use of the VTL (Virtual Test Laboratory)", *MSC Software Virtual Product Development Conference*, 2004.

[4] W. B. Ferry, P. R. Frise, G. T. Andrews, and M. A. Malik, "Combining Virtual Simulation and Physical Vehicle Test Data to Optimize Durability Testing", *Fatigue & Fracture of Engineering Materials & Structures*, vol. 25, pp. 1127-1134, 2002.

[5] R. Edara, S. Shih, N. Tamini, T. Palmer, and A. Tang, "Heavy Vehicle Suspension Frame Durability Analysis Using Virtual Proving Ground", *SAE Technical Paper Series*, (2005-01-3609), 2005.

[6] M. C. Levesley, S. A. Kember, D. C. Barton, P. C. Brooks, and O. M. Querin, "Dynamic Simulation of Vehicle Suspension Systems for Durability Analysis", *Materials Science Forum*, vol. 440-441, pp. 103-110, 2003.

[7] G. M. Prior, "The Use of Multi-body Systems Analysis in the Design and Analysis of Vehicle Suspension Systems ", *SAE Technical Paper Series*, (921463), 1992.

[8] M. Haiba, D. C. Barton, P. C. Brooks, and M. C. Levesley, "Using a Quarter-vehicle Multi-body Model to Estimate the Service Loads of a Suspension Arm for Durability Calculations", *Proc. Instn. Mech. Engrs., Part K: J. Multi-body*

Dynamics, vol. 217, pp. 121-133, 2003.

[9] A. Lepold, G. Ammon, N. Mcgowan, and B. Burdock, "Influence of Active Suspension Components on Durability", *SAE Technical Paper Series*, (2005-01-0981), 2005.

[10] C. W. Mousseau, T. A. Laursen, M. Lidberg, and R. L. Taylor, "Vehicle Dynamics Simulations with Coupled Multibody and Finite Element Models", *Finite Elements in Analysis and Design*, vol. 31, pp. 295-315, 1999.

[11] O. Friberg and P. Eriksson, "Optimization of Ride Comfort", *Multi-body Dynamics: Monitoring and Simulation Techniques - II*, pp. 107-114, 2000.

[12] M. Decker and G. Savaidis, "Measurement and Analysis of Wheel Loads for Design and Fatigue Evaluation of Vehicle Chassis Components", *Fatigue and Fracture of Engineering Materials and Structures*, vol. 25, pp. 1103-1119, 2002.

[13] A. A. Shabana, "Dynamics of Multibody Systems", 2nd ed., *Cambridge University Press*, UK, 1998.

[14] D. Hitchings, "A Finite Element Dynamics Primer." *NAFEMS Ltd.*, Glasgow, 1992.

[15] M. Blundell and D. Harty, "The Multibody Systems Approach to Vehicle Dynamics", *Elsevier Butterworth-Heinemann*, Oxford, 2004.

[16] D. A. Crolla, D. Horton, and G. Firth, "Application of Multi-body Systems Software to Vehicle Dynamic Problems", *Kinematics and Dynamics of Multi-body Systems Seminar (S057)*, 1992.

[17] W. Kortum and R. S. Sharp, "A Report on the State of Affairs on Application of Multibody Computer Codes to Vehicle System Dynamics", *Vehicle System Dynamics*, vol. 20, pp. 177-184, 1991.

[18] D. A. Crolla, D. N. L. Horton, P. C. Brooks, G. R. Firth, D. W. Shuttlewood, M. Woods, and C. K. Yip, "A Systematic Approach to Vehicle Design Using VDAS (Vehicle Dynamics Analysis Software) ", *SAE Technical Paper Series*,

(940230), 1994.

[19] P. J. T. Venhovens, A. C. M. Van Der Knapp, and H. B. Pacejka, "Semi-Active Attitude and Vibration Control", *Vehicle System Dynamics*, vol. 22, pp. 359-381, 1993.

[20] S. Nell and J. L. Steyn, "An Alternative Control Strategy for Semi-Active Dampers on Off-Road Vehicles", *Journal of Terramechanics*, vol. 35, pp. 25-40, 1998.

[21] Y. G. Liao and H. I. Du, "Cosimulation of Multi-Body-Based Vehicle Dynamics and an Electric Power Steering Control System", *Proc. Instn. Mech. Engrs.: Part K*, vol. 215, pp. 141-151, 2001.

[22] D. Danesin, P. Vercellone, F. Mastronardi, M. Fenoglio, A. Fornero, and M. Velardocchia, "Vehicle Dynamics with Real Time Damper Systems", *16th European ADAMS User Conference 2001*, Berchtesgaden, 2001.

[23] W. Kortum, M. Valášek, Z. Šika, W. Schwartz, P. Steinbauer, and O. Vaculin, "Semi-Active Damping in Automotive Systems: Design-by-Simulation", *International Journal of Vehicle Design*, vol. 28, pp. 360-371, 2002.

[24] J. Maiorana, B. P. Minaker, D. Zhang, and M. A. Malik, "Cosimulation of Active Suspension", *SAE Technical Paper Series*, (2005-01-0984), pp. 9, 2005.

[25] M. Ieluzzi, P. Turco, and M. Montiglio, "Development of a Heavy Truck Semi-active Suspension Control", *Control Engineering Practice*, 2005.

[26] O. Vaculin, W. R.Kruger, and M. Valasek, "Overview of Coupling of Multibody and Control Engineering Tools", *Vehicle System Dynamics*, vol. 41, pp. 415-429, 2004.

[27] O. Vaculin, W. Kortum, and W. Schwartz, "Analysis and design of Semi-Active Damping in Truck Suspension - Design-by-Simulation", 2004.

[28] J. Happian-Smith, "An Introduction to Modern Vehicle Design", *Butterworth-Heinemann*, Oxford, 2002.

[29] R. S. Sharp and D. A. Crolla, "Road Vehicle Suspension System Design - a

review", *Vehicle System Dynamics*, vol. 16, pp. 167-192, 1987.

[30] D. A. Crolla, G. Firth, and D. Horton, "An Introduction to Vehicle Dynamics", *School of Mechanical Engineering*, University of Leeds, UK, 2001.

[31] H. Kojima, J. Nakano, H. Nakayama, N. Kawashima, and H. Fujimoto, "Development of New Toyota Electronic Modulated Suspension - Two Concepts for Semi-Active Suspension Control", *SAE Technical Paper Series*, (911900), 1991.

[32] D. Hrovat, "Survey of Advanced Suspension Developments and Related Optimal Control Applications", *Automatica*, vol. 33, pp. 1781-1817, 1997.

[33] M. M. Elmadany and Z. S. Abduljabbar, "Linear Quadratic Gaussian Control of a Quarter-Car Suspension", *Vehicle System Dynamics*, vol. 32, pp. 479-497, 1999.

[34] K. Sharma, "Active Control of Vehicle Suspensions", PhD thesis, *Department of Electronic & Electrical Engineering*, University of Leeds, UK, 1995.

[35] A. G. Thompson, B. R. Davis, and C. E. M. Pearce, "An Optimal Linear Active Suspension with Finite Road Preview", *SAE Technical Paper Series*, (800520), 1980.

[36] R. G. Langlois and R. J. Anderson, "Preview Control Algorithms for the Active Suspension of an Off-Road Vehicle", *Vehicle System Dynamics*, vol. 24, pp. 65-97, 1995.

[37] A. Vahidi and A. Eskandarian, "Influence of Preview Uncertainties in the Preview Control of Vehicle Suspensions", *Proc. Instn. Mech. Engrs., Part K: J. Multi-body Dynamics*, vol. 216, pp. 295-301, 2002.

[38] D. Hrovat, D. L. Margolis, and M. Hubbard, "An Approach Toward the Optimal Semi-Active Suspension", *ASME Journal of Dynamic Systems, Measurement, and Control*, vol. 110, pp. 288-296, 1988.

[39] D. Karnopp, M. J. Crosby, and R. A. Harwood, "Vibration Control Using Semi-Active Force Generators", *Journal of Engineering for Industry*, 1974.

[40] L. R. Miller and C. M. Nobles, "Methods for Eliminating Jerk and Noise in Semi-Active Suspensions", *SAE Technical Paper Series*, (902284), 1990.

[41] E. Teramura, S. Haseda, Y. Shimoyama, T. Abe, and K. Matsuoka, "Semi-active Damping Control System with Smart Actuator", *JSAE Review*, vol. 18, pp. 323-329, 1997.

[42] D. Vetturi, M. Gadola, D. Cambiaghi, and L. Manzo, "Semi-Active Strategies for Racing Car Suspension Control", *SAE Technical Paper Series*, (962553), 1996.

[43] F. Oueslati and S. Sankar, "A Class of Semi-Active Suspension Schemes for Vehicle Vibration Control", *Journal of Sound and Vibration*, vol. 172, pp. 391-411, 1994.

[44] D. Moline, S. Floyd, S. Vaduri, and E. H. Law, "Simulation and Evaluation of Semi-Active Suspensions", *SAE Technical Paper Series*, (940864), 1994.

[45] El-Tawwab and D. A. Crolla, "An Experimental and Theoretical Study of a Switchable Damper", *SAE Technical Paper Series*, (960937), 1996.

[46] K. Sharma, D. A. Crolla, and D. A. Wilson, "Derivation of a Control Law for a 3 State Switchable Damper Suspension System for Improving Road Vehicle Ride Characteristics", *International Symposium on Theory of Machines and Mechanisms*, Nagoya, Japan, 1992.

[47] S. N. Vannucci, "Semi Active Suspensions with Multiple Damping and Levelling Curves", *SAE Technical Paper Series*, (942378), 1994.

[48] Y. I. Yoo and B. W. Jin, "The Characteristic of the Shock Force Induced in the Switchable Damper During its Mode Change", *SAE Technical Paper Series*, (950587), 1995.

[49] M. Ahmadian, X. Song, and S. C. Southward, "No-Jerk Skyhook Control Methods for Semiactive Suspensions", *Journal of Vibration and Acoustics*, vol. 126, pp. 580-584, 2004.

[50] M. Ahmadian and N. Vahdati, "Transient Dynamics of Semiactive Suspensions

with Hybrid Control", *Journal of Intelligent Material Systems and Structures*, vol. 17, 2006.

[51] T. D. Gillespie, "Fundamentals of Vehicle Dynamics", *Society of Automotive Engineers, Inc.*, U.S.A., 1992.

[52] J. Emura, S. Kakizaki, F. Yamaoka, and M. Nakamura, "Development of the Semi-Active Suspension System Based on the Sky-Hook Damper Theory", *SAE Technical Paper Series*, (940863), 1994.

[53] I. Youn, "Optimal Preview Control Design of Active and Semi-Active Suspension Systems Including Jerk", *SAE Technical Paper Series*, (960936), 1996.

[54] P. Barak, "Passive Versus Active and Semi-Active Suspension from Theory to Application in North American Industry", *SAE Technical Paper Series*, 1992.

[55] A. Hac and A. V. Fratini Jr., "Elimination of Limit Cycles Due to Signal Estimation in Semi-Active Suspensions", *SAE Technical Paper Series*, (1999-01-0728), 1999.

[56] T. Katsuda, N. Hiraiwa, S. i. Doi, and E. Yasuda, "Improvement of Ride Comfort by Continuously Controlled Damper", *SAE Technical Paper Series*, (920276), 1992.

[57] F. H. Besinger, D. Cebon, and D. J. Cole, "Force Control of a Semi-Active Damper", *Vehicle System Dynamics*, vol. 24, pp. 695-723, 1995.

[58] S.-H. Hwang, S.-J. Heo, H.-S. Kim, and K.-I. Lee, "Vehicle Dynamic Analysis and Evaluation of Continuously Controlled Semi-Active Suspensions Using Hardware-in-the-loop Simulation", *Vehicle System Dynamics*, vol. 27, pp. 423-434, 1997.

[59] J. Aurell, "The Influence of Different Suspension Parameters on Dynamic Wheel Loads", *IMechE Conference on Road Wear: The Interaction Between Vehicle Suspensions and the Road*, London, 1991.

[60] P. A. Wilkinson, "Advanced Commercial Vehicle Suspensions", *IMechE*

Conference on Road Wear: The Interaction Between Vehicle Suspensions and the Road, London, 1991.

[61] G. Z. Yao, F. F. Yap, G. Chen, W. H. Li, and S. H. Yeo, "MR Damper and its Application for Semi-Active Control of Vehicle Suspension System", *Mechatronics*, vol. 12, pp. 963-973, 2002.

[62] D. H. Wang and W. H. Liao, "Semiactive Controllers for Magnetorheological Fluid Dampers", *Journal of Intelligent Material Systems and Structures*, vol. 16, pp. 983-993, 2005.

[63] M. Yu, C. R. Liao, W. M. Chen, and S. L. Huang, "Study on MR Semi-active Suspension System and its Road Testing", *Journal of Intelligent Material Systems and Structures*, vol. 17, pp. 801-806, 2006.

[64] N. K. Petek, D. J. Romstadt, M. B. Lizell, and T. R. Weyenberg, "Demonstration of an Automotive Semi-Active Suspension Using Electrorheological Fluid", *SAE Technical Paper Series*, (950586), 1995.

[65] S.-S. Han and S.-B. Choi, "Control Performance of an Electrorheological Suspension System Considering Actuator Time Constant", *International Journal of Vehicle Design*, vol. 29, pp. 226-242, 2002.

[66] S.-M. Chen and C.-G. Wei, "Experimental Study of the Rheological Behavior of Electrorheological Fluids", *Journal of Smart Materials and Structures*, vol. 15, pp. 371-377, 2006.

[67] J. Wang and Y. Li, "Dynamic Simulation and Test Verification of MR Shock Absorber under Impact Load", *Journal of Intelligent Material Systems and Structures*, vol. 17, pp. 309-314, 2006.

[68] J. D. Carlson, "What Makes a Good MR Fluid?," *Journal of Intelligent Material Systems and Structures*, vol. 13, pp. 431-435, 2002.

[69] M. Ahmadian and D. E. Simon, "Can Semiactive Dampers with Skyhook Control Improve Roll Stability of Passenger Vehicles?", *SAE Technical Paper Series*, (2004-01-2099), pp. 8, 2004.

[70] H. Decker, W. Schramm, and M. R. Bethell, "An Optimized Approach to Suspension Control", *SAE Technical Paper Series*, (900661), 1990.

[71] M. Valasek, M. Novak, Z. Sika, and O. Vaculin, "Extended Ground-Hook - New Concept of Semi-Active Control of Truck's Suspension", *Vehicle System Dynamics*, vol. 27, pp. 289-303, 1997.

[72] T. J. Gordon, "Non-Linear Optimal Control of a Semi-Active Vehicle Suspension System", *Chaos, Solitons & Fractals*, vol. 5, pp. 1603-1617, 1995.

[73] J. H. E. A. Muijderman, J. J. Kok, R. G. M. Huisman, F. E. Veldpaus, and J. G. A. M. Van Heck, "Preview-Based Control of Suspension Systems for Commercial Vehicles", *Vehicle System Dynamics*, vol. 32, pp. 237-247, 1999.

[74] M. Nagai and T. Hasegawa, "Vibration Isolation Analysis and Semi-Active Control of Vehicles with Connected Front and Rear Suspension Dampers", *JSAE Review*, vol. 18, pp. 45-50, 1997.

[75] A. M. A. Soliman and D. A. Crolla, "Preview Control for a Semi-Active Suspension System", *International Journal of Vehicle Design*, vol. 17, pp. 384-397, 1996.

[76] H. Kim and Y.-S. Yoon, "Semi-Active Suspension with Preview Using a Frequency-Shaped Performance Index", *Vehicle System Dynamics*, vol. 24, pp. 759-780, 1995.

[77] T. J. Gordon and R. S. Sharp, "On Improving the Performance of Automotive Semi-Active Suspension Systems Through Road Preview", *Journal of Sound and Vibration*, vol. 217, pp. 163-182, 1998.

[78] M. Ahmadian and C. A. Pare, "A Quarter-Car Experimental Analysis of Alternative Semiactive Control Methods", *Journal of Intelligent Material Systems and Structures*, vol. 11, pp. 604-612, 2000.

[79] M. Ahmadian and F. D. Goncalves, "A Frequency Analysis of Semiactive Control Methods for Vehicle Application", *SAE Technical Paper Series*, (2004-01-2098), 2004.

[80] P. A. Wilkinson and D. A. Crolla, "Investigations into Alternative Suspensions for Commercial Vehicles (933048)," *SAE Technical Paper Series*, 1993.

[81] D. Cebon, F. Besinger, and D. Cole, "Control Strategies for Semi-Active Lorry Suspensions", *Proc. Instn of Mech. Engrs*, vol. 210 D, pp. 161-178, 1996.

[82] D. J. Cole, D. Cebon, and F. H. Besinger, "Optimisation of Passive and Semi-Active Heavy Vehicle Suspensions", *SAE Technical Paper Series*, (942309), 1994.

[83] D. J. Cole, "Fundamental Issues in Suspension Design for Heavy Road Vehicles", *Vehicle System Dynamics*, vol. 35, pp. 319-360, 2001.

[84] E. M. ElBeheiry and D. C. Karnopp, "Optimal Control of Vehicle Random Vibration with Constrained Suspension Deflection", *Journal of Sound and Vibration*, vol. 189, pp. 547-564, 1996.

[85] S.-B. Choi, H.-S. Lee, and Y.-P. Park, "H infinity Control Performance of a Full-Vehicle Suspension Featuring Magnetorheological Dampers", *Vehicle System Dynamics*, vol. 38, pp. 341-360, 2002.

[86] A. Halfpenny, "A Practical Discussion on Fatigue", *nCode International Ltd.*, 2003.

[87] J. A. Bannantine, J. J. Comer, and J. L. Handrock, "Fundamentals of Metal Fatigue Analysis", *Prentice Hall*, New Jersey, 1990.

[88] S. D. Downing and D. F. Socie, "Simple Rainflow Counting Algorithms", *International Journal of Fatigue*, pp. 31-40, 1982.

[89] A. Halfpenny, "A Frequency Domain Approach for Fatigue Life Estimation from Finite Element Analysis" *International Conference on Damage Assessment of Structures*, Dublin, 1999.

[90] R. I. Stephens, A. Fatemi, R. R. Stephens, and H. O. Fuchs, "Metal Fatigue in Engineering", 2nd ed., *John Wiley and Sons Inc.*, New York, 2001.

[91] L. Huang, H. Agrawal, and P. Kurudiyara, "Dynamic Durability Analysis of

Automotive Structures", *SAE Technical Paper Series*, (980695), 1998.

[92] S. B. Lee, W. S. Han, and H. J. Yim, "Fatigue Analysis of Automotive Suspension System Considering Dynamic Effect", *SAE Technical Paper*, (2003-01-2814), 2003.

[93] G. S. Choi, H. K. Min, and S. H. Paik, "Dynamic Stress Analysis of Vehicle Using Virtual Proving Ground Approach", *SAE Technical Paper Series*, (2000-01-0121), 2000.

[94] M. Haiba, D. C. Barton, P. C. Brooks, and M. C. Levesley, "Review of Life Assessment Techniques Applied to Dynamically Loaded Automotive Components", *Computers and Structures*, vol. 80, pp. 481-494, 2002.

[95] E. Y. Kuo and S. G. Kelkar, "Vehicle Body Structure Durability Analysis", *SAE Technical Paper Series*, (951096), pp. 135-150, 1995.

[96] S. Vellaichamy, "Transient Dynamic Fatigue Analysis of Automotive Structures using Proving Ground Road Profiles", *SAE Technical Paper Series*, (2005-01-0514), 2005.

[97] J. S. Bendat, "Probability Functions for Random Responses", *NASA Report*, on contract NAS-5-4590, 1964.

[98] T. Dirlik, "Application of Computers to Fatigue Analysis", PhD thesis, *University of Warwick*, UK, 1985.

[99] R. Ramli, M. C. Levesley, and D. A. Crolla, "Simulation and Evaluation of Passive and Semi-Active Suspension of Quarter and Full Vehicle Ride Models", *NAFEMS World Congress 2005 - Engineering Simulation: Best Practices and Visions of the Future*, St. Julians, Malta, 2005.

[100] M. C. Levesley, "Simulink Tutorials", *School of Mechanical Engineering*, University of Leeds, UK, 2002.

[101] "MSC Visual Nastran Desktop - User Guide", *The MSC.Software Corporation*, 2003.

[102] "MATLAB/SIMULINK - User Guides", 6.0 ed., *The Mathworks, Inc.*, Natick,

2002.

[103] R. Hudson, "Computer Simulation of Suspension Systems", MSc Dissertation, *School of Mechanical Engineering*, University of Leeds, Leeds, UK, 2002.

[104] J. B. Dabney and T. L. Harman, "Mastering Simulink 4", *Prentice-Hall*, New Jersey, 2001.

[105] K. M. Captain, A. B. Boghani, and D. N. Wormley, "Analytical Tire Models for Dynamic Vehicle Simulation", *Vehicle System Dynamics*, vol. 8, pp. 1-32, 1979.

[106] J. Sui and J. Hirshey, "Evaluation on Analytical Tire Models for Vertical Vibration Simulation Using Virtual Tire Testing Method", *SAE Technical Paper Series*, (1999-01-0786), 1999.

[107] R. J. Hanley, "Tyre Modelling for Misuse Situations", PhD thesis, *School of Mechanical Engineering*, University of Leeds, UK, 2002.

[108] R. Ramli, M. Pownall, M. C. Levesley, and D. A. Crolla, "Dynamic Analysis of Semi-active Suspension Systems Using a Co-simulation Approach", *3rd International Symposium on Multi-body Dynamics: Monitoring and Simulation Techniques*, Loughborough, UK, 2004.

[109] H. Rahnejat, "Multi-Body Dynamics: Vehicles, Machines and Mechanisms", *Professional Engineering Publishing Limited*, London, 1998.

[110] D. J. Inman, "Engineering Vibration", 2nd ed., *Prentice Hall*, New Jersey, 2001.

[111] M. C. Levesley, R. Ramli, N. Stembridge, and D. A. Crolla, "Multi-body Co-simulation of Semi-active Suspension Systems", *Proc. Instn. Mech. Engrs., Part K: J. Multi-body Dynamics*, vol. 220, Number 1/2007, pp. 99-115, 2007.

[112] J.-H. Koo, F. D. Gonclaves, and M. Ahmadian, "A Comprehensive Analysis of the Response Time of MR Dampers", *Journal of Smart Materials and Structures*, vol. 15, pp. 351-358, 2006.

[113] N. D. Sims, N. J. Holmes, and R. Stanway, "A Unified Modelling and Model

Updating Procedure for Electrorheological and Magnetorheological Vibration Dampers", *Smart Materials and Structures*, vol. 13, pp. 100-121, 2004.

[114] N. Stembridge, M. C. Levesley, D. Crolla, N. Sims, and M. Burnett, "Real-Time Control of a Magnetorheological Damper for Vehicle Suspension Systems", *The 8th International Symposium on Advanced Vehicle Control*, Taipei, Taiwan, 2006.

[115] D. J. Peel and W. A. Bullough, "Prediction of Electro-Rheological Valve Performance in Steady Flow", *Proc. Instn of Mech. Engrs*, vol. 208, pp. 253-266, 1994.

[116] "The Schlumberger Oilfield Glossary", http://www.glossary.oilfield.slb.com/, *Schlumberger Limited*, 1998.

[117] S. John and N. M. Wereley, "Nondimensional Quasi-Steady Analysis of Magnetorheological Dampers Utilizing a Herschel Bulkley Model with Preyield Viscosity", *Smart Structures and Materials 2003: Damping and Isolation, Proceeding of SPIE*, vol. 5052, pp. 53-65, 2003.

[118] N. Sims, R. Stanway, D. Peel, W. Bullough, and A. Johnson, "Controllable Viscous Damping: An Experimental Study of an Electrorheological Long-Stroke Damper Under Proportional Feedback Control", *Smart Materials and Structures*, vol. 8, pp. 601-615, 1999.

[119] P. Barak, "Magic Numbers in Design of Suspensions for Passenger Cars", *SAE Technical Paper Series*, (911921), pp. 53-74, 1991.

[120] "ANSYS Online User Manual", *ANSYS, Inc.*, 2003.

[121] M. Matsuishi and T. Endo, "Fatigue of Metals Subjected to Varying Stress", Japan Society of Mechanical Engineers, Fukuoka, Japan, 1968.

[122] "Rainflow with ICE-flow 3.0", Technical Notes, *nCode International*, 2005.

APPENDIXES

APPENDIX I

Lists of Journal Publication, Symposium and Conferences

1) M. C. Levesley, R. Ramli, N. Stembridge, and D. A. Crolla, "Multi-body Cosimulation of Semi-active Suspension Systems," *Proc. Instn. Mech. Engrs., Part K: J. Multi-body Dynamics*, vol. 221, Number 1/2007, pp. 99-115, 2007.

Abstract:

This paper describes the development and use of a multi-body cosimulation approach for predicting the dynamic response of a vehicle containing magnetorheological (MR) semi-active dampers. The approach is used to investigate the effects of various local and global control strategies on the load histories of suspension components for the purpose of assessing their likely impact on fatigue life. The approach adopted aims to exploit the capability of a multi-body system (MBS) code and a mathematical simulation code, by integrating the MBS vehicle models with selected semi-active damper/controller models. Various MBS vehicle models are developed of increasing complexity using MSC.visualNastran, which are linked to three local, two-state switchable (TSS), control algorithms and also two global controllers, each developed in MATLAB/Simulink. The control strategies are implemented within the vehicle model using an MR damper model derived from experimental test data. Road inputs including both bump/pothole and random road excitation, and the tyre model are also implemented within MATLAB/Simulink. Ultimately, the aim is to develop an approach which would allow concurrent structural optimisation and controller optimisation to enable lighter and more durable suspension components to be produced.

Keywords:

Cosimulation, multi-body system, semi-active control systems, magnetorheological damper, service loads, load histories, pitch and roll control, two-state switchable

Multi-body co-simulation of semi-active suspension systems

M C Levesley,* R Ramli, N Stembridge, and D A Crolla
School of Mechanical Engineering, University of Leeds, Leeds, UK

The manuscript was received on 20 March 2006 and was accepted after revision for publication on 25 July 2006.

DOI: 10.1243/14644419JMBD69

Abstract: This paper describes the development and use of a multi-body co-simulation approach for predicting the dynamic response of a vehicle containing magnetorheological (MR) semi-active dampers. The approach is used to investigate the effects of various local and global control strategies on the load histories of suspension components for the purpose of assessing their likely impact on fatigue life. The approach adopted aims to exploit the capability of a multi-body system (MBS) code and a mathematical simulation code, by integrating the MBS vehicle models with selected semi-active damper/controller models. Various MBS vehicle models are developed of increasing complexity using MSC.visualNastran, which are linked to three local, two-state switchable, control algorithms and also two global controllers, each developed in MATLAB/Simulink. The control strategies are implemented within the vehicle model using an MR damper model derived from experimental test data. Road inputs, including both bump/pothole and random road excitation, and the tyre model are also implemented within MATLAB/Simulink. Ultimately, the aim is to develop an approach which would allow concurrent structural optimization and controller optimization to enable lighter and more durable suspension components to be produced.

Keywords: co-simulation, multi-body system, semi-active control systems, magnetorheological damper, service loads, load histories, pitch and roll control, two-state switchable

1 INTRODUCTION

With increasing sophistication and performance of modern software and hardware capabilities, virtual prototyping is rapidly becoming a realistic alternative to physical prototyping. Much interest is currently focused on developing virtual prototyping to allow optimization of automotive components for extended fatigue life while at the same time reducing weight. A key prerequisite of the optimization process is to obtain accurate load histories for the component to be optimized. Ideally, this should be done as early in the design process as possible, preferably before even a rolling chassis prototype is available. In this case, simulation must be relied upon to obtain these load histories. Previous works [1] and [2] have demonstrated that predicting the service load histories of a suspension component from a vehicle with a passive damper using a purely multi-body system (MBS) method is now feasible. The current MBS software allows complex nonlinear passive damper models to be integrated into the suspension model. Semi-active systems, which have been shown to closely match the performance of the more costly and complex active systems [3], can also be integrated within the MBS simulation environment. Of particular interest in the area of semi-active systems are magnetorheological (MR) dampers, which have received increasing attention as a cost effective and reliable semi-active damping device for vehicle suspension applications. Altering the viscosity of MR fluids is achieved by passing a control current through the fluid, essentially changing the damping characteristics of the device. Conventional passive damping is generally a function of the relative velocity across the damper. Skyhook damping, used extensively by a number of

*Corresponding author: Department of Mechanical Engineering, University of Leeds, Leeds LS2 9JT, UK. email: m.c.levesley@leeds.ac.uk

researchers including Sammier *et al.* [4], is a function of the absolute velocity of the sprung mass. This strategy was originally proposed for a single-degree-of-freedom (SDOF) system [5] and excellent isolation of the sprung mass from the road input was observed, at the expense of an increase in the unsprung mass vibration amplitude. Other semi-active control strategies have been identified by Karnopp [5] in the form of a two state switching strategy, and by Cebon *et al.* [6], in the form of modified skyhook damping, which uses a combination of passive and skyhook damping forces to minimize both body acceleration and tyre load fluctuations. Linear optimal control methods for semi-active systems have also been proposed [7], but such control strategies are far more complex and solving such systems within the current MBS software configuration would generate much more computational overheads. It is observed that the MR damper has highly non-linear characteristics, which are found to be control current dependant. Controlling the MR damper to give a desired response can be achieved by applying a force feedback control method, as done by Sims *et al.* [8]. It was demonstrated that the MR damper could be suitably controlled to give a viscous damping force.

The introduction of semi-active damping presents new challenges for the development of automated optimization, because both the algorithms used to adjust the level of damping and the damper itself could potentially cause sudden rapid changes in suspension component loads, thus affecting fatigue life. In addition, these semi-active devices are likely to be linked to a global chassis controller, which again should be included if accurate load histories for a full vehicle are to be simulated. Much controller development for automotive suspension components is currently done within mathematical simulation packages and not within an MBS environment. Currently, research at Leeds is aimed at examining the effect of the suspension component load histories when semi-active control is implemented. In doing so, an alternative approach is introduced, MBS co-simulation, that allows semi-active control models developed in a mathematical program to link to the vehicle models in an MBS code.

A comparable passive suspension system is used as a reference to analyse the performance of the semi-active system. The feasibility of using an MBS co-simulation approach to determine the durability of various suspension components is demonstrated. It provides great flexibility through its modular approach and similar motion accuracies when compared with other methods, but at the expense of increased simulation time. The semi-active damper control strategies, two-state switchable damping coefficient switching (TSS1), and damper force switching (TSS2) demonstrate a reduction not only in the body acceleration but also in the load histories of the suspension component. In contrast, semi-active damper control with current switching (TSS3) produces better body acceleration reduction than TSS1 and TSS2, but exhibits higher acceleration histories at the suspension arm. For the full vehicle model (FVM) application, the beneifits of incorporating pitch and roll control for a two-state switchable semi-active damper on a relatively smooth road surface appear to be insignificant.

2 MBS CO-SIMULATION

MBS simulation has long been recognized as an excellent tool to predict dynamic response of vehicles [1, 2, 9, 10]. The accuracy of the simulation results relies on the accuracy of the representative model as compared to the physical system, in terms of geometrical properties, material properties as well as the interfaces with other components. One of the key advantages of the MBS approach is that it allows non-linear elements such as bump stop and suspension bushings to be modelled readily.

The introduction of semi-active suspension components that require extensive use of mathematical functions and control algorithms presents challenges for current software that use the MBS method and may restricted its use in these applications. Such restrictions may result in the unwanted simplification of models to suit the MBS software capability and, therefore, inaccurate results may be produced. MBS co-simulation offers an alternative approach where each subsystem is developed in a simulation environment that is most appropriate to it, without sacrificing overall accuracy.

On the basis of these conditions, the approach adopted here integrates the MBS software (MSC. visualNastran) used for modelling complex multi-body vehicle suspensions configurations, with MATLAB/Simulink used for the development of the semi-active controllers, tyre and road models, as shown in Fig. 1. MSC.visualNastran is a computer aided engineering tool for MBS analysis. It is capable of simulating motions, vibration, stress, and thermal analysis. Measured parameters in static, kinematic, and dynamic analysis include positions, velocities and accelerations, constraint force, length and torque, joints forces, and moments. The application of MBS in this study assumes all connecting components as rigid bodies.

Here, each program executes its respective simulation simultaneously, where at each time step, both codes update one another with new state values before advancing to the next step. Simulation

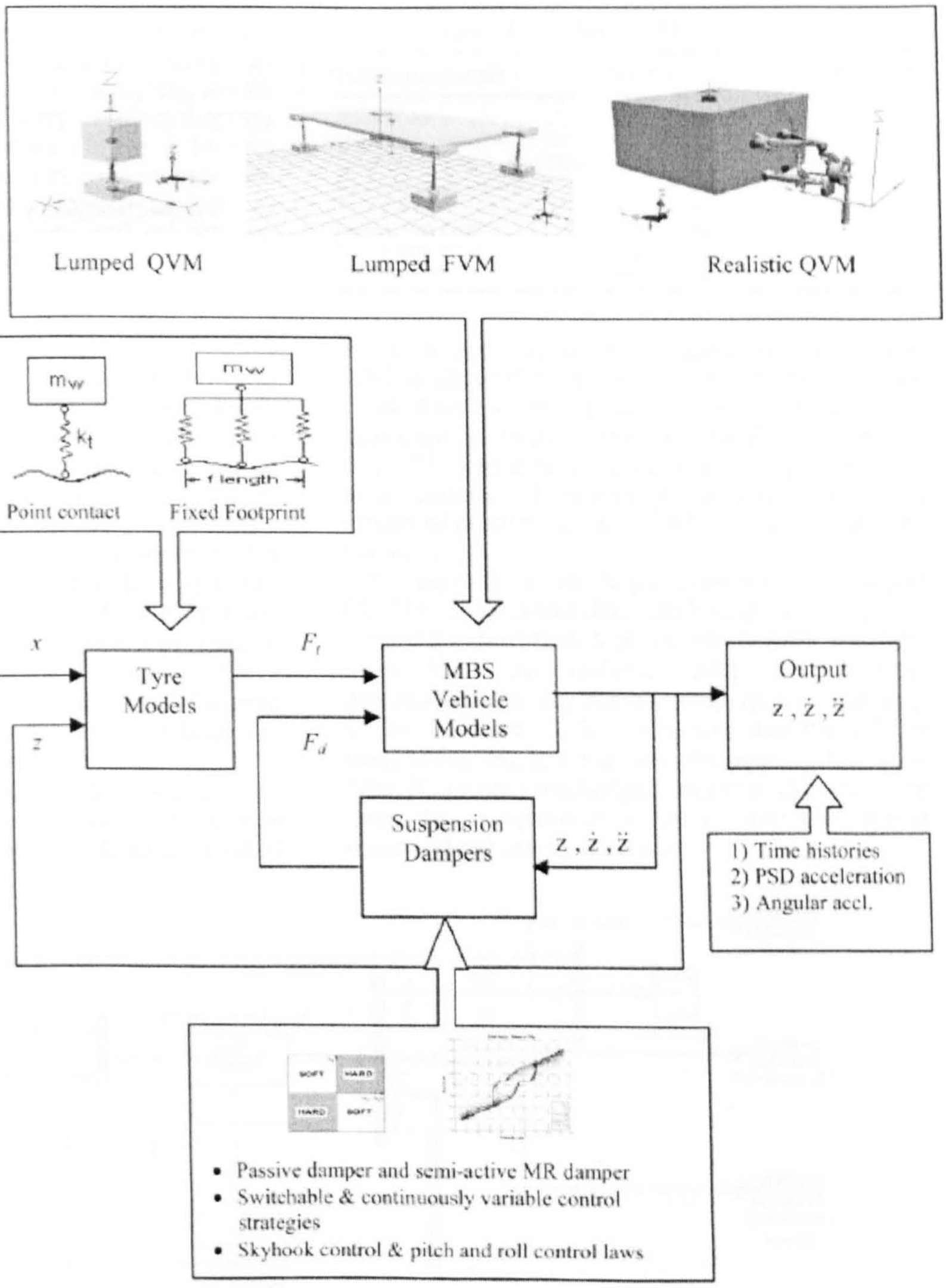

Fig. 1 MBS co-simulation modelling strategy

begins when MATLAB/Simulink computes the road displacement, x at t_0. The tyre subsystem calculates the tyre force, F_t, from both road and MBS vehicle model inputs. In the tyre subsystem, various mathematical tyre models can be created, although only two are shown in Fig. 1 for illustrations purposes.

The MBS vehicle model accepts force inputs from the tyre and suspension damper subsystems. These inputs are represented as linear force actuators in the MBS environment. Feedback input to MATLAB/Simulink for both subsystems is taken from the state output of the MBS vehicle model in the forms of displacements, relative velocities, and accelerations. Non-linear, passive damper, and semi-active damper models are generated in the suspension damper subsystem, whereas the linear suspension stiffness is modelled within the MBS vehicle model. This approach allows easy model substitution when

evaluating the performance of various suspension systems. The suspension damper subsystem produces the damper force, F_d by accepting inputs from the MBS vehicle model. A typical block diagram of the proposed method is shown in Fig. 2. Motion histories generated from the MBS co-simulation are used as key inputs to finite-element analysis to calculate the stress distributions and to estimate fatigue life of suspension components.

2.1 Vehicle models

The realistic quarter vehicle model (QVM) shown in Fig. 1, is developed by Haiba *et al.* [1]. The suspension components were first modelled using a CAD package. Then, the suspension model is exported to the MBS software, where appropriate mass, inertia properties, and joint constraints are assigned. The model consists of twelve degree-of-freedom, which have been formulated as outlined by Rahnejat [11]. Vehicle data for the realistic QVM (unladen) are given in Table 1. The realistic QVM is then used to obtain the equivalent vehicle parameters for a lumped mass QVM. The lumped mass QVM is used in this study to validate both MBS and MBS co-simulation modelling approaches.

A lumped mass FVM is also built to evaluate the holistic effect of various semi-active controllers to the suspension components as well as their effect on pitch and roll in the dynamic response. The FVM is allowed to move in the vertical direction at all four corners of the unsprung mass but is restrained in both lateral and longitudinal directions. The constraint put on the sprung mass permits translational motion in the vertical axis and rotational motions around the lateral and longitudinal axes.

Table 1 Realistic QVM vehicle data

Vehicle parameters	Symbol	Units	Two-DOF/QVM
Body mass	M_b	kg	535
Front hub mass	M_h	kg	38.75
Suspension torsional stiffness	K_{tor}	N m/deg	46.74
Suspension damping	C	Ns/m	3800
Tyre stiffness	K_t	N/m	239 000
Upper arm mass	M_{ua}	kg	2
Lower arm mass	M_{la}	kg	5
Tie rod mass	M_{tr}	kg	2

The equivalent vehicle parameters of the lumped QVM in Table 2 were obtained by logarithmic decrement [12] calculation, δ, of the vehicle body displacement from the realistic QVM. The method determines the equivalent suspension damping, C, and stiffness, K_s. It is assumed that the vehicle body mass, M_b, and the one-dimensional tyre stiffness, K_t, remain unchanged, whereas the unsprung mass, M_w, is equivalent to the combination of hub mass and the linkages masses.

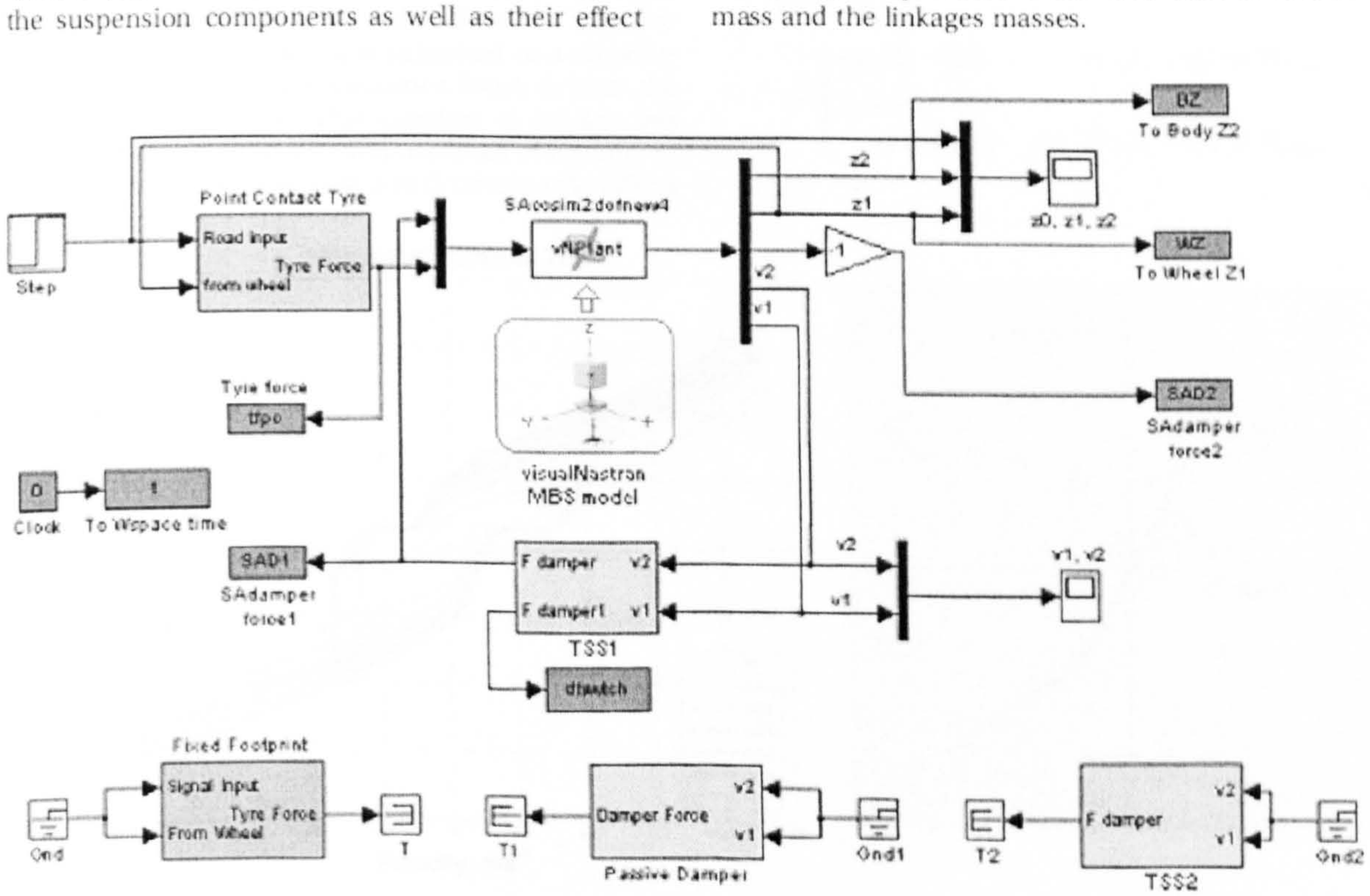

Fig. 2 Example of MBS co-simulation of MATLAB/Simulink and MSC.visualNastran

Table 2 Lumped QVM vehicle data

Vehicle parameters	Symbol	Units	Two-DOF QVM
Effective sprung mass	M_b	kg	535
Unsprung mass	M_w	kg	47.75
Suspension stiffness	K_s	N/m	31 000
Suspension damping	C	Ns/m	1500
Tyre stiffness	K_t	N/m	239 000

The vehicle dynamic characteristics are calculated [13], based on the lumped parameter data. The vehicle body resonance occurs at 1.14 Hz and the wheel hop frequency occurs at 12 Hz. The ride rate, K_{eq}, and the damping ratio, ζ, are determined as 27.4 kN/m and 0.2, respectively. The lumped mass QVM and realistic QVM have been validated for various simulation configurations using MATLAB/Simulink alone, MBS alone, and MBS co-simulation, results of which are outlined in section 4.3 and section 4.4.

2.2 Tyre models

From a study by Ramli *et al.* [14], a number of tyre models were developed as subsystems within the MATLAB/Simulink environment. The work presented here concentrates on the point contact tyre model to study the dynamic response of several vehicle models equipped with different suspension systems. This simple tyre model allows the wheel to leave the ground when it is subjected to a negative force, by introducing a saturation block to limit the minimum tyre force. This simplest of models has been chosen due to its computational efficiency, as the main focus of this work is to determine the effects of various semi-active suspension configurations on load histories.

2.3 Damper models

The force characteristics of an MR damper can be varied considerably with the application of a suitable control current, as shown in the experimental force velocity data for a Carrera Magneshock™ MR damper in Fig. 3(a). It can be seen that a zero control current has similar characteristics to a standard passive damper. As a control current is applied, the characteristics change dramatically. Peel and Bullough [15] have shown that this current dependant flow can be approximated by a Bingham plastic flow, which has a finite yield force at zero velocity. The discontinuous nature of the Bingham flow model makes control difficult and is therefore unsuitable for vehicle applications. The bi-viscous model is a further development of the Bingham model, and was introduced by John and Wereley [16] and further developed by Sims *et al.* [17]. Unlike the Bingham model, the bi-viscous model assumes there is preyield flow. This quasi-steady representation of the MR fluid flow is shown in Fig. 3(b) and is described by the following equation

$$c(\dot{z}_1 - \dot{z}_2, I) = \begin{cases} c_{pre}(\dot{z}_1 - \dot{z}_2) & \text{if } (\dot{z}_1 - \dot{z}_2) \leqslant F_y c_{pre} \\ c_{post}(\dot{z}_1 - \dot{z}_2) & \\ \quad + F_y \text{sgn}(\dot{z}_1 - \dot{z}_2) & \text{if } (\dot{z}_1 - \dot{z}_2) \geqslant F_y c_{pre} \end{cases} \quad (1)$$

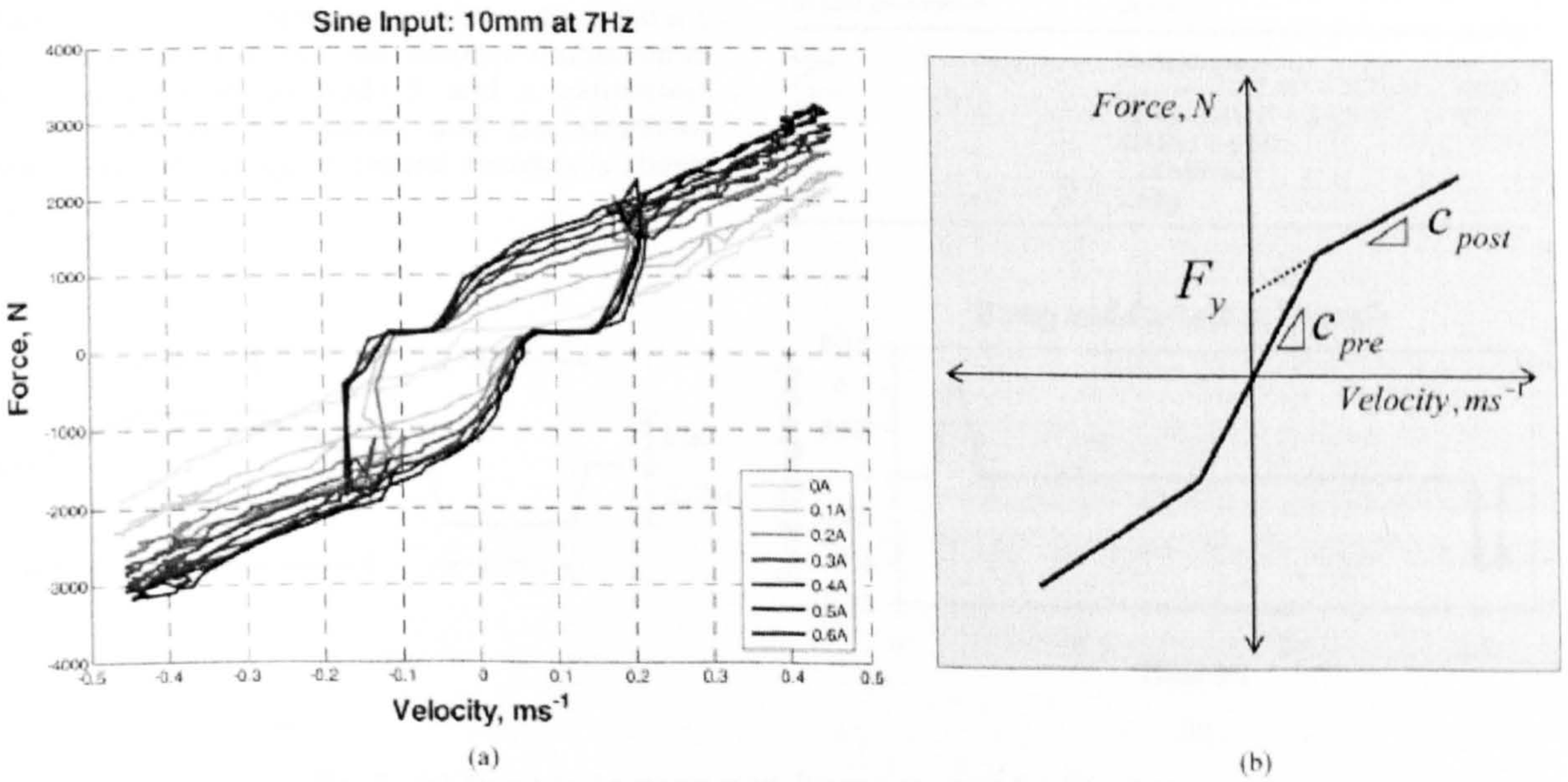

Fig. 3 (a) MR damper experimental characteristics and (b) MR fluid flow characterization

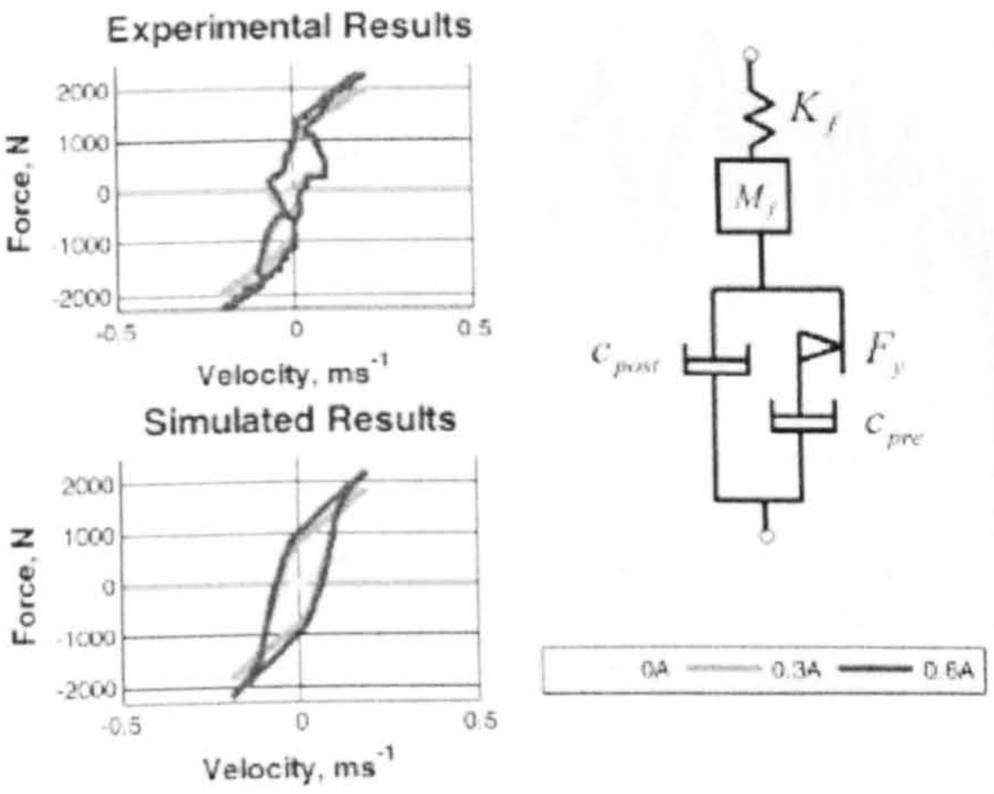

Fig. 4 Mechanical analogy of MR damper model with experimental and simulated results

where c_{pre} is the preyield damping, c_{post} the post yield damping, and F_y the yield force. The dynamic characteristics of the damper, resulting from the fluid compressibility and inertia, must also be considered. By representing the fluid inertia by a mass and the compressibility of the fluid by a spring, the dynamic characteristics of the damper can be predicted, as demonstrated by Sims *et al.* [8]. A mechanical analogy of this model is shown in Fig. 4. The parameters F_y, K_f, c_{post}, and c_{pre} have been derived from experimental data and M_f is estimated from knowledge of the volume and density of the MR fluid within the damper. It was found that both F_y and c_{post} are control current dependant, whereas the remaining values are constant. The values used in the MR damper model simulations are shown in Table 3, and a comparison of the experimental results and the simulated results over the range of control currents is shown in Fig. 4.

2.4 Road models

Two types of road inputs are used in this paper. A bump and pothole input is used to evaluate transient vertical events with intention of validating vehicle models, simulation methods, and semi-active models. The transient road input in Fig. 5 combines a bump profile from Blundell and Harty [18] and pothole from Sui and Hirschey [19]. Once, acceptable criteria have been achieved, a random road input is used to excite the various models. In this paper, all vehicle models are subjected to traversing the virtual random road surface at a constant velocity of 34 km/h. The power spectral density (PSD) of this random road input is shown in Fig. 6.

3 SEMI-ACTIVE CONTROL MODELS

3.1 Two-state switchable

The TSS semi-active control strategy used in this work was first proposed by Karnopp *et al.* [5]. In terms of the lumped two-DOF QVM in Fig. 7, the semi-active control strategy is given by

$$\begin{aligned} &\text{if } \dot{z}_2(\dot{z}_2 - \dot{z}_1) > 0; \quad \text{switching parameter} = C_{\text{hard}} \\ &\text{else} \qquad\qquad\quad ; \quad \text{switching parameter} = C_{\text{soft}} \end{aligned} \tag{2}$$

The TSS system in Equation (1), uses an on/off control logic to select between two discrete damper settings

Table 3 MR damper model parameters

MR damper model parameter	Value
C_{pre}	55.76 kNsm^{-1}
C_{post}	$C_{post} = -5257.3I^2 + 7671.5I + 3203.3$
F_y	$F_y = -13417I^4 + 25233I^3 - 17787I^2 + 6145.8I + 1.33$
K_f	1.29 MN/m
M_f	1.5 kg

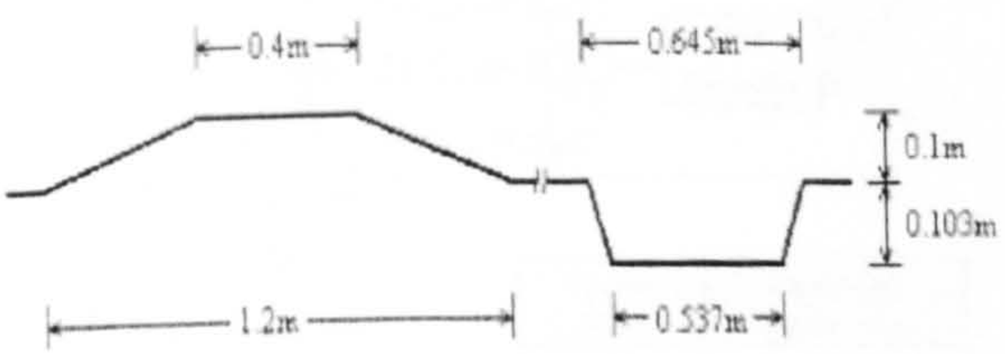

(a)

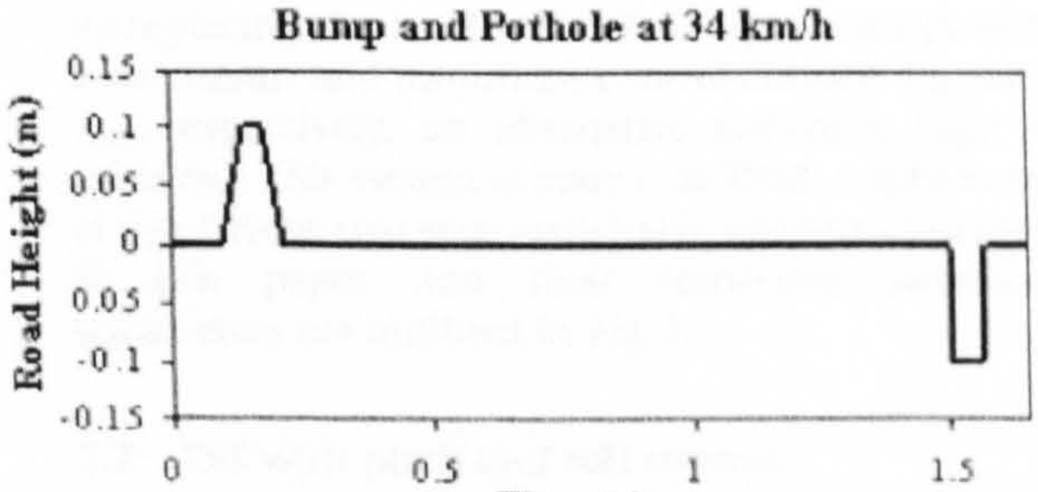

(b)

Fig. 5 (a) Bump and pothole road dimensions and (b) time history

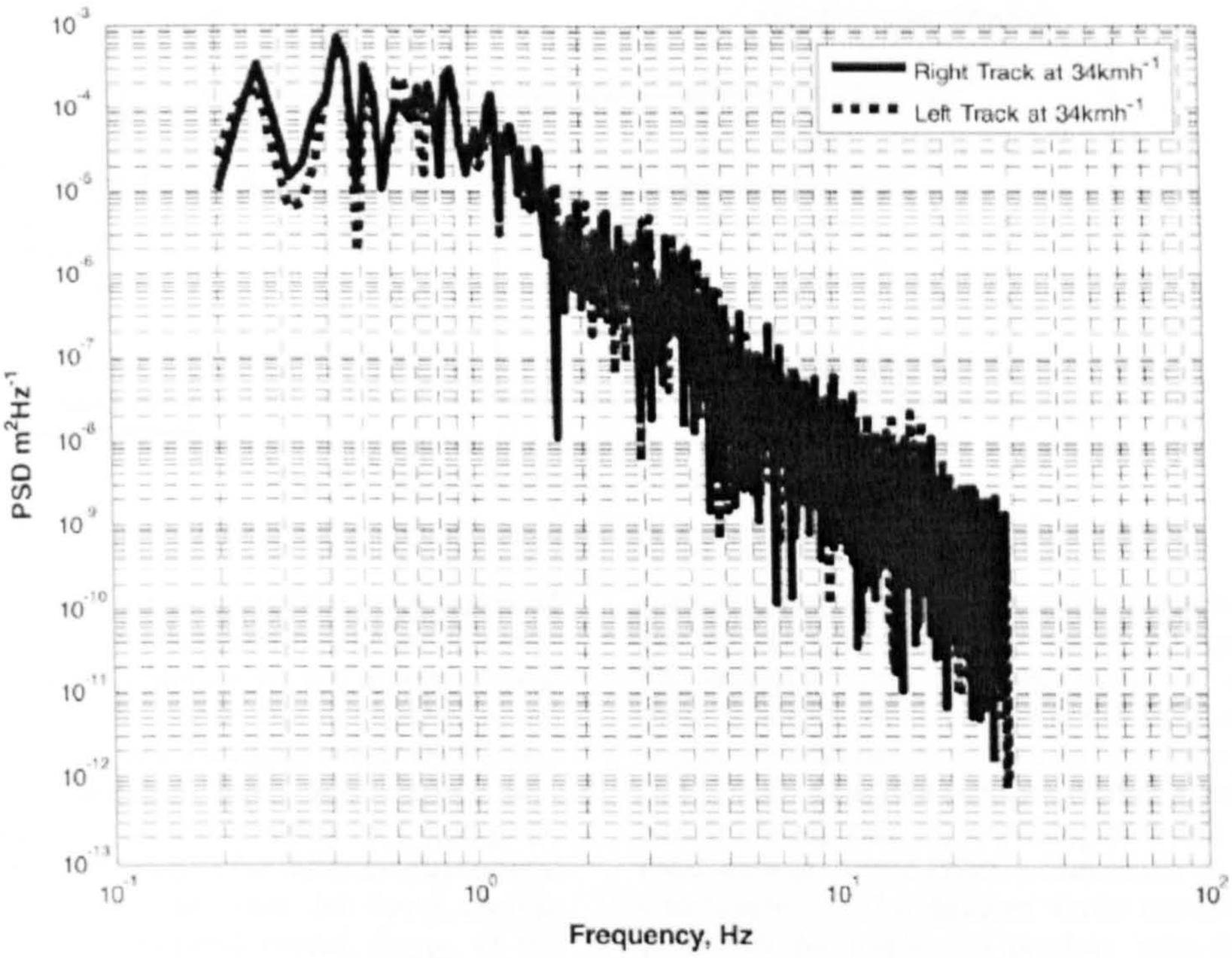

Fig. 6 Random road input at 34 km/h

C_{hard} and C_{soft}, both linear damping coefficients. Throughout the remainder of this paper, this system is referred to as TSS1. The response of the MR damper to an applied control current is highly nonlinear, as shown in Fig. 3(a). This makes accurate control of the device more difficult. Sims *et al.* [8] developed a feedback linearization control method whereby the response of the damper can be shaped in an attempt to produce a linear viscous response. The control scheme is shown in Fig. 8, where the controller gains have been optimized with values, $B = 0.8$ and $G = 0.001$. The gain D_{hard} is the hard linear damping coefficient, providing the viscous force which the MR damper emulates. To apply Karnopp's switching control strategy to the MR damper, two different approaches can be adopted. First, by shaping the response of the MR damper to give a linear damping force, suitable control logic is developed to emulate the general case given in equation (2). In this case, the damping coefficients C_{hard} and C_{soft} are replaced by D_{hard} and D_0, respectively, where D_{hard} is the hard viscous damping coefficient and D_0 is the soft viscous damping coefficient of the MR damper, which is achieved when a 0A control current is applied. This system is referred to as TSS2. Second, by replacing the hard and soft damper settings with a maximum and minimum control current, I_{max} and I_{min} respectively, an alternative switching logic is achieved. This system is known as TSS3. A schematic of the various two state switchable systems examined in this paper and their respective switching parameters are outlined in Fig. 7.

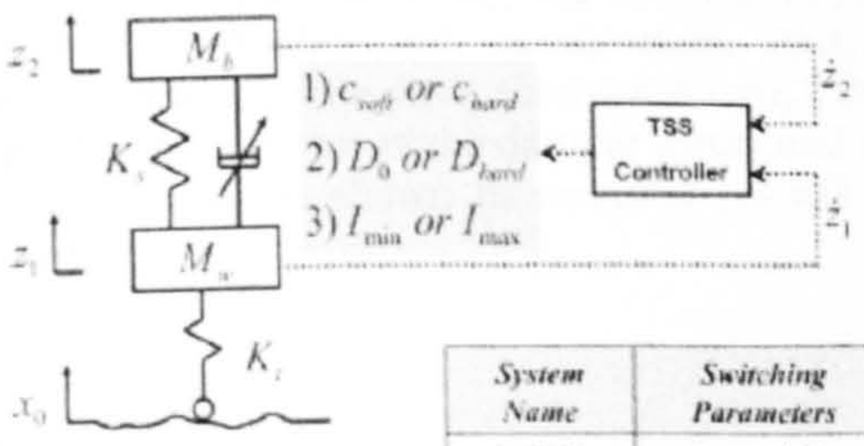

System Name	*Switching Parameters*
1) TSS1	C_{hard} and C_{soft}
2) TSS2	D_0 and D_{hard}
3) TSS3	I_{min} and I_{max}

Fig. 7 TSS system schematic and switching parameters

3.2 TSS with pitch and roll control

The controller model adopted from Nell and Steyn [20] intends to improve ride performance for an off-road vehicle. It was based on (body bounce, pitch, and roll

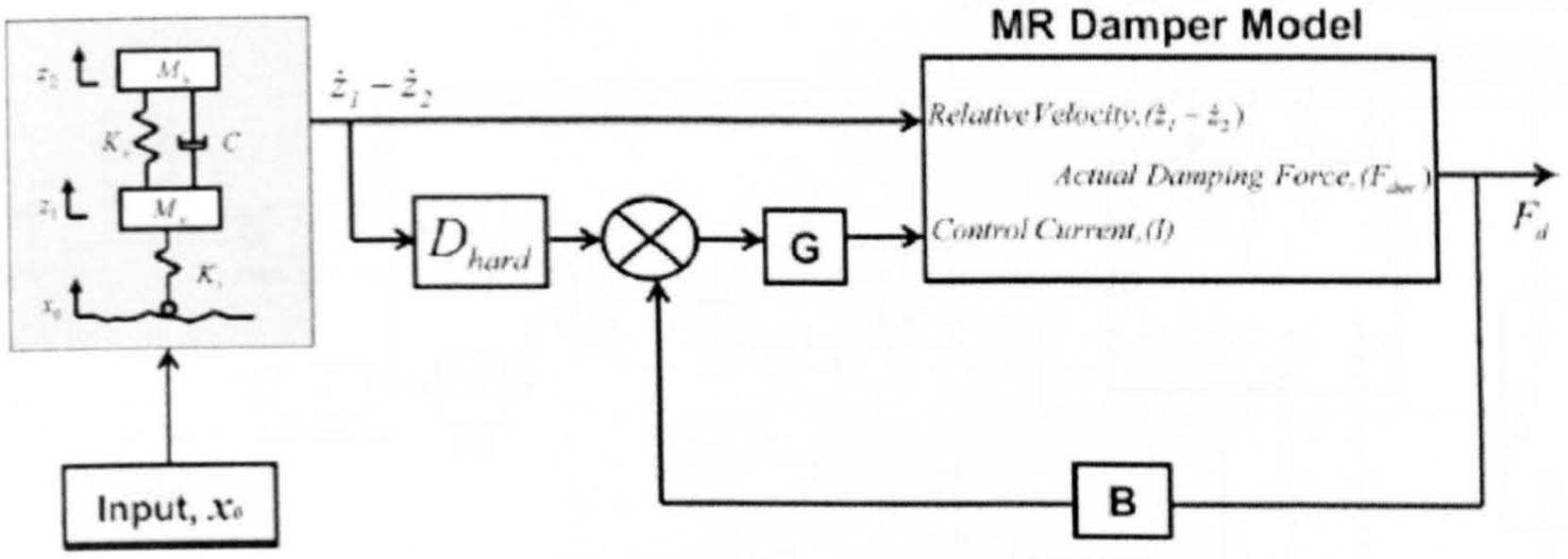

Fig. 8 Feedback control of MR damper model

motions with respect to the axes of the body centre of gravity) that chooses the minimum product of acceleration as a selection criterion for the damper states at each corner. In this paper, the controller model has been modified to suit a lumped seven-DOF FVM. It compares the absolute pitch acceleration, $|\ddot{\Theta}_x|$ against the absolute roll acceleration, $|\ddot{\Theta}_y|$. The pitch acceleration, $\ddot{\Theta}_x$, is defined as the difference of vertical accelerations between the front left-hand corner, $\ddot{z}_{F\_LHS}$ and the rear left-hand corner, $\ddot{z}_{R\_LHS}$ of the vehicle divided by α, as shown in equation (3). In a similar manner, the roll acceleration $\ddot{\Theta}_y$ can be determined by taking the difference of the vertical acceleration between the front left corner, $\ddot{z}_{F\_LHS}$ and the front right corner, $\ddot{z}_{F\_RHS}$ of the vehicle dividing the difference with the width, β, as shown in equation (4)

$$\ddot{\Theta}_x = \frac{\ddot{z}_{F\_LHS} - \ddot{z}_{R\_LHS}}{\alpha} \tag{3}$$

$$\ddot{\Theta}_y = \frac{\ddot{z}_{F\_LHS} - \ddot{z}_{F\_RHS}}{\beta} \tag{4}$$

In equation (5), if the absolute pitch acceleration, $|\ddot{\Theta}_x|$, is greater than, $|\ddot{\Theta}_y|$, then the product of the summation of the damper forces and the pitch acceleration as in equation (6), will be used. In contrast, if the absolute roll acceleration, $|\ddot{\Theta}_y|$, is larger than the absolute pitch acceleration, $|\ddot{\Theta}_x|$, than the product of the sum of the damper forces and the roll acceleration, as shown in equation (7) will be selected.

If

$$|\ddot{\Theta}_x| > |\ddot{\Theta}_y| \tag{5}$$

then

$$(d_{F\_LHS} + d_{F\_RHS} - d_{R\_LHS} - d_{R\_RHS})_{t=1:16} \times \ddot{\Theta}_x \tag{6}$$

else

$$(d_{F\_LHS} + d_{R\_LHS} - d_{F\_RHS} - d_{R\_RHS})_{t=1:16} \times \ddot{\Theta}_y \tag{7}$$

Each of the damper force in either equation (6) or (7) has two discrete settings, a soft and a hard settings. The damper forces are determined by multiplying these damping constant with the relative velocities across the damper, as shown in equations (8) to (11). As there are four damper forces (one at each corner), which are capable of switching between soft or the hard settings, there exists a maximum of 16 damper combinations. The damper force combination that produces the minimum product with the pitch or roll acceleration will be used as the output force to the linear actuators. For example, the first combination is when all soft damping settings are selected and the last combination is when all hard settings are chosen. With the use of logic operators, all 16 combinations will be checked. The configuration that gives the minimum product of damper forces with the pitch or roll acceleration will be selected and the corresponding damper forces will be used as output to each corner of the MBS vehicle model. This process will be calculated at each time step as defined by the MBS co-simulation.

$$d_{F\_LHS} = C_{soft/hard} \cdot \dot{z}_{rel\ F\_LHS} \tag{8}$$

$$d_{F\_RHS} = C_{soft/hard} \cdot \dot{z}_{rel\ F\_RHS} \tag{9}$$

$$d_{R\_LHS} = C_{soft/hard} \cdot \dot{z}_{rel\ R\_LHS} \tag{10}$$

$$d_{R\_RHS} = C_{soft/hard} \cdot \dot{z}_{rel\ R\_RHS} \tag{11}$$

This TSS with pitch and roll control algorithm is developed in the MATLAB/Simulink environment using block diagram method, as shown in Fig. 9. It requires body acceleration output from the MBS vehicle suspension model at each corners of the vehicle to calculate pitch and roll accelerations. Concurrently, the relative velocities between the body and the corresponding unsprung mass are used to compute damper forces. The damper combination that gives minimum product of pitch or roll acceleration (Fig. 10) will be fed back to the MBS vehicle model via a linear force actuator.

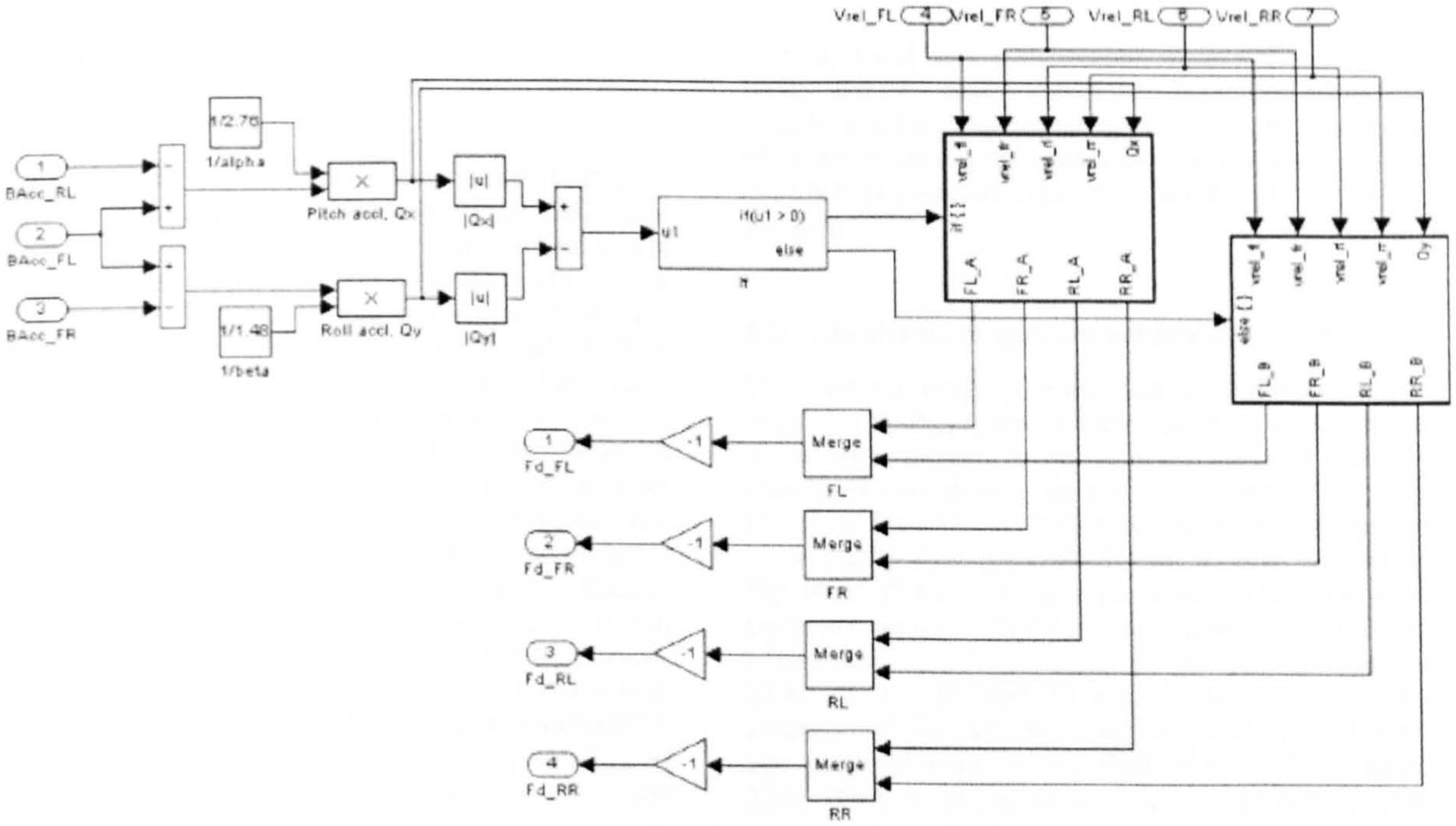

Fig. 9 TSS with pitch and roll controller model

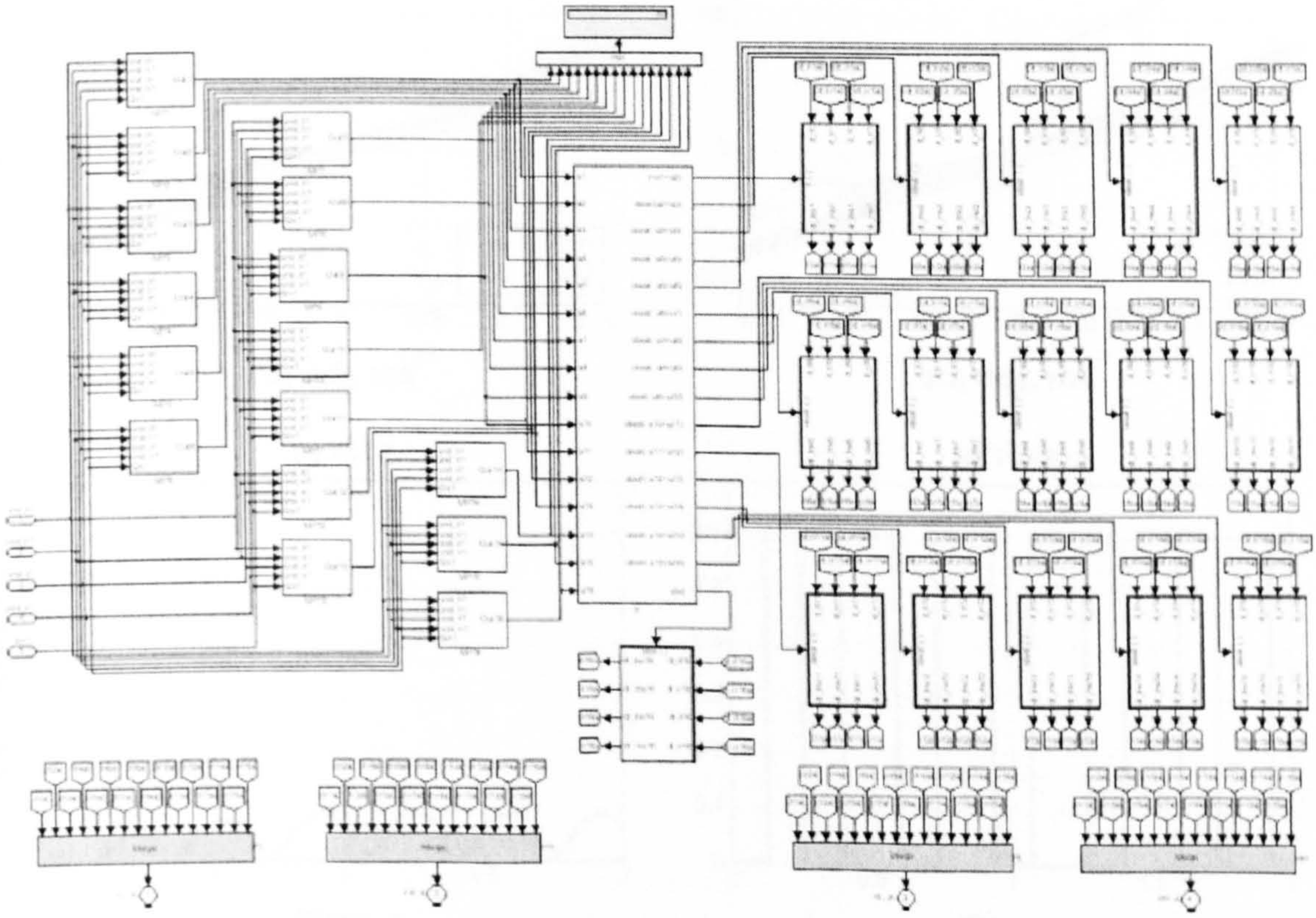

Fig. 10 Simulink block diagram for the 16 damper force combinations

4 SIMULATION RESULTS

4.1 MR damper force control

Figures 11 and 12 show the force velocity characteristics for the various TSS systems, TSS1, TSS2, and TSS3. The input is a sinusoidal displacement signal with a 10 mm amplitude at 1.5 Hz (Fig. 11) and at 5 Hz (Fig. 12). The control current is also shown for the two MR controlled systems, TSS2 and TSS3 at 1.5 Hz, Figs 11(c) and (d) and at 5 Hz, Figs 12(c) and (d), respectively. It can be seen from the results of TSS2 in Fig. 11(a) that by applying the feedback control loop, the force velocity characteristics match those of TSS1 very closely. However, the results of TSS3 in Fig. 11(b) show much higher forces are achieved at low velocities. Similar results for a 5 Hz input are shown in Fig. 12. It can be seen that by increasing the excitation amplitude, both force velocity characteristics and control current of TSS3 resembles the TSS2 characteristics much closer. In general, using both I_{min} and I_{max} as the switching parameters, as done for the TSS3 system, yield less predictable results than for the TSS2 system and, therefore, less desirable for vehicle control applications. The effects that both of these control strategies have on the response of the QVM is presented and discussed in the following section.

4.2 Results from quarter vehicle response

The vertical body acceleration and damper force response of the lumped mass QVM to a sinusoidal input with 10 mm amplitude for each of the TSS strategies are shown in Fig. 13(a) for 1.5 Hz and Fig. 13(b) for 5 Hz. A similar quarter vehicle response to a bump and pothole input is also shown in Fig. 14(a). The root mean square values of the vertical body acceleration, RMS_{ACC}, are shown in Fig. 14(b), where the input is the random surface traversed at 34 km/h, as defined in Fig. 6. As expected, the response of the vehicle using the TSS2 control strategy matches very closely that of the vehicle using TSS1. This is observed at both input frequencies,

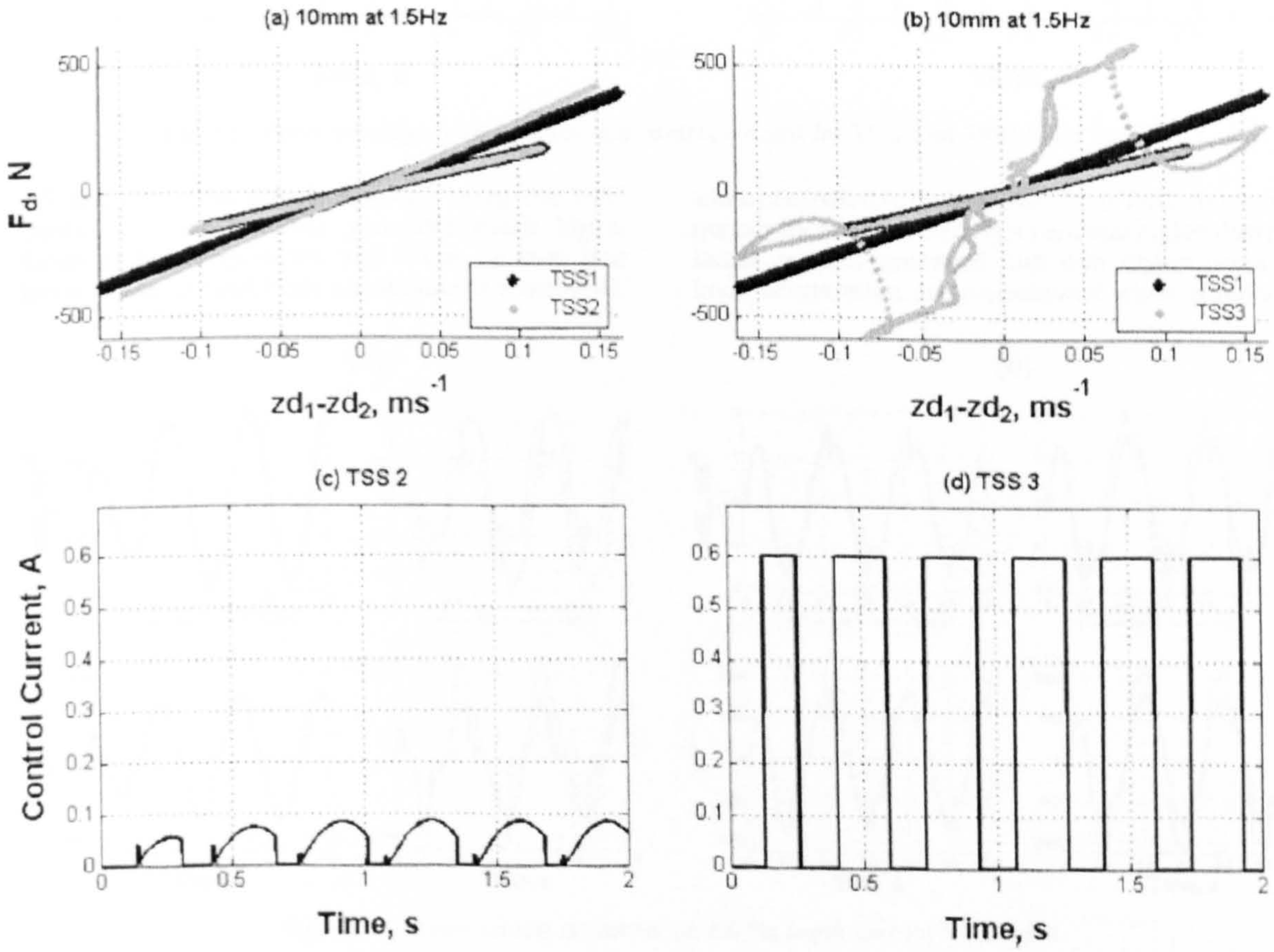

Fig. 11 Force velocity characteristics and control current for TSS2 and TSS3 (1.5 Hz)

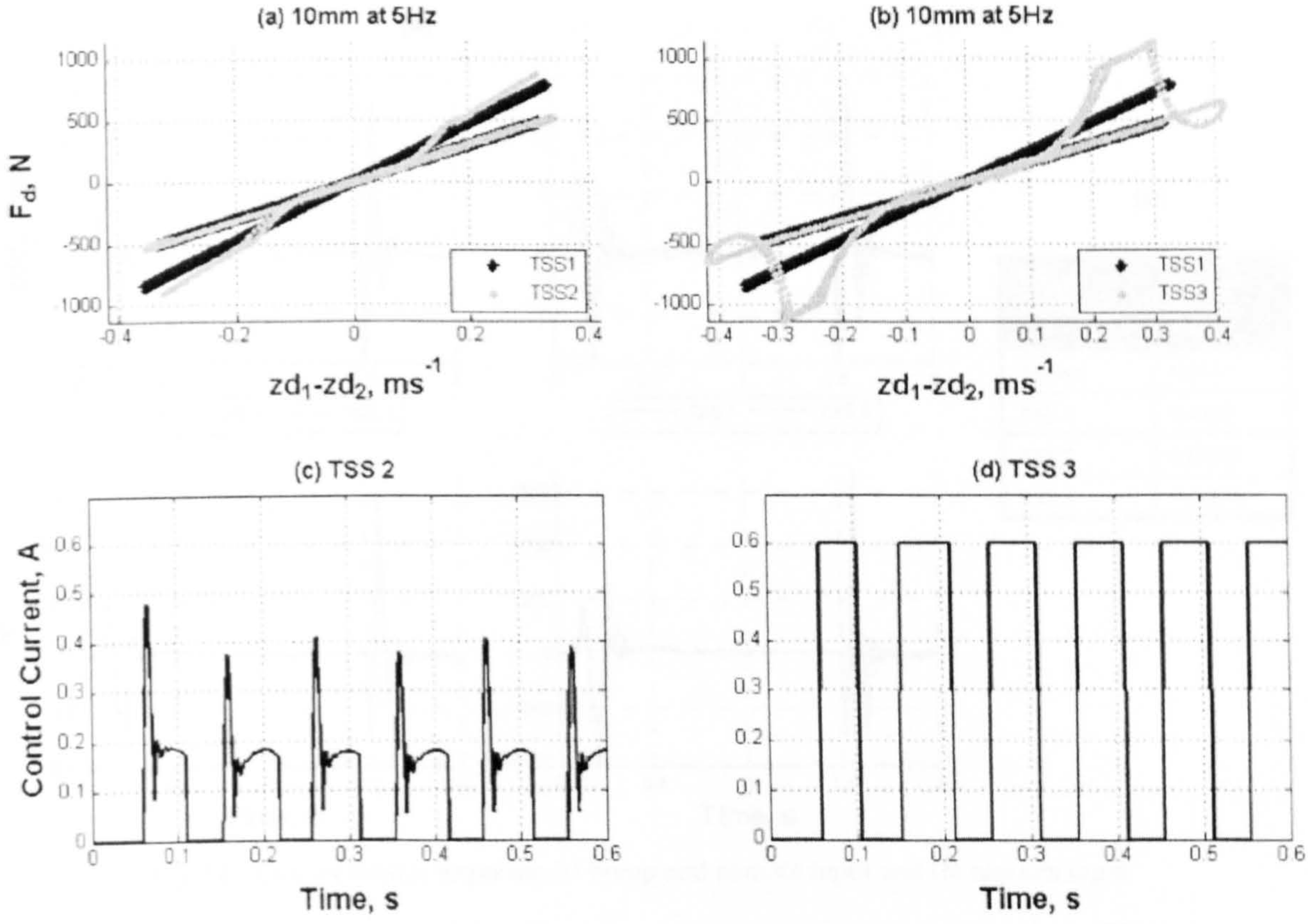

Fig. 12 Force velocity characteristics and control current for TSS2 and TSS3 (5 Hz input)

1.5 and 5 Hz. The vehicle response using the TSS3 control strategy, however, generates much higher forces at low frequencies, and it can be seen that lower values of peak body acceleration are achieved, when compared to the response from TSS1. As the frequency increases to 5 Hz, it is seen that higher damper forces are still generated, but now higher levels of body acceleration are experienced when compared

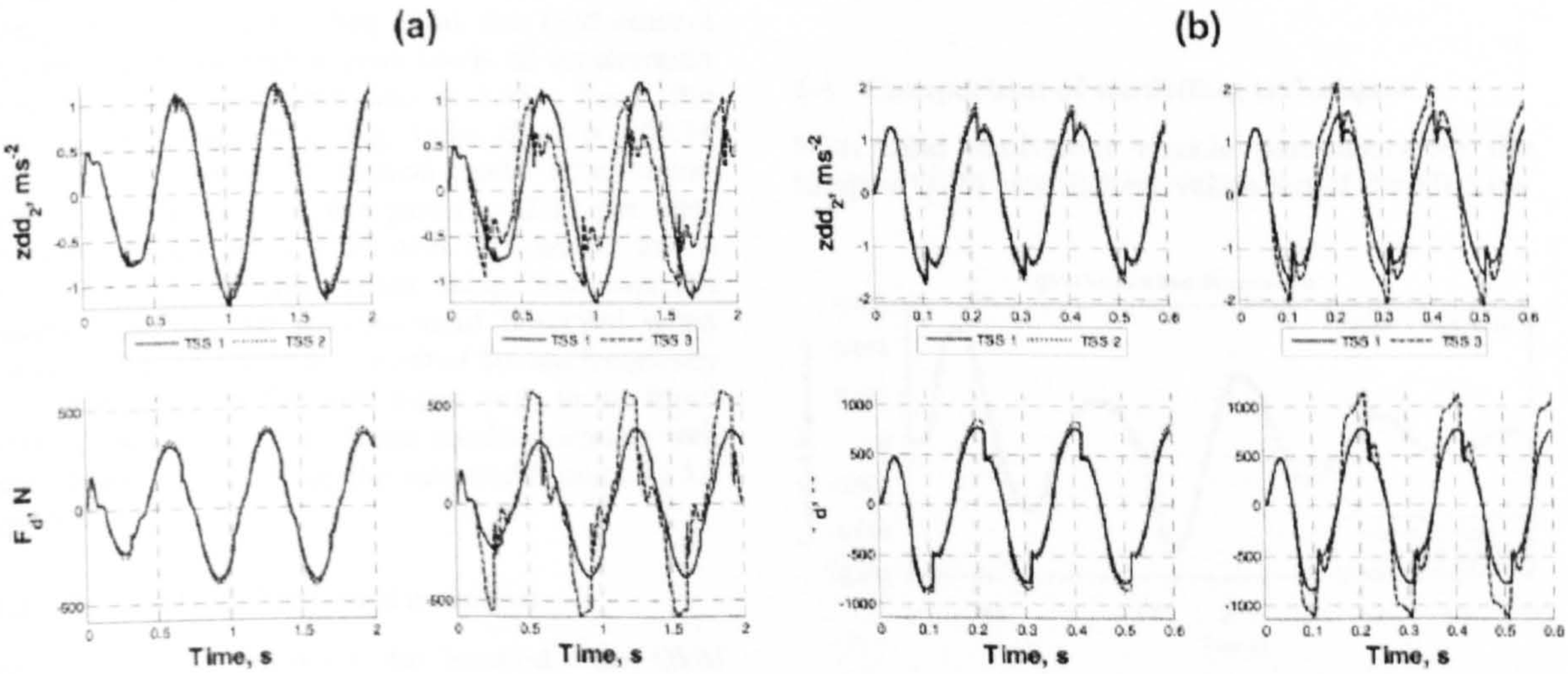

Fig. 13 Quarter vehicle response: (a) 1.5 Hz input and (b) 5 Hz input

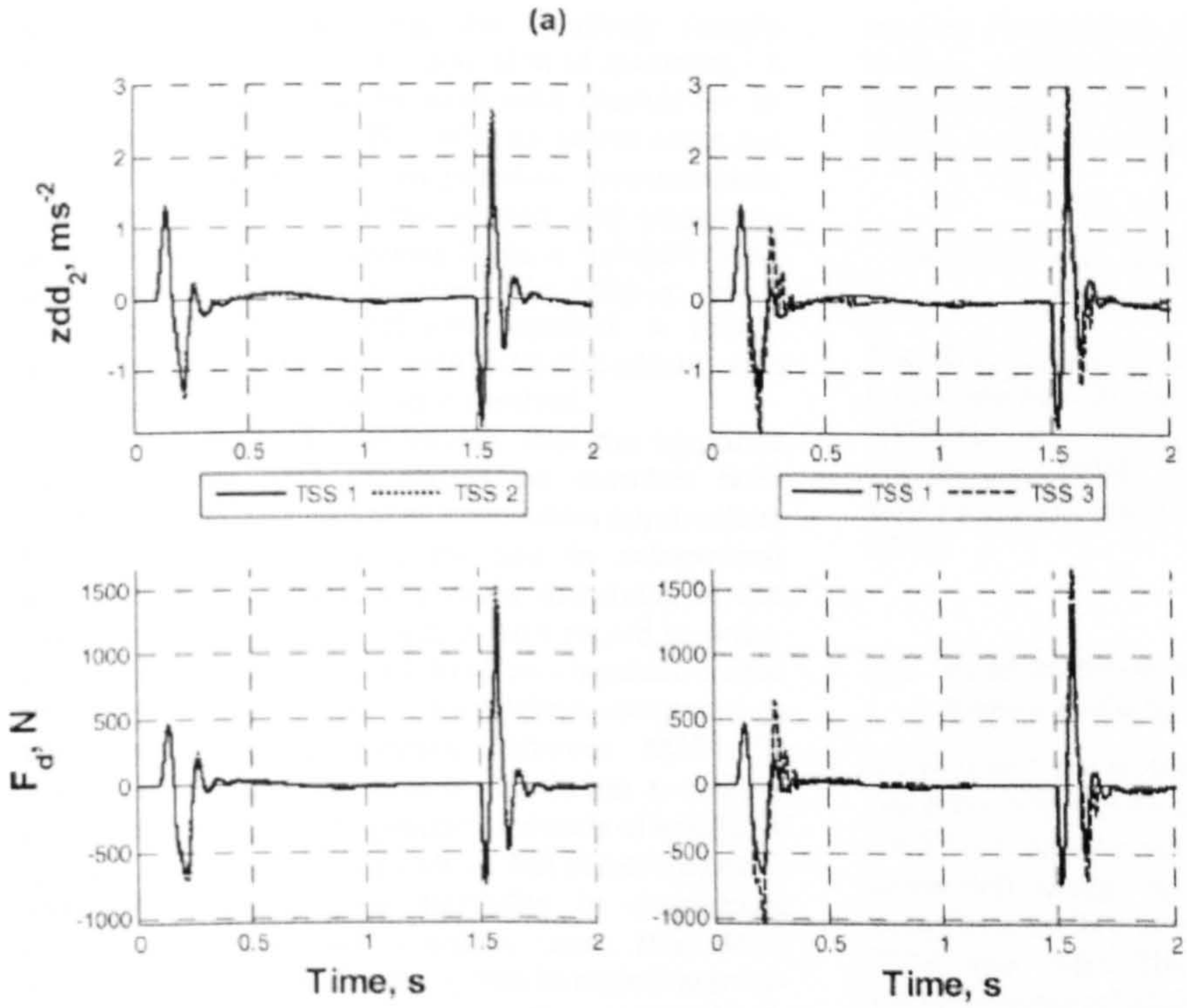

(b)

Suspension System	Random Input RMS_{ACC}
Passive	0.803
TSS 1	0.6524
TSS 2	0.62298
TSS 3	0.51619

Fig. 14 Quarter vehicle response: (a) bump and pothole input and (b) random input

to TSS1. While lower levels of body acceleration are observed for TSS3 at low frequencies, the sudden changes in vertical acceleration observed when using this control strategy, resulting in the highly non-linear nature of the damper when using simple current switching, may have an adverse effect on the durability of the suspension components. This issue is further addressed in section 4.5. For the bump and pothole response in Fig. 14(a), the TSS3 control strategy produces higher peak levels of acceleration over TSS2, at 0.25 s and also at 1.65 s. From the RMS_{ACC} values shown in Fig. 14(b), there is a 22.14 per cent reduction in vertical body acceleration when using TSS1 over the passive, 22.42 per cent reduction when using TSS2 over the passive and a 35.72 per cent reduction when using TSS3 over the passive system. The improvement observed when using TSS3 is primarily as a result of the low frequency (< 1.3 Hz) power of the road input, seen in the input PSD as shown in Fig. 6. These results correlate well with those presented for the sinusoidal input at 1.5 and 5 Hz.

4.3 Results from MBS co-simulation

In section 2.1, parameters for lumped mass QVM were presented as determined from a more realistic QVM that included suspension geometry. Once, determined simulation in the MBS environment was used to assess its validity. Figure 15 shows the vehicle body/sprung mass response when subjected to the transient road profile defined in Fig. 5. Both lumped mass and realistic model data are presented, which can be seen to match well. Similar close comparison was also observed in the hub/unsprung mass response (not shown).

4.4 Comparison of modelling techniques

With valid equivalent vehicle parameters for the lumped QVM established, validation of the MBS co-

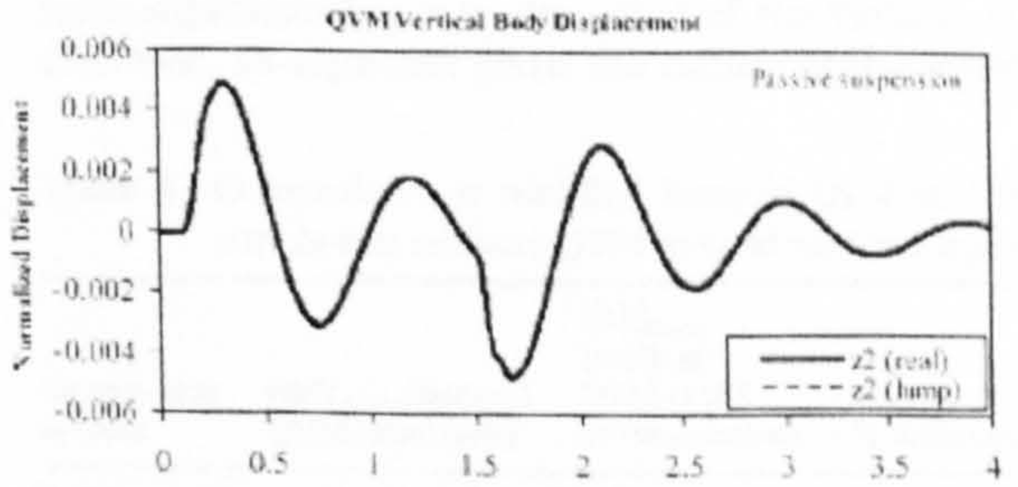

Fig. 15 Comparison between the realistic QVM and the lumped mass two-degree-of-freedom QVM

simulation approach using this relatively simple model is possible, with the intention of assessing its accuracy, so that it can be used with confidence to further investigate the effect of semi-active damping on the durability of suspension components. Again,the analysis uses the sprung and unsprung mass displacement response from a lumped QVM for a passive suspension system. The MBS co-simulation approach is evaluated against a purely mathematical approach (MATLAB/Simulink) and with a purely MBS simulation method.

Response from Fig. 16 implies that the response obtained from MBS co-simulation matches both MATLAB/Simulink and MBS simulation approaches. Confirming its suitability for use in subsequent sections of this paper. The main drawback of the MBS co-simulation approach is with regard to simulation run time. At present, MBS co-simulation uses the longest simulation run time when compared to the other two approaches, whereas MATLAB/Simulink recorded the fastest simulation run time. However, modelling the geometric details of a realistic QVM is prohibitively difficult in MATLAB/Simulink, although it offers great flexibility in developing controller models and is widely used. Pure MBS simulation provides a better option in regard to modelling complex geometrical properties and load histories from suspension components can be extracted and exported to finite-element packages for stress analysis. However, creating complex semi-active damper models and controllers within the MBS environment is not currently possible. All simulations ran on a desktop computer with AMD Athlon™ XP 2200+ processor at 1.81 GHz with 512 MB of RAM. With the availability of faster computing speed and higher access memory, simulation run time can be significantly reduced making the MBS co-simulation more attractive approach. As a means of comparing the various simulation methods (Simulink and MBS co-simulation) as well as the various vehicle models used (lumped QVM and realistic QVM), the RMS_{ACC} values, in response to the random road input, are presented in Table 4. The RMS_{ACC} values are derived from the power spectral density, S_{ACC} of the time domain body acceleration signal, $\ddot{z}_2$ and described as follows

$$RMS_{ACC} = \sqrt{\int_{f_1}^{f_h} S_{ACC} df} \tag{12}$$

The difference as a percentage of the lumped QVM results are also shown. It can be seen that the realistic QVM has consistently higher values of RMS_{ACC} than the lumped QVM. This is due to additional non-linear force created by the bump stop in the realistic QVM.

4.5 Load histories of suspension component from a realistic QVM

To evaluate the potential effect on fatigue life, load histories in the form of acceleration PSD were evaluated for a passive system and compared with those generated using the three semi-active TSS laws described earlier in section 3.1, these being TSS1, TSS2, and TSS3. The assessment uses the realistic QVM, as detailed analysis of suspension components is not possible using the lumped QVM. The vehicle model was subjected to the right-hand side of the random road input travelling at a forward velocity of 34 km/h. The RMS accelerations recorded in x, y, and z directions were measured at the hub, vehicle body, and two at the locations along the lower arm, namely Location 1 (Loc1) and Location 2 (Loc2), as illustrated in Fig. 17. The two locations at the lower suspension arm are at the same positions as chosen by references [1] and [21].

Table 5 presents the results including the percentage improvement with reference to the passive suspension system. Positive and negative values indicate improvement and deterioration, respectively, with the applied semi-active laws. Results shown in Table 5 suggested that the influence of the longitudinal (x) and lateral (y) load histories were significantly lower than that of the vertical (z) direction, as expected given the nature of the input.

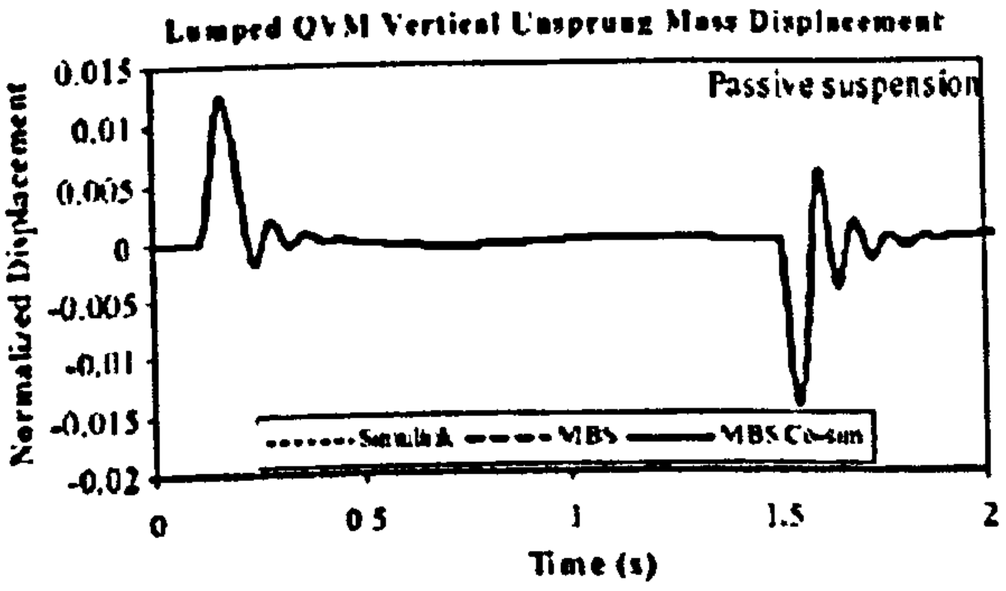

Fig. 16 Comparison of modelling techniques

Table 4 Comparison of simulink lumped QVM and co simulation realistic QVM to random road input

Suspension system	RMS_{ACC} (lumped QVM–simulink)	RMS_{Body} (realistic QVM–MBS co-simulation)	% difference
Passive	0.803	0.833 45	3.8
TSS1	0.6524	0.671 78	2.97
TSS2	0.622 98	0.644 38	3.43
TSS3	0.516 19	0.570 06	10.45

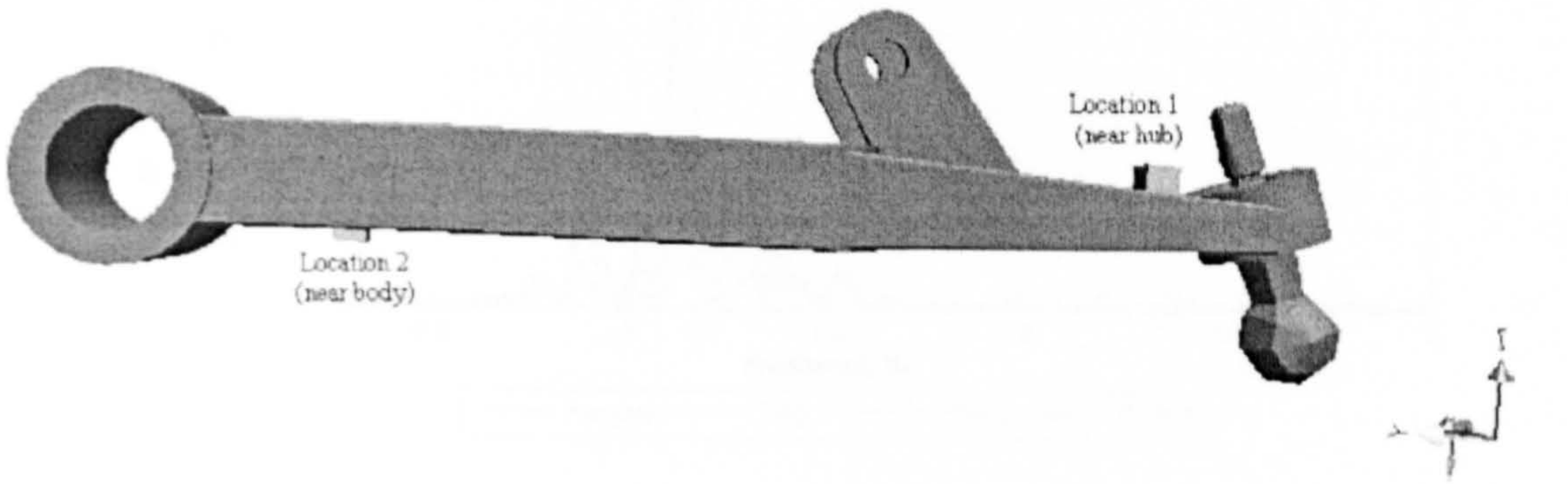

Fig. 17 Suspension arm

This is true for both passive and all semi-active systems. Closer inspection of the RMS accelerations shows a gradually decreasing trend of the vibration energy as it progresses from the hub to the vehicle body. Clearly, significant reduction in the vehicle body accelerations can be observed, resulting from implementation of the TSS control strategies. TSS2 provides the best overall reduction at all four locations. In contrast, TSS3 appears to produce higher RMS values than those of the passive system at all locations except at the vehicle body, where the highest reduction is recorded. It implies, despite the considerable improvement in ride comfort, this control law is not optimum, because the increase in loading at higher frequencies may greatly reduce the fatigue life of the suspension component. These results correlate well with those presented in section 4.2. PSD accelerations of the suspension lower arm at Location 2 for vertical directions (z) are displayed in Fig. 18. Owing to the proximity of Location 2 to the body, it can be seen that TSS3 has a much lower peak than both TSS1 and TSS2 around the body resonance frequency range (0–3 Hz), as shown in Fig. 18(a). Examining the same PSD plot around wheel hop resonance range (10.5–15 Hz), as in Fig. 18(b), it can be seen that in general there appears to be higher peaks using TSS3. The results presented in this section highlight the significance of linearizing the response of the MR damper of terms of reducing the energy at the lower arm suspension component, which will have a significant affect on the durability and fatigue life of the component.

4.6 Evaluation of pitch and roll control strategies for a lumped mass FVM

As the results from previous sections (4.3 and 4.4) indicated that for a QVM, good accuracy can be achieved from the MBS co-simulation approach, the work is extended here to examine the ride performance of a lumped mass FVM subjected to two alternative semi-active vehicle control strategies.

Table 5 RMS acceleration for the competing suspension systems

Direction	RMS_{Hub} (Passive)	RMS_{Hub} (TSS1)	% improve	RMS_{Hub} (TSS2)	% improve	RMS_{Hub} (TSS3)	% improve
x	0.151 85	0.134 93	11.1	0.123 12	18.9	0.235 37	−55.0
y	0.156 35	0.120 64	22.8	0.113 95	27.1	0.16	−2.3
z	2.1501	1.9643	8.6	1.8132	15.7	3.4835	−62.0
Direction	RMS_{Loc1} (Passive)	RMS_{Loc1} (TSS1)	% improve	RMS_{Loc1} (TSS2)	% improve	RMS_{Loc1} (TSS3)	% improve
x	0.002 4727	0.001 965	20.5	0.001 87	24.4	0.002 2779	7.9
y	0.1853	0.158 59	14.4	0.141 02	23.9	0.273 84	−47.8
z	1.8712	1.7111	8.6	1.5827	15.4	3.0176	−61.3
Direction	RMS_{Loc2} (Passive)	RMS_{Loc2} (TSS1)	% improve	RMS_{Loc2} (TSS2)	% improve	RMS_{Loc2} (TSS3)	% improve
x	0.002 2736	0.002 0336	10.6	0.001 9187	15.6	0.003 1968	−40.6
y	0.073 985	0.064 739	12.5	0.060 339	18.4	0.108 28	−46.4
z	0.792 74	0.671 23	15.3	0.643 11	18.9	0.773 77	2.4
Direction	RMS_{Body} (Passive)	RMS_{Body} (TSS1)	% improve	RMS_{Body} (TSS2)	% improve	RMS_{Body} (TSS3)	% improve
x	0.001 7784	0.001 4335	19.4	0.001 375	22.7	0.001 2164	31.6
y	2.95E-05	2.38E-05	19.4	2.28E-05	22.7	2.02E-05	31.6
z	0.833 45	0.671 78	19.4	0.644 38	22.7	0.570 06	31.6

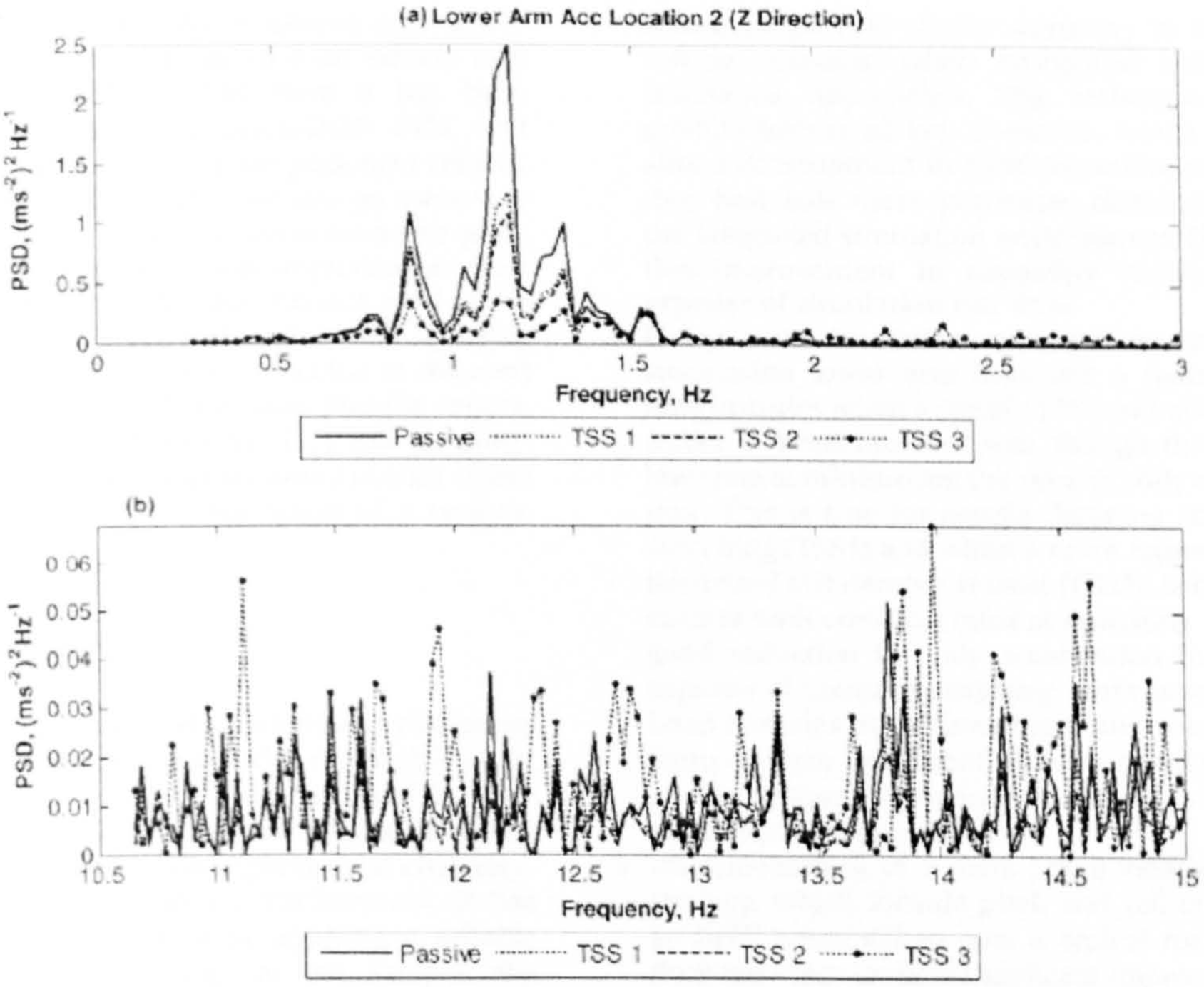

Fig. 18 PSD at Location 2 for vertical direction(z): (a) 0–3 Hz and (b) 10.5–15 Hz

Passive independent suspension is used as a reference. The idealized TSS1 damper control strategy is selected for the analysis of the two semi-active vehicle control strategies because of its computational simplicity (though results in section 4.5 suggest that very similar performance using the more representative TSS2 is achieved). Additionally, TSS1 can be simulated at lower sampling rates (500 Hz), when compared to TSS2 and TSS3 (2 kHz), without significantly affecting accuracy of the response. This reduces considerable simulation run times.The first vehicle control strategy simply allows four fully independent semi-active controllers to operate at each corner, whereas the second incorporates pitch and roll control, as described in section 3.2. The vehicle traverses the left and the right-hand side of the virtual road at a constant velocity of 34 km/h. The results, as shown in Table 6, illustrate the RMS accelerations at all corners of the vehicle body.

Simulation results suggested that both semi-active suspension systems registered more than 10 per cent improvement in ride performance compared with the independent passive system. The RMS accelerations from TSS1 with pitch and roll control showed mixed results when compared to the independent TSS1. A modest ride comfort improvement is observed at the front right and rear left of the vehicle body, when compared with the independent semi-active controller, whereas at the other two locations the performance was only marginally improved. This is probably be due to the smoothness of the tracks where the contribution of pitch or roll may not be significant. Similar trends were recorded by Nell and Steyn [20] though only the front right and the rear left were presented and they concluded that their minimum product strategy performs much better as the road becomes rougher.

Table 6 Vertical acceleration RMS of the lumped FVM (vehicle body)

	Independent passive (m/s^2)	Independent TSS1 (m/s^2)	% improve	TSS1 with P&R ctrl (m/s^2)	% improve
Body FL	0.842 68	0.675 57	19.8	0.673 42	20.1
Body FR	0.883 64	0.699 88	20.8	0.727 59	17.7
Body RL	0.843 15	0.695 31	17.5	0.728 39	13.6
Body RR	0.846 47	0.689 86	18.5	0.6742	20.3

While Nell and Steyn [20] employed semi-active pitch and roll control for an off-road vehicle in a three-degree-of-freedom FVM, here it has been extended and used in a seven-DOF FVM and implemented on a multi purpose passenger vehicle. The extension to more DOF may also go some way to explain why the results for the semi-active pitch and roll controller deliver less improvement than may be expected over the independent semi-active controller. Further work will explore the dynamic response when the vehicle is subjected to different forward velocities and bump and pothole inputs. Virtual durability road sections [21] will be introduced to examine the effect on load histories of the lower arm using MBS co-simulation of a realistic FVM.

5 CONCLUSIONS

1. The MR damper model developed in this paper has been shown to predict with reasonable accuracy the force-velocity characteristics of the Carerra Magneshock MR damper. Simulated results have been matched with experimental characterization of the MR device. Furthermore, it has been demonstrated that by applying a suitable feedback control strategy to the damper, the highly non-linear response of the damper can be shaped to give a near viscous damping characteristic (TSS2). Alternatively, by applying a minimum and maximum control current to the damper based on Karnopp's two state switchable control strategy, a simpler but highly non-linear switchable damper achieved, which has the potential to deliver higher forces at lower frequencies (TSS3). Comparison of the two when applied to a lumped mass QVM shows the later produces larger transient forces which have the potential to have a significant affect on suspension component durability.
2. In terms of reducing the vertical acceleration of the body mass, TSS3 seemed to give the best results. However, for higher frequencies, the performance of this control strategy appeared to degrade. TSS2 appears to perform much better in terms of reducing peak accelerations on the lower arm, thus providing better control in terms of durability and fatigue of suspension components. Though TSS2 requires a much more sophisticated controller, it offers a much more predictable and tuneable response, fitting in much better with the modular concept of the co-simulation approach presented here.
3. An approach to obtaining load histories of suspension components has been demonstrated which uses MBS co-simulation. It has been shown to provide similar accuracy in terms of vehicle response when compared with other simulation approaches. The technique allows modularization of key elements, which in turn allows development in their respective programs that best suit these particular elements within the integrated simulation environment. However, this improvement in capability comes at the expense of simulation run time.
4. Using a co-simulation approach analysis of a suspension lower arm indicates a reduction in load histories when a simple TSS semi-active controller is implemented even though the control law aims at minimizing the vehicle body acceleration. This is true for simple damping coefficient switching (TSS1) and when a more representative linearized MR damper is used (TSS2). Semi-active control with constant current switching provides good reduction in body acceleration but at the expense of increase unsprung mass acceleration. Load histories in the lower arm and results from damper show significant increase in acceleration and force thus generating greater stress intensity to the suspension arm.
5. Implementation of a semi-active vehicle control strategy, which include pitch and roll control, in an MPV when driven over a typical road profile does not seem to show significant improvement in ride over an independent TSS method. Hence, for multi-purpose vehicles or passenger vehicles that travel most of the time on asphalt, the use of simple independent TSS control may be sufficient in improving ride. Conversely, the inclusion pitch and roll control strategy might be useful only when examining durability issue, where the vehicle is subjected to virtual durability tracks that induce high levels of pitch and role.

ACKNOWLEDGEMENTS

The authors wish to express their gratitude to MSC Software Corporation, MathWorks Inc., MIRA Ltd., and Neil Sims at Sheffield University for their support. The second named author would like to thank the University of Malaya for financially supporting him during the progress of this research.

REFERENCES

1 Haiba, M., Barton, D. C., Brooks, P. C., and Levesley, M. C. Using a quarter-vehicle multi-body model to estimate the service loads of a suspension arm for durability calculations. *Proc. Instn Mech. Engrs, Part K: J. Multi-body Dynamics*, 2003, 217, 121–133.

2 Levesley, M. C., Kember, S. A., Barton, D. C., Brooks, P. C., and Querin, O. M. Dynamic simulation of vehicle

suspension systems for durability analysis. *Mater. Sci. Forum*, 2003, 440–441, 103–110.
3 Sharp, R. and Hassan, S. An evaluation of passive automotive suspension systems with variable stiffness and damping parameters. *Veh. Syst. Dyn.*, 1986, 15, 335–350.
4 Sammier, D., Sename, O., and Dugard, L. Skyhook and H infinity control of semi-active suspensions: some practical aspects. *Veh. Sys. Dyn.*, 2003, 39, 279–308.
5 Karnopp, D., Crosby, M., and Harwood, R. Vibration control using semi-active force generators. *ASME J. Eng. Ind., Trans. ASME*, 1974, 96, 619–626.
6 Cebon, D., Besinger, F., and Cole, D. Control strategies for semi-active lorry suspensions. *Proc. Instn Mech. Engrs, Part D: J. Automobile Engineering*, 1996, 210 (D), 161–178.
7 Sharp, R., and Hassan, S. Performance and design considerations for dissipative semi-active suspension systems for automobiles. *Proc. Instn Mech. Engrs*, 1987, 201(D2), 149–153.
8 Sims, N., Stanway, R., Peel, D., Bullough, W., and Johnson, A. Controllable viscous damping: an experimental study of an electrorheological long-stroke damper under proportional feedback control. *Smart Mater. Struct.*, 1999, 8, 601–615.
9 Liao Y. G. and Du, H. I. Cosimulation of multi-body-based vehicle dynamics and an electric power steering control system. *Proc. Instn Mech. Engrs, Part K*: 2001, 215, 141–151.
10 Malorana, J., Minaker, B. P., Zhang, D., and Malik, M. A. *Cosimulation of active suspension*. SAE technical paper series, 2005-01-0984, 2005, p. 9.
11 Rahnejat, H. *Multi-body dynamics: vehicles, machines and mechanisms*. 1st edition, 1998, (Professional Engineering Publishing Limited, Bury St Edmunds and London).
12 Inman, D. J. *Engineering vibration*. 2nd edition, 2001 (Prentice Hall, New Jersey).
13 Gillespie, T. D. *Fundamentals of vehicle dynamics*. 1992 (Society of Automotive Engineers, Inc., Warrendale).
14 Ramli, R., Pownall, M., Levesley, M. C., and Crolla, D. A. Dynamic analysis of semi-active suspension systems using a co-simulation approach. 3rd International Symposium on *Multi-body dynamics: monitoring and simulation techniques*, 2004 Loughborough, UK, pp. 391–400.
15 Peel, D. J. and Bullough, W. A. Prediction of electro-rheological valve performance in steady flow. *Proc. Instn Mech. Engrs*, 1994, 208, 253–266.
16 John, S. and Wereley, N. M. Nondimensional quasi-steady analysis of magnetorheological dampers utilizing a herschel bulkley model with preyield viscosity. Smart structures and materials 2003: damping and isolation, Proceeding of SPIE, San Diego, CA, USA, 2003, vol. 5052, pp. 53–65.
17 Sims, N. D., Holmes, N. J., and Stanway, R. A unified modelling and model updating procedure for electrorheological and magnetorheological vibration dampers. *Smart Mater. Struct.*, 2004, 13, 100–121.
18 Blundell M. and Harty, D. The multibody systems approach to vehicle dynamics, 2004 (Elsevier Butterworth-Heinemann, Oxford).
19 Sui J. and Hirshey, J., *Evaluation on analytical tire models for vertical vibration simulation using virtual tire testing method*. SAE technical paper series, 1999-01-0786, 1999.
20 Nell S. and Steyn, J. L., An alternative control strategy for semi-active dampers on off-road vehicles. *J. Terramech.*, 1998, 35, 25–40.
21 Ramli, R., Levesley, M. C., and Crolla, D. A. Simulation and evaluation of passive and semi-active suspension of quarter and full vehicle ride models. NAFEMS World Congress 2005 – Engineering Simulation: Best Practices and Visions of the Future, St. Julians, Malta, 2005.

APPENDIX

Notation

c_{pre}	pre-yield MR fluid damping coefficient
c_{post}	post-yield MR fluid damping coefficient
C	viscous damping coefficient
C_{hard}	high damping coefficient
C_{soft}	low damping coefficient
d_{F_LHS}	damper force on the front left hand
d_{F_RHS}	damper force on the front right hand
d_{R_LHS}	damper force on the rear left hand
d_{R_RHS}	damper force on the rear right hand
F_d	damper force
F_t	vertical tyre force
F_y	MR fluid yield force
I	control current
K_f	MR fluid stiffness
K_s	passive suspension stiffness
K_t	tyre stiffness
K_{eq}	ride rate
M_b	vehicle body mass or sprung mass
M_f	MR fluid mass
M_h	hub mass
M_w	wheel mass or unsprung mass
x	displacement road profile
z	displacement of vehicle components
$\dot{z}$	velocity of vehicle components
$\ddot{z}$	acceleration of vehicle components
$\dot{z}_1$	unsprung mass velocity
$\dot{z}_2$	sprung mass velocity
α	wheelbase
β	track width
δ	logarithmic decrement
ζ	damping ratio
$\ddot{\Theta}_x$	angular acceleration about x-axis (pitch acceleration)
$\ddot{\Theta}_y$	angular acceleration about y-axis (roll acceleration)

2) R. Ramli, M. C. Levesley, and D. A. Crolla, "Simulation and Evaluation of Passive and Semi-Active Suspension of Quarter and Full Vehicle Ride Models," presented at NAFEMS World Congress 2005 - Engineering Simulation: Best Practices and Visions of the Future, St. Julians, Malta, 2005.

Summary:

This paper describes an ongoing project to accurately determine the dynamic response of vehicles with passive and semi-active suspension systems, for the purpose of durability calculations. The overall aim of the research is to predict the fatigue life based on durability loads, of suspension components from a realistic model. A reliable fatigue life prediction requires accurate estimation of the dynamic response i.e. the service load histories of the suspension components. In this paper, an alternative modelling and simulation approach (cosimulation) is introduced. It combines a mathematical modelling method with a multi-body system (MBS) technique, intended to offer flexibility in modelling of the road, tyre, suspension and the vehicle. Cosimulation of a lumped parameter two-degree-of freedom model (2DOF) and a realistic quarter-vehicle model (QVM) with passive and semi-active suspension systems traversing a transient input (pothole) and a virtual durability road are evaluated. The study is further extended to a lumped seven-degrees-of freedom full-vehicle model (7DOF FVM) in order to examine the dynamic response of the suspension where the influence of body pitch and roll are considered.

Keywords:

Cosimulation, semi-active suspension, durability, fatigue life multi-body system, quarter vehicle model, full vehicle model.

Introduction

In the automotive industry, physical testing of vehicle components for vehicle durability assessment is accurate and reliable. Nevertheless, it requires a vehicle prototype, which is a time consuming and exhaustive process, and most importantly it incurs high operating costs, particularly in the early design stages, as reported by Ferry et al. [1]. With the rapid advancement in computer technology and software development, the use of virtual durability assessment appears to present a better option. Production cost can be reduced with a reduction in product development time. Virtual simulation allows vehicle models to be tested and analyzed under different road conditions with a selection of suspension configurations without the need of actual physical testing. Minor changes to the component design can be tested without building another prototype. If one is to consider durability effects in the early design stage, an accurate representation of the component loading must be produced from a virtual vehicle model, predominantly when the vehicle is driven over a damaging road input. Building on these advances, research at the University of Leeds is seeking to use virtual prototyping as an alternative method to physical durability testing.

Simulation Technique

The proposed simulation approach integrates MBS (MSc Visual Nastran) vehicle models, with mathematical simulation (MATLAB/Simulink) for the tyre model and road input. MATLAB/Simulink is also chosen for the implementation of suspension control, since the code is well suited for control system modelling. It is expected that each code will perform its task efficiently in their own simulation environment. Known as cosimulation, [2], the method described in this paper provides simple integration of these subsystems, as illustrated in Figure 1, allowing each of the subsystems of different complexities to be developed, analysed, and validated separately. This process simultaneously computes the solutions for both modelling codes.

In previous work [3], the cosimulation technique generated comparable dynamic response to the purely mathematical method, for a lumped 2DOF quarter vehicle model (QVM) subjected to step input. In this paper the research is extended to evaluate the dynamic response of vehicle models of different complexities with passive and semi-active suspension systems under the influence of pothole and durability road excitations. The cosimulation scheme, as shown in Figure 1, begins with the numerical road input in the form of displacement, x. It then enters a tyre subsystem containing the tyre model which produces a force input, F_t , to the MBS vehicle subsystem. Here the tyre force, represented as a linear actuator exerts a force at the centre of the unsprung mass. The suspension damper force F_d , either from the passive subsystem or the semi-active subsystem, is calculated from the relative velocities of the sprung and unsprung masses and fed back to the MBS vehicle subsystem. Similarly, the response of the unsprung mass is fed back to the tyre model. The subsystem sends a force output, F_t , back to the MBS vehicle model to represent the actuator force in response to the road excitation. The output displays dynamic responses of the body and wheel in the form of displacement, z, velocities, $\dot{z}$ or accelerations, $\ddot{z}$, concurrently in MSc Visual Nastran and MATLAB/Simulink.

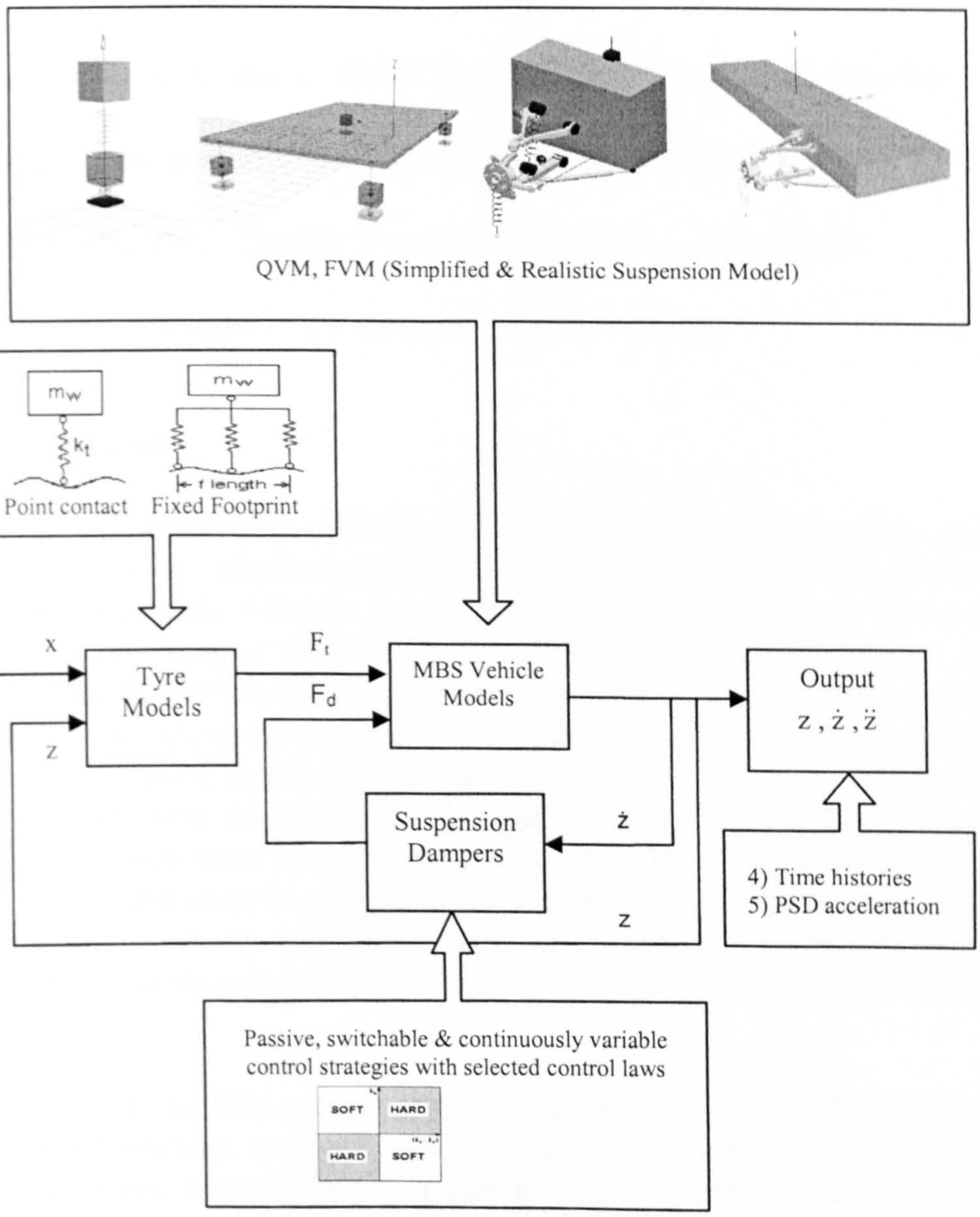

Figure 1: Cosimulation scheme

Vehicle Models

The vehicle models utilized in this study are confined to ride dynamics where only the vertical ground excitation and vertical tyre force are considered. The vehicle parameters and the realistic passive suspension configuration are adopted from [4, 5]. It comprises of a lumped 2DOF quarter vehicle model (QVM), a 7DOF full vehicle model (FVM) and a realistic quarter vehicle suspension. Static analysis is conducted prior to the simulation to allow the suspension components to achieve their equilibrium states. Dynamic analysis of the vehicle models centres on sprung and unsprung mass response for the lumped 2DOF QVM and 7DOF FVM. As for the realistic suspension model, the lower front suspension arm is selected. The acceleration response of this component from cosimulation are compared to experimental results obtained from earlier research [4]. The vehicle parameters are given as follows:

- Effective sprung mass, m_b: 535 kg (2DOF QVM); 1600 kg (7DOF FVM)

- Front and rear unsprung mass, m_w: 47.8 kg (2DOF QVM & 7DOF FVM)
- Front and rear suspension stiffness, k_s: 22000 N/m (2DOF QVM & 7DOF FVM)
- Front and rear suspension damping, c_s: 1500 Ns/m (2DOF QVM & 7DOF FVM)
- Front and rear tyre stiffness, k_t: 239000 N/m (2DOF QVM & 7DOF FVM)
- Centroidal Inertia, Ixx: 1580 kgm^2; Iyy: 628 kgm^2; Izz: 1540 kgm^2;

Road Input and Tyre Model

The simulation begins with evaluation of the vehicle model under the influence of a damaging pothole excitation. A pothole representation from [6] was adopted, as shown in Figure 2. All vehicle models traverse the pothole input at a constant forward velocity of 10 m/s. For the lumped 7DOF FVM, only the front right suspension is allowed to strike the pothole. Next, a virtual durability road is used (Figure 2), to study the effect of dynamic excitation on the loading of the vehicle suspension components. The road consists of a short track made of elements which create significant loading to the vehicle. The road data were measured and sampled every 2 milliseconds as the vehicle traversed the durability track at a constant speed of 34 km/h. To simulate this, the right hand side of the pavè track is applied to the realistic QVM cosimulation. The acceleration response of the lower suspension arm at Location 1 (near hub) and Location 2 (near gearbox), as shown in Figure 8, will be compared to the experimental response.

At present only vertical tyre models are employed in the study. The tyre force in the lateral and longitudinal directions, typically used in issues concerning handling, have negligible effects on forces transmitted to suspension components, thus are not considered. During this phase of the investigation, a point contact tyre model is used. It consists of a spring and a damper arranged in parallel to each other. However, the tyre damping is neglected since its effects are small when compared to the suspension damping. A saturation block in MATLAB/Simulink is introduced to allow the wheel to leave the ground when the tyre encounters a negative slope.

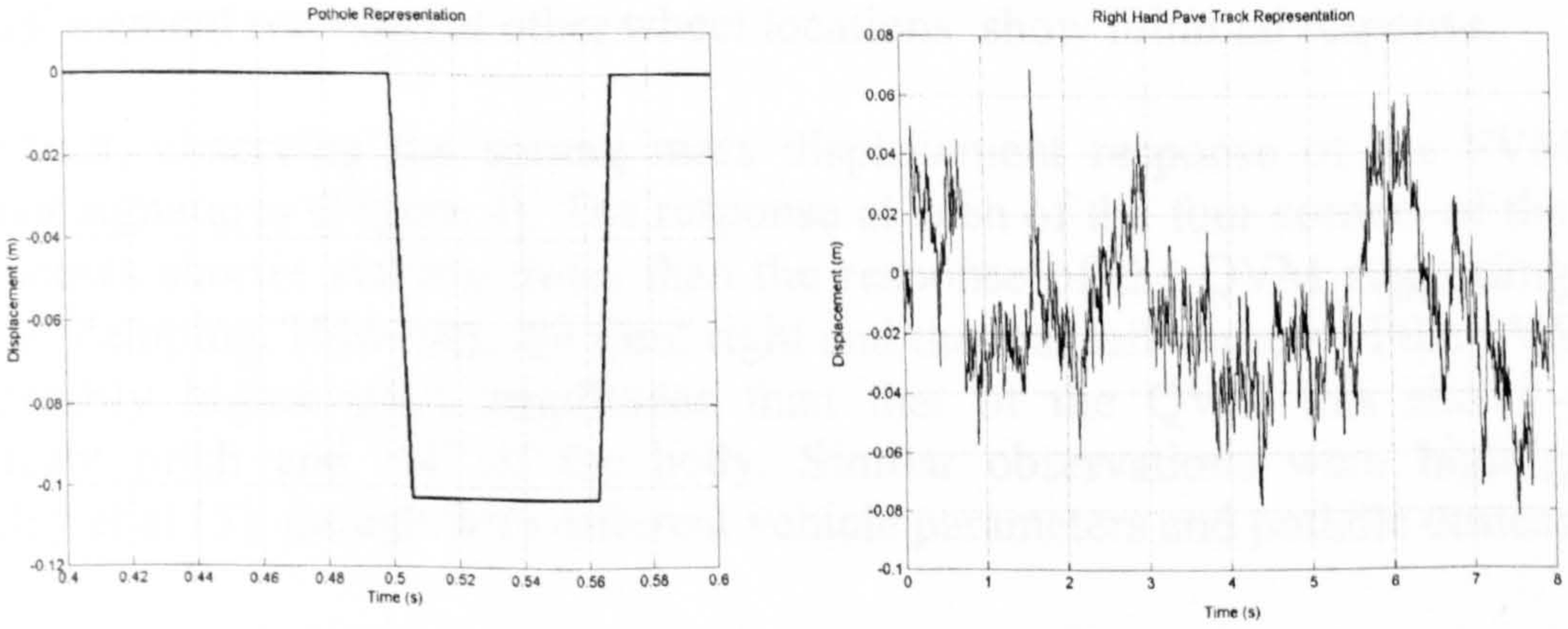

Figure 2: Pothole and Durability Road Numerical Representation

Semi-active Control Model

The semi-active control system presented in this paper adopts a switchable (on-off) strategy with skyhook control law [7], which aims to minimise vehicle body acceleration as shown in the equation below.

$$F_d = \begin{cases} C_{hard} \cdot \left(\dot{z}_b - \dot{z}_w\right) \cdots\cdots \text{if } \dot{z}_b \cdot \left(\dot{z}_b - \dot{z}_w\right) > 0 \\ C_{soft} \cdot \left(\dot{z}_b - \dot{z}_w\right) \cdots\cdots \text{if } \dot{z}_b \cdot \left(\dot{z}_b - \dot{z}_w\right) < 0 \end{cases}$$

Where, F_d is the actual damper force; C_{hard} stands for the damping coefficient for the higher damper setting; C_{soft} represents the damping coefficient for the lower damper setting; $\dot{z}_b$ symbolizes the velocity of the sprung mass; and $\dot{z}_w$ corresponds to the velocity of the unsprung mass.

The implementation of the control law using this approach requires velocity responses of the sprung and unsprung mass which then generates a force feedback to the suspension damper in the MBS environment. For the passive suspension system, a simple damper model is used. For the 7DOF full vehicle model the suspension system of all four wheel station are assumed to be independent. The tyre model subsystem produces a force feedback to the MBS vehicle model which is represented as a linear force actuator acting at the centre of the hub. Validation of the simulation method has been conducted in an earlier investigation [3].

Simulation Results and Discussions

The evaluation begins with the simulation of a lumped 7DOF FVM with passive suspension subjected to the pothole input, where unsprung mass and sprung mass displacement response at all four corners are compared against those from the lumped 2DOF QVM.

In Figure 3, it can be seen that the peak amplitude of the wheel displacement for the QVM is slightly higher than that from the front right wheel of the FVM. The FVM was developed by assuming all four corners of the suspensions are fully independent, thus the displacement recorded at other wheel locations show minimal response.

In contrast, observing the sprung mass displacement response of the FVM shows different signatures (Figure 4). The response at each of the four corners of the vehicle body shows shorter settling times than the response of the QVM suggesting greater affect of damping. However, the front right and the rear left corners of the FVM shows considerably higher peak amplitudes than that of the QVM this shows there is significant pitch and roll of the body. Similar observations were highlighted by Levesley et al [5], though with different vehicle parameters and pothole dimensions.

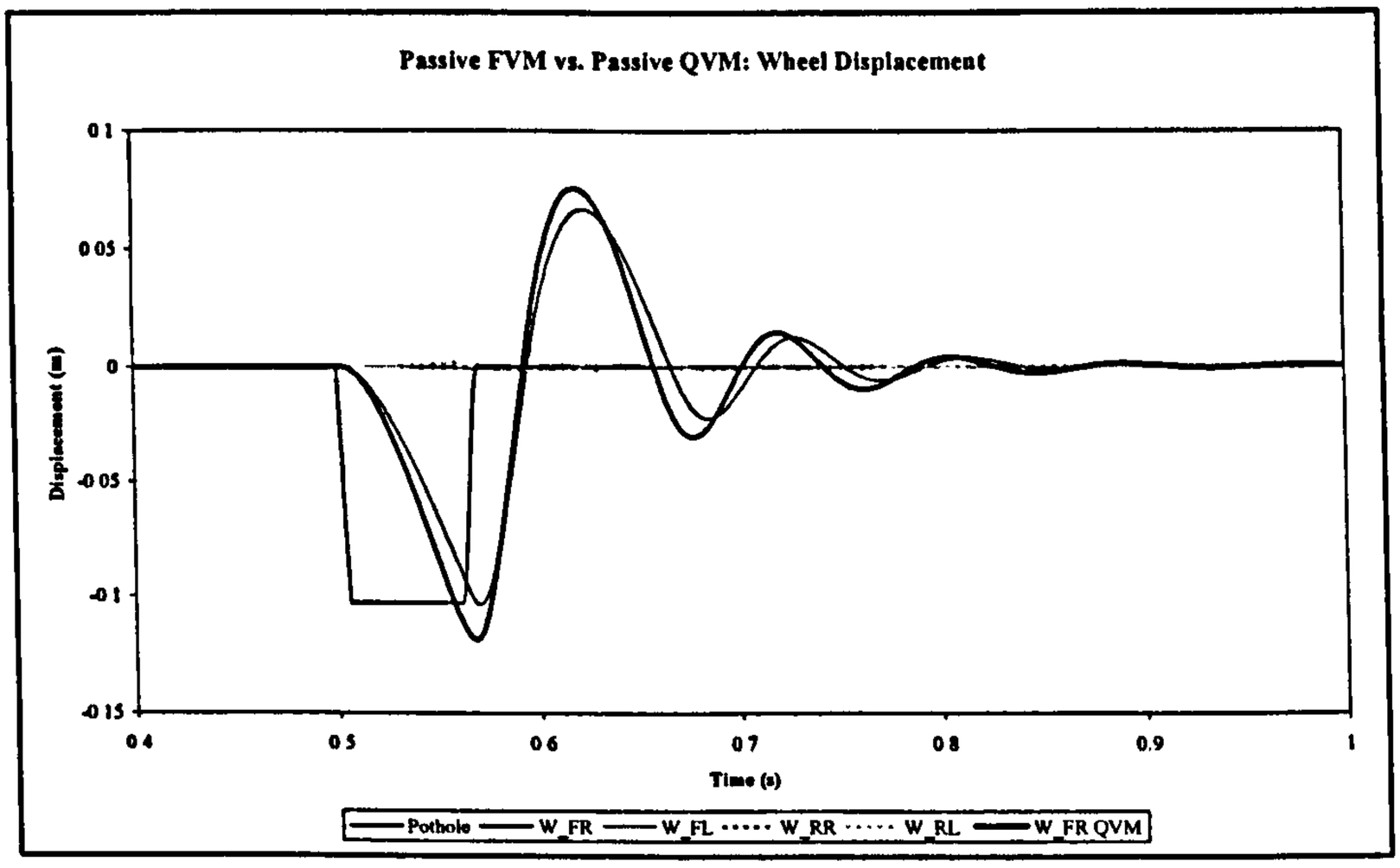

Figure 3: Unsprung Mass Displacement Comparison

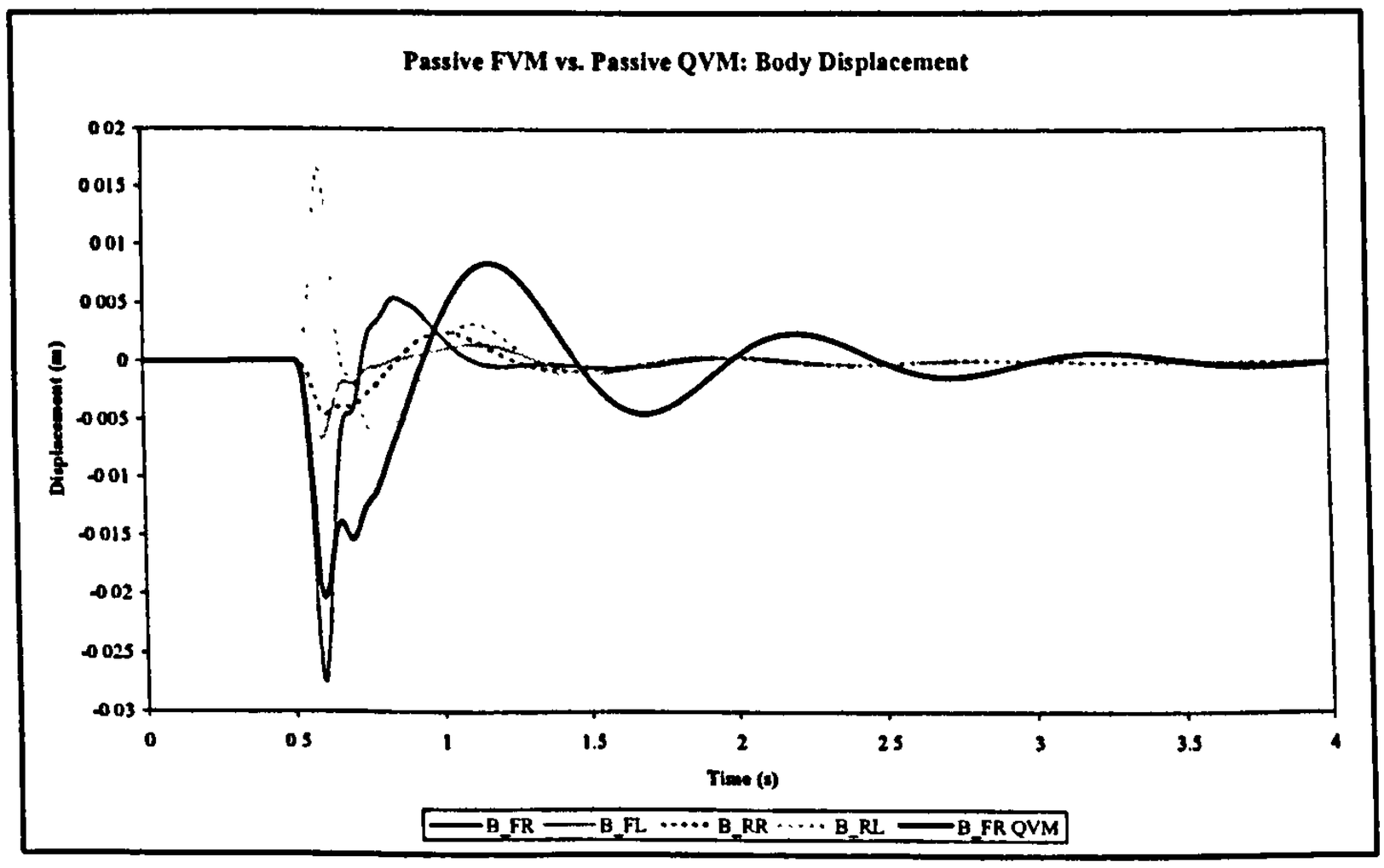

Figure 4: Body Displacement Comparison

Further simulation to assess passive suspension and semi-active suspension systems for lumped 2DOF QVM and 7DOF FVM, now takes place, focussing on the front right hand side of the wheel striking the pothole. Figure 5 describes the unsprung mass profiles of the competing vehicle models and suspension systems. The general trend indicates slightly higher peak amplitudes along with some phase lag, for the semi-active system in comparison with the passive system.

The body displacement characteristics as illustrated in Figure 6 highlight several key issues. For the QVM, implementation of the semi-active control strategy provides significant reduction in peak amplitude compared to the passive system. On the contrary, employing the same strategy on the FVM at all four corners independently shows major differences, principally the peak amplitude with the semi-active system is twice that of the passive system. Next, comparison between different vehicle models employing the semi-active system reveals that the QVM response is better than that of the FVM. It can be concluded, the semi-active strategy used operates well with the QVM in minimizing sprung mass vibration. Unfortunately, it does not present similar performance improvement when used with the FVM, primarily because the effects of

the vehicle body pitch and roll motions are not taken into consideration in the controller. Thus, the implementation of the semi-active control system based on a QVM is inappropriate for the FVM, even if all four corners of the suspensions remain independent. Further investigation is in progress to include pitch and roll effects in the controller algorithm.

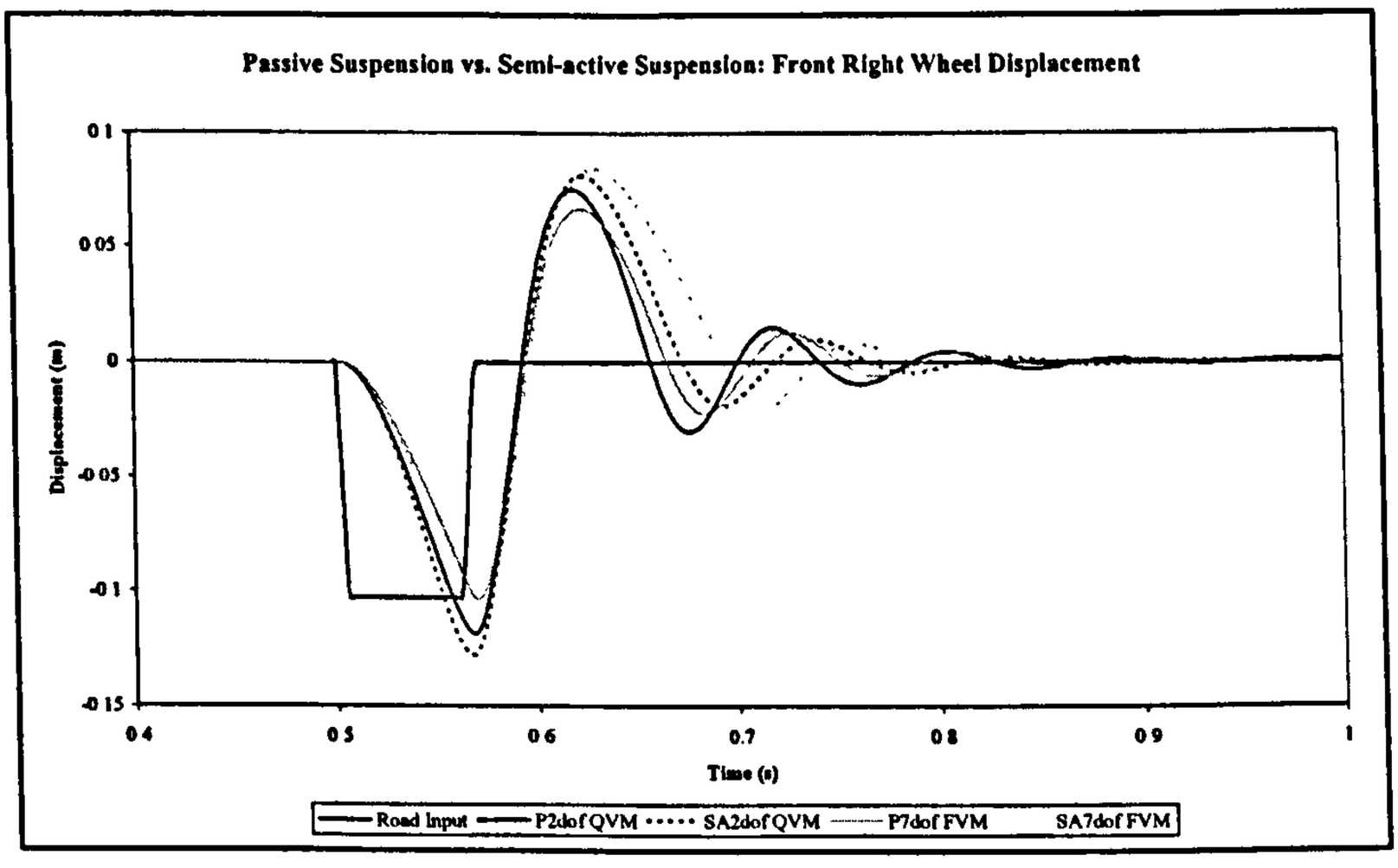

Figure 5: Front Right Wheel Displacement Comparison

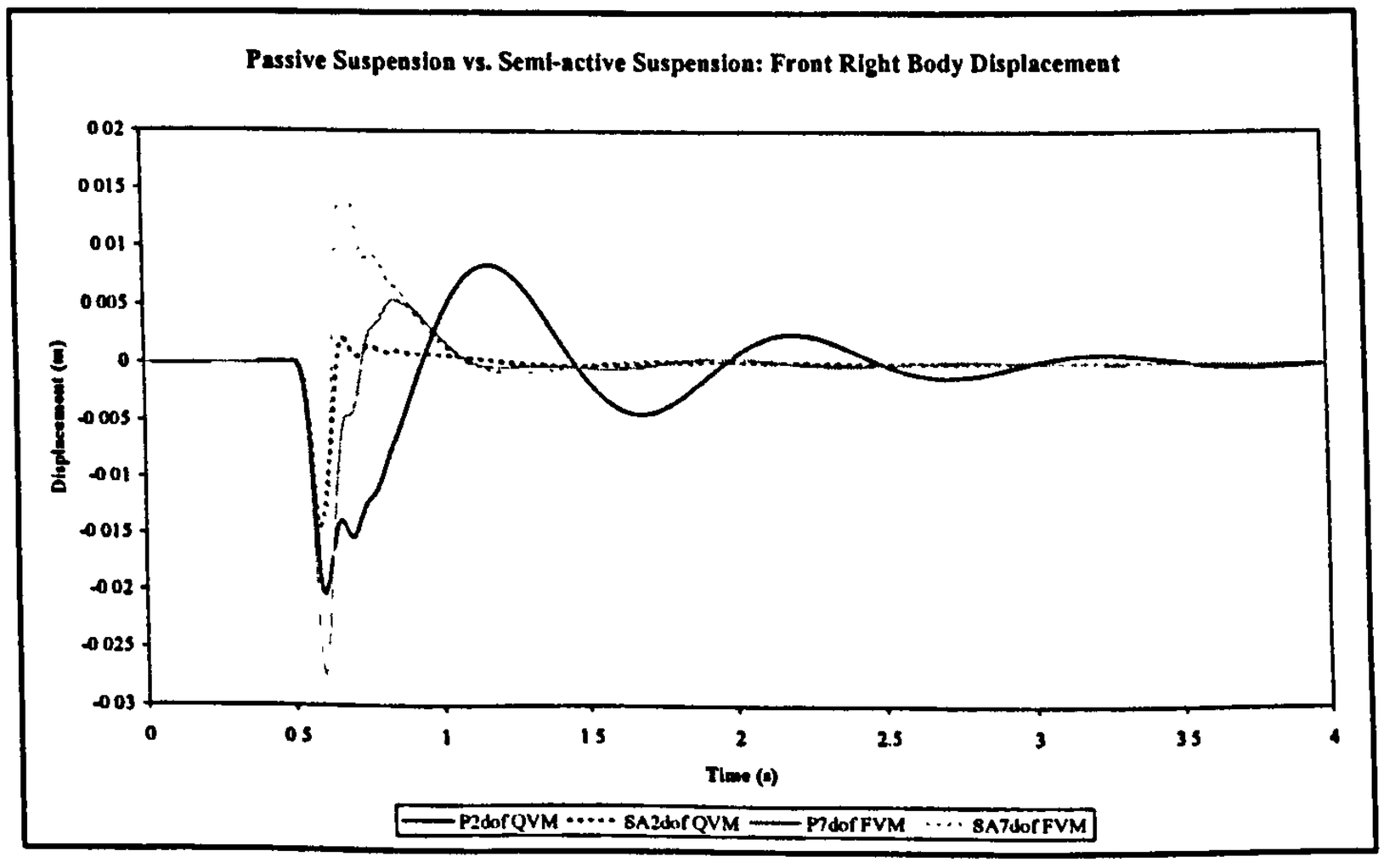

Figure 6: Front Right Body Displacement Comparison

In the subsequent analysis, a realistic QVM (Figure 1) with passive suspension system traversing a pothole is shown. The hub and sprung mass displacement exhibit more oscillatory responses than those from the lumped 2DOF model. This is because the two vehicle models have different geometrical properties, material properties and the boundary conditions. Vehicle parameters of the realistic suspension system consist of components of different properties and constraints, than the simple lumped 2DOF model. Observing the sprung mass displacement suggests differences in results in the model output. In general, body oscillation in figure 6 tends to subside much faster than those recorded in Figure 7. Further modelling is in progress to study the dynamic response of a realistic FVM and the effects of applying a semi active suspension.

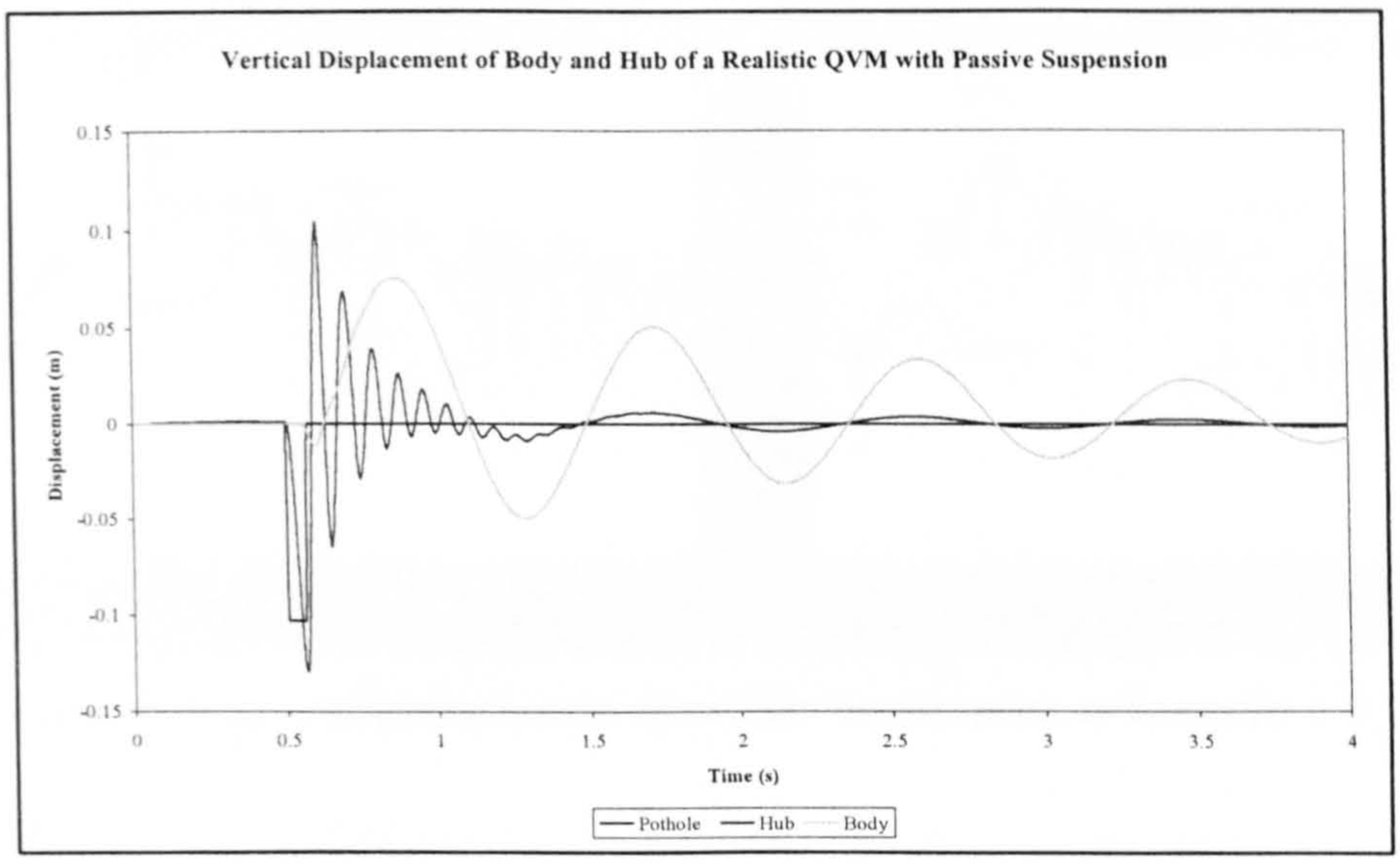

Figure 7: Body and Hub Vertical Displacement Comparison

Finally, the simulation evaluates a realistic QVM with passive suspension where the vehicle is subjected to durability road input. Analysis focuses on the lower arm acceleration at Location 1 (near hub) and Location 2 (near gearbox), as shown in Figure 8. The cosimulation results are compared with the experimental results taken at these locations. The experimental acceleration response from Haiba et al. [4], is sampled every 2 milliseconds (equivalent to sampling frequency, Fs of 500 Hz).

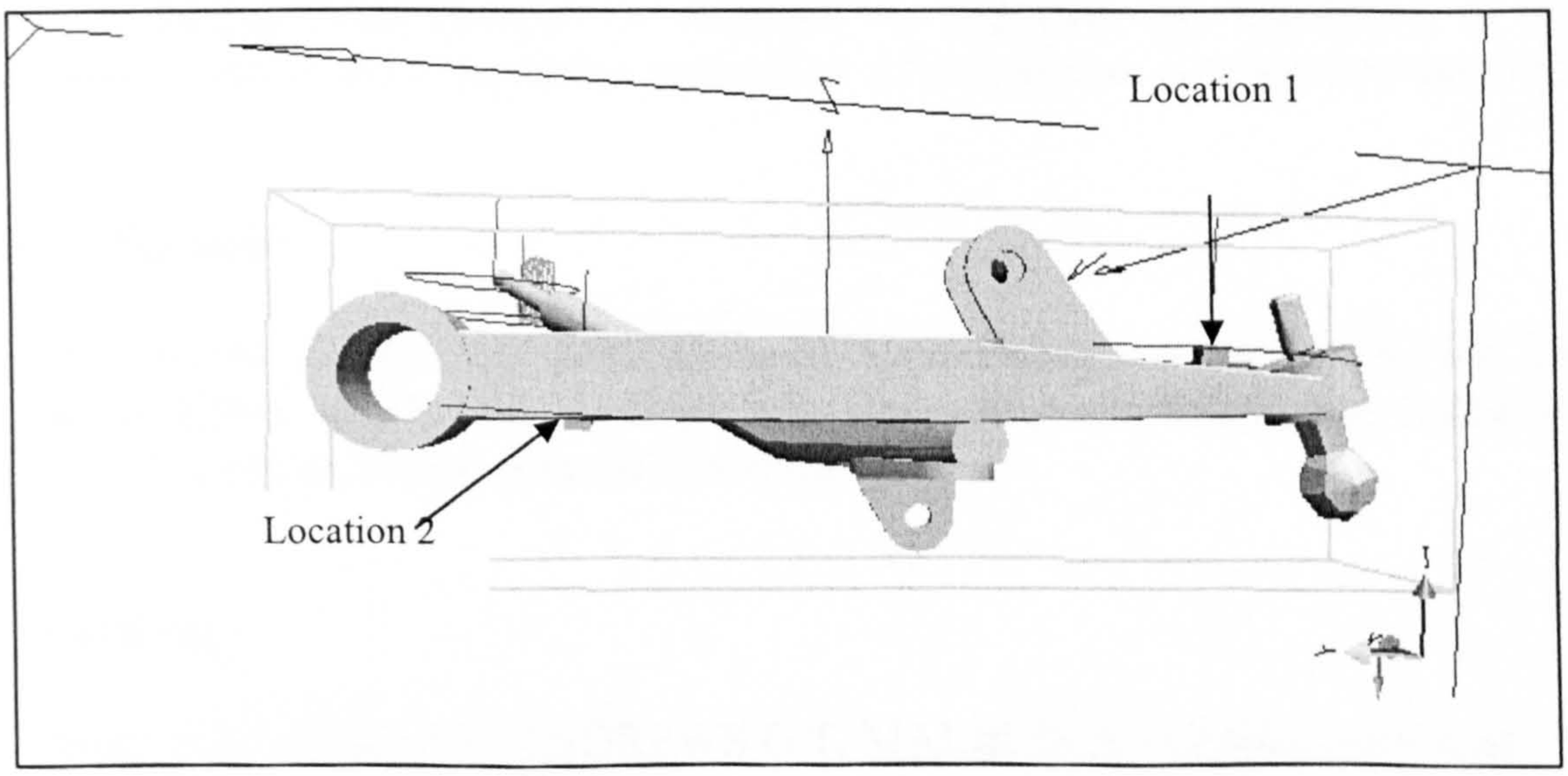

Figure 8: Lower Arm Representation and the Location of Measurement

Acceleration power spectral density (PSD) is used to evaluate the results from cosimulation. In Figure 9, response at Location 1 and 2 indicate significant overestimation from the cosimulation, generally at all frequencies above 7 Hz. The predictions are quite acceptable below this frequency which includes the body resonance occurring at 1Hz (calculated). In contrast, there is large overestimation at the wheel hop frequency of 11.8Hz (calculated). This suggests that the analysis for the lower arm using the QVM is inappropriate due to the discrepancies at frequencies above 7 Hz. At present, results obtained from cosimulation using the QVM to evaluate dynamically loaded suspension components are not acceptable. Further refinement is necessary in order to assess whether the accuracy of the prediction increases when pitch and roll are allowed for.

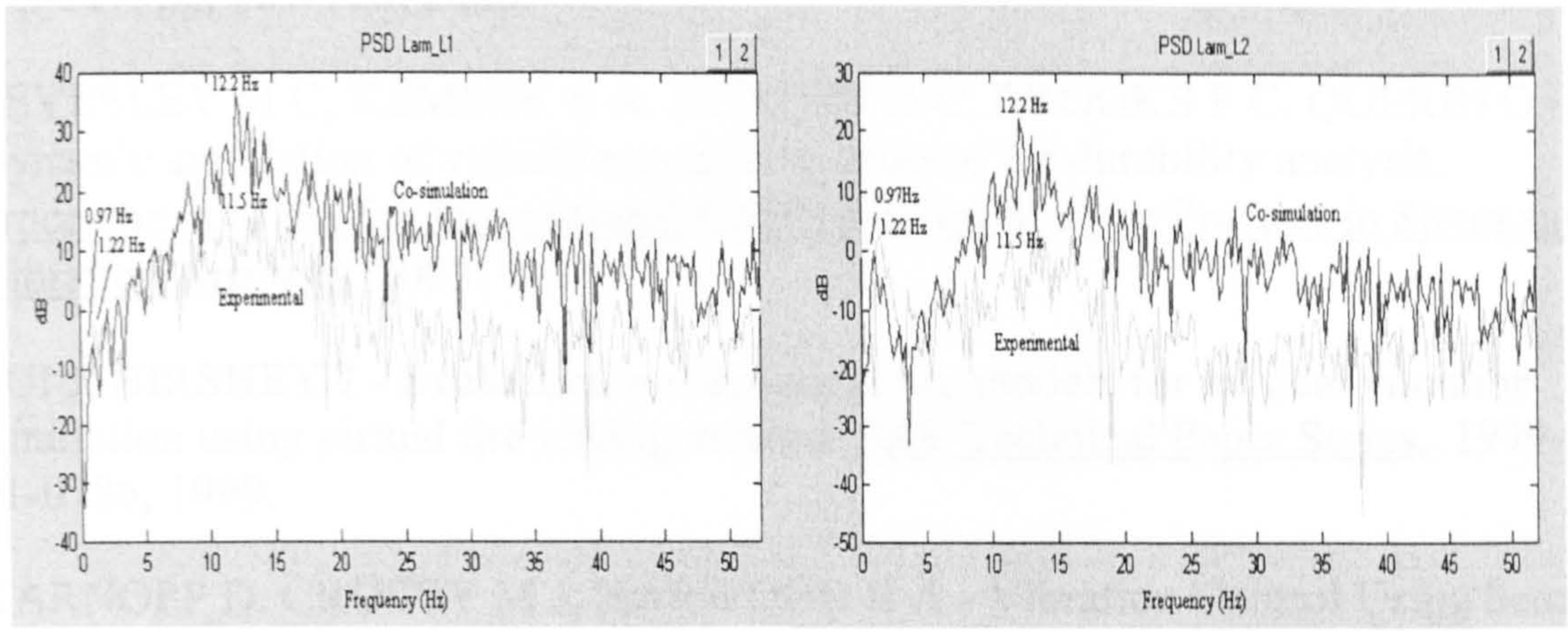

Figure 9: Corresponding Lower Arm PSD Acceleration at Location 1 & 2

Conclusions

An alternative method of determining durability loads of suspension components is presented. Several vehicle models in addition to different suspension systems are simulated and evaluated. The use of a quarter vehicle model (QVM) either in the form of a simple lumped parameter model or realistic model may not be appropriate for durability studies. Similarly, implementing semi-active control based on a QVM to a full vehicle model (FVM) results in deterioration in ride quality, even with each suspension corner acting independently. A suitable control strategy needs to be implemented, to take into account the effect of pitch and roll of the vehicle body. Further modelling enhancement is required to improve the capability of the cosimulation method allowing better estimation of suspension components durability loads.

Acknowledgement

The authors would like to thank MSC Software Corporation and MathWorks Inc. The first named author would like to thank the University of Malaya for financially supporting him during the progress of this research.

REFERENCES

1. FERRY W B, FRISE P R, ANDREWS G T, MALIK M A - Combining virtual simulation and physical vehicle test data to optimize durability testing. Fatigue & Fracture of Engineering Materials & Structures, Vol 25, pp. 1127-1134, 2002.

2. BLUNDELL M, HARTY, D – The multibody systems approach to vehicle dynamics. Elsevier Butterworth-Heinemann, 2004.

3. RAMLI R, POWNALL M, LEVESLEY M C, CROLLA D A - Dynamic analysis of semi-active suspension systems using a cosimulation approach. 3rd International Symposium on Multi-body Dynamics: Monitoring and Simulation Techniques, 391-399, 2004.

4. HAIBA M, BARTON DC, BROOKS PC, LEVESLEY MC - Using a quarter-vehicle multi-body model to estimate the service loads of a suspension arm for durability calculations. Proc. Instn. Mech. Engrs., Part K: J. Multi-body Dynamics,

Vol 217, pp. 121-133, 2003.

5. LEVESLEY M C, KEMBER S A, BARTON D C, BROOKS P C, QUERIN O - Dynamic simulation of vehicle suspension systems for durability analysis. Proceedings of the 5th International Conference on Modern Practice in Stress and Vibration Analysis, 2003.

6. SUI J, HIRSHEY J - Evaluation on analytical tire models for vertical vibration simulation using virtual tire testing method. SAE Technical Paper Series, 1999-01-0786, 1999.

7. KARNOPP D, CROSBY M J, HARWOOD R A - Vibration Control Using Semi-Active Force Generators. Journal of Engineering for Industry, 1974.

3) R. Ramli, M. Pownall, M. C. Levesley, and D. A. Crolla, "Dynamic Analysis of Semi-active Suspension Systems Using a Cosimulation Approach," presented at 3rd International Symposium on Multi-body Dynamics: Monitoring and Simulation Techniques, Loughborough, UK, 2004.

Abstract:

The aim of this paper is to demonstrate how the principles of cosimulation can be used to calculate the ride response of a vehicle with semi-active suspension. The ultimate goal is to use the approach developed for the estimation of component service loads, enabling optimisation of components based on fatigue life to be implemented. The cosimulation technique employed allows a dynamic vehicle model to be constructed in a Multi Body System (MBS) environment, while two key components, the tyre and active suspension systems, are concurrently simulated in a mathematical simulation environment. The packages used are MSC Visual Nastran MBS software and Mathworks MATLAB/Simulink software.

Since previous research [1, 2] has shown that a quarter vehicle model (QVM) is inappropriate for this type of analysis, a lumped parameter full vehicle model (FVM) has been developed in the MBS environment, though for preliminary validation the QVM is used. Using the cosimulation approach, the effects of the semi-active system and the tyre model on the vehicles response to potentially damaging transient inputs (step and potholes for example) are examined.

Results show that while the semi-active suspension system employed in this study significantly affects the response of the sprung mass (vehicle body), it has less effect on the unsprung mass (wheel and hub). The converse is true for the tyre model, where the results show different tyre models greatly affect the loads applied to the hub. The paper concludes that the approach adopted is an effective method of integrating the semi-active device, control strategy, and tyre model into the MBS vehicle model. It has significant benefits over alternative methods and has potential for use in the optimisation of suspension components based on fatigue life.

Keywords:

Cosimulation, multi-body system, semi-active vehicle suspension, vertical tyre modelling, service loads, load histories.

Nomenclature

C_{hard} = high damping coefficient

Cs = viscous damping coefficient

C_{soft} = low damping coefficient

F_d = damper force

F_t = vertical tyre force

Ks = passive suspension stiffness

Kt = tyre stiffness

Mb = vehicle body mass or sprung mass

Mw = wheel mass or unsprung mass

x = displacement road profile

z = displacement of vehicle components

$\dot{z}$ = velocity of vehicle components

$\ddot{z}$ = acceleration of vehicle components

$\dot{z}_b$ = sprung mass relative velocity

$\dot{z}_w$ = unsprung mass relative velocity

Introduction

The emerging trend in vehicle durability assessment is to utilise virtual prototyping, as a tool for dynamic design verification and as an alternative to physical durability testing. This is made possible with increased computing speed and improved software performance, allowing significant cost saving compared to physical testing. Research at the University of Leeds is seeking to link results from MBS analysis to FE models with structural optimisation algorithms, to generate a method for automating the design of light weight components with maximum fatigue life [3, 4]. Central to this method is the assumption that accurate load histories can be generated from MBS vehicle models when subjected to appropriate road inputs. Further, since the technique is currently being designed to remove the need for physical durability tests, the predicted load histories must be accurate for road inputs specifically intended to apply significant damage to a vehicle's components, such as large amplitude transient inputs generated by a step and potholes for example.

Clearly the tyre model is a key component of the model, converting road

displacements into forces applied to the suspension system. While some MBS software packages contain purpose made tyre models, the compromise between model complexity and accuracy/solution time as well as the ability to populating these models with appropriate parameters remains an issue. An alternative approach [1] is to build a the tyre model from spring and damper elements within the MBS model, though this approach may lack the flexibility to be able to assess quickly various tyre models with different MBS vehicle models.

Another key component within the suspension system is the main damper element. While most MBS packages allow complex non-linear passive dampers to be included in the model, few will allow easy integration of active or semi-active elements, which are of increasing interest in the automotive industry. Clearly, different actuators and control algorithms could have a profound affect on service loads applied to the suspension system, which need to be taken into account.

The aim of this paper is to show how these two key components can be integrated efficiently within an MBS vehicle model. The approach integrates an MBS based vehicle model representation, with tyre models and semi-active control models developed in a mathematical simulation environment. The intention of evaluating the load histories using this method is to enable the user to combine specific and specialised modelling tasks with different complexities, into one simulation code. The paper examines the efficacy of the modelling approach and compares preliminary results from the cosimulation method to a mathematical approach, in terms of tyre force, actuator force, sprung and unsprung mass displacements.

Cosimulation

The approach adopted for this study integrates an MBS model of the vehicle, with separate simulation codes for the semi-active controller and the for the tyre model. The main reason behind the approach, is to allow easy integration of subsystems i.e. vehicle models, suspension types, and tyre models, to be controlled under one simulation environment as illustrated in Figure 1. This, allows each of the subsystems to be developed, analysed, and validated separately. The input/output interface is controlled in MATLAB/Simulink [5] environment. An MBS modelling code, Visual Nastran [6] models the suspension system, whilst MATLAB/Simulink is again used to

develop semi-active control laws and tyre models. The output of the system, in the form of acceleration, velocity or displacement, is fed back to the MATLAB/Simulink code at predefined time steps. This process simultaneously computes the solution for both modelling codes.

In Figure 1, the cosimulation plant is divided into two phases. The first phase involves cosimulation of tyre models with a passive suspension system. The initial analysis is centred on vertical tyre forces generated from point contact (PC) and fixed footprint (FFP) models, to allow verification against other research. The cosimulation flow may be understood as follows. The tyre subsystem (PC or FFP models) receives a displacement input from the road profile, x, in the form of transient (steps or bumps) input or random input. The product of this displacement and tyre stiffness generates a force output, F_t , which is then fed to the MBS vehicle subsystem as a force input. The force input excites the unsprung mass producing displacement, velocity and acceleration responses of the bodies within the model. With passive suspension in use, the forces exerted by the spring and passive damper are calculated within the MBS model from the relative displacement and relative velocity, between the sprung and unsprung mass, respectively. The response of the unsprung mass is fed back to the tyre model. The output displays dynamic responses of the body and wheel in the form of displacement, z, velocities, $\dot{z}$ or accelerations, $\ddot{z}$.

Detailed analyses of the tyre force from the PC and FFP models were performed initially within MATLAB/Simulink for the purpose of validating the models against published data. Once achieved, the same models are linked to the MBS system and used in the cosimulation environment, as illustrated in Figure 1. Sprung and unsprung mass displacement profiles, and the tyre force are compared with the conventional simulation using MATLAB/Simulink.

The second phase of the cosimulation introduces the semi-active controller subsystem. The dynamic responses from the MBS vehicle model in the form of displacement, velocity, or acceleration are fed to a semi-active controller subsystem where suitable algorithm are coded in the MATLAB/Simulink environment. Then, the subsystem sends a force output, F_d, back to the MBS vehicle model to represent the actuator force in response to the road excitation. In these preliminary studies, a simple 2 degree of

freedom (2DOF) quarter vehicle model (QVM), constructed in Visual Nastran, is used to allow validation against other published data. The MBS model requires a force signal from MATLAB/Simulink to drive the actuator that is built into the hub. The position of the hub is fed back into the MATLAB/Simulink tyre model from the MBS model and simulation parameters are controlled from MATLAB/Simulink. Initial results are given focusing on the effects of the semi-active system on the vehicle and comparing these to a passive system.

Vehicle Models

The vehicle models describe in this section are confined to vertical dynamics. Haiba *et. al.* [1] concluded that the predicted acceleration power spectral density of a quarter vehicle model (QVM) overestimated the experimental results particularly in vertical acceleration. Since a QVM does not take into account vehicle body roll and pitch, analysis of the suspension arm load histories should consider a full vehicle model (FVM). This was confirmed by Levesley *et. al.* [2] with a simplified FVM. Both of the studies were based on vehicle modelling in multi-body system (MBS) alone with passive suspension only. In light of this research, it is planned that the complexity of the vehicle models used will grow in stages, starting with validation of the cosimulation approach (the main focus of this paper) using of a 2DOF QVM. A full vehicle model (FVM) in a simplified format (7DOF) has subsequently been developed (though results are not presented in this paper). Ultimately, an MBS model of realistic complexity, will be required in which each of the main components of the suspension is represented. This will allow investigation into the effects of including a semi active suspension element on the service load histories of the individual suspension components such as the arms, for subsequent stress analysis and optimisation. Through out this study the parameters given in Table 1 have been used which represent a generic Multi-Purpose Vehicle (MPV).

Vehicle Parameters	Units
Sprung Mass, Mb	400 kg
Unsprung Mass, Mw	47.75 kg
Suspension Stiffness, Ks	22000 N/m
Damping constant, Cs	1500 N.s/m
Tyre Stiffness, Kt	239000 N/m

Table 1 Quarter vehicle model parameters of a multi-purpose vehicle

Tyre Models

The development of the tyre models is based on vertical tyre dynamics, modelled in MATLAB/Simulink. Following an initial study, it was concluded that the fixed footprint tyre model (FFP) [7] offered a substantial improvement in simulating tyre forces over the single point contact (PC) spring model, without unduly effecting model complexity and hence simulation times. Although other models have also been developed, it is the FFP model that has been presented in this cosimulation study. Results are compared to the PC model to due to its simplicity, wide spread usage and hence ease of validation. Both tyre models require a negative tyre force saturation to facilitate the ability of the tyre to leave the ground if a negative step is encountered. This non-linearity is an important element in the tyre model.

Semi-active Control Model

The principal aim of incorporating semi-active systems is to evaluate its effect on the suspension component service load histories compared to those generated from a passive system, [1]. Unlike the active system, semi-active systems are chosen because of their minimal power consumption, simplicity in developing appropriate control laws, and minimal weight addition. In approximating the ideal skyhook concept [8, 9], a switchable semi-active control strategy is adopted as shown in the equation below.

$$F_d = \begin{cases} C_{hard} \cdot \left(\dot{z}_b - \dot{z}_w\right) \cdots\cdots \text{ if } \dot{z}_b \cdot \left(\dot{z}_b - \dot{z}_w\right) > 0 \\ C_{soft} \cdot \left(\dot{z}_b - \dot{z}_w\right) \cdots\cdots \text{ if } \dot{z}_b \cdot \left(\dot{z}_b - \dot{z}_w\right) < 0 \end{cases}$$

For this initial study, a 2-state switchable controller is selected for its simple controller development which has been experimentally verified. The controller objective minimises vehicle body response by controlling the relative velocity of the sprung, $\dot{z}_b$ and unsprung mass, $\dot{z}_w$, across the damper. A positive value of the relative velocity and the quantity $\dot{z}_b$ $(\dot{z}_b - \dot{z}_w)$ would switch the damper to a hard setting, C_{hard}. It occurs when the vehicle body velocity, $\dot{z}_b$ is larger than the velocity of the wheel, $\dot{z}_w$, placing the damper in tension. This large damper force, F_d acts in a direction opposite to the relative motion of the masses. In contrast, if the sprung mass velocity, $\dot{z}_b$ is smaller than that of the unsprung mass, both quantities, $(\dot{z}_b - \dot{z}_w)$ and $\dot{z}_b$ $(\dot{z}_b - \dot{z}_w)$ shall be negative in which case the damper is compressed. The damper then switches off, creating a low or minimal force, F_d, from the soft damper setting, C_{soft}.

Road Input Representations and Simulation Solver

In this preliminary study, the road input is modelled as a simple step with a height of 0.023 m. The model is simulated to run at a constant forward velocity of 47 km/hr. The input is applied after three seconds, allowing static deflection of the vehicle to reach its equilibrium state. More realistic road inputs, including potholes and a durability pavé road input [1], have been developed but results presented in this paper are confined to the step input, due to ease of validation. The ultimate aim is to generate road inputs that match typical transient inputs known to induce significant damage within a suspension system. All simulation in MATLAB/Simulink uses the variable step (ODE 113 Adams-Bashforth-Moulton PECE multi-step) solver for tight tolerance with relative tolerance of $1e^{-6}$. In cosimulation the same solver is used in conjunction with the MBS Kutta-Merson integrator having a variable integration step size.

Results and Discussions

In order to obtain validated results from the cosimulation approach, preliminary analysis of the quarter vehicle model (QVM) focused on comparison with established results. A QVM with point contact (PC) tyre model was simulated both in MATLAB/Simulink and using the MBS software and results compared with those from [2]. Similar sprung and unsprung mass displacements were observed suggesting that the QVM models from both software were valid for further analysis.

Cosimulation with Tyre Model – Phase 1

Two basic vertical tyre models were selected for this study i.e. the point contact (PC) and the fixed footprint (FFP). Results for QVM response to the step input are shown in Figure 2. The peak tyre force of the PC model can be seen to exceeded the force of the FFP model by 600-700 N, with the latter lagging by a few milliseconds. The corresponding unsprung mass displacement profiles revealed similar characteristics to the tyre force in terms of the delay, however differences in peak amplitude are much smaller. Very minimal difference was observed when comparing the displacement of the sprung mass (not shown). Investigations using QVMs of a variety of other vehicles shows similar trends, i.e. the type of tyre model has a significant influence on the load histories generated but has less effect on the unsprung mass response and very little effect on the sprung mass.

To investigate the effects of parameter variation in the tyre model, the tyre stiffness in the PC model was varied between 191,200 and 286,800 N/m, as indicated in Figure 3. As expected and in line with the previous results, varying tyre stiffness can be seen to have a significant impact on the load history but less effect on the unsprung mass response. Less still effect was observed on the sprung mass response (not shown).

Due to the simplicity of the MBS vehicle model at this stage (2DOF QVM), direct comparison between results from the cosimulation approach and a model simulated in MATLAB/Simulink alone is possible. Results, compared well highlighting some important issues related to efficiency verses accuracy. For ease of validation, this initial study uses a step input with a PC tyre model. As can be seen in Figures 2 and 3, this results in an instantaneous application of force to the MBS model. Clearly this is not a true representation of the actual tyre. In reality there would be a more gradual rise in force due to the geometry and flexibility of the tyre as it rolls over the step. This can be taken into account in a number of ways. The response of the FFP tyre model generates the force in discrete stages depending on the number of springs used. This can be seen in Figure 2. Instantaneous step changes in force still exist, however the more springs used the more representative the model becomes but this occurs at the expense of computational efficiency. An alternative would be to use the PC tyre model but alter the step input to take account of the geometry affects of a rigid wheel rolling over the step. This profile would however need to be applied as a series of discrete steps. Again, more steps would result in a more gradual application of the force and hence a more representative model, but once more at the cost of computational efficiency. Sudden changes in force affect the integration step size required to produce an accurate simulation. This can be seen in Figure 4 where results from the MATLAB/Simulink simulation using a variable integration step size are compared to the cosimulation results with two integration step sizes limits imposed. With a minimum step size of 0.005 seconds, the responses are markedly different. As the step size is reduced to 0.001 seconds the unsprung mass response is seen to agrees closely with the variable step simulation, though significant differences in the force remain. These differences are however as a result of the over simple PC tyre model, which produces a large instantaneous increase in force, hence a simple model with a simple input may not necessarily be computationally efficient if small integration step sizes are require to model it accurately.

Cosimulation with Semi-active Controller – Phase 2

In phase 2, efforts were focused on the development and validation of the semi-active suspension system in a form suitable for integration within the cosimulation environment established in phase 1. The control laws and algorithms have been implemented in MATLAB/Simulink. Inputs are in the form of sprung and unsprung mass velocities and output is in the form of an actuator force, based on relative velocity and a switchable damper. Simulation results were obtained and validated against established data [10]. The simulation for the MPV is given in Figure 5. It confirms that the semi-active control strategy improves the ride quality in terms of lower body displacement. Both the unsprung mass and actuator force registered significant differences when compared to the linear passive damper. Clearly this may unduly affect durability of the suspension components at the expense of improving comfort.

Conclusions

i. A cosimulation environment has been established and validated for relatively simple vehicle and tyre models. It allows simple development and integration of key subsystems, in this case the tyre model and a semi-active suspension device.

ii. The influence of the tyre model on the sprung mass response was found to be minimal. Though its effect on the unsprung mass displacement was also small, its effect on the load history applied to it was significant. This has important implications if these load histories are to be used for optimisation of suspension components based on fatigue life.

iii. A relatively simple point contact tyre model may not be as computationally efficient as expected due to the small integration step sizes required to cope with the large and unrealistic instantaneous changes in force it generates.

iv. Evaluation of the semi-active suspension system revealed that the control strategy improves the vehicle body response, but has a significant influence on both the unsprung mass response and the force applied by the actuator to the suspension components.

References

[1] M. Haiba, D. C. Barton, P. C. Brooks, and M. C. Levesley, "Using a Quarter-vehicle Multi-body Model to Estimate the Service Loads of a Suspension Arm for Durability Calculations," *Proc. Instn. Mech. Engrs., Part K: J. Multi-body Dynamics*, vol. 217, pp. 121-133, 2003.

[2] M. C. Levesley, S. A. Kember, D. C. Barton, P. C. Brooks, and O. M. Querin, "Dynamic Simulation of Vehicle Suspension Systems for Durability Analysis," presented at Proceedings of the 5th International Conference on Modern Practice in Stress and Vibration Analysis, Glasgow, 2003.

[3] M. Haiba, D. C. Barton, P. C. Brooks, and M. C. Levesley, "Review of Life Assessment Techniques Applied to Dynamically Loaded Automotive Components," *Computers and Structures*, vol. 80, pp. 481-494, 2002.

[4] M. Haiba, D. C. Barton, P. C. Brooks, and M. C. Levesley, "The Development of an Optimisation Algorithm Based on Fatigue Life," *Internal Journal of Fatigue*, vol. 25, pp. 299-310, 2003.

[5] Anon., "MATLAB-SIMULINK - User Guides," 6.0 ed. Natick: The Mathworks, Inc., 2002.

[6] Anon., "MSC Visual Nastran Desktop - User Guide," The MSC.Software Corporation, 2003.

[7] K. M. Captain, A. B. Boghani, and D. N. Wormley, "Analytical Tire Models for Dynamic Vehicle Simulation," *Vehicle System Dynamics*, vol. 8, pp. 1-32, 1979.

[8] D. Karnopp, M. J. Crosby, and R. A. Harwood, "Vibration Control Using Semi-Active Force Generators," *Journal of Engineering for Industry*, 1974.

[9] D. Moline, S. Floyd, S. Vaduri, and E. H. Law, "Simulation and Evaluation of Semi-Active Suspensions," *SAE Technical Paper Series*, 1994.

[10] K. Sharma, D. A. Crolla, and D. A. Wilson, "Derivation of a Control Law for a 3 State Switchable Damper Suspension System for Improving Road Vehicle Ride Characteristics," presented at International Symposium on Theory of Machines and Mechanisms, Nagoya, Japan, 1992.

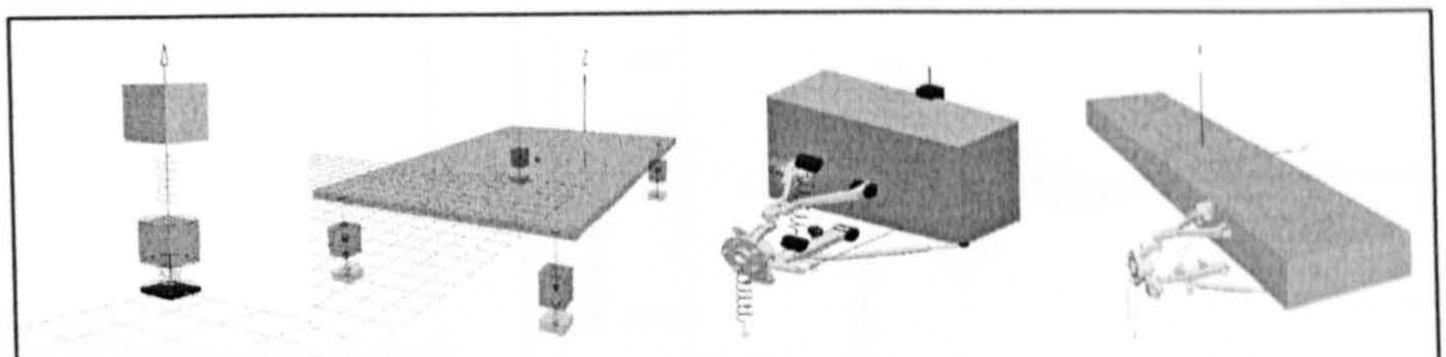

QVM, FVM
(Simplified & Realistic Suspension Model)

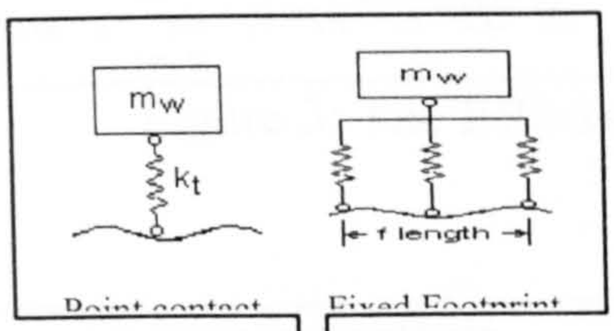

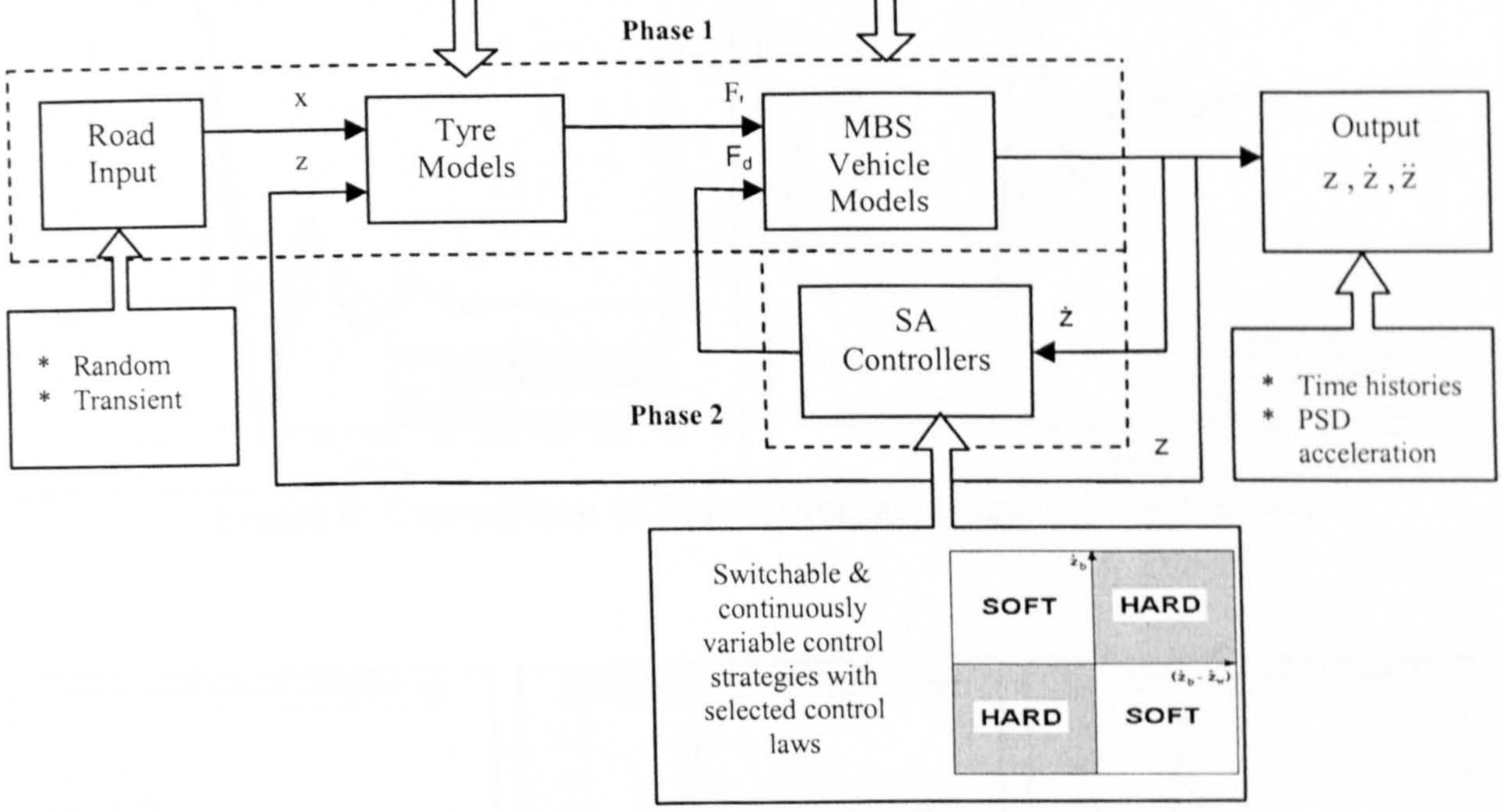

Figure 1: Cosimulation Plant

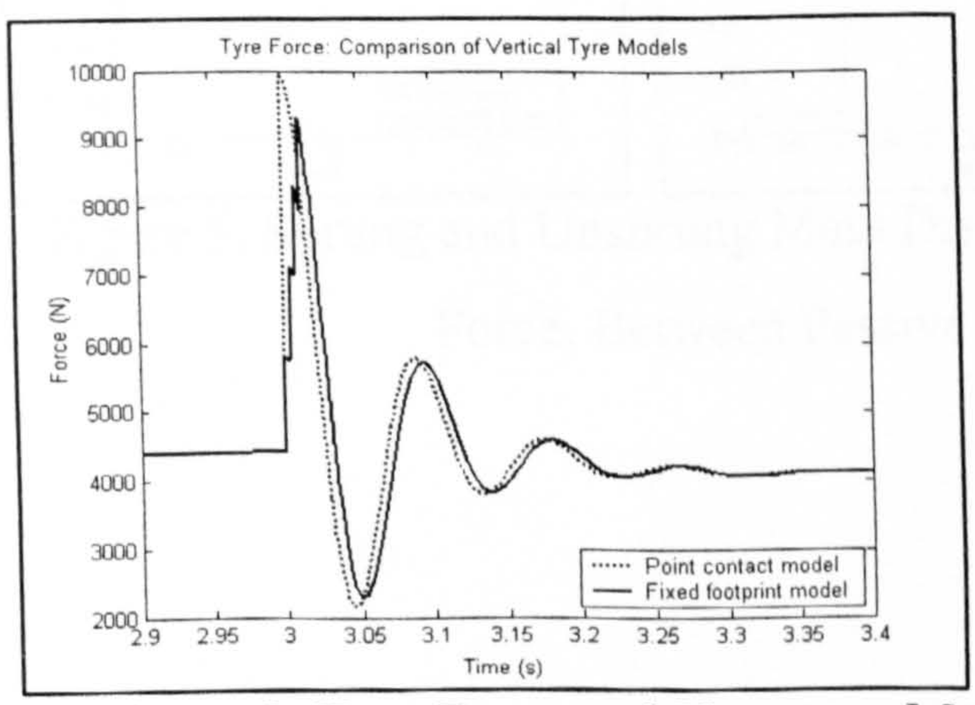

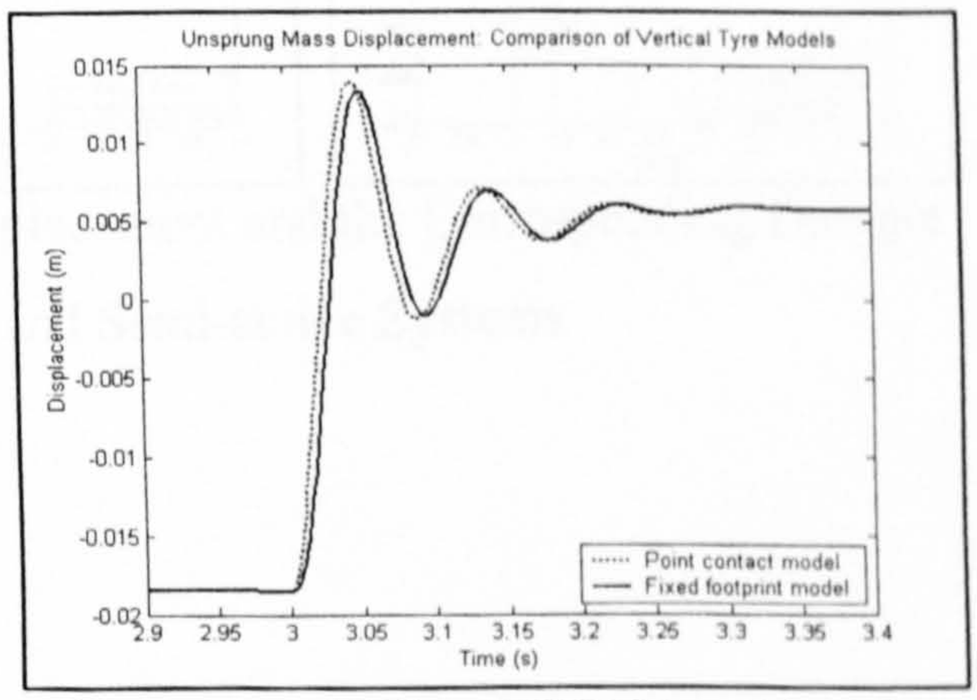

Figure 2: Tyre Force and Unsprung Mass Response of PC and FFP Tyre Models

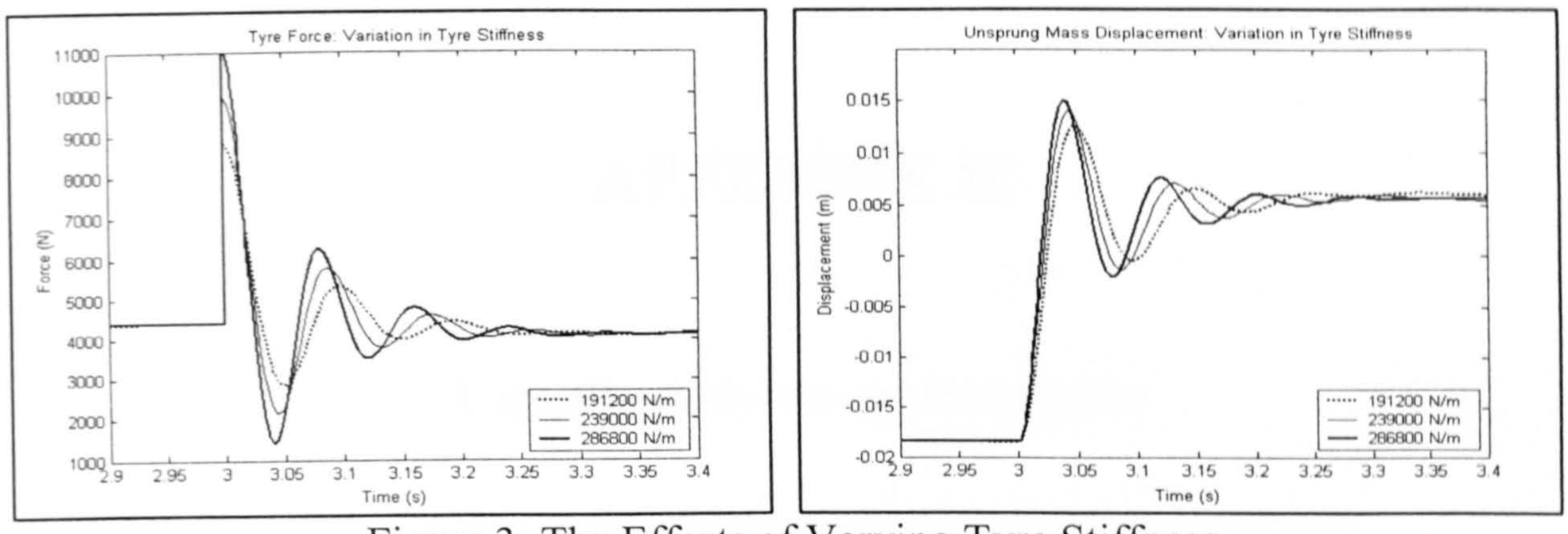

Figure 3: The Effects of Varying Tyre Stiffness

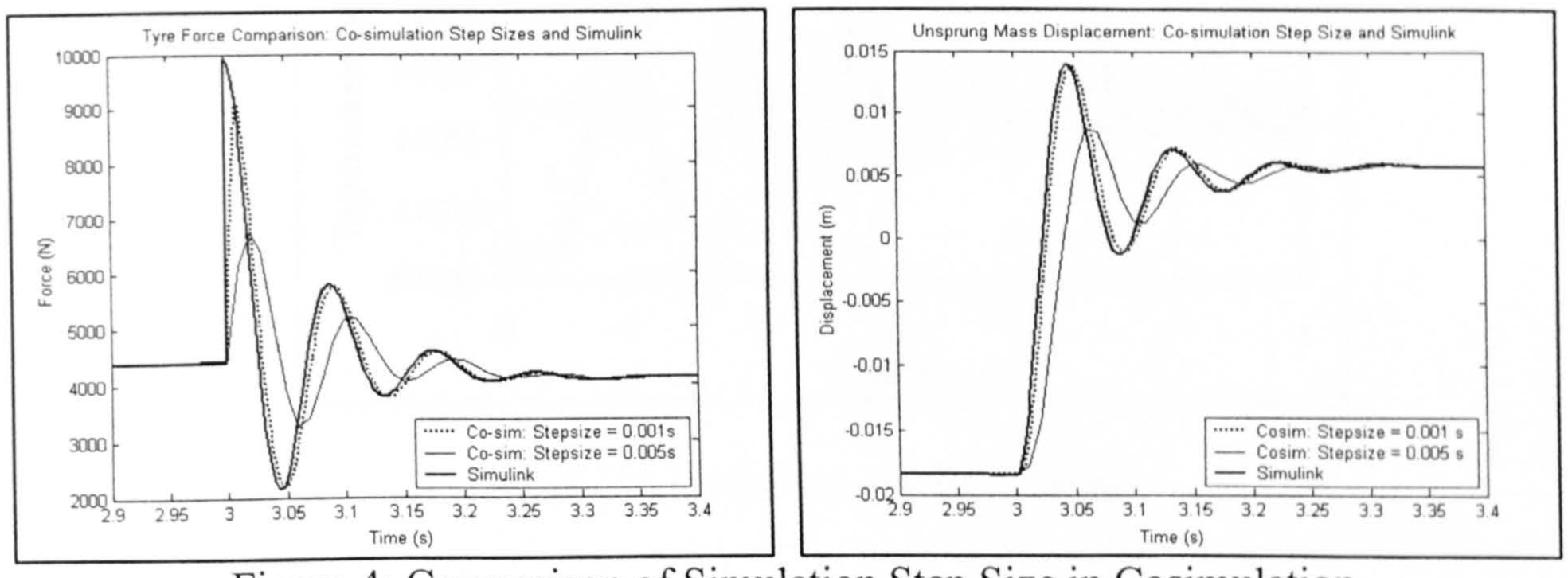

Figure 4: Comparison of Simulation Step Size in Cosimulation

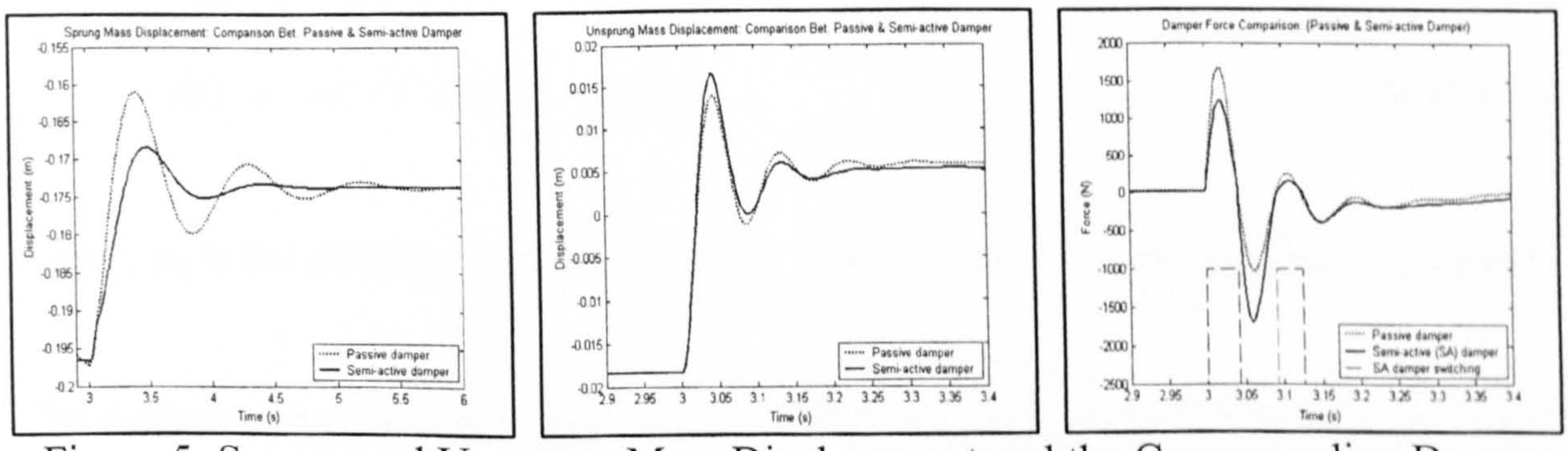

Figure 5: Sprung and Unsprung Mass Displacement and the Corresponding Damper Force, Between Passive and Semi-active Systems

APPENDIX II

Logarithmic Decrement Calculation

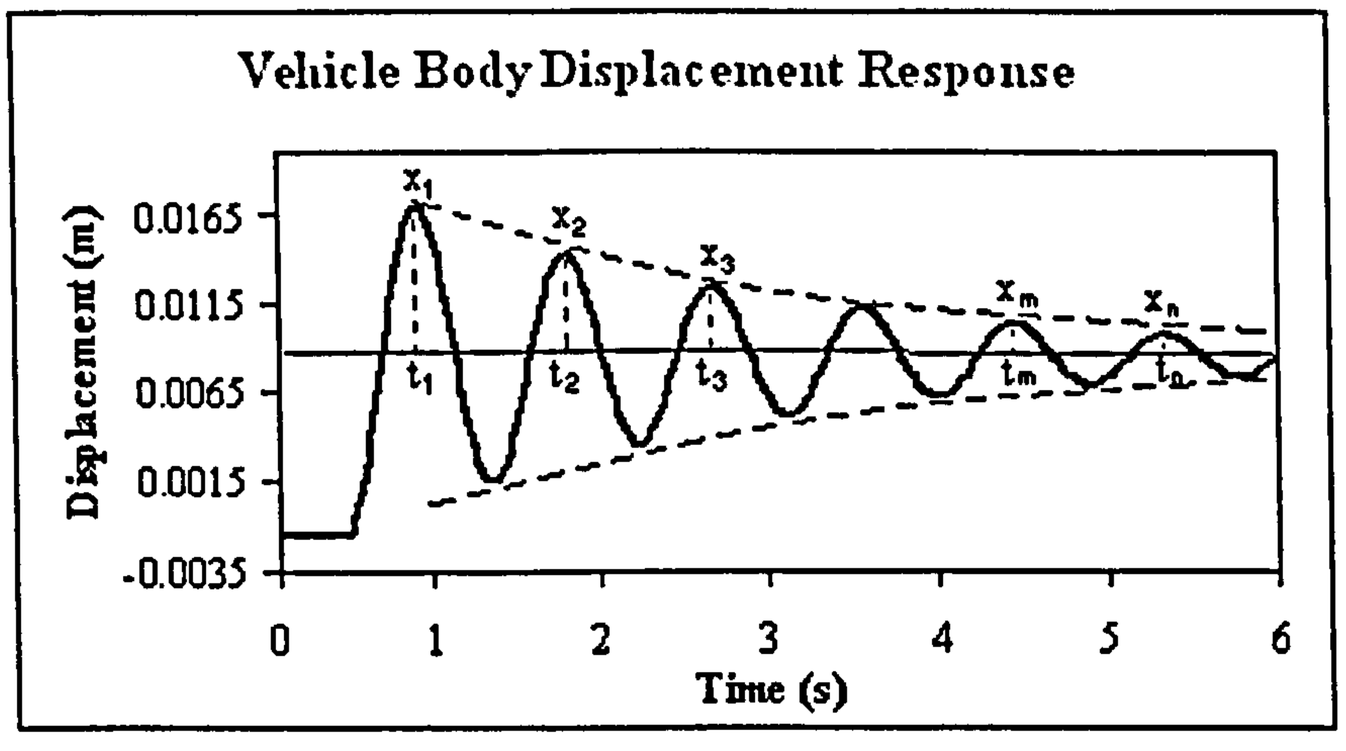

Figure A2.1: Response of Realistic QVM

Figure A2.1 shows a typical solution for an underdamped system where the general solution can be written as:

$$x(t) = Ae^{-\zeta\omega_n t}\sin(\omega_d t + \theta) \qquad \textbf{Eq A2.1}$$

where, ω_d is the damped natural frequency, while A and θ is the integration constant.

The dashed curve lines in Figure A2.1 refers to the decay rate and is equals to $Ae^{-\zeta\omega nt}$, where $\zeta\omega_n$ is a constant. Therefore, the general form of logarithmic decrement δ may be expressed as:

$$\delta = \ln\frac{x(t)}{x(t+T)} \qquad \textbf{Eq A2.2}$$

for which T is the period of a complete oscillation.

If T is measured at the peak amplitude, then Eq A2.2 can be rewritten as:

$$\delta = \ln\frac{x_1}{x_2} = \ln\frac{x_2}{x_3} = \ln\frac{x_m}{x_n} \qquad \textbf{Eq A2.3}$$

where x_1/x_2, x_2/x_3 ... and x_m/x_n are ratio of successive peaks.

With the damped natural frequency, $\omega_d = 2\pi/T$, substituting Eq A2.1 into Eq A2.2, reduces the term δ to:

$$\delta = \ln e^{\zeta\omega_n T} = \zeta\omega_n T \qquad \textbf{Eq A2.4}$$

where, T is measured between two successive peaks.

For example, taking the first ratio in Eq A2.3, the corresponding $T = t_2 - t_1$. Since, $\omega_d = \omega_n\sqrt{1-\zeta^2}$ and $T = \omega_d / 2\pi$, substituting these expressions into Eq A2.4 and the damping ratio, ζ yields:

$$\zeta = \frac{\delta}{\sqrt{4\pi^2 + \delta^2}} \qquad \textbf{Eq A2.5}$$

With known damping ratio, ζ the natural frequency, ω_n can be determined with Eq A2.5. Thus, the equivalent suspension stiffness, $k_s = m_b\omega_n^2$. Using $\zeta = c_s/c_{cr}$, where $c_{cr} = 2\sqrt{k_s m_b}$, the equivalent suspension damping, c_s can be obtained. This formulation can be calculated using a spreadsheet program to estimate the equivalent vehicle parameters from other ratio of successive peaks.

APPENDIX III

Natural Frequency Calculations of a Lumped Quarter Vehicle Model

1. Ride Rate (RR)

The formulation assumes that the suspension stiffness and the tyre stiffness are in series.

$$RR = \sqrt{\frac{k_s . k_t}{k_s + k_t}} \qquad \textbf{Eq A3.1}$$

2. Body Bounce Natural Frequency, W_{n1} or f_{n1}

$$W_{n1} = \sqrt{\frac{RR}{M_b}} \quad (in\ rad/\sec) \qquad \textbf{Eq A3.2}$$

or

$$f_{n1} = \frac{W_{n1}}{2\pi} \quad (in\ Hz) \qquad \textbf{Eq A3. 3}$$

3. Wheel Hop Frequency:

$$W_{n2} = \sqrt{\frac{k_s + k_t}{M_w}} \quad (in\ rad/\sec) \qquad \textbf{Eq A3.4}$$

or

$$f_{n2} = \frac{W_{n2}}{2\pi} \quad (in\ Hz) \qquad \textbf{Eq A3.5}$$

where,

k_s = suspension stiffness (in N/m)
k_t = tyre stiffness (in N/m)
M_b = sprung mass (m)
M_w = unsprung mass (m)

Example 1:

Quarter Car Data from Crolla *et al.*:

Ks = 22000 N/m
Kt = 192000 N/m
Mb = 317.5 kg
Mw = 45.4 kg

Bounce Natural Frequency = 7.9 rad/sec (1.3 Hz)

Wheel Hop Frequency = 68.7 rad/sec (10.9 Hz)

Example 2:

MPV Quarter Car Data :

Ks = 31000 N/m
Kt = 239000 N/m
Mb = 535 kg
Mw = 47.75 kg

Bounce Natural Frequency = 7.2 rad/sec (1.14 Hz)

Wheel Hop Frequency = 75.2 rad/sec (11.97 Hz)

APPENDIX IV

Obtaining PSD and RMS Values using MATLAB Commands.

MATLAB Script File

```
% STEP 1: LOAD RESULT FILE FROM MICROSOFT EXCEL (in .csv format)
% Ensure no headers and footers in the spreadsheet. Just plain data file.
% Ensure current directory in MATLAB is in the same directory of the file location.
data=csvread('LArmLoc2_PasifExpVsCosim.csv');
%
% STEP 2: ASSIGN VARIABLE NAMES TO LOADED DATA
% time values in 1st column of the (.csv) file
t=data(:,1);
% data values in the 2nd, 3rd and 4th columns.
X1=data(:,2);  % corresponds to results in longitudinal (x) direction
X2=data(:,3);  % corresponds to results in lateral (y) direction
X3=data(:,4);  % corresponds to results in vertical (z) direction
%
% STEP 3: GENERATING PSD & CALCULATING RMS VALUES
fs=500;          % sampling frequency
q=1; r=3000;   % index values to select frequency range of interest
%
% STEP 4: GENERATE PSD DATA
[P1,f1]=periodogram(X1,[],[],fs);          % P1 = PSD in x direction; f1 = frequency vector
% STEP 5: GENERATE RMS VALUES
LArmL2_Exp1RMS=trapz(f1(q:r),P1(q:r)); % integral gives area under PSD plot over freq (q to r)
LArmL2_Exp1RMS=sqrt(LArmL2_Exp1RMS);   % square root of area to obtain RMS value
%
% REPEAT FOR THE OTHER TWO DIRECTIONS
%
% GENERATE PSD DATA
[P2,f2]=periodogram(X2,[],[],fs);          % P2 = PSD in Y direction; f2 = frequency vector
% GENERATE RMS VALUES
LArmL2_Exp2RMS=trapz(f2(q:r),P2(q:r)); % integral gives area under PSD plot over freq (q to r)
LArmL2_Exp2RMS=sqrt(LArmL2_Exp2RMS);   % square root of area to obtain RMS value
%
% GENERATE PSD DATA
[P3,f3]=periodogram(X3,[],[],fs);          % P3 = PSD in Z direction; f3 = frequency vector
% GENERATE RMS VALUES
LArmL2_CosimRMS=trapz(f3(q:r),P3(q:r)); % integral gives area under PSD plot over freq (q to r)
LArmL2_CosimRMS=sqrt(LArmL2_CosimRMS);  % square root of area to obtain RMS value
%
% READ RMS VALUES IN MATLAB WORKSPACE
%
% Plot Time Histories and PSDs
figure
hold on
plot(t,X1,'k-','LineWidth',2.0)
plot(t,X2,'k-','LineWidth',1.0)
plot(t,X3,'k:','LineWidth',2.0)
legend('Longitudinal','Lateral','Vertical')
xlabel('Time (s)')
ylabel('Acceleration (m/s^2)')
```

```
title('Lower Arm Location 2: Acceleration Histories')
%
figure
hold on
plot(f1(q:r),P1(q:r),'k-','LineWidth',2.0)
plot(f2(q:r),P2(q:r),'k-','LineWidth',1.0)
plot(f3(q:r),P3(q:r),'k:','LineWidth',2.0)
legend('Longitudinal','Lateral','Vertical')
ylabel('PSD Acceleration (m/s^2)^2/Hz')
xlabel('Frequency (Hz)')
title('Lower Arm Location 2: PSD Acceleration')
%
```

Sample Time and PSD Plot

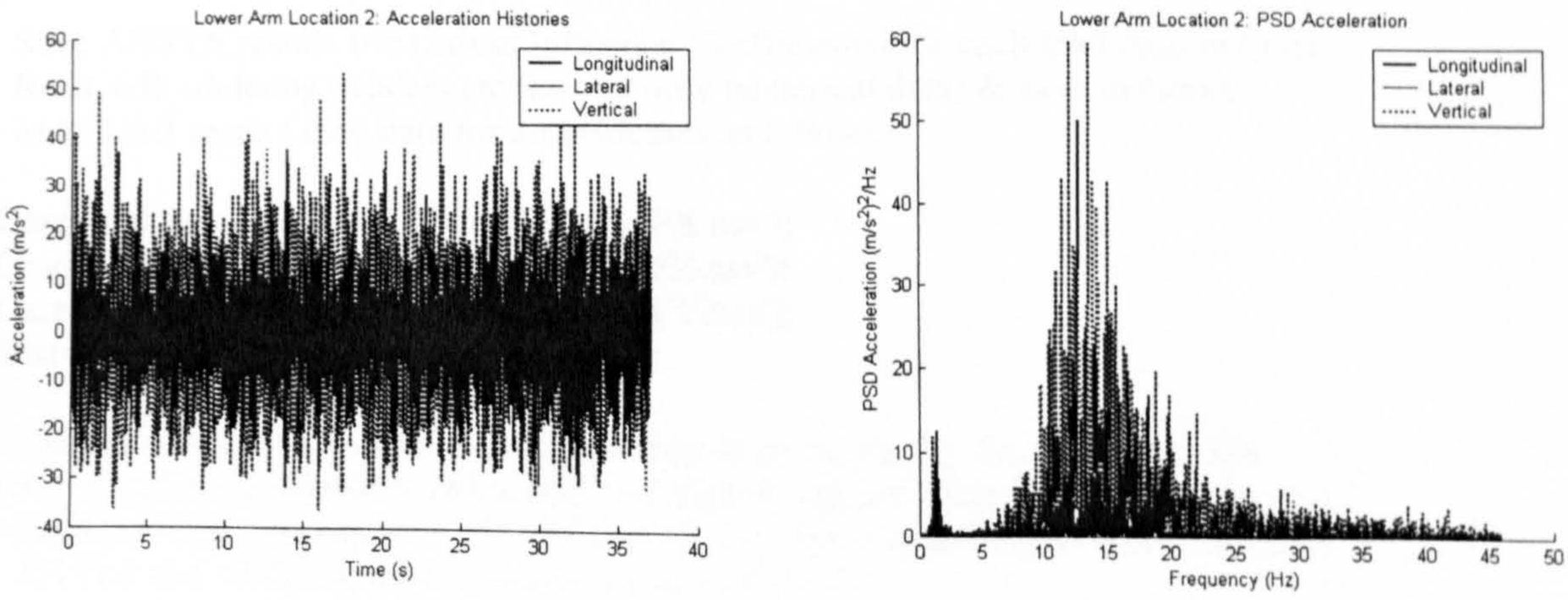

Figure A4.1: (a) Time and (b) PSD plots

APPENDIX V

Calculating Total Dynamic Stress Histories and Cyclic Stress Ranges

Calculating Total Stress Histories with MATLAB Script File

```
% Calculating Total Stress Histories for Fatigue Estimation
%
% Save ANSYS results file (Stress Influence Coefficients) for each load case in (.txt)
% Read, edit (deleting headers etc leaving only numerical data) & save in (.csv)
% MATLAB reads (.csv) data for all loadcases as follows:
%
LCase1 = csvread ('LCase1_CompStress12FX.csv');
LCase2 = csvread ('LCase2_CompStress12FZ.csv');
LCase3 = csvread ('LCase3_CompStress12FY.csv');
LHist = csvread ('LHistPasif_tFxyz.csv');
%
% Each load case (SIC) consists of component stresses: Sx, Sy, Sz, Sxy, Syz, Szx
% Sx, Sy & Sz are normal stresses; and Sxy, Syz & Szx are shear stresses
% Load histories consists of: t, FX, FY and FZ directions according to vN4D output
% ANSYS and vN4D sign conventions are not the same
% Note:
%     LCase1_-FX in ANSYS corresponds LHist_FY in vN4D
%     LCase2_-FZ in ANSYS corresponds LHist_FX in vN4D
%     LCase3_+FY in ANSYS corresponds LHist_FZ in vN4D
%
% Extracts the component stresses from each load case
%
SxLC1=LCase1(:,1);SyLC1=LCase1(:,2);SzLC1=LCase1(:,3);SxyLC1=LCase1(:,4);SyzLC1=LCase1(:,
5);SzxLC1=LCase1(:,6);
SxLC2=LCase2(:,1);SyLC2=LCase2(:,2);SzLC2=LCase2(:,3);SxyLC2=LCase2(:,4);SyzLC2=LCase2(:,
5);SzxLC2=LCase2(:,6);
SxLC3=LCase3(:,1);SyLC3=LCase3(:,2);SzLC3=LCase3(:,3);SxyLC3=LCase3(:,4);SyzLC3=LCase3(:,
5);SzxLC3=LCase3(:,6);
%
% Extracts load history components
FX=LHist(:,2);FY=LHist(:,3);FZ=LHist(:,4);t=LHist(:,1);
%
% Calculate Stress Histories for ALL nodes (i=1:42)
% Multiply each load case with the corresponding load history
% Determine Total Dynamic Stress Histories for each component stresses by applying superposition
principle
% Note that the output sampling interval is 2ms equivalent to sampling rate of 500 Hz
%
        for i=1:42;
                Sxt(:,i)=(SxLC1(i).*FY(:))+(SxLC2(i).*FX(:))+(SxLC3(i).*FZ(:));
                Syt(:,i)=(SyLC1(i).*FY(:))+(SyLC2(i).*FX(:))+(SyLC3(i).*FZ(:));
                Szt(:,i)=(SzLC1(i).*FY(:))+(SzLC2(i).*FX(:))+(SzLC3(i).*FZ(:));
                Sxyt(:,i)=(SxyLC1(i).*FY(:))+(SxyLC2(i).*FX(:))+(SxyLC3(i).*FZ(:));
                Syzt(:,i)=(SyzLC1(i).*FY(:))+(SyzLC2(i).*FX(:))+(SyzLC3(i).*FZ(:));
                Szxt(:,i)=(SzxLC1(i).*FY(:))+(SzxLC2(i).*FX(:))+(SzxLC3(i).*FZ(:));
        end
% Randomly verify stress histories at nodes by cross checking with MSoft Excel or through calculation
```

```
Sxt((1:3),(1:3))
plot(t,Sxt(:,1),t,Sxt(:,5))
```

Sample of Dynamic Stress Histories

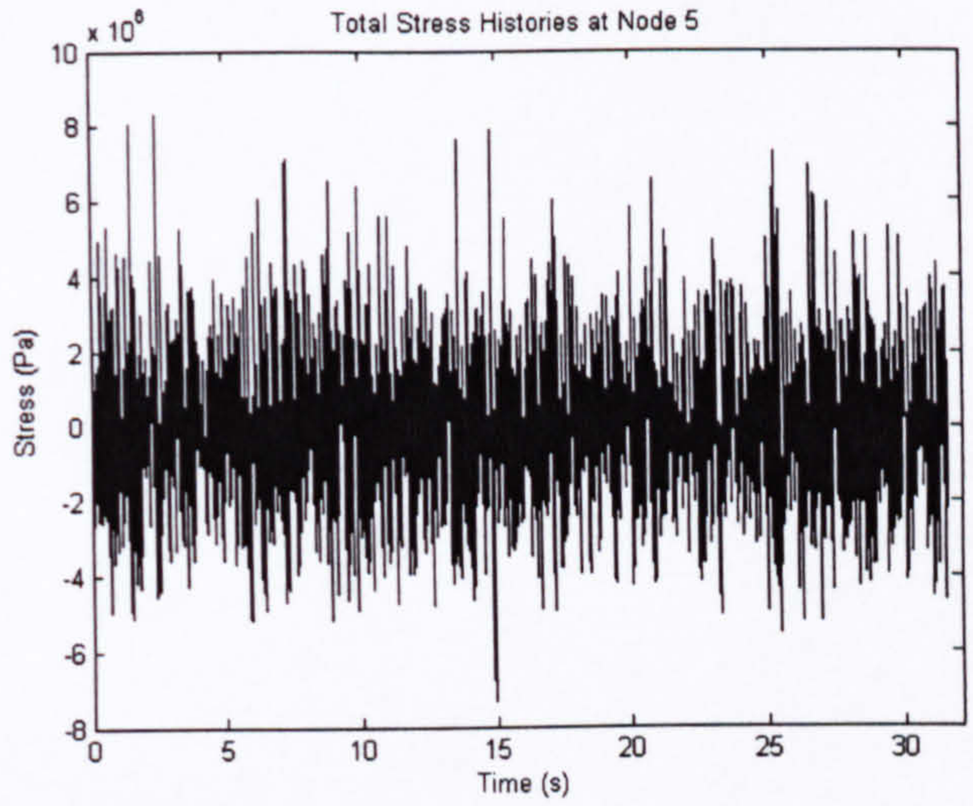

Figure A5.1: Component Stress Histories (Sxt)

Identifying Cyclic Stress Ranges using Rainflow Cycle Counting Method

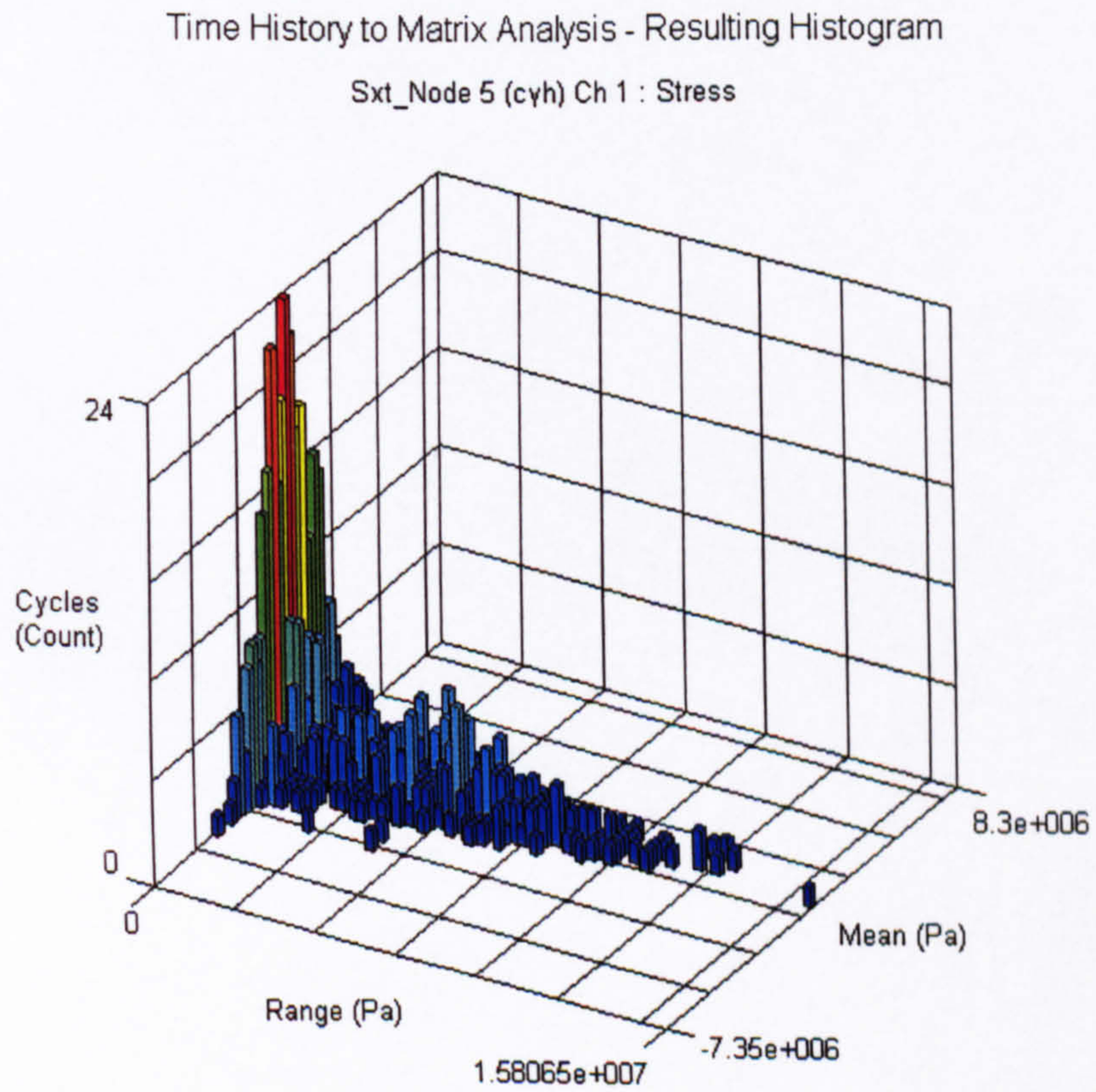

Figure A5.2: Rainflow Cycle Counting with nCode ICE-flow